Natural Convection in a Vertical Channel Related to Passive Solar Systems

A thesis presented for the degree of
Doctor of Philosophy in Mechanical Engineering

by

ABDUL RASSOL H. AL-AZZAWI, B.SC., M.SC.

Department of Mechanical and Process Engineering
Division of Thermodynamics and Fluid Mechanics

University of Strathclyde
Glasgow

September 1987

To my family

ACKNOWLEDGEMENTS

I wish to thank Professor H.C. Simpson, B.Sc, SM, Sc.D., FInstP, AMAICHE, CEng, FIMechE, FRSE, Head of the Division of Thermodynamics and Fluid Mechanics, for giving me the opportunity to study at Strathclyde University.

I also wish to express my sincere thanks to my supervisors, Dr A.A. Nicol, B.Sc, Ph.D, MInstP, and Dr A. Gilchrist, M.Sc., Ph.D., ARCST, for their guidance, help, advice and critical suggestions throughout the project.

I would like to thank Dr S. Fraser and Dr C. Carey for their assistance with the PHOENICS programming problems.

I also wish to thank Mr A.A. Moustafa for his discussion and company during the late working hours and at weekends.

I am grateful to the technical staff of the Thermodynamics Laboratory for their diverse contribution and in particular to Mr J. Lowe, chief technician and Mr R. MacIntyre for their considerable input to the construction of the test facility.

My thanks also to Mrs M. Mitchell, Miss A. Ross and Mrs M. Floyd for their assistance with the typing of this thesis.

Finally, my thanks to the Scientific Research Council, Solar Energy Centre, Baghdad for offering me this Scholarship and my family for their extensive support.

ABSTRACT

Heat transfer and fluid flow characteristics for natural convection of air in a vertical parallel channel system have been examined. The results of both theoretical and experimental work are reported in this thesis.

The system of differential equations governing the fluid flow was solved using the PHOENICS code program. The PHOENICS solution gave velocities, temperatures and pressures throughout the field and velocity and temperature profiles are presented at different vertical locations for three channel heights, 1, 2 and 3 m, each for three different channel widths, 50, 100 and 150 mm. A further PHOENICS sub-routine was written to obtain relevant dimensionless parameters such as the Nusselt Number, which characterises the heat transfer to the air, the Rayleigh Number, the dimensionless air flow rate and dimensionless channel length. The results obtained have been compared with experimental results and with existing data for channels with constant wall temperatures. Non-isothermal wall cases were also considered and the resulting velocity and temperature profiles are presented.

The channel used in the experimental work was formed from two vertical plates, one of which was electrically heated, while the other was glass. Heated plates of height 1 m and 2 m were used and combination of these formed a plate of height 3 m. The width of the plates was 1 m. A double glazed cover plate of the same dimensions could be adjusted to give spacings between the heated plate and glass from 25 mm to 150 mm. The electrically heated plate could be controlled to give the required constant plate temperature (range 35-125°C) and heating could be augmented by a solar simulator consisting of 50 Tungsten Halogen Lamps of 150 Watts each.

From the experimental results, relationships between the Nusselt number, Rayleigh number, dimensionless air flow rate and dimensionless channel height have been obtained. In addition, the effect of diffuser sections at the channel inlet and outlet and transient operating conditions were investigated experimentally. Effects of atmospheric pressure and humidity were also considered.

The experimental results are compared with those from the PHOENICS solution and with existing data for constant wall temperature conditions and they show good agreement.

A discussion of the use of the correlating equations for the heat transfer coefficient and air flow rate in the design of passive solar heating systems, such as the Trombe wall, is also included.

CONTENTS

NOMENCLATURE

b	width of channel, m
β	coefficient of volumetric thermal expansion, K^{-1}
C_p	specific heat of fluid, kJ. kg^{-1}. K^{-1}
g	gravitational acceleration, 9.806 m. s^{-2}
Gr	Grashof number, g. $\beta(\bar{T}_w-To)$. b^3. ν^{-2}
h	average heat transfer coefficient, kJ. m^{-2}. K^{-1}. s^{-1}
K	thermal conductivity of fluid, kJ. m^{-1}. K^{-1}. s^{-1}
l	height of channel, m
L	dimensionless height of channel
ν	kinematic viscosity, m^2. s^{-1}
Nu	average Nusselt number
p	pressure at elevation x, N. m^{-2}
p_a	ambient pressure at elevation x, N. m^{-2}
P	dimensionless pressure, b^2. $(p-p_a)\nu^{-2}$. Gr^{-2}. ρ^{-1}
Pr	Prandtl number = $C_p \mu/K$
$\dot{q}$	volume flow rate, m^3. m^{-1}. s^{-1}
$\dot{Q}$	dimensionless volume flow rate
R	gas constant for air = 287 $J.Kg^{-1}.K^{-1}$
Ra	Rayleigh number, Gr.Pr
ρ	fluid density, kg. m^{-3}
T	temperature, K
Θ	dimensionless temperature, (T-To)/(Tw-To)
u	fluid velocity, x-direction, m. s^{-1}
U	dimensionless fluid velocity, X-direction

v fluid velocity, y-direction, m. s^{-1}

V dimensionless fluid velocity, Y-direction

x,y cartesian coordinates, m

X,Y dimensionless cartesian coordinates

Subscripts

g glass

o inlet

t total

x elevation

w wall

CHAPTER 1

INTRODUCTION

Natural convection flow along vertical surfaces

occurs in a wide range of technological situations, for example, heat dissipation from radiators, heat exchangers, fire propagation, solar collectors and driers, cooling of electronic equipment and storage of spent nuclear reactor fuel assemblies. The increasing importance and development of alternative energy sources has stimulated great interest in recent years in the use of passive solar energy systems for both heating and ventilation and natural convection plays an integral part in all such systems.

Passive solar energy systems include the Trombe wall concept and the solar chimney both of which rely on absorbed solar energy heating a vertical wall to a temperature which is high enough to induce convective air flow. Normally such systems are glazed to maximize energy collection and thus the arrangement usually takes the form of a vertical, parallel plate channel with the walls at different temperatures. To design such a passive solar system, the transient conduction wall storage problem has to be solved simultaneously with those of radiation and convection heat transfer on the surface exposed to the

incident radiation to enable wall surface temperatures to be obtained. However the convective heat transfer coefficient is dependent on the wall temperature and thus the problem is a coupled one, i.e. if a computer simulation of the complete system was made then an iterative method of solution would be required. Although the solution for the complete system is time dependent, the time constant for the solid wall is such that the transient response is slow and hence the system can be considered to be in the steady state at any instant in time (i.e. a quasi-steady state approach can be used). Thus a system comprising a vertical solid wall and a glazed wall separated by a space, can be regarded as a vertical solar collector where the air flow rate through the channel is determined by the buoyancy effects caused by heat transfer to the air from the solid walls. Detailed analysis of such installations is too complex a problem for architectural design purposes and simpler procedures giving approximate solutions are therefore required. Information on the effective heat transfer coefficient and air flow rates in relatively short ducts in which flow is still developing is required before such methods can be applied with reasonable confidence.

Although a great deal of theoretical work is available for fully developed flows, these being more amenable to analysis, relatively little information is available on developing flow, particularly for channels

where the two walls are at different temperatures and where the wall temperatures vary with height.

The present study was undertaken to investigate the heat transfer and air flow for developing flow in parallel, vertical, channels for both constant and variable wall temperatures. The channels used in the investigation consisted of one composite wall with an aluminium plate in contact with the air and one double glazed wall. The design of the system permitted the aluminium plate to be heated in a controlled manner using electric resistance heaters embedded in the composite wall and also allowed for additional heating using a solar simulator.

Experiments were performed to investigate the behaviour of the system for a range of channel widths and heights, and a range of wall temperatures. Further experiments were conducted to examine the influence of atmospheric pressure and humidity, the use of inlet and outlet diffuser sections and transient effects.

Theoretical solutions were obtained using the PHOENICS computer package. Solutions were obtained for a range of plate heights and channel widths and a range of wall temperatures for comparison with the experimental results and with existing data available in the literature. Finally the experimental and theoretical results obtained

are plotted and compared using dimensionless parameters normally used in natural convection studies.

CHAPTER 2

LITERATURE REVIEW

2.1 Introduction

This chapter presents in chronological order the literature presently available on natural convection heat transfer in a vertical constant wall temperature channel. This literature is discussed in detail in Section 2.2. Heat transfer correlations and derivation of the dimensionless groups for the fluid flow in a channel are presented in Section 2.3. Since natural convection of air between parallel flat plates is only one aspect of a much more general problem in the collection of solar energy, a section devoted to references on basic passive solar energy systems is also included. The systems referred to consist essentially of parallel plate channels one of which is heated using absorbed solar energy and are presented in section 2.4. Finally, the literature concerned with natural convection heat transfer and fluid flow in the Trombe-wall system is discussed in Section 2.5. Some references on the utilization and design of such systems are also included.

2.2 Literature Review on Natural Convection Between Two Vertical Parallel Plates

Heat transfer by natural convection in a fluid layer between two vertical parallel plates has been studied extensively due to its relevance to many problems of practical interest such as air flow in solar collectors, nuclear reactors, furnaces, electronic circuit cards, fins, radiators, heat-exchangers, etc.

The earliest experimental study is that of Carpenter and Wassell (1), who used a system consisting of two pairs of square plates, 121.92 cm^2 and 40.64 cm^2 respectively, mounted vertically. The variation of the convective loss per unit area, averaged over the whole surface of a plate, was determined for different heights, spacings, and temperature excesses above ambient air. Some observations were made on the effect of extending the plates upwards by means of a chimney section of wood. All their work was experimental and observational, and, they did not present any correlation between the variables.

Experiments by Kennard (2) were performed using a Mach-Zehnder interferometer to investigate the temperature distribution and heat flux in the air flow through a rectangular channel with heated walls. Photographs were presented showing the interference fringes for flow between

two vertical parallel plates for four different plate spacings.

The most widely quoted study is that of Elenbaas (3) who worked with a system consisting of a pair of square plates open to the ambient along all edges (lateral, top and bottom). In his first study he measured heat transfer from vertical parallel plates, 12 cm by 12 cm for different spacings between the plates. The plates had a uniform temperature higher than the ambient temperature. He also developed an approximate simplified mathematical model by fitting a modified parabolic velocity profile and a modified exponential temperature profile for the region between the plates. The optimum distance between the plates as a function of the height for different values of wall temperature were plotted. His measured heat dissipation, when corrected for finite size of the plates, shows good agreement with his mathematical treatment. The measured results of Nusselt number as a function of GrPr b/l are shown in Figure 2.1. Elenbaas (4,5,6) later extended his theory to vertical channels of different cross section including circular, square, rectangular and triangular shapes. Elenbaas' results are frequently used as the basis for optimisation calculations for vertical plates and are often compared with analytical results for parallel plate channels.

An analysis of natural convection phenomenon carried out by Ostrach (7,8), shows that the flow and heat transfer are not only functions of the Prandtl and Grashof numbers but also depend upon another dimensionless parameter, $\bar{K} = Gr\beta f_x b/C_p$, where f_x is the x-component of body force per unit mass. Attention was given to the particular case of fully developed natural convection flow of fluids between two long parallel vertical surfaces. These surfaces were taken to have constant but not necessarily equal temperatures. The velocity and temperature distributions in the flow for this special case were determined and it was observed that increasing the ratio of wall and air temperature differences increased the flow velocities, the net mass flowrate and of course the temperatures. No relationships between the variables governing the mass and heat transfer were presented in this study.

Kobayashi and Fujimoto (9) studied the dissipation of heat from hot surfaces to the air flow caused by natural convection in the narrow space between two parallel walls facing each other. The amount of heat dissipated from any particular point on the hot surface was determined from the product of the temperature gradient in the boundary layer and the thermal conductivity of the air film. Heat dissipated from the hot surface was observed using the Schlieren method and the air temperature was measured using

thermocouples. The heat transfer coefficient at any point on the hot surface is affected by the temperature difference between the hot surface and the cold air current at inlet and the gap between the two parallel walls.

Siegel and Norris (10), measured free-convection heat transfer coefficients as a function of spacing for two parallel, electrically heated, vertical plates. The walls were substantially uniformly heated, and the Grashof number, based on plate height, was of the order of 10^{10}. The experimental results demonstrated that the surface temperature rise increases, or the local Nusselt number decreases, as either of the cross-section dimensions of the free convection space is reduced. The decrease in Nusselt number was less rapid than was expected from purely two dimensional flow considerations. This was ascribed to the effect of the asymmetrical flow pattern observed in the convection space. When the space between plates was made sufficiently large, the results obtained were reasonably consistent with the correlation proposed by Jakob (11) for a single vertical plate with a turbulent boundary layer and with the theoretical correlation for uniform heat flux,single vertical plates with laminar boundary layers which was derived by Siegel (12). The results of Siegel and Norris (10) were almost independent of the spacing between the heated surfaces down to the minimum value tested. Experimental local Nusselt number

as a function of GrPr for different channel widths were correlated.

Bodoia and Osterle (13,14) were the first to obtain a numerical solution to the basic governing equations, the continuity, momentum and energy equations, for the channel problem with constant wall temperature. The equations were expressed in finite difference form and solved numerically using a digital computer. Results were obtained for the variations of velocity and temperature. The fluid was assumed to enter the channel with ambient temperature, atmospheric pressure, a flat velocity profile and leave the channel at atmospheric pressure. Dimensionless velocity and temperature profiles versus elevation were presented for a channel of dimensionless length L = 0.333. The flow and heat transfer characteristics of the channel were studied. Figure 2.2 shows the results for the dimensionless flow rate plotted against dimensionless channel length for the fully developed flow case. The pressure variation through the channel is shown in Figure 2.3. The pressure distribution in the channel reaches a negative maximum at some point in the channel, beyond which the pressure increases and returns to atmospheric pressure at the channel exit. Nusselt number as a function of GrPr b/l for a Pr = 0.7 is shown plotted in Figure 2.4 and is given by the following equation

$$Nu = 0.680\ (GrPr\ b/l)^{1/4} \qquad (2.1)$$

The heat dissipation from two parallel plates held vertically in free air was studied experimentally by Aihara (15). From Schlieren photographs taken under various conditions of spacing between the plates and temperature difference between the heated surfaces and the environment the heat transfer coefficients were calculated. The following correlation representing the mean Nusselt number was obtained for the range $10 < GrPr\ b/l < 10^4$

$$Nu = \frac{1}{24}\ GrPr\ \frac{b}{l}\ [1-e^{-(32.4\ 1/GrPrb)^{3/4}}] \qquad (2.2)$$

The transport properties of the air were determined at the wall temperature.

Results of an analytical investigation were presented by Engel and Mueller (16) for a wide range of Prandtl and Rayleigh numbers for both the constant wall temperature and constant heat flux boundary conditions for the development of natural convection in channels of finite length with particular emphasis on channels in which the boundary layer development region occupies a significant portion of the channel length. These results were obtained by an integral technique which, although fairly complex, is far simpler than numerical integration of the governing partial differential equations. The velocity

and temperature profiles, pressure variation in the channel and Nusselt numbers predicted by the integral technique compared favourably with the numerical results presented by Bodoia and Osterle (13) as shown in Figures 2.5 to 2.7.

Numerical integration solutions were presented by Rao and Morris (17) for laminar flow between two vertical parallel plates when one of the plates has a uniform temperature gradient in the direction of flow and the other is thermally insulated, for the case where a gravitational effect was taken into account. Two sets of solutions were derived depending on whether the flow was in an upward or downward direction. Velocity and temperature profiles, heat transfer and friction factor were obtained. The bulk Nusselt number variation with Rayleigh number > 150 is given by the following equation

$$Nu_b = \frac{2\sqrt{2}}{3} (Ra)^{1/4} \qquad (2.3)$$

A series of experimental studies were made by Aihara (20,21,22,23), for natural convection from vertical rectangular fin arrays. Effect of fin geometry and temperature on the average heat transfer coefficient was investigated and an empirical correlation was obtained. In addition, a theoretical analysis of the case of large fin spacing was made by using a stationary air layer model.

Experimental investigation of the natural convection of air between two isothermal vertical surfaces was made by Currie and Newman (24). Measurements were made of the temperature and velocity profiles across the air gap at various streamwise locations for various gap sizes. From the results the volume flow rate and heat transfer coefficient between the two surfaces were calculated. The temperature profiles were found to be fitted by a hyperbola while the velocity profiles were fitted by a parabola. The heat transfer coefficient was found to be in agreement with published experimental results of Elenbaas (3). The induced flow rate calculated from the experiments was found to be in good agreement with the theoretical analysis of Bodoia and Osterle (13) and Engle and Mueller (16).

Ofi and Hetherington (25), conducted an experimental and theoretical work on natural convective air flow between a pair of rectangular isothermal, vertical parallel flat plates each 30 x 40 cm. Measurements were made of the exit temperature and velocity distributions midway along the channel breadth for gap sizes varying from 0.68 to 4.48 cm, and channel surface temperature from 72°C to 380°C. The finite element method was used to obtain approximate numerical solutions for steady state natural convection from the open vertical channel with uniform wall temperature. The natural boundary conditions generated by

the variational technique were invoked at the channel entrance and exit. Temperature, and velocity profiles were obtained for a Rayleigh number range of 0.1 to 10^7. Nusselt numbers against Rayleigh numbers are shown in Figure 2.8 and were found to be related by the following equations:

for Wide channel $\quad Nu = 0.75\ (GrPr\ b/l)^{1/4} \qquad (2.4)$

for Narrow channel $\quad Nu = {}^{1}/_{24}\ (GrPr\ b/l) \qquad (2.5)$

These correlations compare very closely with those obtained by Bodoia and Osterle (13) using a finite difference solution.

Miyatake and Fujii (26) obtained the Nusselt number by performing a numerical analysis of free convection heat transfer between vertical parallel plates, with one of the plates uniformly heated and the other thermally insulated, for Prandtl numbers of 0.7 and 10 over a range of Rayleigh number from 1 to 10^3. A forward marching, implicit method with iteration was used to solve the nonlinear partial differential equations governing the fluid flow. Pressure boundary conditions at the inlet and outlet were assumed atmospheric. Numerical results were obtained for the variations of induced flow rate, fluid temperature, fluid pressure, and Nusselt numbers based on the properties of the air evaluated at the film temperature (Tw + To)/2.

The pressure reduces up to a particular height then increases to atmospheric at the channel exit. The pressure defect along the channel length is shown in Figure 2.9. The predicted mean Nusselt number was found to agree with experimental data of Nakamura et al (27) and Bodoia and Osterle (13) respectively as shown in Figure 2.10. Average Nusselt number for developing flow is given as:-

$$Nu = 0.613\ (GrPr\ b/l)^{0.25} \qquad (2.6)$$

Numerical and experimental investigation of the developing laminar free convection heat transfer in vertical parallel plate channels with asymmetric heating was presented by Aung (28, 29). Thermal boundary layer conditions of uniform wall heat flux and uniform wall temperature were considered. The boundary conditions of the pressure at the channel inlet and outlet were assumed to be atmospheric. Axial pressure variation along the channel length and the average Nusselt number as a function of Gr Pr b/l for different wall heating ratios are shown plotted in Figures 2.11 and 2.12 respectively. Fluid properties were evaluated at a temperature $(\bar{T}+To)/2$ where $\bar{T}$ is the average of the wall temperatures. The developing dimensionless flow rate was obtained for air at different ratios of the wall temperature differences and is shown plotted in Figure 2.13. The numerical solutions were shown to approach the closed form solution for fully

developed flow. Results indicated that for uniform wall temperature, the Nusselt number characterising the total heat transfer to the fluid was found to be very nearly related to the Rayleigh number by a universal curve for all ratios of wall temperature differences. The experimental data were obtained using an interferometer. Some interferometer fringe patterns were obtained in the vicinity of the mid-height of the channel. These interferograms were intended for a qualitative study of the temperature field in the fluid at different test conditions. Full details of the experimental procedure and test results were presented by Sernas et al (30) and Aung and O'Regan (31). Good agreement between the numerical solution and experimental data was noted. The numerical solution agreed with the Bodoia and Osterle (13) solution for a channel with symmetrical uniform wall temperature.

A theoretical investigation was carried out by Aihara (32) to solve the governing equations of laminar convection between vertical parallel plates of uniform temperature by an implicit finite difference method, taking into consideration the pressure drop due to the acceleration of the fluid to the channel inlet which was neglected in all other theoretical studies. Solutions were obtained for both inlet velocity conditions of flat and parabolic profiles for Prandtl number of 0.7 and 10. From the differences in velocity, temperature and pressure

distribution between this solution and Bodoia and Osterle's results (13), the effects of the inlet boundary conditions and an applicable limit of Bodoia and Osterle's (13) inlet conditions were clarified. Figure 2.14 presents the variations of the pressure with channel height and shows that the pressure decreased with the development of the flow near the channel inlet to a negative maximum value at a location along the channel height, then increased gradually to atmospheric pressure at the channel outlet. By taking account of the pressure at the channel inlet section,which was neglected in all other theoretical studies , as in Aihara's investigation the result still shows a similarity in the pressure behaviour throughout the channel for low Rayleigh number conditions. The fluid properties were evaluated at the wall temperature. The average Nusselt number versus GrPr b/l is shown plotted in Figure 2.15 and is given by the following relations for developing flow for Pr = 0.7:

for parabolic velocity profile $Nu = 0.386\ (GrPr\ b/l)^{1/4}$ (2.7)

for flat velocity profile $Nu = 0.515\ (GrPr\ b/l)^{1/4}$ (2.8)

The results for average Nusselt number agree well with other theoretical studies. This is an important paper which provides a link between the previous papers in which the pressure and velocity conditions were artificial to a

certain extent in that the velocity profile of the incoming fluid was not recognised.

Akbari and Borgers (33) performed a theoretical investigation of free convection laminar heat transfer between vertical parallel plates of different temperature in the Trombe wall system. A finite difference procedure was used to solve the governing equations of continuity, momentum and energy in dimensionless form with the boundary conditions similar to those described by Aihara (32). A uniform inlet velocity profile and the pressure drop corresponding to flow acceleration at the channel entrance were selected as the starting conditions. Details of the dimensionless velocity and dimensionless temperature profiles were given at four stages of flow development for three different glass temperatures at dimensionless volume flow rates of 0.02, 0.002 and 0.0005. The resulting correlations for calculating the Nu number, dimensionless channel length and volume flow rate were long and complex. These correlations were functions of dimensionless glass temperature. These correlations were developed to enable important performance characteristics to be estimated given the channel geometry, surface temperatures and inlet air temperature. No comparison with available theoretical or experimental data was made.

This investigation was extended by Borgers and Akbari (34) to study the free convection turbulent flow

within the Trombe wall channel and the results were presented using the same procedures.

Pratt and Karaki (35) used a slightly different numerical technique from that of Akbari and Borgers (33). The flow in the duct, as part of a more complex system, was again treated as being two-dimensional laminar free convective flow between vertical plates of unequal and non-uniform temperature where vent friction losses are significant. Given surface temperature distributions and the geometry of the vent flow restrictions, the mass transport through the channel and the heat transfer from the plates is determined by solving simultaneously the momentum, energy and continuity equations. Uniform initial velocity profile, known pressure gradient and two-dimensional boundary layer equations, including buoyancy effects, were assumed for the numerical solution. Solutions were presented for the Trombe wall designs used in this study. The dimensionless temperature and velocity profiles and heat transfer coefficient were presented for selected conditions of the wall and glass temperature and inlet velocity. No comparison between this study and existing results was made and no correlations were given.

Natural convection between two parallel square vertical plates was investigated experimentally by Sparrow and Bahrami (36) using the naphthalene sublimation

technique instead of direct heat transfer to enable elimination of radiation effects, extraneous convective/conductive heat losses, and variable property effects. The experiments encompassed three types of hydrodynamic conditions along the lateral edges (1) fully open to ambient, (2) blockage of one of the edge gaps, (3) blockage along both of the edge gaps. The results for the fully open-edged case cast substantial doubt on the often quoted data of Elenbaas (3) for the low range of the parameter GrPr b/l. Uncertainties in Elenbaas' results owing to large fluid property variations were also demonstrated. Suppression of fluid flow along one lateral edge gap generally has only a modest effect on the heat transfer coefficient and no effect for GrPr b/l > 4. When both edges were blocked, 30 percent (or more) reduction in the heat transfer coefficient occurred at low values of GrPr b/l. When GrPr b/l > 10, the lateral edge conditions did not affect the results.

A computer program was developed by Melhus (38, 39) for the steady, two-dimensional natural convection in vertical ducts. The computer program was based on a method using finite differences and the SIMPLE algorithm, presented by Spalding and Patankar (65). The solution method was elliptic and it was possible to calculate a flow field for which the velocity profile at the inlet of

the calculation domain, or the mass flowrate, were unknown initially. Static pressure must be specified where fluid crosses the boundaries, as a function of the velocity at the boundaries. At the inlet of the duct Bernoulli's equation was used to find the relationship between static pressure and velocity. At the outlet of the duct the static pressure was that of the surroundings. The velocity and temperature profiles at the inlet and outlet of the calculating domain were directly calculated. In contrast to the use of parabolic methods in which the velocity profile at the inlet must be prescribed and the correct velocity is found by trial and error, the elliptical method avoids any specification of these parameters prior to calculation. Calculations were performed for ducts heated in three different ways, (a) a duct with uniformly distributed heat source in the fluid and with walls insulated on the outside, (b) isothermal wall duct and (c) a duct with simple heating element fixed vertical at the centre. The results for the velocity and temperature profiles were compared with experimental data, investigated by use of laser-doppler-anemometry. The comparison showed that the computed velocity and temperature values are smaller and greater than the measured values respectively. Some of the theoretical results were compared with results obtained using the parabolic computer program "GENMIX". It was concluded that the elliptic method for calculation of natural

convection in vertical ducts as used by Melhus (39) was better than the earlier used parabolic methods. No correlations between the flow variables were presented in this work.

Numerical analysis of free convection between parallel plates was carried out by Nakamura et al (40), without using the boundary layer approximation. An approach that can determine the flow rate by consideration of the pressure drop was proposed. A comparison of the results was made with Kettlebrough's (41) model for numerical calculations and Aihara's (32) results and agreement was found to be reasonable.

A theoretical method was presented by Tichy (42) for study of air flow in a Trombe wall channel. Flow was assumed to be laminar, Newtonian and two-dimensional. The method was based on linearising the convective terms of the governing equations by an Oseen-type approximation. By including an empirical parameter in the approximation, results agree very well with the numerical solution due to the Akbari and Borgers (33), for the case of no flow losses through the channel inlet and exit sections. Results were presented for dimensionless temperature and velocity fields, flow rate and heat transfer in terms of a loss coefficient, surface temperature ratio and Grashof number.

When flow losses at channel inlet and exit are included, it is seen that air flow delivery to the enclosed space is decreased significantly.

Bar-Cohen and Rohsenow (43) presented a theoretical study of fully developed two-dimensional flow between parallel plates at different conditions (symmetric or asymmetric isothermal plates). The practical application was heat dissipation in vertical parallel plate arrays encountered in electronic equipment. Several correlations for Nusselt number and optimum spacing were obtained for the range of conditions considered in this study. A comparison showed good agreement between the variation of the Nusselt number with GrPr b/l with the work of Miyatake and Fujii (26) and Nakamura et al (44).

Flow visualization methods using holographic interferometry were used by Cordier and Durou (45) to investigate natural convection in heated wall channels. These methods have the advantage of not disturbing the fluid flow being studied. Interference fringe patterns were presented for the air flow in channels with a range of wall temperatures. These allowed optimization of the channel geometry in order to control the flow in the channel at different wall and inlet temperatures.

Laminar natural convection between vertical plates was investigated by Burch et al (46) using a finite-difference procedure. Since the solution was parabolic, velocity and temperature conditions at the channel exit were not required. At the channel inlet uniform velocity and temperature profiles were specified. The pressure was specified to be the same at both the channel inlet and exit. The dimensionless temperature and velocity profiles were obtained for Gr b/l of 10, 10^3 and 10^6 and aspect ratios of 5 and 0.5 respectively. The axial pressure results are shown plotted in Figure 2.16 for Gr b/l = 10 and 10^6 which shows that the pressure decreases after the channel inlet to a minimum value at some location within the channel and of course increases back to the prescribed value at the channel exit. The dimensionless mass flow rate and total heat transfer at Gr b/l = 10, 10^3 and 10^6 were presented in tables for different aspect ratios.

Theoretical predictions of natural convection in a Trombe wall system were presented by Ormiston et al (47) using a finite-volume method similar to the method described by Patankar (75). Assumptions made were that the flow is laminar, two-dimensional and the glass and wall are isothermal. Dimensional analysis showed that, for a given geometry, the flow and heat transfer are characterized by two Rayleigh numbers, one Rayleigh number

governs the natural convection interaction between the wall and glass, the other governs the natural convection interaction between the room and the channel. These predictions are believed to be the first that take account of the interaction between the room and the channel and which include the important case where the glass temperature is lower than the room temperature. The streamlines and isotherms of the flow were presented for the channel and the interior space of the room. A comparison between the predicted Nusselt number for the Trombe wall channel with the experimental results of Elenbaas (3) is shown in Figure 2.17 and agreement is seen to be reasonable.

In conclusion, analyses of the flow and thermal fields between two vertical flat plates have been performed by many authors considering either prescribed symmetrical or non-symmetrical wall temperatures. All the above investigators cited analyses considering laminar flow and were based on the assumption that both walls are at higher temperatures than the ambient air inlet temperature thus ensuring that the flow is moving upwards because of the buoyancy effect. This allows simplification of the non linear governing equations of continuity, momentum and energy so that they may be solved by a marching technique either using finite difference or finite element methods.

As may be seen from the literature review, a number of different pressure boundary conditions at the channel inlet and exit have been considered.

Most theoretical research work has been performed using boundary conditions where the inlet and outlet pressures are equal to the ambient pressure at these levels. The pressure defect in the channel for these cases has been shown to decrease to a minimum value somewhere along the length of the channel and subsequently increases to the boundary value at outlet.

When a different pressure boundary condition was used by Aihara (32), using the pressure drop due to the acceleration of the fluid at channel inlet to obtain the inlet pressure condition, both linear and the above described pressure distributions along the channel were obtained depending on the magnitude of the Rayleigh number. In this paper parabolic inlet velocity profiles as well as uniform velocity profiles were examined and these also influenced the pressure distributions.

The theoretically predicted flow in a channel is evidently dependent on the pressure boundary conditions used and the inlet velocity distribution and from the work of Aihara (32), it would appear that very small

dimensionless pressure differences between inlet and outlet, of the order of $\dot{Q}^2/2 = 3.2 \times 10^{-3}$ for $GrPrb/l = 10^2$, have a marked effect on the flow.

Since for a vertical channel of length l without flow the static pressure difference between the bottom and top is ρgl, which for a 1 m length is considerably larger than the pressure drop caused by fluid acceleration when flow is induced by heating, then the effect of the inlet velocity profile will be small and the use of a pressure boundary condition dictated only by the static head of the ambient fluid should give sufficiently accurate results.

2.3 Derivation of the Dimensionless Groups Generally Used in Natural Convection Analysis:

The first step in analysing a fluid flow problem is to write down in mathematical form the physical laws which govern the flow. These physical laws include the conservation of mass, momentum and energy plus any auxiliary information, boundary conditions and assumptions required to complete the solution.

The system to be analysed is shown in Figure 2.18. It consists of two vertical flat parallel plates of height l and spacing b which form a vertical channel. Boundary conditions of uniform equal wall temperatures and uniform but different wall temperatures are considered in the analysis. The channel walls are heated and as a result of the heat transfer to the fluid, the temperature of the latter increases. The resulting density changes causes the fluid to rise through the channel due to the buoyancy effect. The fluid that enters the channel at the bottom at uniform temperature T_o is assumed to have a uniform velocity profile u_o.

The following simplifying assumptions were made:

1. The flow mode is laminar, steady state and two-dimensional

2. The fluid is a continuum, Newtonian, and of uniform composition

3. The transport properties of the fluid are constant

4. The flow is one of natural convection developing between smooth vertical walls

5. The pressure at the inlet and outlet of the channel are equal to the static pressure in the ambient fluid

6. Air is used as the heat transfer fluid with constant Prandtl number 0.7.

For moderate differences between Tg, Tw and To, the flow is governed by the so-called incompressible natural convection equations expressing conservation of mass, momentum and energy, which simplify to:

$$\frac{\partial u}{\partial x} + \frac{\partial v}{\partial y} = 0 \qquad (2.9)$$

$$u\frac{\partial u}{\partial x} + v\frac{\partial u}{\partial y} = \nu\frac{\partial^2 u}{\partial y^2} - \frac{1}{\rho}\frac{dp}{dx} - g \qquad (2.10)$$

$$u\frac{\partial T}{\partial x} + v\frac{\partial T}{\partial y} = \frac{K}{\rho C_p}\frac{\partial^2 T}{\partial y^2} \qquad (2.11)$$

By rewriting Equation (2.10) using static pressure p_a of the ambient fluid and thermal expansion coefficient β,

$$\beta = -\frac{1}{\rho}\left(\frac{\partial \rho}{\partial T}\right)_p \qquad (2.12)$$

then

$$u\frac{\partial u}{\partial x} + v\frac{\partial u}{\partial y} = \nu\frac{\partial^2 u}{\partial y^2} - \frac{1}{\rho}\frac{d(p-p_a)}{dx} + \beta g(T-To) \qquad (2.13)$$

The term $(p-p_a)$ represents the pressure defect, i.e. the difference between the local pressure within the channel and the ambient pressure at the same elevation.

The boundary conditions for uniform wall temperatures are:

For $x=0$ and $0<y<b$; $u=uo$, $v=0$, $T=To$ (2.14)

For $y=0$ and $x\geq 0$; $u=0$, $v=0$, $T=Tg$ (2.15)

For $y=b$ and $x\geq 0$; $u=0$, $v=0$, $T=Tw$ (2.16)

At $x = 0$; $p-p_a = 0$ (2.17)

At $x = l$; $p-p_a = 0$ (2.18)

The following dimensionless quantities are defined

$$U = \frac{bu}{\nu Gr} \tag{2.19}$$

$$V = \frac{bv}{\nu} \tag{2.20}$$

$$X = \frac{x}{bGr} \tag{2.21}$$

$$Y = \frac{y}{b} \tag{2.22}$$

$$P = \frac{(p-p_a)b^2}{\rho \nu^2 Gr^2} \tag{2.23}$$

$$Pr = \frac{Cp\mu}{k} \tag{2.24}$$

$$\Theta = \frac{T-To}{Tw-To} \tag{2.25}$$

$$Gr = \frac{g\beta(\bar{T}_w-To)b^3}{\nu^2} \tag{2.26}$$

$$\bar{T}_w = \frac{Tw+Tg}{2} \tag{2.27}$$

Equations (2.9), (2.13) and (2.11) can be written in dimensionless form using equation (2.19) to (2.26). Thus

$$\frac{\partial U}{\partial X} + \frac{\partial V}{\partial Y} = 0 \tag{2.28}$$

$$U\frac{\partial U}{\partial X} + V\frac{\partial V}{\partial Y} = \frac{\partial^2 U}{\partial Y^2} - \frac{dP}{dX} + \Theta \tag{2.29}$$

$$U\frac{\partial\theta}{\partial X} + V\frac{\partial\theta}{\partial Y} = \frac{1}{Pr}\frac{\partial^2\theta}{\partial Y^2} \qquad (2.30)$$

The corresponding dimensionless boundary conditions are:

For X=0 and 0<Y<1 ; U=Uo, V=0, θ=0 (2.31)

For Y=0 and X≥0 ; U=0, V=0, $\theta=\theta g$ (2.32)

For Y=1 and X≥0 ; U=0, V=0, $\theta=\theta w$ (2.33)

At X=0 ; P=0 (2.34)

At X=L ; P=0 (2.35)

Some solutions to equations (2.28), (2.29) and (2.30) and the stated boundary conditions have been obtained by Bodoia and Osterle (13), Aung (28), Miyatake and Fujii (26), and Aihara (32) using numerical techniques to find the heat transfer coefficient in the channel as mentioned in Section 2.2.

The volume flow rate is defined as follows:

$$\dot{q} = \int_o^b u\,dy \qquad (2.36)$$

The dimensionless volume flow rate is defined by

$$\dot{Q} = \int_o^b \frac{bu}{\nu Gr}\,dy = \int_o^1 U\,dY \qquad (2.37)$$

This flow rate must be constant throughout the channel.

The mass flow rate throughout the channel can be defined as

$$M = \int_0^b \rho u dy \tag{2.38}$$

The rate of heat absorption by the fluid up to a particular elevation in the channel can be written as

$$\dot{Q}_x = \int_0^b \rho C_p u(T-To)dy \tag{2.39}$$

and, the average heat transfer coefficient h at a location x along the channel height can be defined as

$$h_x = \frac{\dot{Q}_x}{2x(\bar{T}_w - To)} \tag{2.40}$$

Accordingly, the average Nusselt number is given by the following equation

$$Nu_x = \frac{h_x b}{k} \tag{2.41}$$

The dimensionless channel length L is the value of X when x=l, that is

$$L = \frac{l}{bGr} \tag{2.42}$$

The dimensionless groups and equations 2.36 to 2.42 were used in the analysis of the data collected during the experimental tests. Also, they were used in the GROUND subroutine of the PHOENICS code for the theoretical solution of the problem, and full details are given in Appendices C and J.

2.4 Passive Solar Heating

The oil crisis of 1973 has, perhaps more than any other single factor, drawn worldwide attention not only to the rate at which man is depleting the resources of fossil fuels but also to the need for investigating the use of alternative sources of energy.

With the ever growing concern for alternative energy applications, a great deal of interest has recently been shown in the use of solar energy for the heating of dwellings. The designs offered as possible configurations are many and varied. They can be conveniently divided into two classes, the so-called "active" and "passive" designs. The former utilizes solar collectors, separate thermal storage units, and controls as shown in Figure 2.19. Thermal energy collected from the insolation is transported from the collector to the energy storage unit and subsequently from the storage unit to the building thermal control system in a completely regulated way using liquid

or air as a heat transport fluid. This type of system has come to be known as an "active" solar energy system due to the requirement for pumping the heat transport fluid through the system's components. Such units are suitable for almost any site installation, Kreider and Kreith (48), McVeigh (49) , and therefore tend to be expensive.

Passive designs on the other hand are intended to be as simple as possible. Solar energy gains through windows or walls into the building are utilized to effect a net reduction in the total building energy requirement. Generally there are no continuously pumped fluids. Heat is transported by natural convection or radiation, as shown in Figure 2.20. Since solar gains are present in every building, each is passively solar heated to some extent. It is when solar energy utilization becomes a major objective of the architectural design and solar energy supplies a major fraction of the building energy that the building would be described as being a solar building. Frequently these buildings are referred to as sun-tempered structures, Greeley et al (50), Ohanessian and Charters (51).

The two predominant categories of passive solar heating systems are indirect and direct gain systems. All other categories are subsets within these two main categories.

The following subsets are included within the indirect heat gain category:

a. Trombe-Michel wall

b. Water wall

c. Roof pond

d. Attached/isolated sunspace (or greenhouse)

e. Thermosyphoning collectors (air or water)

In contrast there are only two types of direct heat gain systems:

a. Diffusing direct gain

b. Non-diffusing direct gain

Examples of the above categories are illustrated in Figures 2.21 and 2.22, Wright (52), Haltz and Place (53).

2.5 Trombe-Michel Wall

A number of examples of passive solar heating concepts have been built into structures and have received widespread attention. Most use extensive south exposure glass to admit low-angle winter sunshine to the building and extensive use of thermal capacity inside the thermal envelope of the building to store thermal energy.

The basic principle is that thermally massive south facing walls, usually made of concrete, are painted black, and covered with glass on the outside, leaving an air gap between the wall and the glass. The wall is both a thermal energy collector and a thermal energy store. Solar radiation passes through the glass and is absorbed by the wall. Ducts at the top and bottom of the wall allow heated air to be circulated into the room at ceiling level, with the colder air from the room at floor level drawn in at the bottom. For summer cooling, valves at the top of the wall can be used to vent heated air to atmosphere and valves at the rear of the building, at ceiling level, are opened to allow cooler air to flow through into the building.

This increasingly used principle was invented and patented by E.L. Morse in the U.S.A. in 1881, Jäger (54), McVeigh (49). It was developed by Felix Trombe and his collaborator Jacques Michel in 1967 in France, and incorporated into the construction of the first house heating system with thermal storage wall in Odeillo in Southern France as shown in Figure 2.23, Trombe et al (55), Lebens (56). This has been perhaps the most important contribution to solar space heating to date and has promoted world-wide interest in the potential of passive

solar heating systems. Trombe's name is now firmly attached to the principle.

The Odeillo house uses a black-painted, 600 mm thick concrete, south facing wall to collect and store energy from the sun and heat losses are reduced by the use of double glazing across the face of this wall. The method of heating is by convection from the inside surface of this massive concrete wall to the room. It takes 10 to 15 hours for the heat to travel through the wall so instantaneous heating is made possible by circulating room air in the gap between the glass and wall. This is achieved by natural circulation. Dampers are used on the lower openings to stop the air circulation at night. The overhang of the roof shades the south wall completely during the summer and the glazing vents can be opened to encourage cross ventilation. Trombe attempted to measure the bulk heat transfer by measuring the mass flow rate of air and the temperature rise up the duct. His results showed a 30-35 per cent thermo-circulation contribution to the total heat transfer. No experimental results on the nature of the duct flow were presented, but Trombe suggested that the mass flow limit was caused as a result of turbulent flow over the entire length of the duct. The horizontal air inlet was felt to be the probable cause of the turbulence.

There are some new ideas which have been independently developed and which go a long way to reducing some of the disadvantages of the Trombe system. The main disadvantages are slow response of the system to the incident solar radiation and slow heat absorption by the wall in the early hours in the morning. Some of the modifications of the Trombe wall have been proposed at the University of Arizona (57) such as the use of vertic1 fins attached to the wall so that their east side is painted black and their west side is reflective, as shown in Figure 2.24. Morning insolation strikes the blackened side of the fins and hot air is quickly supplied to the room by convection. Thus the room is heated long before the Trombe wall is. In the afternoon the reflective side of the fins is seen by the sun and therefore all the energy is directed on to the wall.

Another modification by Bier (58) was built into a house in Ferrum, Virginia, U.S.A. in which he divided the conventional Trombe wall into five short lengths, as shown in Figure 2.25, each turned so that it is at an angle of 45° to the south glazing. This has become a mixed passive system consisting of half direct gain and half indirect gain. By so doing it has reduced many of the architectural disadvantages of the Trombe wall. It allows morning sunlight in, it intercepts and stores afternoon

sunlight thus preventing overheating, and it allows vision and access through the south collecting surface.

Most experimental data published on Trombe-wall performance has been in the form of overall building performance.

Balcomb et al (88,89,90), Wray and Balcomb (91) have presented temperature profiles for a Trombe wall test cell at Los Alamos, New Mexico, U.S.A. Data for overall performance is of limited use as it only provides seasonal estimates of heat gains for specific building designs, wall configurations and climates. Because of the large number of parameters and the wide range of climatic conditions that affect the performance of the Trombe-wall, assessment of performance lends itself more towards the use of thermal simulation techniques. However, before simulation techniques can be used properly, a fuller understanding of the heat transfer process is required. The nature of transient heat conduction through slabs is well known but further detailed information on the thermo-circulation heat transfer is needed. Balcomb et al (92,93,94) modelled cell temperatures using simple one-dimensional implicit thermal network analysis techniques, which have been validated by comparison with test room results, to predict the annual contribution of a passive solar heating concept which utilises a thermal storage wall of either

water or masonry located behind a vertical double glass, south-facing window. Hour-by-hour calculations for a one-year period are used based on solar radiation and weather data from nine cities. The effect of air thermo-circulation and wall thickness is studied. It is concluded that these approaches to passive solar heating are viable in all the climates studied and will provide a net energy gain to the building of 40,000 to 70,000 BTU per year per square foot of solar wall. The comparative analysis includes parametric variation of fundamental design parameters including building load, glazing area, total mass, mass thickness, number of glazings, night insulation value and allowable temperature swing. Thermal comfort within the two generic types of buildings was considered as well as energy efficient performance, Balcomb (95,96,97).

Work at Melbourne University was based on an extensive numerical simulation by Ohanessian and Charters (51). They performed a comparative analysis between a Trombe-wall heated house and a conventional house over a typical 28-day Melbourne Winter period. The convection heat transfer in the duct was assumed to be turbulent free convection over only the wall surface with the heat transfer from the glazing taken to be small in comparison. Optimisation studies for various glazing networks, wall thickness and auxiliary heating were performed. The

conclusions from this study were (i) the "Odeillo" wall model appears to work quite well under typical Melbourne winter conditions; (ii) the thermal advantage of double glazing seems to be minimal and it is therefore unlikely that double glazing is cost effective in moderate climate zones; (iii) heat conduction through the slab is a critical factor in obtaining acceptable internal temperatures, the use of an overthick slab appears to be a positive disadvantage; (iv) with auxiliary heating a thickness of 250 mm seems to be near optimal for the particular case studied; and (v) energy savings of approximately 40 per cent are obtainable with such design.

An experimental investigation was carried out by Casperson and Hocevar (59) to determine the performance characteristics of a Trombe-wall passive solar heating system. The principal objective of the project was to provide experimental information regarding the heat transfer characteristics of the collector system proper. A secondary objective was to evaluate the overall thermal performance of the test building. The cell on which the experiments were performed incorporated vents across the full width of the wall which was covered with double glazing to allow the gap between the wall and the glazing panel to be varied and the inlet and outlet duct geometries to be changed. A velocity probe and a thermocouple were attached to a traversing mechanism to provide air velocity

and temperature measurements across the width of the gap. Measurements are taken at various vertical and horizontal locations to allow investigation of flow regime development and asymmetric effects. Typical wall and air gap temperature distributions and air gap velocity profiles were given. The shape of the velocity profiles indicate that the air flow was turbulent in the gap. The preliminary experimental results of the concrete wall thermal behaviour and Trombe wall performance were presented. No mathematical correlations for the heat transfer coefficient and flow rate were presented.

Bilgen and Chaaban (60) presented theoretical and experimental studies of a modified Trombe wall collector. A numerical solution for two-dimensional free convection laminar flow was used for the thermal performance analysis of the solar collector. The theoretical results for temperature distribution in the channel and in the wall were presented. The calculated thermal efficiency of the wall storage and the typical results of temperature and velocity measurements in the collector were also presented. These studies have shown that the specific system considered, or its variations could perform quite satisfactorily in Canadian climatic conditions and that an overall thermal performance of about 35 per cent was achievable. The solar convective channel was sufficient to collect and to generate the necessary thermo-circulation

to distribute the warm air without the need of a booster fan.

Akbarzadeh et al (18), carried out an experimental investigation, involving flow visualisation studies of the fundamental flow mechanisms in a Trombe wall channel. Air velocity and temperature measurements were used to examine the natural convection heat transfer processes involved in the thermo-circulation flow. Particular attention was paid to the effects on operational performance of wall parameters such as wall/glazing distance and vent size. Adequate correlation of the experimental results was achieved by using expressions derived by Warner and Arpaci (19) for turbulent free convection from an isothermal vertical flat-plate. It is considered that this type of fundamental heat transfer information is vital so that the overall performance of Trombe wall systems can be adequately modelled using the large range of simulation techniques currently available for thermal network analysis.

The later study of Tichy and Quinn (37), differed from their earlier studies in that primary focus was on natural convection aspects of the air flow in the channel rather than thermal storage and conduction in the wall. The air flow was described by the Akbari and Borgers (33) correlations which are based on numerical solution of the

continuity, momentum and energy equations for the case of the laminar flow at low Grashof numbers and on turbulence modelling at high Grashof numbers. Geometric description, construction materials, insulation and heat conduction were handled using BLAST, a detailed Public Domain Building Analysis Program. Several important aspects relating particularly to commercial buildings were studied for the first time including the effect of climate on the efficiency of the Trombe wall, the effect of wall height, the effect of a low-mass insulated wall, air flow by thermo-circulation and the effect of time lag on heat delivery.

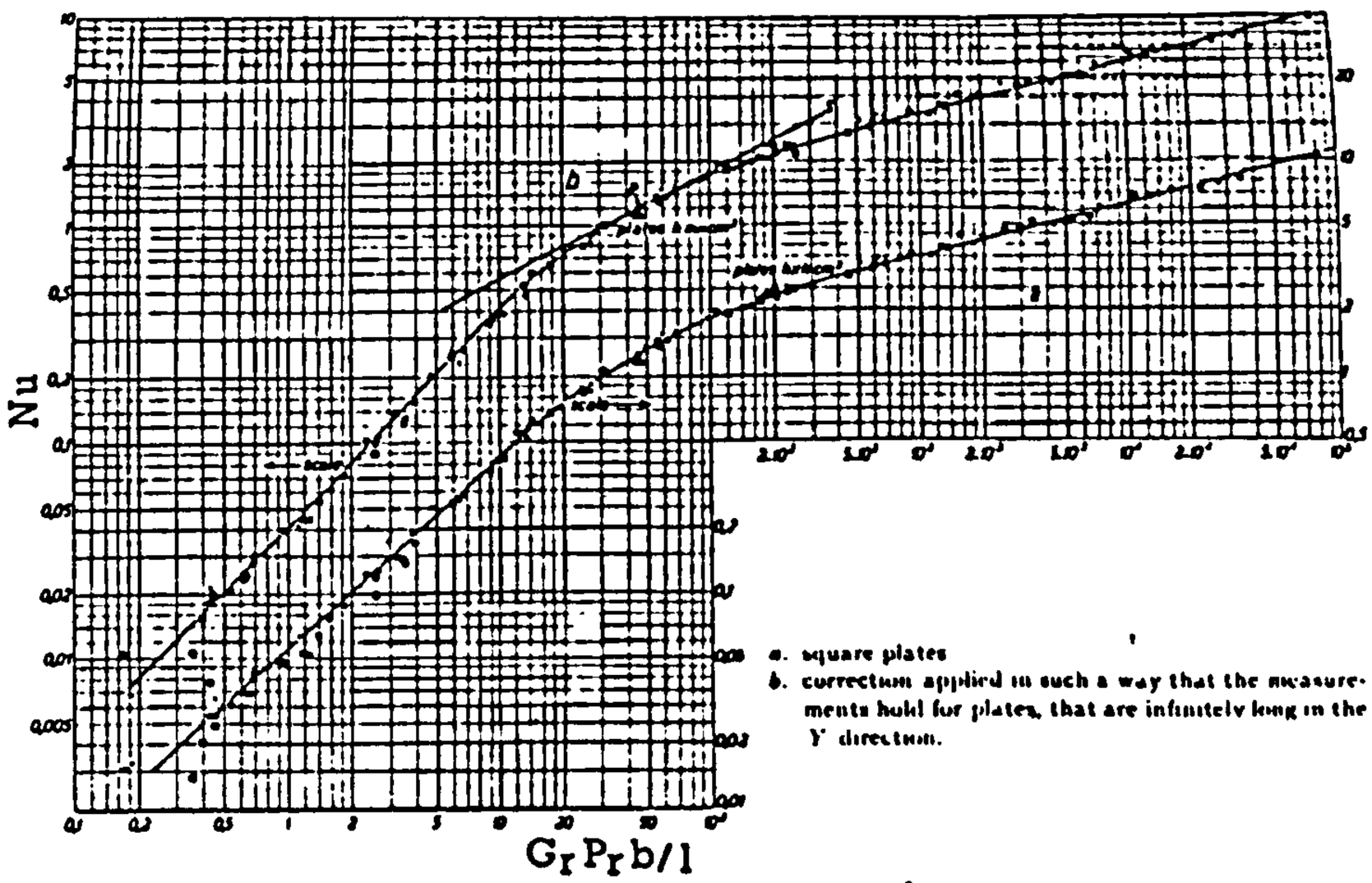

Figure 2.1 Results of Elenbaas (3)

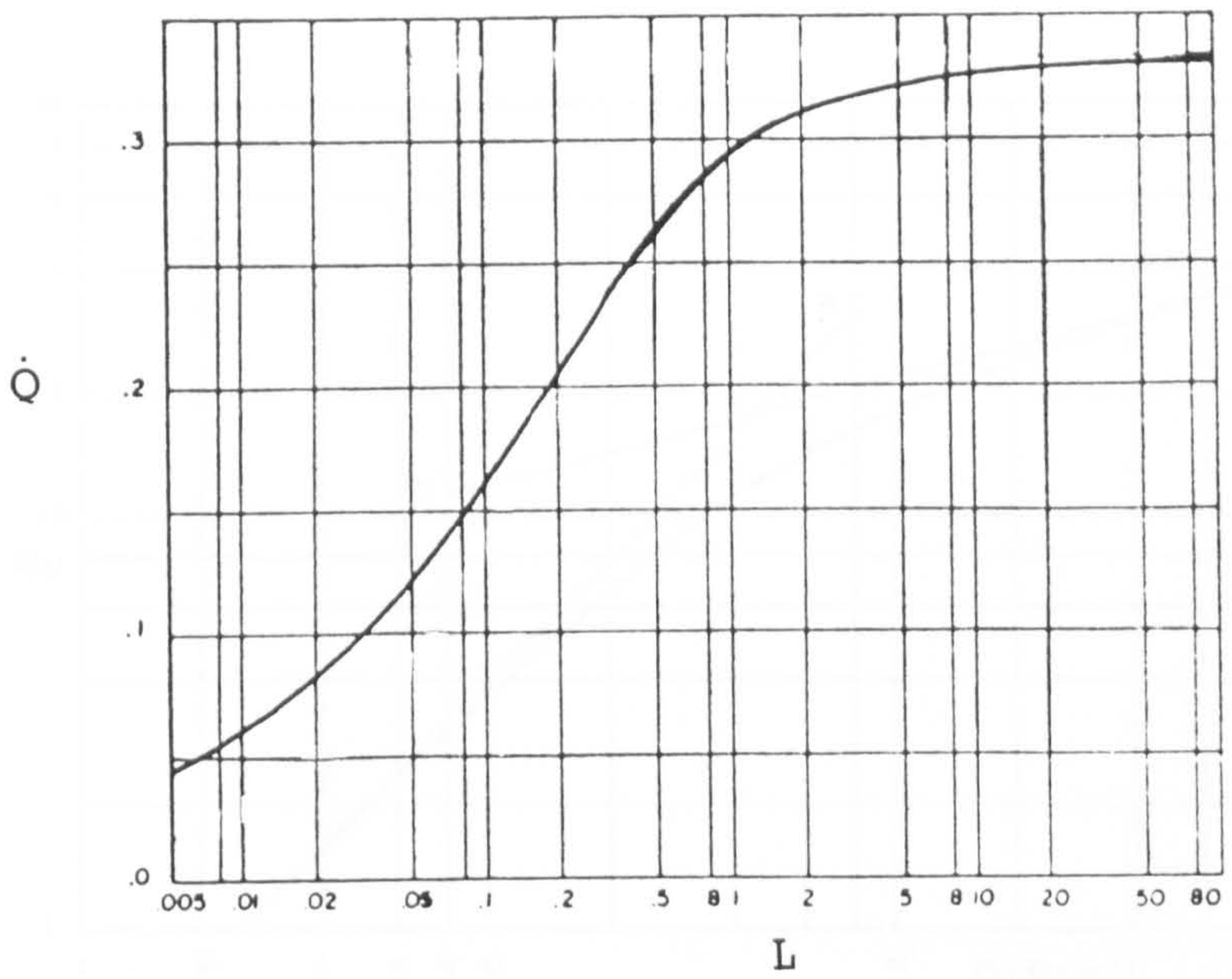

Figure 2.2 Dimensionless Flowrate Versus Dimensionless Channel Length.

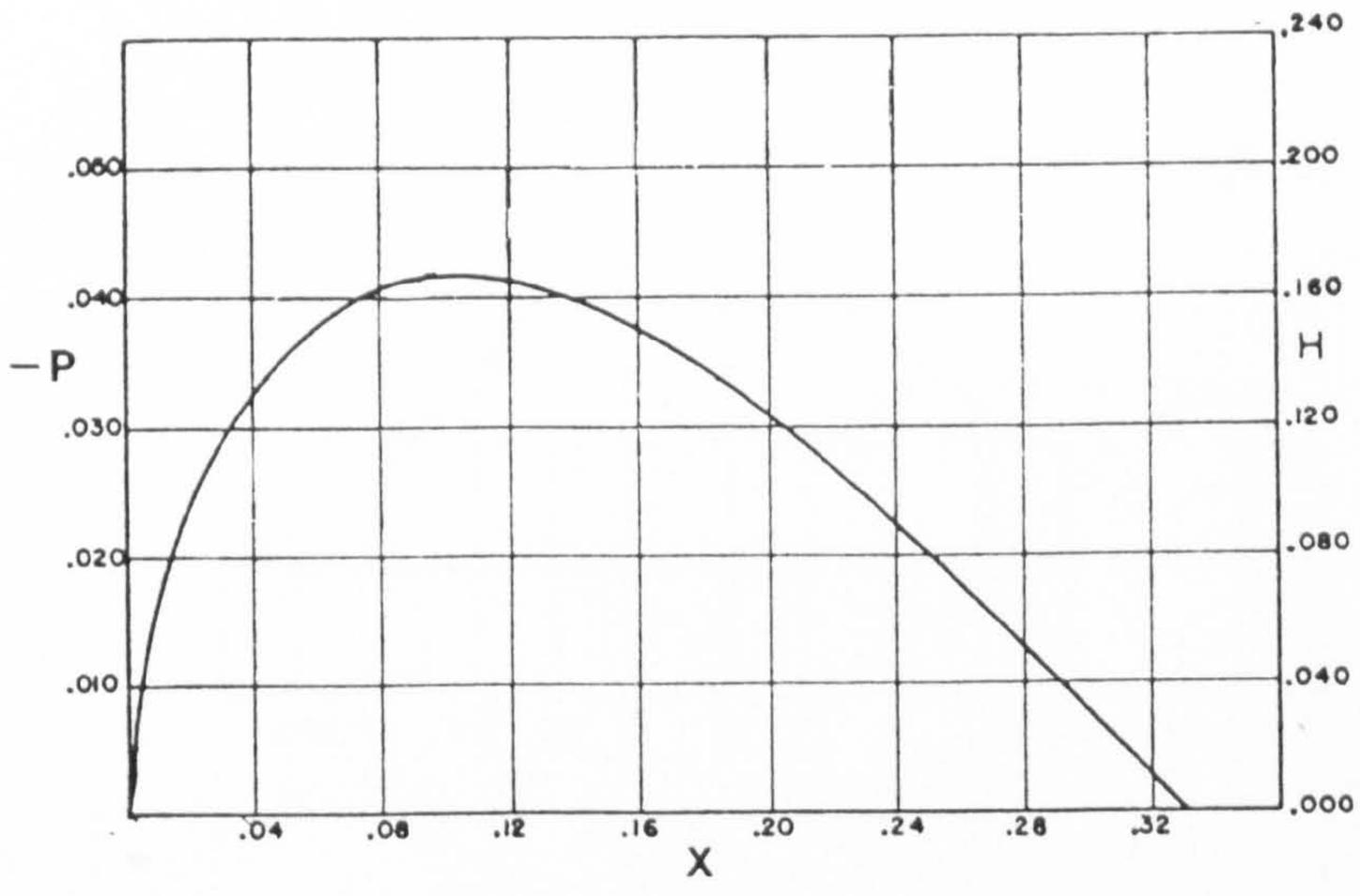

Figure 2.3 Variation of Pressure with Elevation in Channel with L = 0.333

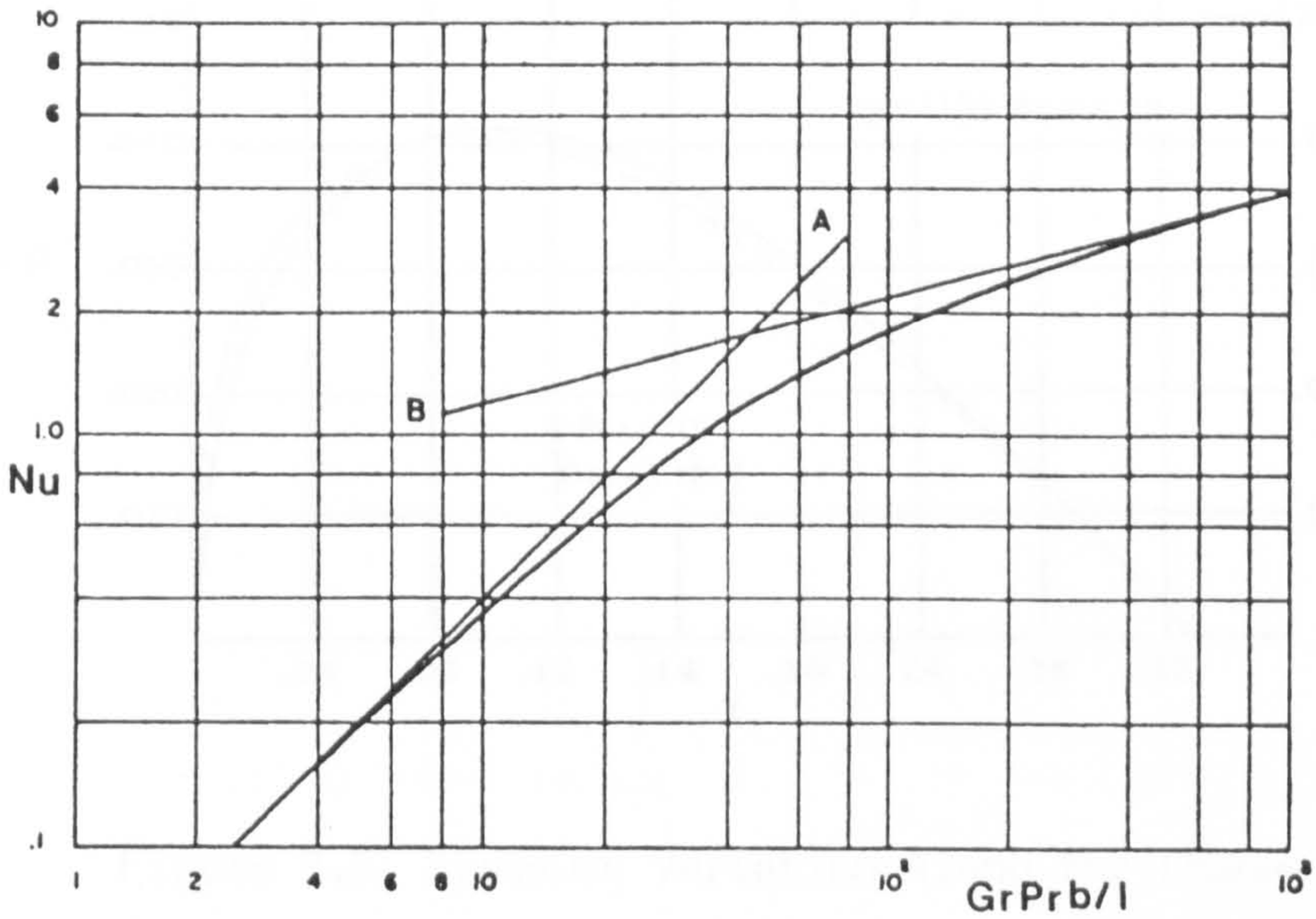

Line A denotes theoretical fully developed solution
Line B denotes theoretical solution for developing flow
Curve denotes correlated line

Figure 2.4 Theoretical Results of Bodoia and Osterle (13)

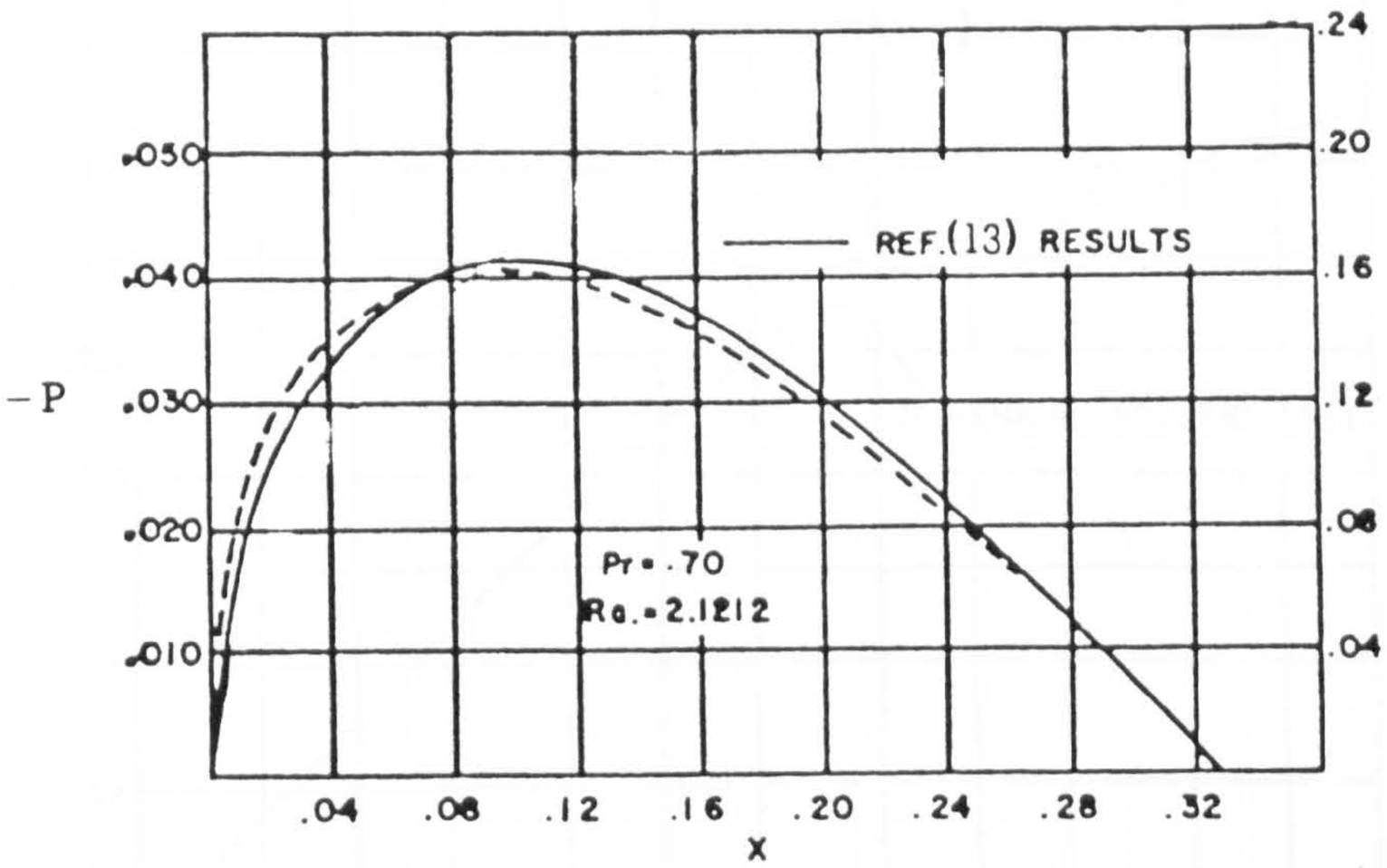

Figure 2.5 Pressure Variation Along the Channel

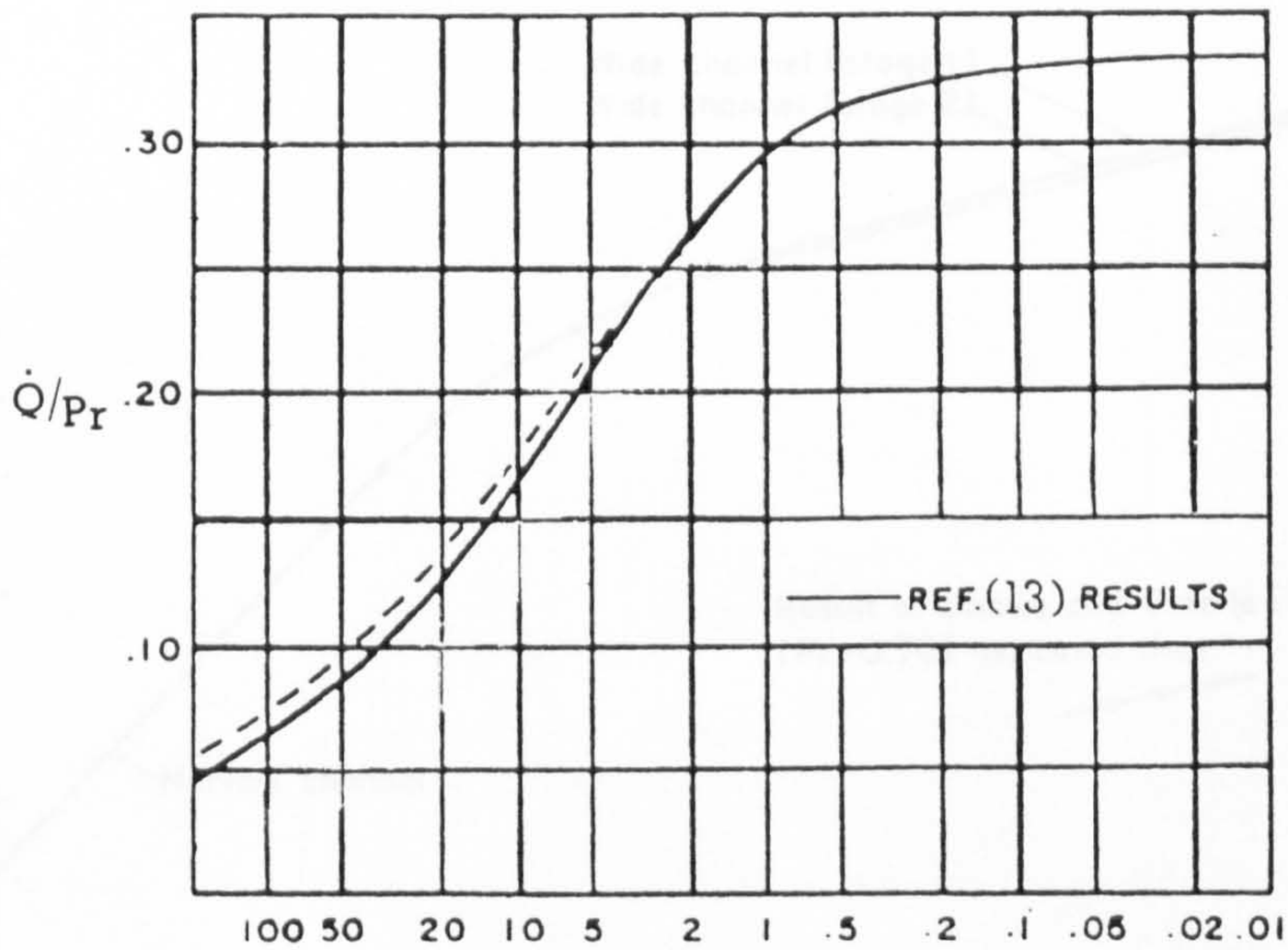

Figure 2.6 Dimensionless Flow Rate as a function of Dimensionless Channel Length.

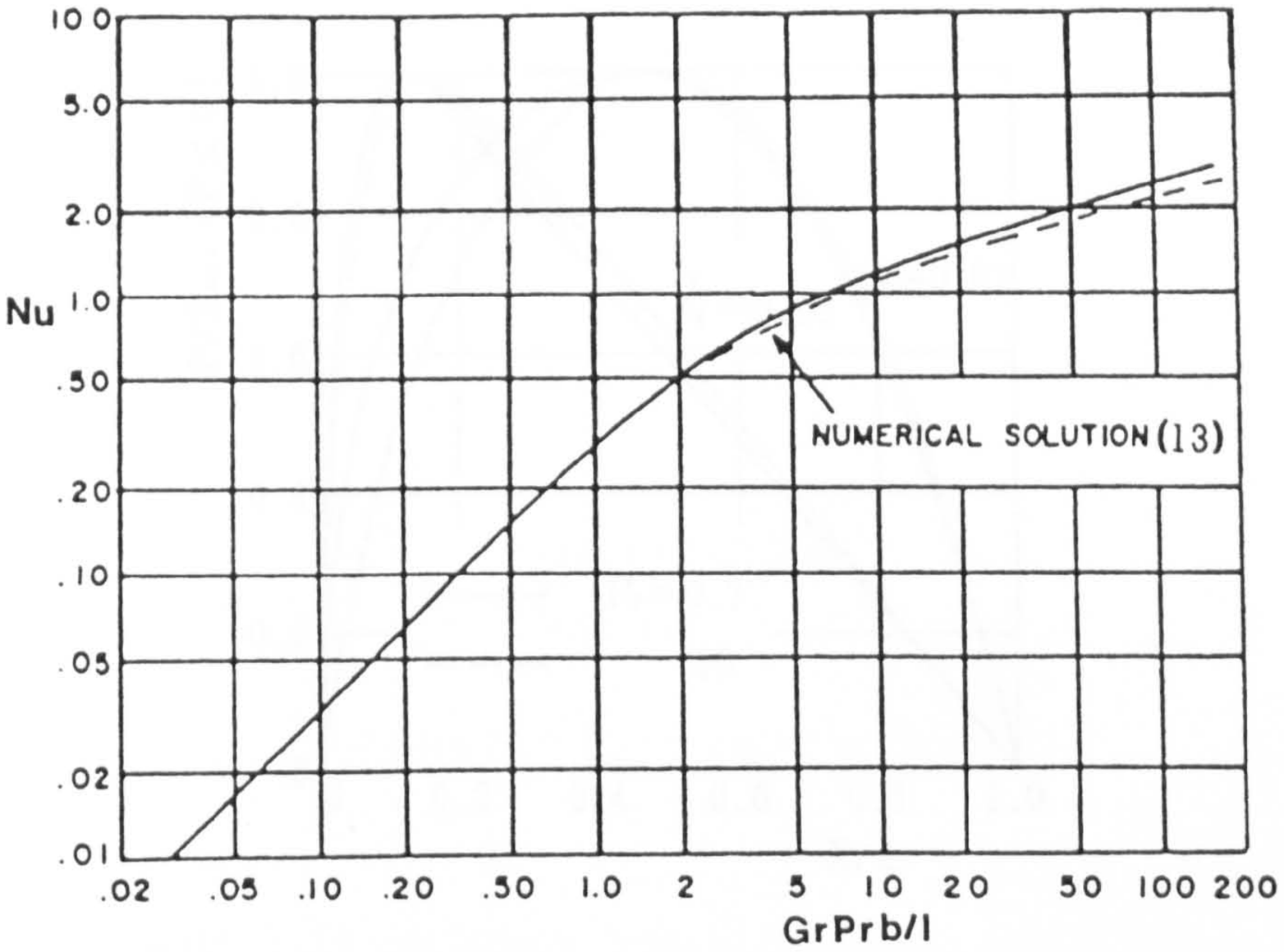

Figure 2.7 Theoretical Results of Engel and Mueller (16)

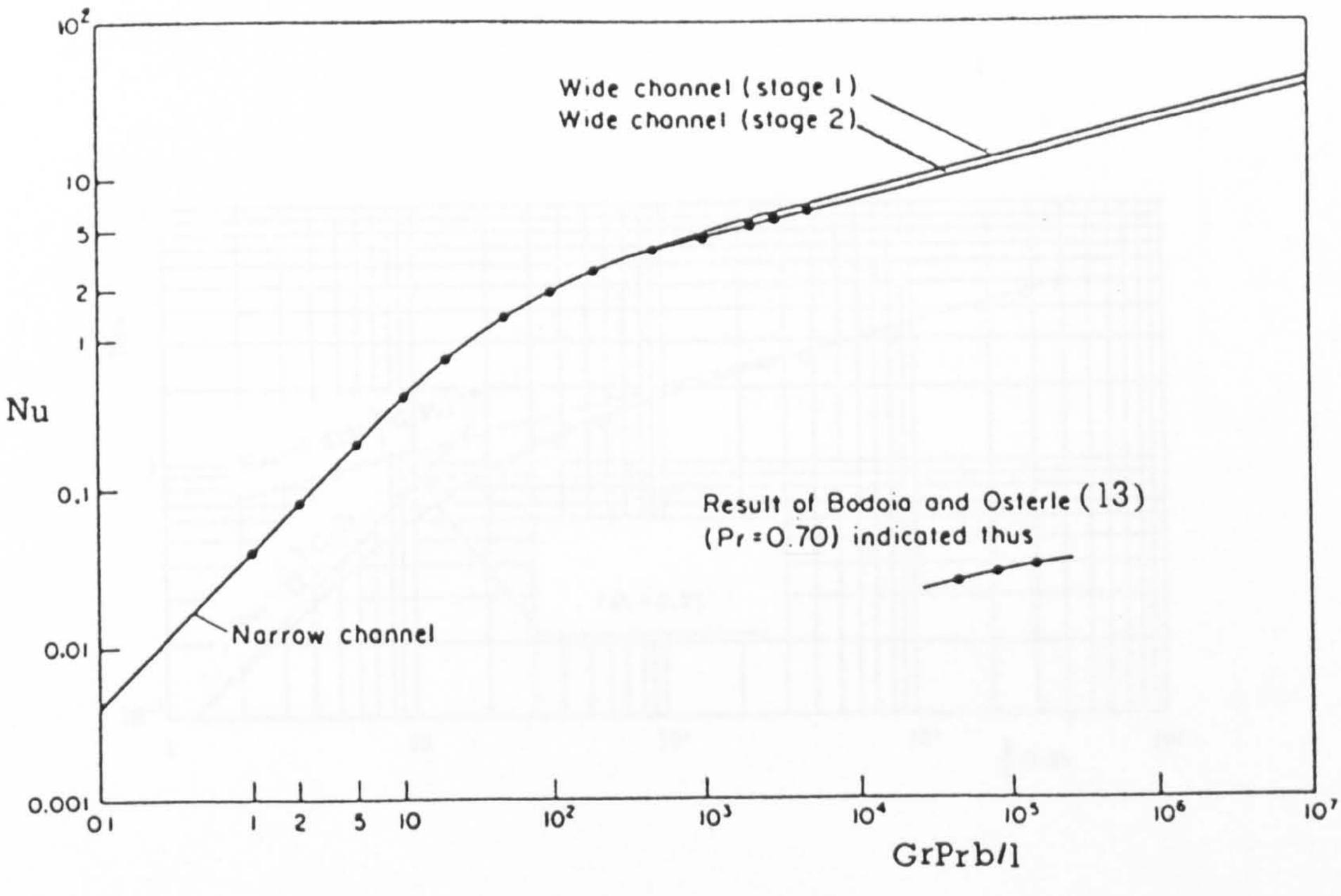

Figure 2.8 Theoretical Results of Ofi and Hetherington (25)

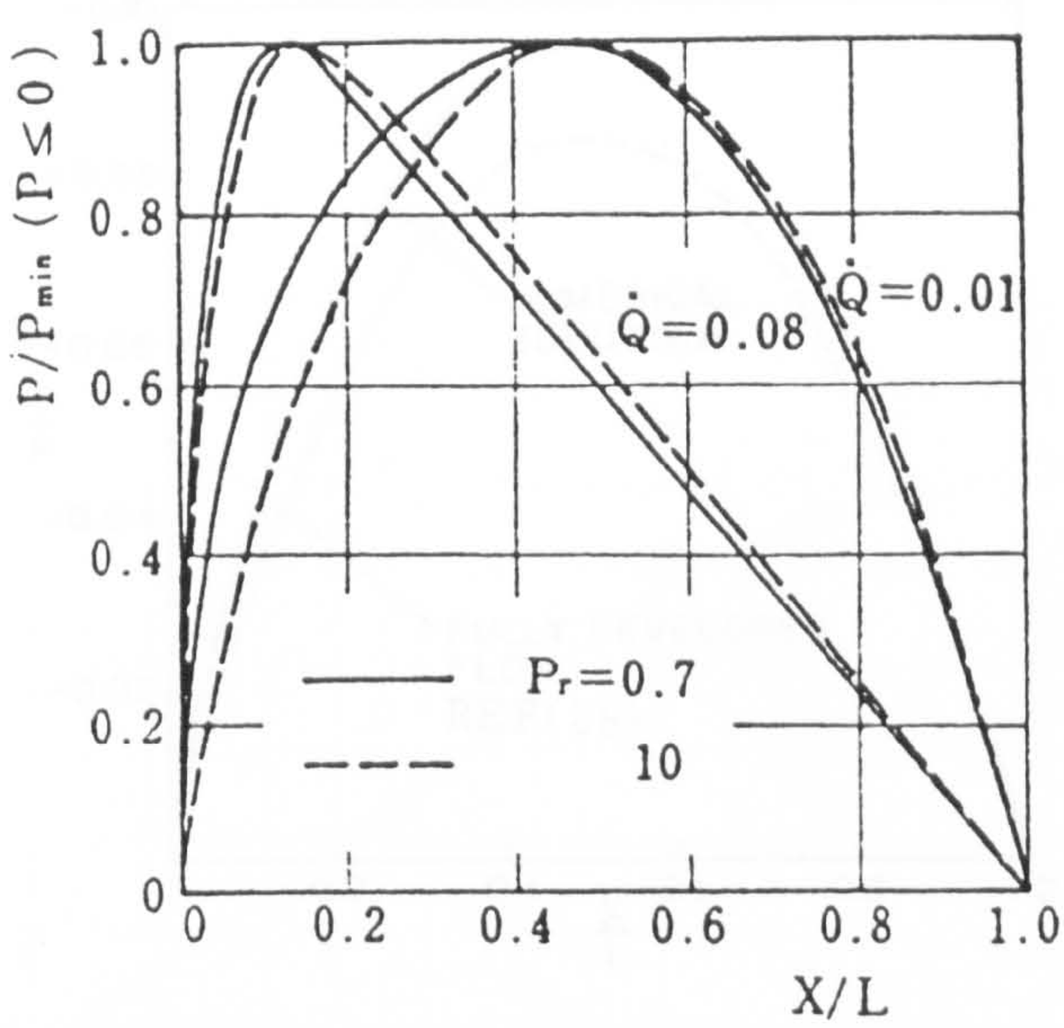

Figure 2.9 Pressure Variation Along the Channel

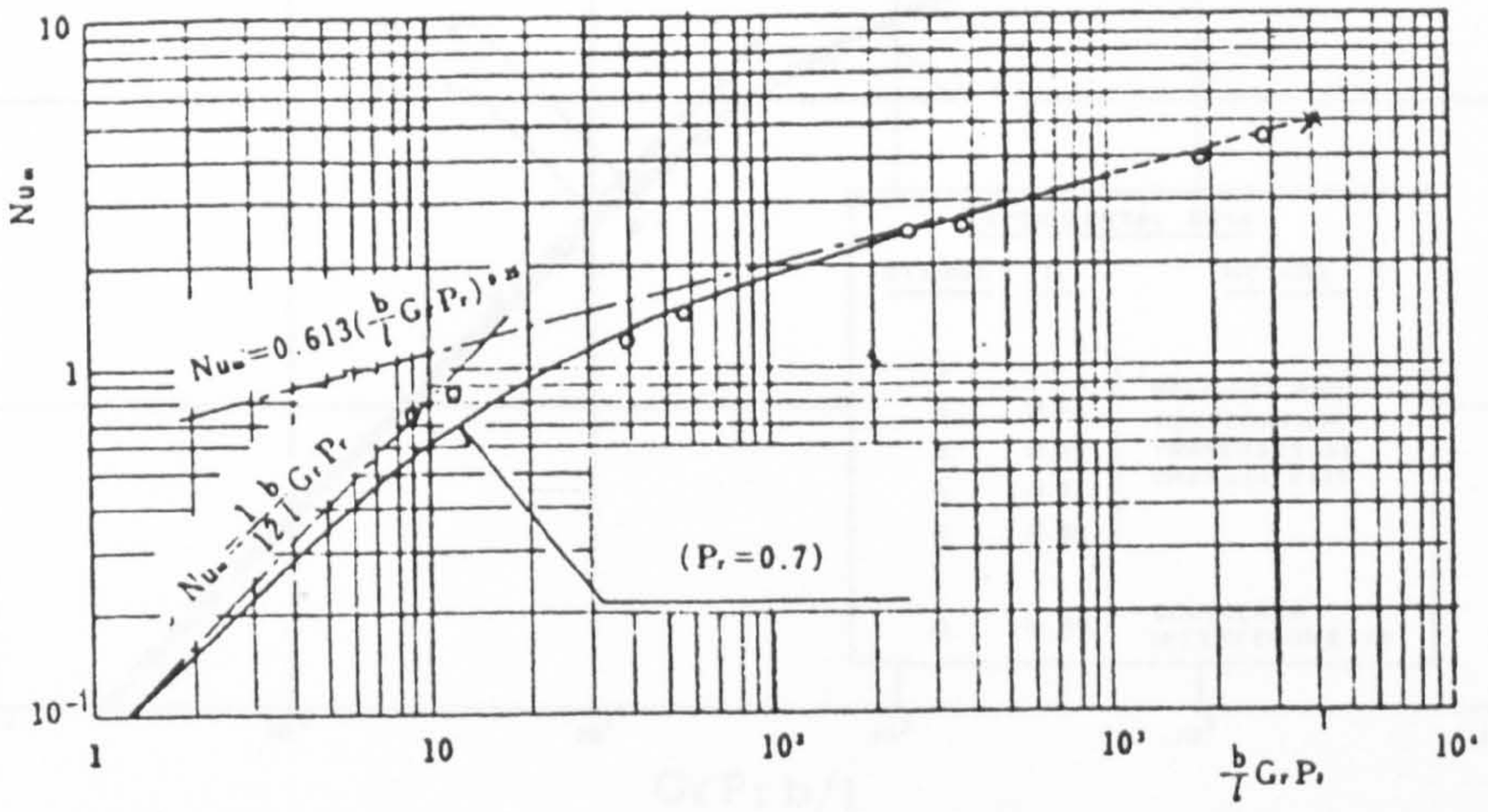

Figure 2.10 Theoretical Results of Miyatake and Fujii (26)

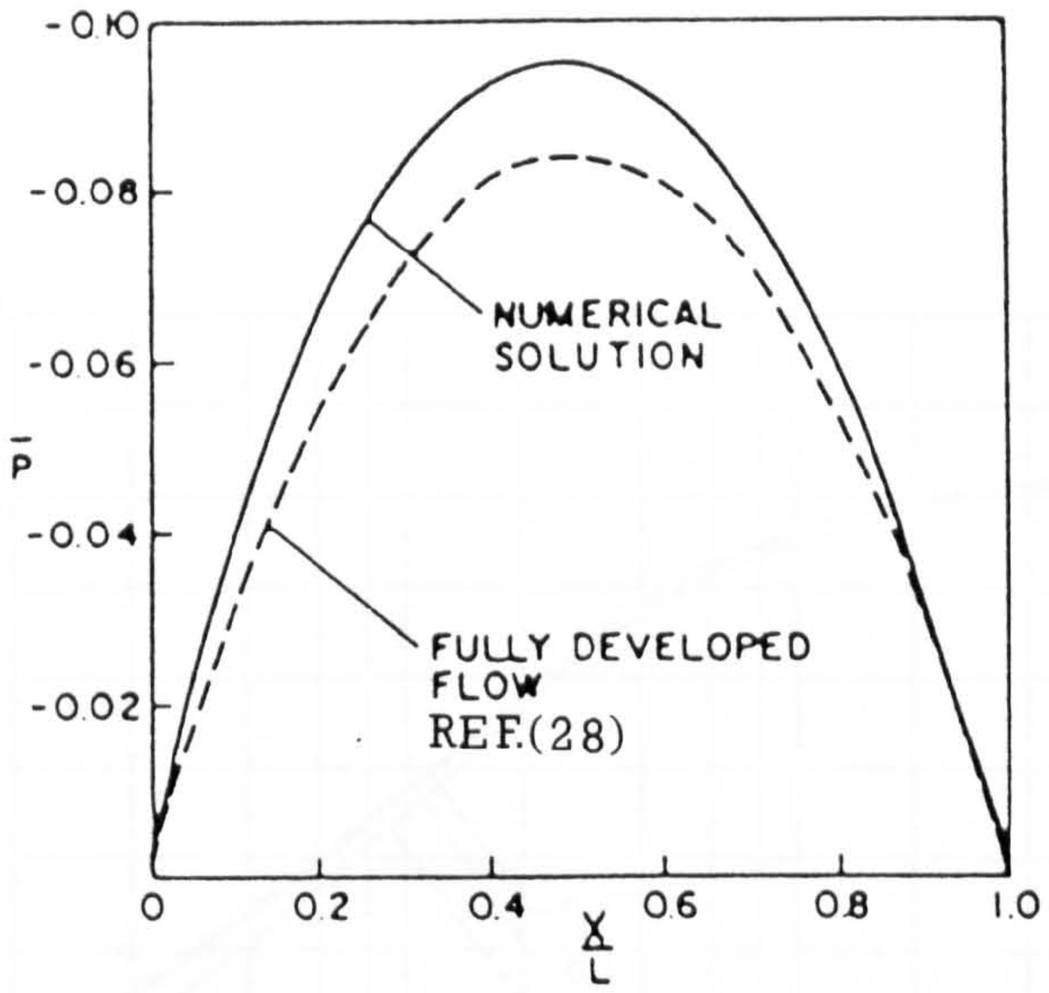

Figure 2.11 Pressure Variation Along the Channel

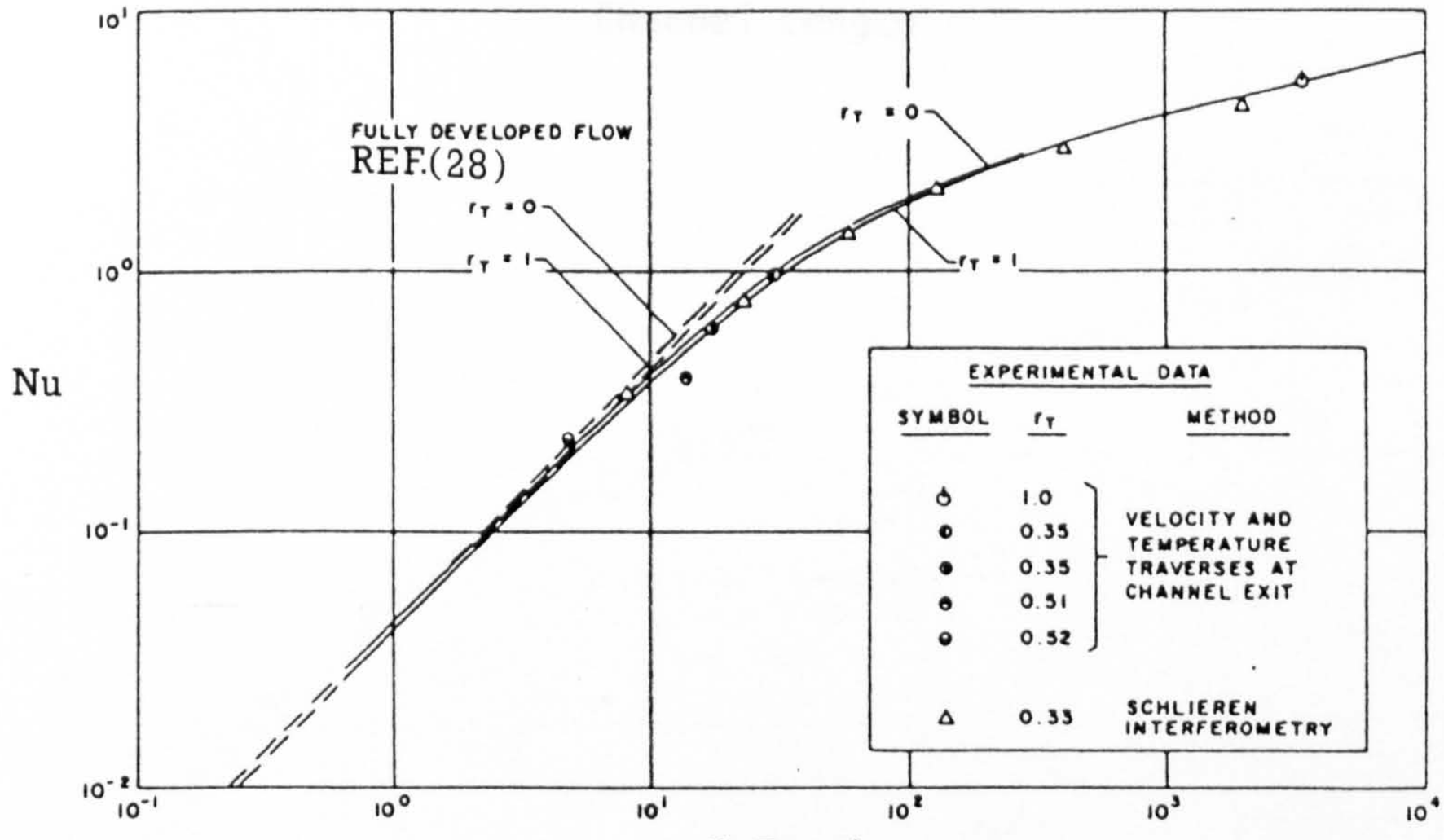

Figure 2.12 Results of Aung et al (29)

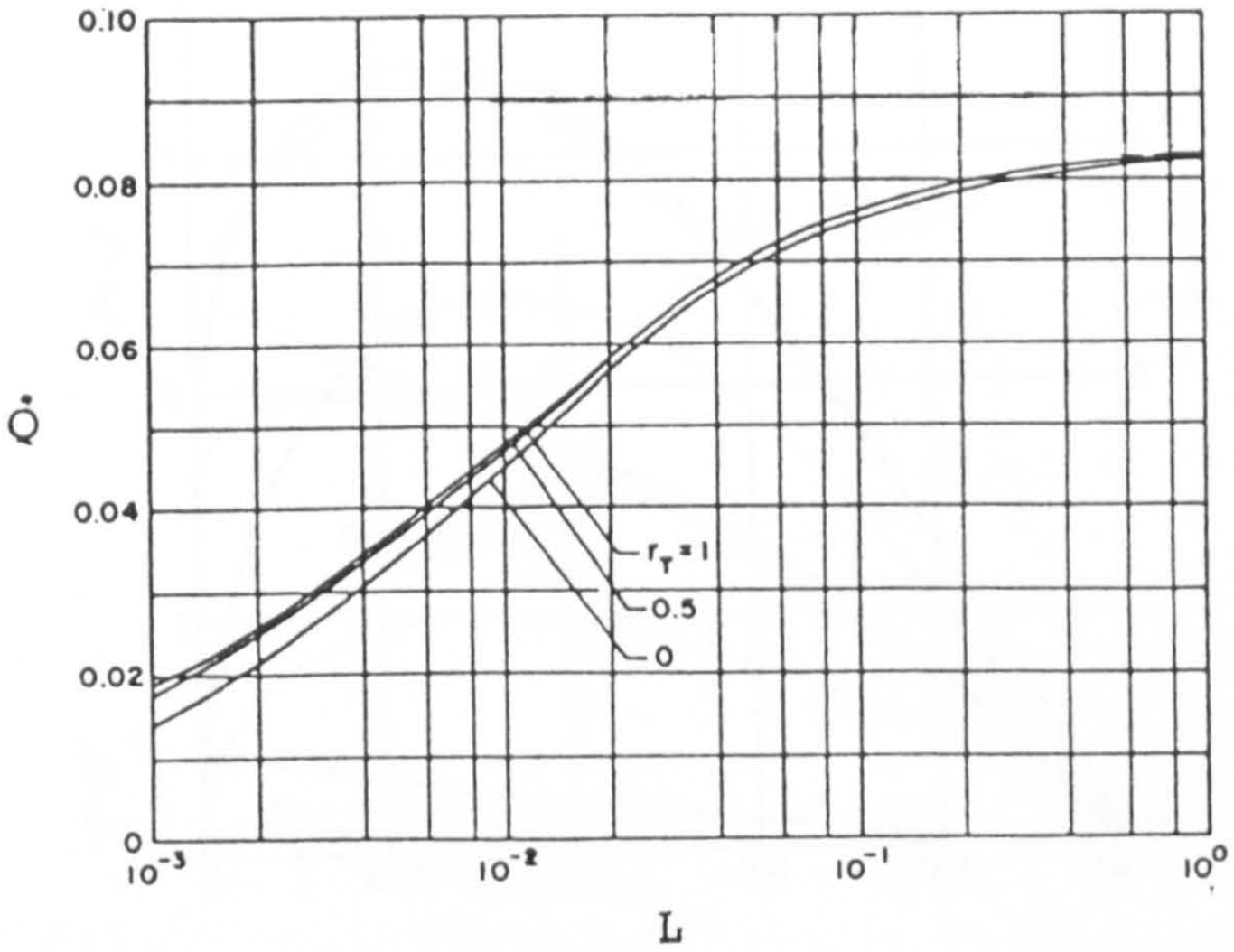

Figure 2.13 Relation Between Dimensionless Volume Flow Rate and Dimensionless Channel Length

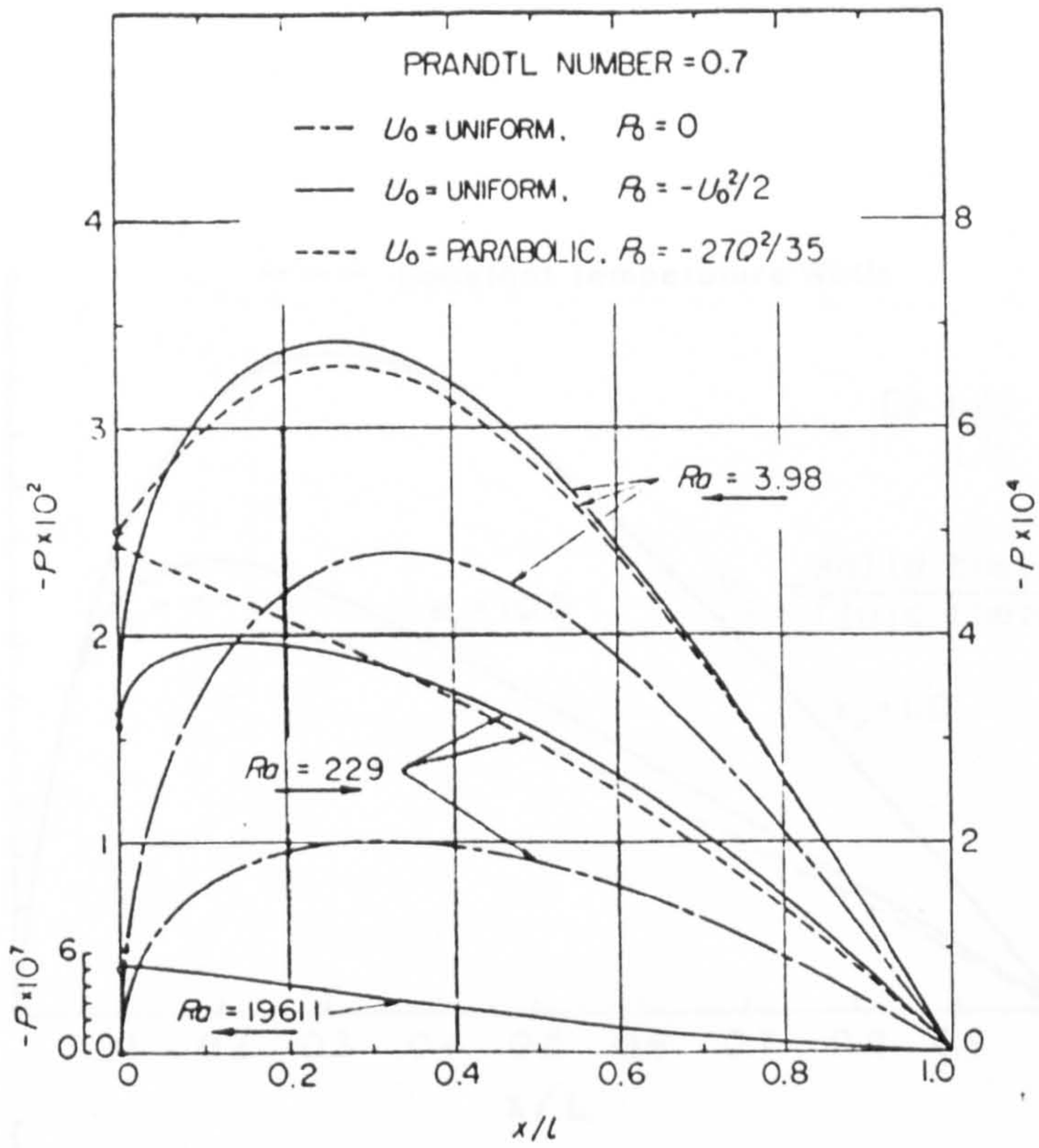

Figure 2.14 Variation of Pressure With Elevation in Channel

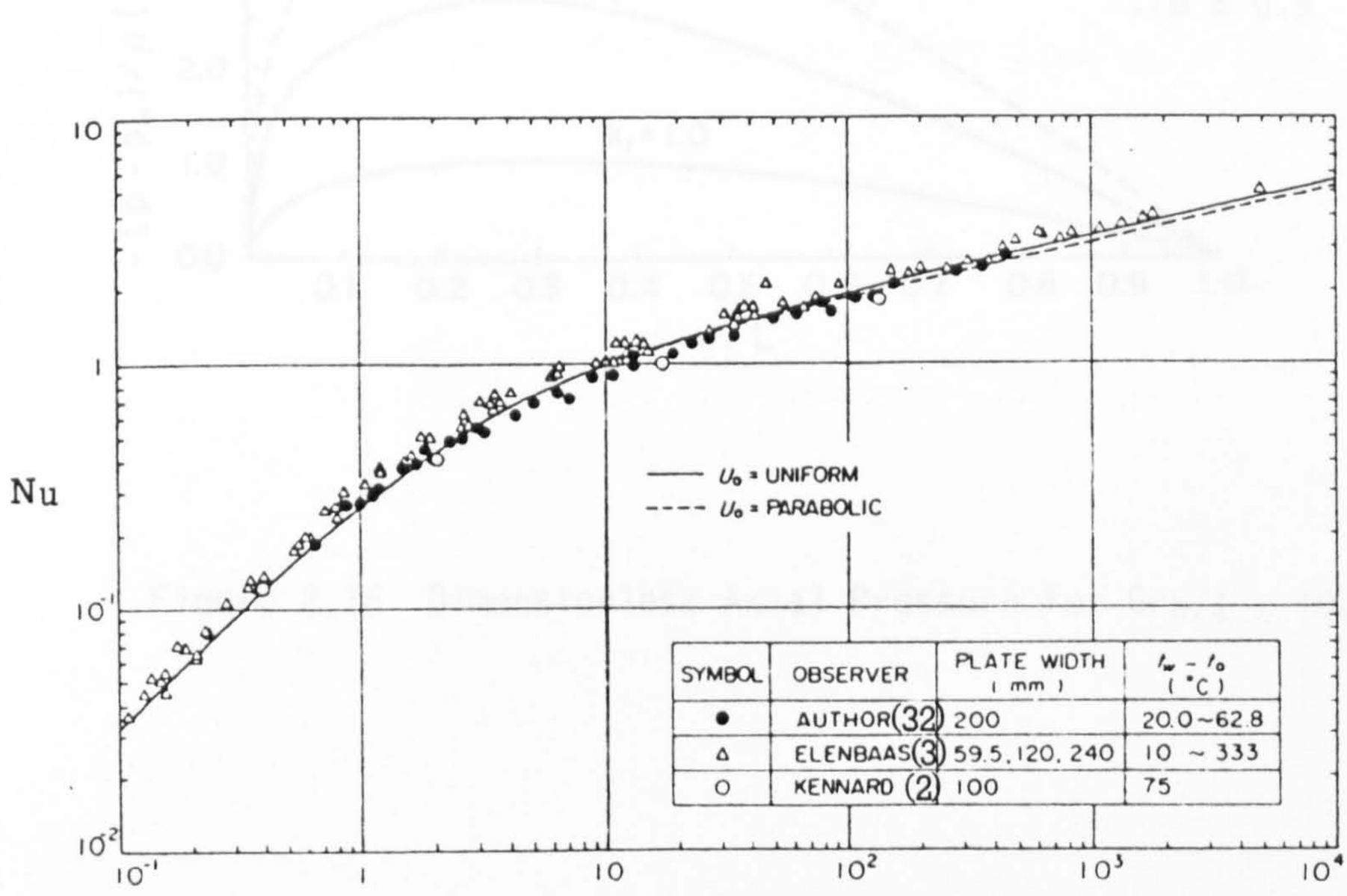

Figure 2.15 Theoretical Results of Aihara (32)

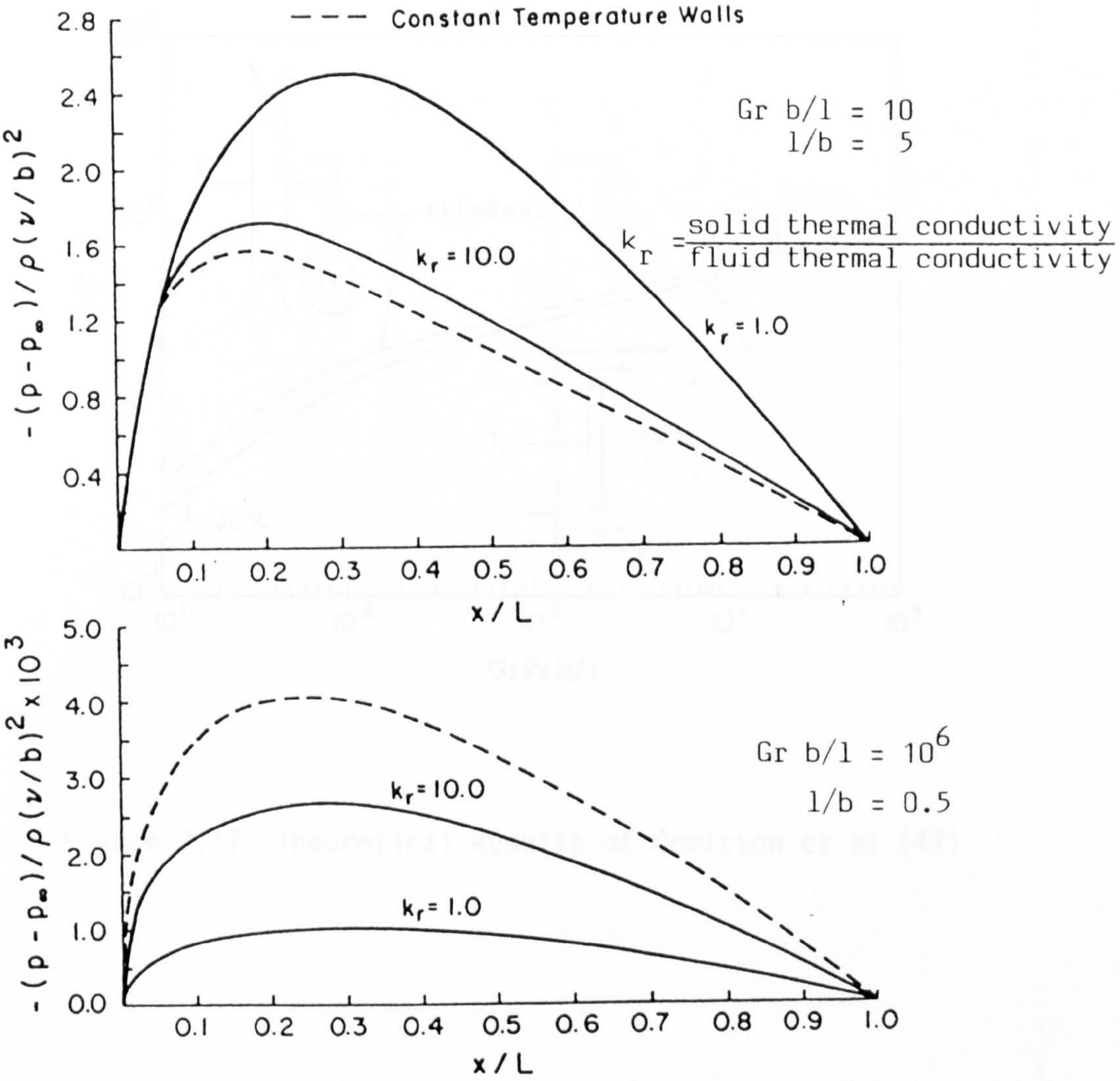

Figure 2.16 Dimensionless Axial Pressure for $Gr_b/l = 10, 10^6$

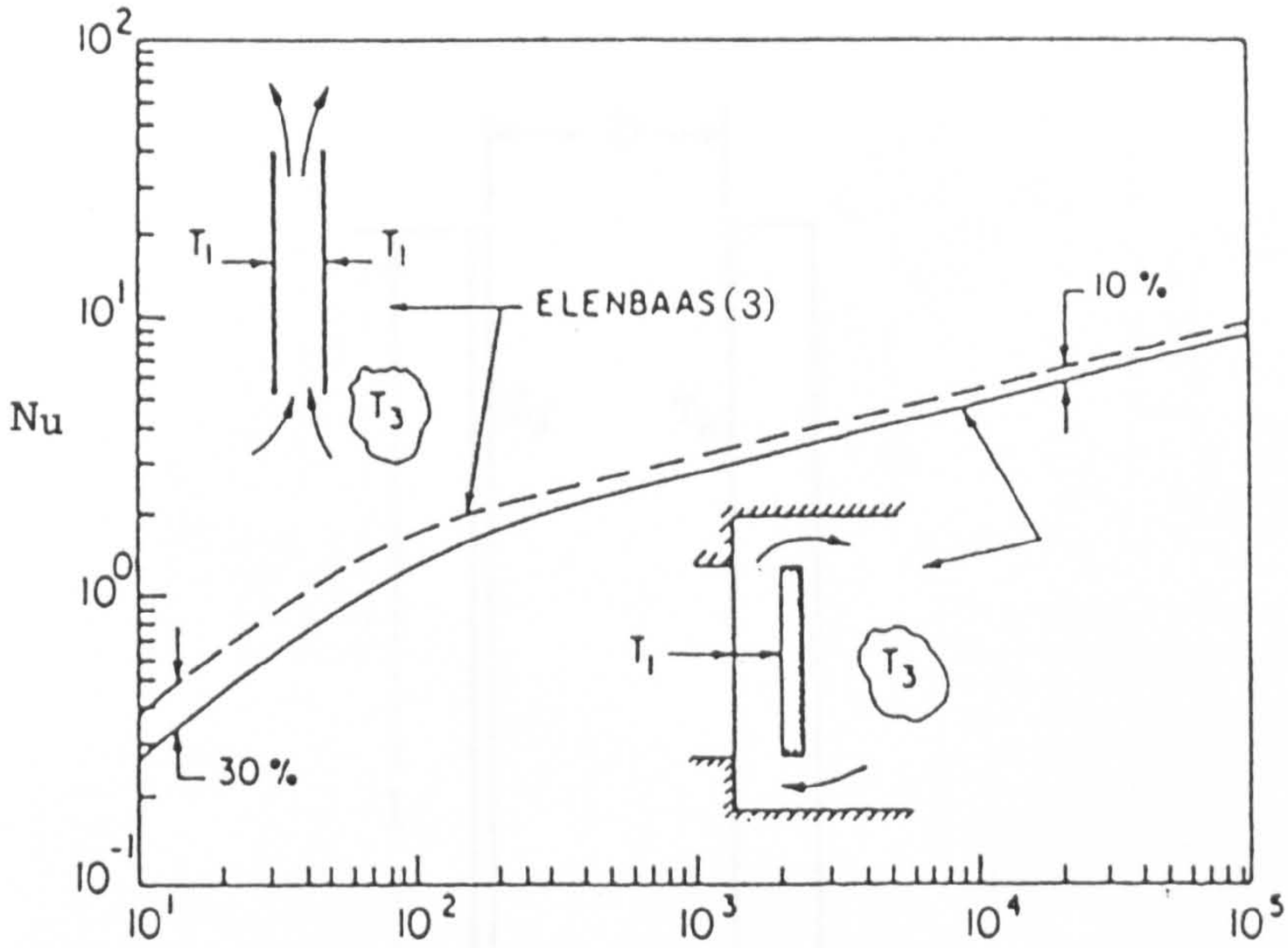

Figure 2.17 Theoretical Results of Ormiston et al (47)

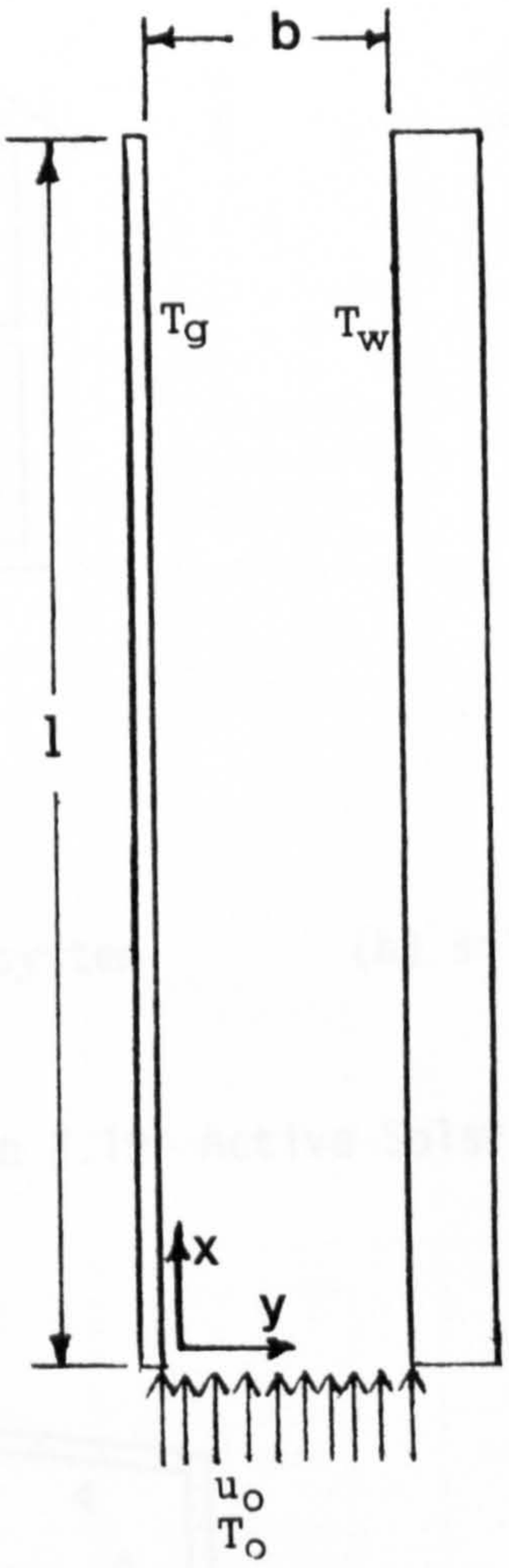

Figure 2.18 Analytical System and Coordinates

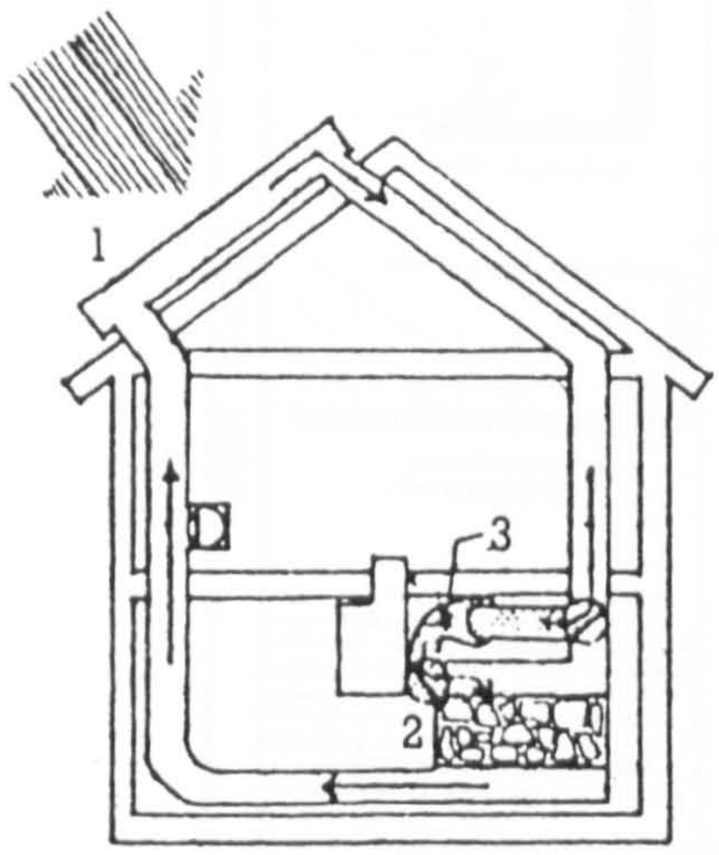

1 collector
2 rock store
3 fan

(a) solar air heating system

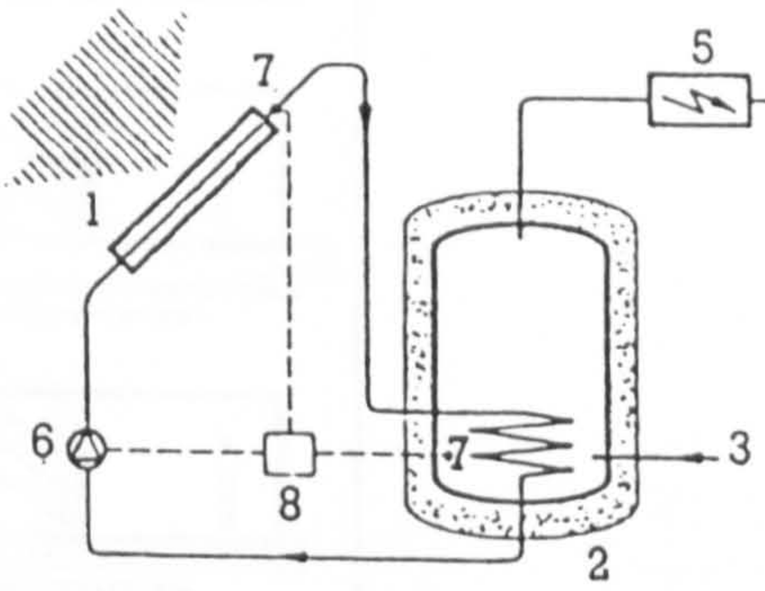

1 flat-plate collector
2 solar hot water store
3 cold water inlet
4 hot water outlet
5 auxiliary heating
6 circulating pump
7 temperature sensor
8 differential temperature controller

(b) solar water heating system

Figure 2.19 Active Solar Systems

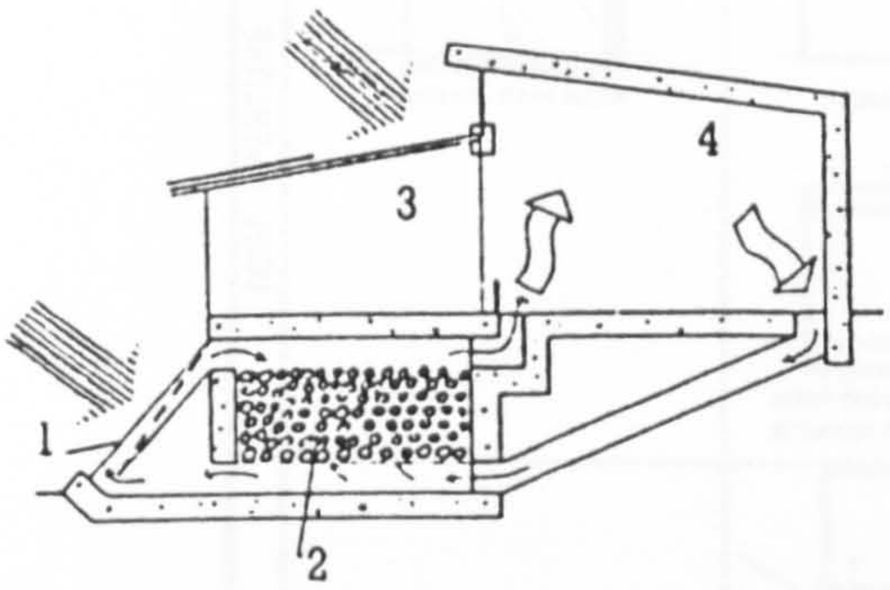

1 collector
2 rock store
3 & 4 living room

(a) solar air heating system

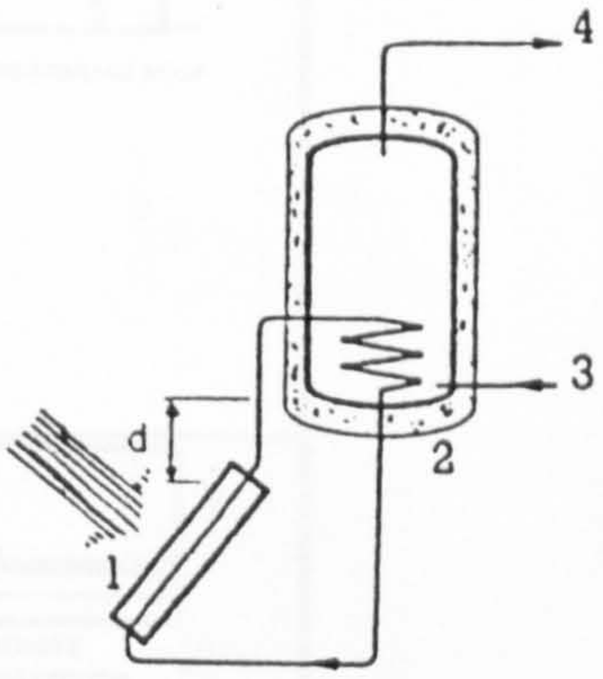

1 collector
2 solar hot water store
3 cold water inlet
4 hot water outlet

(b) solar water heating system

Figure 2.20 Passive Solar Systems

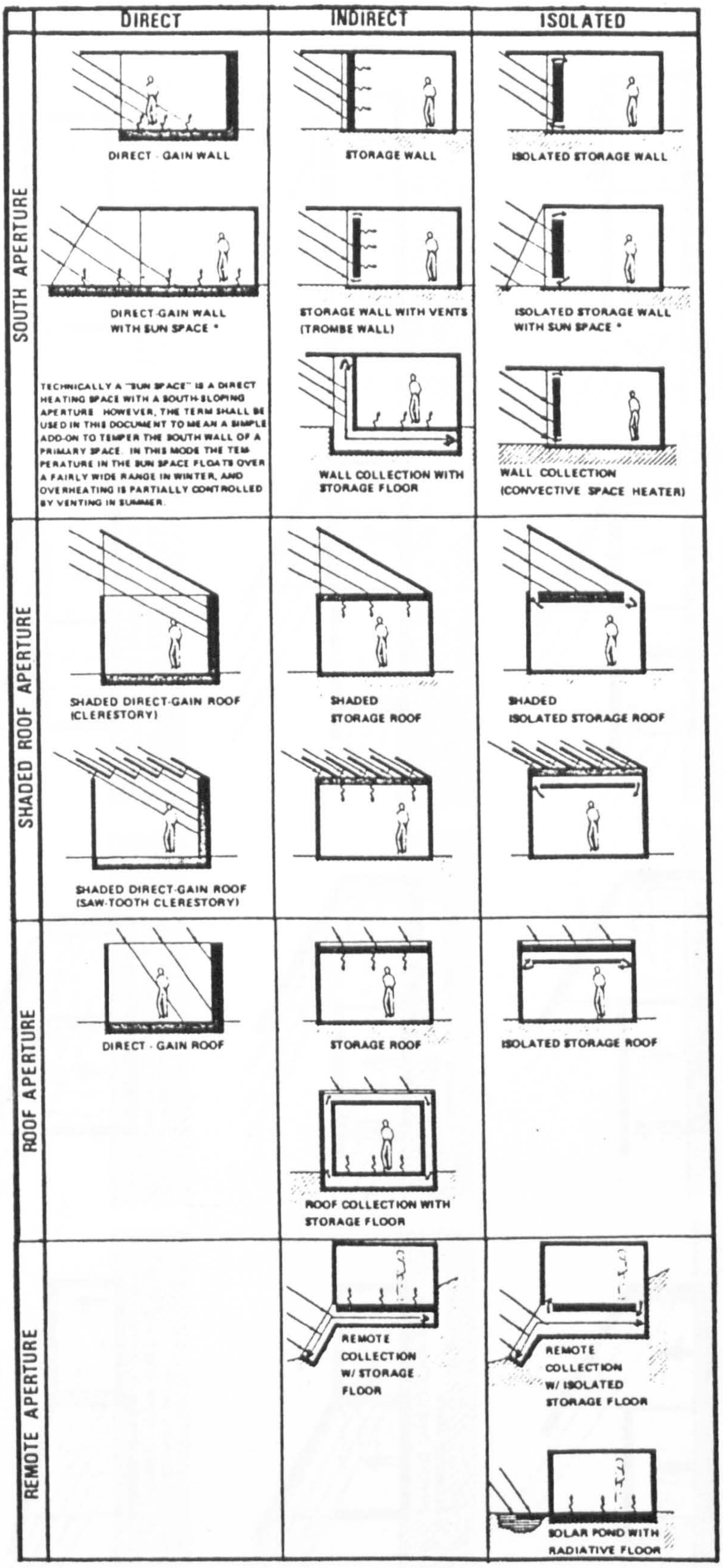

Figure 2.21 Examples of Passive Solar Heating Systems

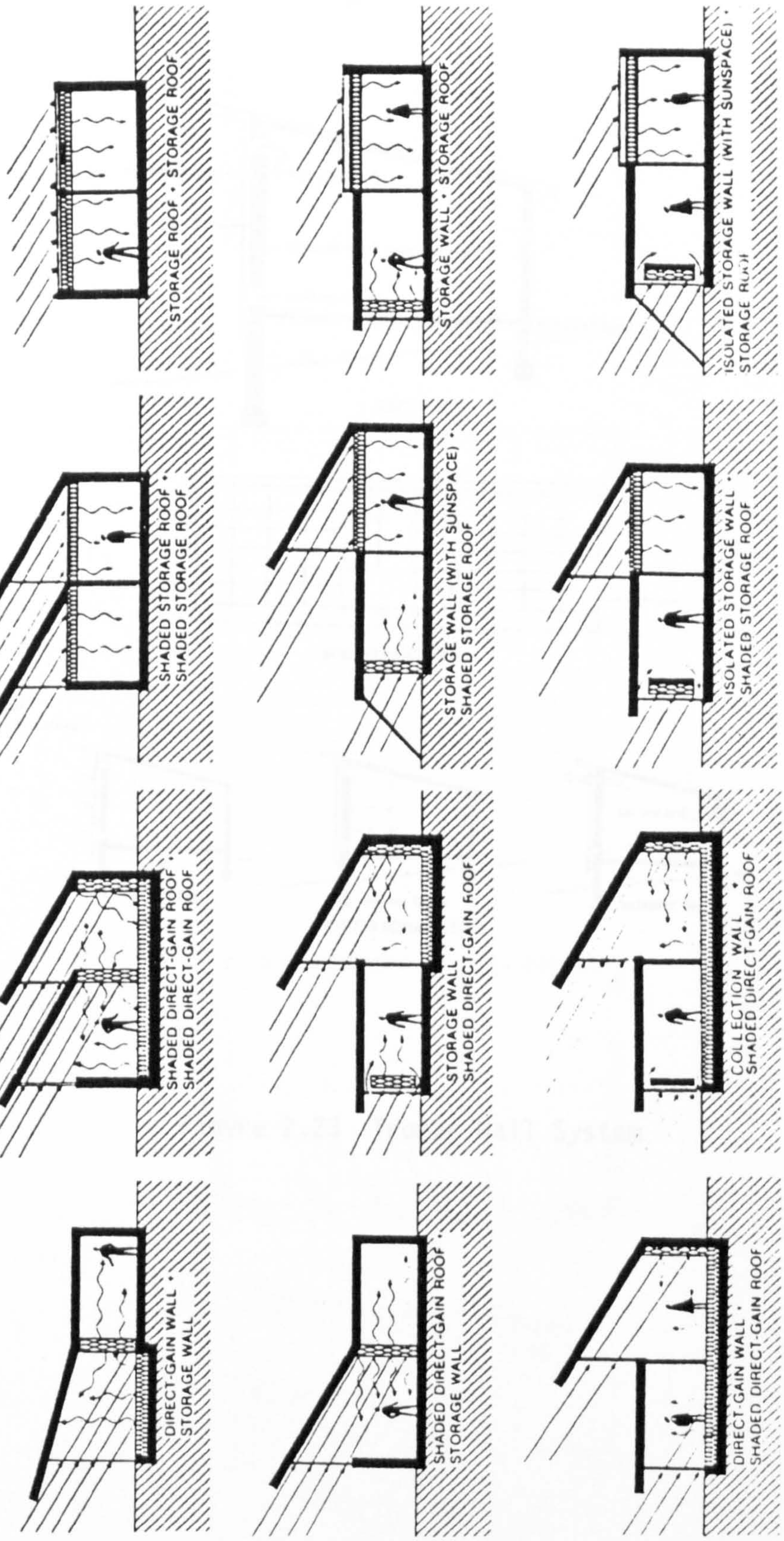

Figure 2.22 Examples of Single-story, Multi-zone, Passive Solar Systems

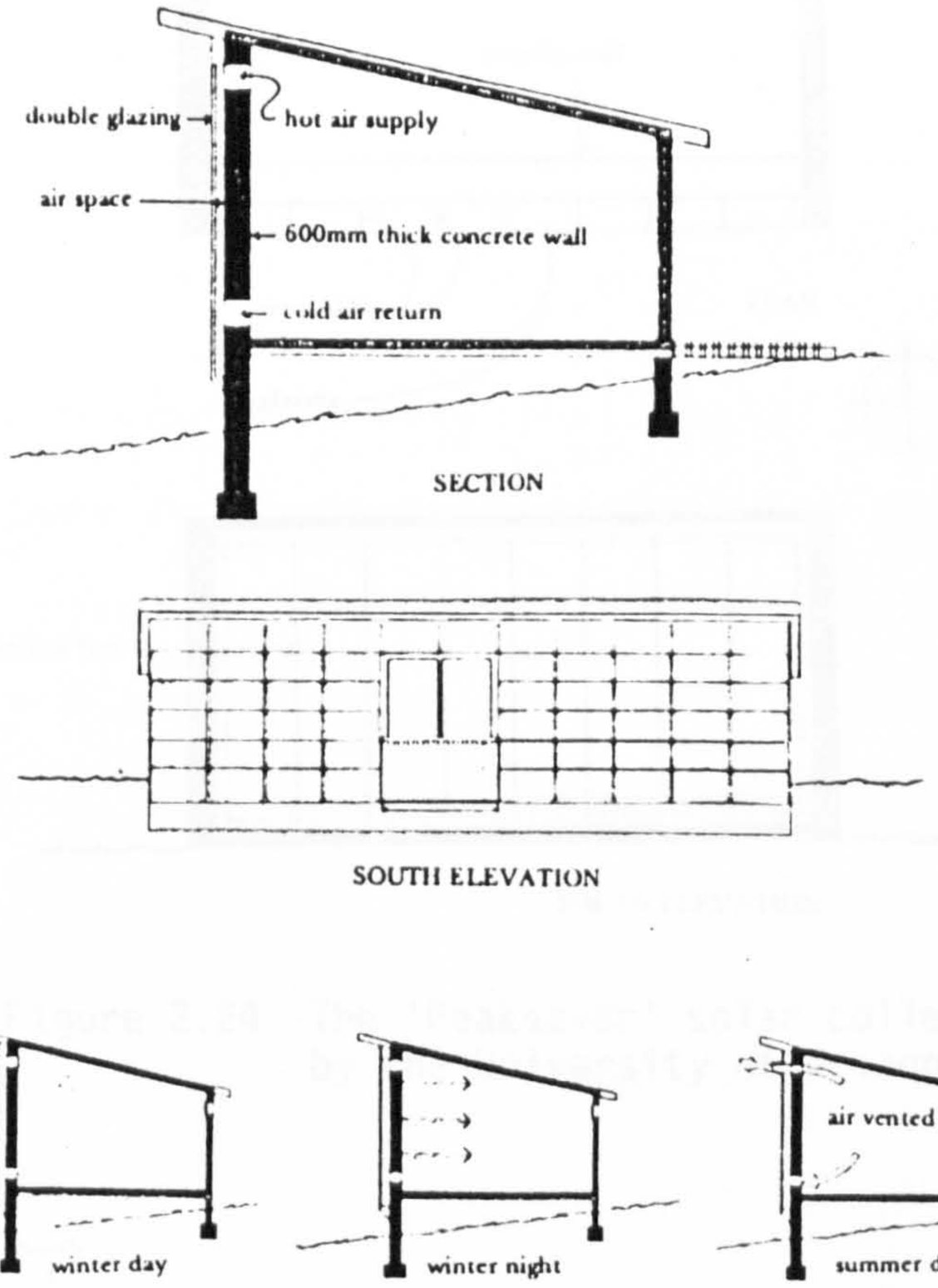

Figure 2.23 Trombe Wall System

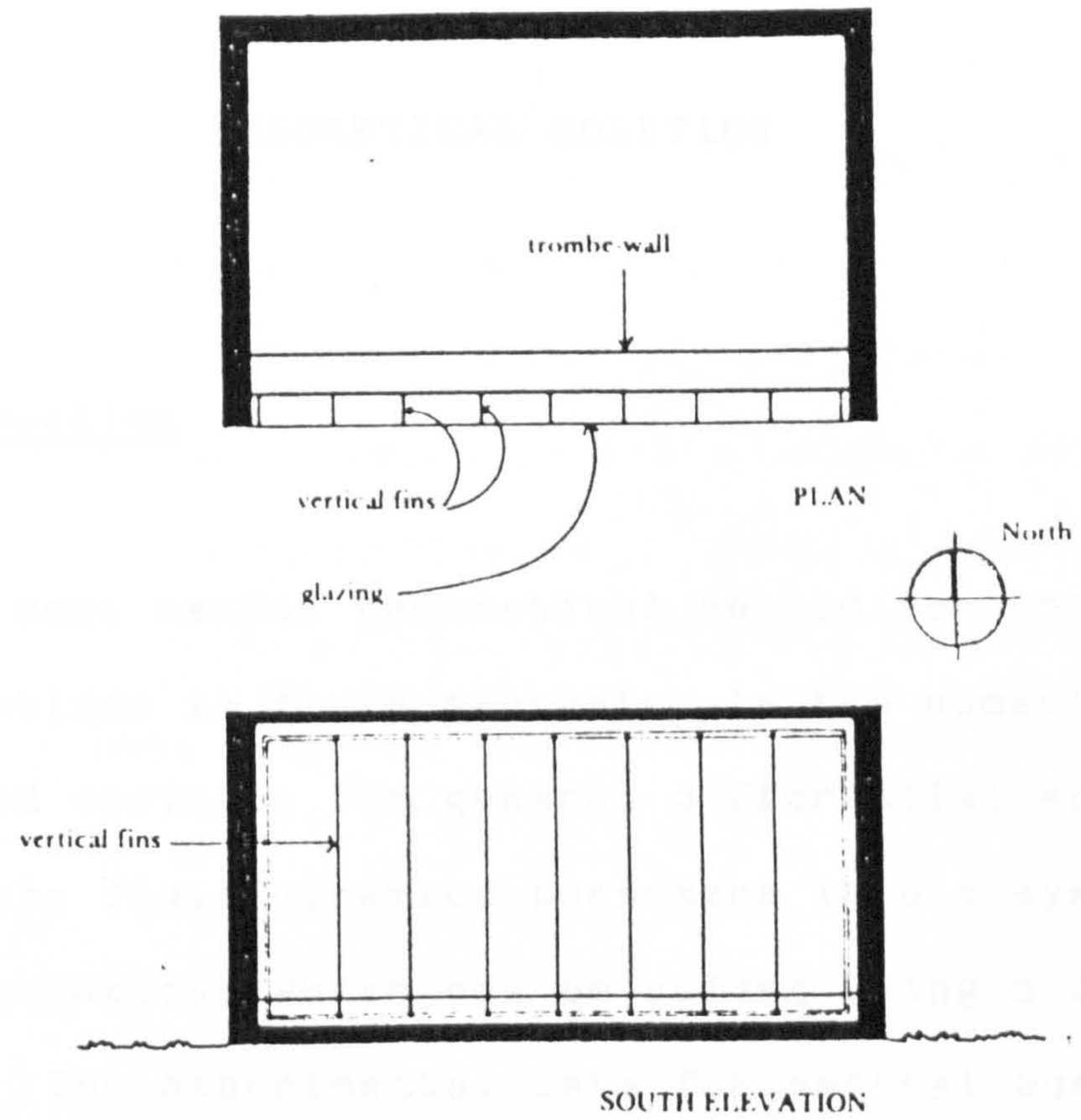

Figure 2.24 The 'Peaksaver' solar collector by the University of Arizona

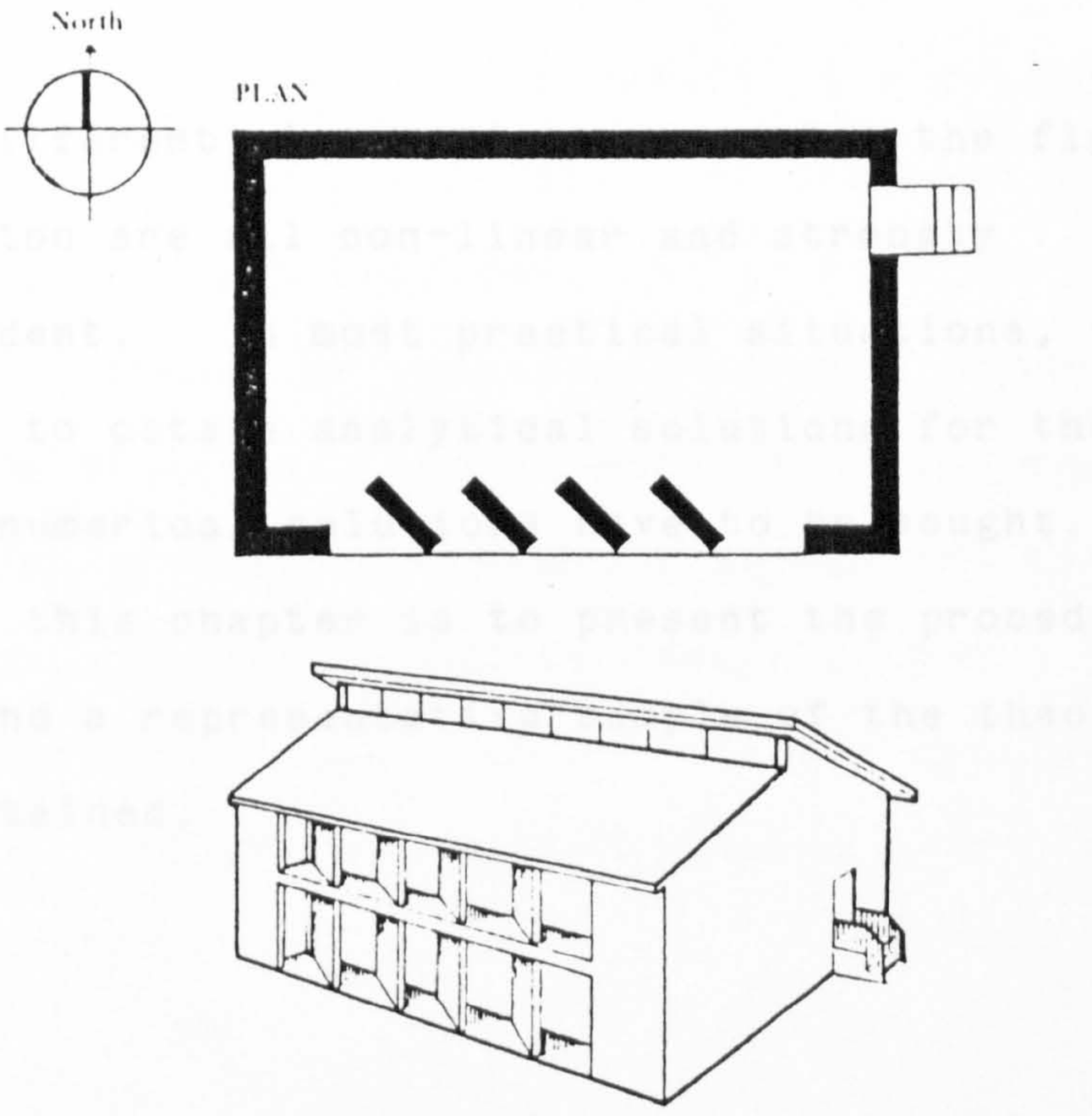

Figure 2.25 James Bier's house in Virginia, USA

CHAPTER 3

THEORETICAL SOLUTION

3.1 Introduction

The most useful theoretical method for solving complex problems in fluid mechanics is the numerical method. This method converts the general differential equations governing the fluid-dynamics phenomena into a system of algebraic equations which can be solved using a digital computer. The experimental data for natural convection flow in a vertical parallel channel obtained in the present study can be compared with results obtained using a suitable numerical method.

The differential equations governing the flow under consideration are all non-linear and strongly interdependent. In most practical situations, it is impossible to obtain analytical solutions for them and therefore numerical solutions have to be sought. The purpose of this chapter is to present the procedure employed and a representative sample of the theoretical results obtained.

This chapter is composed of four sections in which the theoretical solution is detailed. Section 3.2 describes briefly the background of the PHOENICS code. Section 3.3 describes in some detail some of the operating procedures of the PHOENICS code for the present problem since a correct formulation of the problem is an essential part of the elliptical solution. Finally Section 3.4 presents a selection of the velocity and temperature profiles and heat transfer correlations obtained.

3.2 PHOENICS

The governing equations were solved by means of the PHOENICS code developed by Spalding (61, 62). The name PHOENICS is an acronym: it stands for Parabolic, Hyperbolic or Elliptic Numerical-Integration Code Series CHAM (63), Rosten and Spalding (64). PHOENICS is a general purpose computer program for the solution of problems in single or two-phase flow, heat transfer, and in chemical reaction processes. Steady or unsteady phenomena in one, two or three space dimensions can be handled. The equations for conservation of matter, momentum, energy and chemical species are solved by a finite-domain method. The solution method is described by Patankar and Spalding (65), Rosten et al (66). Appendix A gives a brief introduction to the PHOENICS code.

The solution procedure consists of the following major steps:

(a) The flow domain is divided into many discrete regions by constructing a finite-difference grid which generates 'control volumes' for each variable.

(b) The transformation of the partial-differential equations into algebraic ones (finite-domain equations) for each variable at each cell. This is accomplished by intregrating the differential equations over the control volumes using appropriate assumptions for the variation of the variables between grid nodes.

(c) The solution of the resulting set of algebraic equations by means of an appropriate algorithm.

(d) The solution obtained using finite-domain solution of differential equations depends on the number of grid nodes employed. However, a 'grid-independent' solution may be obtained provided that this number is large enough. The only way to determine how large this number needs to be is to perform the calculation several times using increasing numbers of grid nodes until the solution is not appreciably affected by further increases. This practice is necessary to

obtain an accurate solution and therefore, has been adopted in this work.

Over six hundred flow-simulation problems are provided in the PHOENICS Library as input files (CHAM (67)). The files are available for direct access to PHOENICS users. Some of the cases call for special GROUND files, the listings of which are provided in a separate document entitled "special GROUND's and SATLIT for PHOENICS Input Library" Edwards and Rosten (68). Some of the examples which PHOENICS can simulate includes the aerodynamic drag of a road vehicle, heat conduction phenomena in foundations and in structures, two-phase flow problems and heat exchanger design. The example available in the PHOENICS Input Library closest to the present problem is that of laminar natural convection in an enclosed cavity (case 251) CHAM (67), Markatos and Pericleous (69). Markatos and Pericleous (70) extended this case to laminar and turbulent natural convection in an enclosed cavity.

3.2.1 Components of PHOENICS

PHOENICS comprises two distinct computer programs. The smaller one is called "satellite", and the larger one called "EARTH". More details are given in Appendix A. EARTH is always the same; but satellites differ from one

problem to another, at least in their data-input files, and possibly in the Fortran of one of their subroutines. Figure 3.1 shows a PHOENICS-84 flow chart which illustrates the relation of the satellite to the EARTH program, and to auxiliary files and devices.

EARTH contains the main flow-simulating software, and so incorporates coding sequences which represent the laws of physics applied to elements of space and time. The satellite can be set to accept any case to be simulated, which is then converted into a set of data inputs which will appropriately activate EARTH, and then transmits these inputs to EARTH by way of a data file.

The satellite can be regarded as an interpreter. It turns instructions expressed in the so-called PHOENICS Input Language (PIL) into commands to which the computer responds. It is easy to extend the simulating capability of PHOENICS by using the "GROUND" program (standing for 'ground-station') which contains any special coding sequences which must be active while EARTH is carrying out its flow-simulating function. An exemplary GROUND, called GREX1, is a commonly-required feature possessing many of the standard functions required in fluid flow problems which may or may not be used, CHAM (64).

3.2.2 The PHOENICS Description of Physical Phenomena

PHOENICS describes phenomena involving the flow of heat or material in terms of distributions in space and time of temperatures, velocities, pressures, concentrations and other physically meaningful quantities.

These distributions involve ascribing numerical values to the temperatures, velocities, etc. at each of an orderly array of locations, called 'nodes' or 'grid-points'; and, if the process is a time dependent one, such distributions are created for each of a succession of instants of time.

The locations in space and time at which temperature and other dependent variables are computed are finite in number; and they are imagined to lie within a finite set of "cells" which, added together, make up the whole space-time domain that is being considered. The grid may be distributed either uniformly or non-uniformly over the integration domain. Using a non-uniform distribution it is possible to locate more grid nodes in regions where large gradients of the flow variables are expected thus giving a more economic solution without sacrificing accuracy. However, once the grid density and dimensions are chosen, they remain fixed during the solution process. The grid density and dimensions have to be chosen in such a

way that the solution obtained is independent as much as possible of the grid spacing. Of course the degree of independence may be limited by economic considerations, e.g. store requirements and computational times.

Figure (3.2) illustrates (a) a space-time domain and (b) a two-dimensional control cell in cartesian coordinates in which P is the centre of the cell or the grid-point. The neighbouring points are defined as points N, S, E and W (North, South, East and West) and the lines joining P to its neighbouring points cut the cell faces at n, s, e and w; the values of the variables at P, N, S, E and W are regarded as representing values over the whole of the faces of the cell.

3.2.3 Location of the Flow Variables

Figure (3.2) shows a typical grid configuration and identifies the locations at which the flow variables are stored. The pressure, density, exchange coefficient and any scalar variables such as temperature are stored at the grid nodes, while the velocity components are stored at the cell-face locations and are denoted u_e, u_w, v_n and v_s.

This arrangement is called the "staggered grid" configuration, which is similar to the one that was first

used by Harlow and Welch (72), and which has the following advantages:

(a) The stream velocity components are conveniently located for the calculation of the convective flux contributions of flow properties stored at the grid nodes.

(b) The calculation of a mass balance over the region surrounding a grid node is made easy because the velocities normal to the boundaries of this region are located on the boundaries.

(c) The pressures are stored so as to make it easy to calculate the pressure gradients which affect the velocities.

As shown in Figure 3.3, the velocities are enclosed in dashed enclosures taking an 'L' shape in the yz plane. The purpose of these enclosures is to help in identifying the velocity components which refer to a particular grid node, Patankar and Spalding (65).

3.2.4 Control Volumes

The 'control volume' refers to these imaginary regions over which the partial differential equations are

integrated so as to convert them into their finite-domain form. Because there are three different types of locations for the variables on the staggered-grid, there are three types of control volumes: (a) main or grid node control volumes for the variables stored at each grid node; (b) u-velocity control volumes for the u-velocities storage locations; and (c) v-velocity control volumes for the v-velocities storage locations. Examples of each one of these control volumes are shown in Figure 3.4. The boundaries of the grid node control volumes lie halfway between the grid nodes; thus, the surfaces of these control volumes pass through the locations where the normal velocities are stored. The velocity control volumes are bounded in a similar way on the side perpendicular to the velocity component, but in the direction of the velocity component the boundaries of the control volumes pass through the grid nodes in front of and behind the velocity locations.

3.2.5 The Mathematical Model

In analysing a fluid flow problem it is necessary to write down in mathematical form the physical laws which govern the flow under consideration, for example that illustrated in Figure 3.5. These physical laws include the conservation of mass, momentum and energy differential

equations written with reference to the Cartesian Co-ordinate, Schlichting (73), Eckert (74).

In order to simplify the equations to be solved, it will be assumed that:

(a) The flow is laminar and two-dimensional in y-z direction

(b) The fluid has constant thermal conductivity, specific heat and laminar viscosity.

(c) The viscous heat dissipation term is negligible in the energy equation.

The set of differential equations for unsteady laminar flow with the above assumptions is as follows:

Continuity equation

The partial differential equation governing the conservation of mass over a control volume may be written as

$$\frac{\partial \rho}{\partial t} + \frac{\partial (\rho v)}{\partial y} + \frac{\partial (\rho w)}{\partial z} = 0 \qquad (3.1)$$

In this equation, t is the time, v and w are the velocity components in the y- and z- directions respectively and ρ is the fluid density.

Momentum equations

The law of conservation of momentum can be applied to the control volume. The momentum equations for a two-dimensional flow under unsteady conditions is given by the following differential equations:-

y- direction momentum

$$\frac{\partial(\rho v)}{\partial t} + \frac{\partial}{\partial y}(\rho v^2) + \frac{\partial}{\partial z}(\rho vw) = -\frac{\partial p}{\partial y} + \rho g_y + \mu\left(\frac{\partial^2 v}{\partial y^2} + \frac{\partial^2 v}{\partial z^2}\right) \quad (3.2)$$

z- direction momentum

$$\frac{\partial(\rho w)}{\partial t} + \frac{\partial}{\partial y}(\rho vw) + \frac{\partial}{\partial z}(\rho w^2) = -\frac{\partial p}{\partial z} + \rho g_z + \mu\left(\frac{\partial^2 w}{\partial y^2} + \frac{\partial^2 w}{\partial z^2}\right) \quad (3.3)$$

where p is the fluid pressure, μ is the laminar viscosity, and (g_y, g_z) are body accelerations in the (y, z) co-ordinate directions.

Energy equation

The differential equation governing the conservation of energy for a fluid with constant transport properties.

$$\rho C_p\left(\frac{\partial T}{\partial t} + v\frac{\partial T}{\partial y} + w\frac{\partial T}{\partial z}\right) = \frac{\partial p}{\partial t} + v\frac{\partial p}{\partial y} + w\frac{\partial p}{\partial z} +$$

$$K\left(\frac{\partial^2 T}{\partial y^2} + \frac{\partial^2 T}{\partial z^2}\right) \qquad (3.4)$$

The density is dependent on the temperature and pressure and for a perfect gas is obtained using:

$$\rho = p/RT$$

3.2.6 The General Transport Equation

The elliptic differential equations (3.2), (3.3) and (3.4) for the variation of the dependent variables in a cartesian co-ordinate system can be conveniently presented as:

$$\frac{\partial}{\partial t}(\rho\phi) + \frac{\partial}{\partial x}(\rho u\phi) + \frac{\partial}{\partial y}(\rho v\phi) + \frac{\partial}{\partial z}(\rho w\phi) = \frac{\partial}{\partial x}\left(\Gamma_\phi \frac{\partial \phi}{\partial x}\right) +$$

$$\frac{\partial}{\partial y}\left(\Gamma_\phi \frac{\partial \phi}{\partial y}\right) + \frac{\partial}{\partial z}\left(\Gamma_\phi \frac{\partial \phi}{\partial z}\right) + S_\phi \qquad (3.5)$$

and in the general differential equation form as (Patankar (75), Broyd et al (76)).

$$\frac{\partial}{\partial t}(\rho\phi) + \text{div}(\rho\vec{u}\phi) = \text{div}(\Gamma_\phi \text{ grad } \phi) + S_\phi \qquad (3.6)$$

transient term | convection term | diffusion term | source term

where ϕ stands for the dependent variable, $\Gamma\phi$ is the appropriate exchange coefficient for the variable ϕ which can stand for any property which can be convected and diffused, e.g. stagnation enthalpy, chemical-species concentration, and turbulence energy; $S\phi$ is the corresponding volumetric source/sink term of ϕ. The advantage of writing the equation in the form given by (3.6) is that additional equations can be incorporated very easily into the solution sequences of a computer program.

3.2.7 The General Finite-Domain Equation

The derivation of the finite-domain equation has been described by Spalding (78, 79). It is obtained by integrating the differential transport equations over each of the control volumes that subdivide the flow domain. The integrations entail "interpolation assumptions" which are commonly referred to as the "fully-implicit" and "upwind-differencing scheme" formulations.

The general finite-domain equation for the transport of a scalar ϕ is derived by integrating Equation (3.6) over the control cell P (see Figure 3.4) as follows:

$$\iiint_V \frac{\partial(\rho\phi)}{\partial t}\, dV + \iint_A (\rho\vec{u}\phi).d\vec{A} = \iint_A \vec{J}_\phi.d\vec{A} + \iiint_V S_\phi dV \qquad (3.7)$$

where V denotes the cell volume, A its total surface area and $\vec{J}_\phi$ the diffusion flux defined as:

$$\vec{J}_\phi = -\Gamma_\phi \text{ grad } \phi \qquad (3.8)$$

The transport of variable ϕ across the faces and throughout the time, yields transient convection and diffusion terms. Other terms which result from the integration of the general differential equation over the control volume are called source terms. Each one of these terms will now be discussed.

Transient Term

Since the variable ϕ, is assumed to be uniformly distributed throughout the control cell, the integration of the transient term over the control volume can be written as:

$$\iiint_V \frac{\partial(\rho\phi)}{\partial t} dV = V \frac{\partial(\rho\phi)}{\partial t} = \frac{V}{\Delta t} (\rho_p \phi_p - \rho_{p,o} \phi_{p,o}) \qquad (3.9)$$

where the subscript o refers to values prevailing at the start of the time interval. The transient procedure adopted is fully implicit in that all neighbouring ϕ's of ϕ_p and related values are late-time values, i.e. present values.

Convection Term

If all the variables are presumed constant over each cell face, the surface integral of the convection term in Equation (3.7) gives:

$$\iint_A (\rho \vec{u} \phi).d\vec{A} = \sum_{n,s,e,w} (\rho \vec{u} \phi).\vec{A} \qquad (3.10)$$

Since ϕ_p is the value associated with the nodal point P, interpolations are required for the cell-face value of ϕ to be used in the surface integral Equation (3.10). In the present study, the 'upward-differencing scheme' of Spalding (80) is used to evaluate the convection fluxes across the control volume faces. Thus, for the convection term, the value of ϕ to be convected across a cell face is taken to be the nodel value prevailing at the upstream side of the face; for example when the convective flux is calculated at the north face n, the value of ϕ_n specified is:

$$\phi_n = \phi_N \quad \text{if} \quad v < 0$$

or (3.11)

$$\phi_n = \phi_p \quad \text{if} \quad v > 0$$

where v is the velocity component normal to the north face; and similar rules apply for the other faces and directions.

Equation (3.10) can be expressed in terms of the convection flux, C_i where:

$$C_i \phi = \rho_{up} U_i A_i \phi \qquad (3.12)$$

where the subscript, i, refers to the cell faces and ρ_{up} is the density of the 'upstream fluid'.

Diffusion Term

As before, all the variables are presumed constant over each cell face so the surface integral of the diffusion term in Equation (3.7) gives:

$$\iint_A \vec{J}_\phi . d\vec{A} = \sum_{n,s,e,w} \vec{J}_\phi . \vec{A} \qquad (3.13)$$

With the aid of the general flux law, Equation (3.8), this can be expressed as:

$$\sum_{n,s,e,w} \vec{J}_\phi . \vec{A} = - \sum_{n,s,e,w} \Gamma_\phi \text{ grad } \phi . \vec{A} \qquad (3.14)$$

Source Term

For constant variables assumed over each cell, the source term can be written as:

$$\iiint_V S_\phi dV = S_\phi V \qquad (3.15)$$

The source term of ϕ may then be linearised to be written in the form:

$$S_\phi V = S_u V + S_p V \phi_p \qquad (3.16)$$

where S_u and S_p are the appropriate components numerically designated for the source term.

3.2.8 The PHOENICS Finite-Domain Equations

A numerical solution of a differential equation consists of a set of numbers from which the distribution of the dependent variable ϕ can be constructed. Thus, a numerical method treats as its basic unknowns the values of the dependent variable at a finite number of locations in the calculation domain. The method includes the tasks of providing a set of algebraic equations for these unknowns and of prescribing an algorithm for solving the equations, Patankar (75).

This set of algebraic equations is embodied in PHOENICS as the 'finite-volume' (also called 'Finite-domain') equations. The integration leads to "finite-domain equations" (FDE's), having the form, in 3-dimensional, unsteady state, CHAM (63).

$$a_p\phi_p = a_N\phi_N + a_S\phi_S + a_E\phi_E + a_W\phi_W + a_H\phi_H + a_L\phi_L + a_T\phi_T + b \qquad (3.17)$$

where:

a_p, a_N --- etc. are coefficients,

b is a representation of the source appropriate to ϕ for the cell,

subscripts have the following meanings:

p grid node within cell,

N north- neighbour node in positive-y direction,

S south- neighbour node in negative-y direction,

E east- neighbour node in positive-x direction,

W west- neighbour node in negative-x direction,

H high- neighbour node in positive-z direction,

L Low- neighbour node in negative-z direction, and

T grid node at earlier time.

Figure 3.6 shows the space coordinate system.

3.2.9 Procedures for solving the Finite-Domain Equations

There is a finite-domain equation for each variable for each control cell in the domain of integration. Each equation, as already explained, can be expressed in the general form as given in Equation 3.17, and although linear in appearance, they are in fact non-linear, because the coefficients and sources are functions of the ϕ's. In addition, the momentum equations are coupled one to the other through the unknown pressure field. Thus, an iterative procedure must be employed for their solution.

The following procedures are used in the present study for solving the variables as specified in Group 6 of the Q1 file which is explained in Appendix B.

(a) Jacobi point-by-point

The finite-domain equations for the velocities, i.e. v1 and w1 are solved by the Jacobi point-by-point procedure, CHAM (63). The algebraic 'finite-domain' equations are derived by integration of the differential equations over grid cells. All finite-difference equations are cast into a standard form as follows:

$$\phi_p = \frac{\sum_i a_i \phi_i + b}{\sum_i a_i - c} \qquad (3.18)$$

where ϕ_p is the dependent varible at point P, and $\sum_i$ denotes summation over the neighbouring grid points. The coefficient a_i represents the effects of convection and diffusion and are formulated using upwind differencing. With all ϕ's on the right-hand-side having the values which they possessed before the updating 'sweep' through the grid was commenced. At the next sweep, the ϕ's on the right-hand side will have the values created in the previous one.

(b) Slab-wise simultaneous

Most of the equation sets are solved slab-by-slab by means of slab-wise linear solver which proceeds as follows:

- Treat off-slab values (H,L,T) as known (temporarily), reducing the equation to:

$$a_p\phi_p = a_N\phi_N + a_S\phi_S + a_E\phi_E + a_W\phi_W + b' \qquad (3.19)$$

where $b' = b + a_H\phi_{H*} + a_L\phi_{L*} + a_T\phi_{T*}$

- Postulate the existence of the subsidiary equation set:

$$\phi_p = N_{\phi_N} + E_{\phi_E} + B$$

and derive equations for N,E and B by algebraic substitution, in terms of a_N, a_S, a_E, a_W, b', ϕ_{NW} and ϕ_{SE}.

- Compute values of N, E and B, from these equations by recurrence starting in the south-west corner.

- Compute values of ϕ_p, starting in north-east corner.

- Repeat the process until convergence.

(c) Whole-field solver

The equations can also be solved in a "whole-field" procedure. This procedure is similar in nature to that for the single slab. It proceeds as follows:

- Treat only ϕ_T as known, writing the equation:

$$a_p\phi_p = a_N\phi_N + a_S\phi_S + a_E\phi_E + a_W\phi_W + a_H\phi_H + a_L\phi_L + b' \qquad (3.20)$$

where $b' = b + a_T\phi_T$*

- Postulate that the ϕ's can also be connected by:

$$\phi_p = N\phi_N + E\phi_E + H\phi_H + B$$

and derive equations for N, E, H and B in terms of a_N, a_S, etc by algebraic substituion

- Compute values of N,E,H and B, from these equations, by recurrence, starting in the south-west-low corner.

- Thence compute values of ϕ_p, starting in the north-east-high corner and working back.

- Repeat the process until convergence, the iteration being necessary because the B's contain ϕ's for the north-west, south-east, high-south, low-north, high-west and low-east neighbours of point P.

The whole-field procedure differs from the slab-by-slab one in taking z-direction links into account simultaneously with x- and y- direction links. It therefore reaches the solution more rapidly. This procedure is used for solving the pressure in this study.

There are other solution procedures employed in the PHOENICS code like the hybrid methods which are often used for the pressure correction equation and the partial elimination algorithm which is used for two phase flow. The above procedures can be solved elliptically or parabolically for steady or transient flow. More details on these procedures are given in CHAM (63).

3.2.10 Auxiliary Information

The differential equations alone do not specify the problem; additional information of two kinds is needed: initial and boundary conditions for all the dependent

variables (u, v, w, p, ϕ); and auxiliary equations allowing the density, shear stresses, diffusion fluxes, body force and sources to be computed in terms of the dependent variables at each point in the field.

3.3 Application to the Parallel Plates Natural Convection Problem

The problem simulated is shown schematically in Figure 3.5 which shows laminar free convection of air in a parallel-plate, vertical, smooth walled channel of infinite depth along the x-axis. Both walls are maintained at constant temperatures. Heat transfer through the walls causes density changes of the air in the channel, and leads to buoyancy driven flow along the z-axis.

3.3.1 Description of the Solution Procedure

This study is to analyse the natural convection flow in a vertical heated wall channel having its inlet and outlet open to ambient pressure. The PHOENICS simulation procedure is to obtain the heat transfer coefficient in a channel for different widths, heights and wall temperatures. Some simplifying assumptions are considered in this solution:

(a) the flow is laminar, two-dimensional and the flow moves in the z-direction by means of buoyancy effects

(b) the fluid is air (Pr=0.7)

(c) the transport properties are constant and the density is a function of the temperature only and is calculated using the perfect gas law with the pressure taken as 1 bar

(d) the velocity and temperature profiles at the channel inlet are assumed uniform

(e) the pressure gradient is zero across the channel width at inlet and outlet.

In order to produce a theoretical solution and make a comparison between this solution, the experimental results of this study and existing reference works concerned with this type of problem, a Q1 file and special GROUND subroutine were created to simulate the flow in the channel. The dimensionless groups, volume and mass air flowrates and heat transfer coefficient, as outlined in Section 2.3, are obtained using GROUND subroutine with some PHOENICS programming modification to suit the operation procedure of the PHOENICS system.

A brief description of the steps which were taken to obtain a successful PHOENICS solution is given below.

Many PHOENICS runs were made using the above assumptions with the flow taken as being steady and the pressure equal to atmospheric at the channel inlet using the parabolic method of solution. Other runs were made treating the problem as elliptic where the pressure was specified equal to atmospheric at the channel exit as a boundary condition. All the above runs gave a flow circulation within the domain which of course is not in agreement with experimental findings.

Other runs were made with the pressure value at the channel inlet specified via the mass flow rate and with the channel inlet velocity imposed as boundary conditions, using the parabolic solution. Further runs were made with the above boundary conditions at the channel inlet and with the pressure at exit equal to atmospheric and the temperature of any inflowing air if it occurred at the channel exit being the same as that in the last cell of the domain. The elliptic solution was applied. Both cases gave reasonable results for the solution of the fluid parameters. Results for the elliptic solution showed that the pressure at inlet was equal to that at outlet plus $\rho g l$, the ambient static head across the channel.

The inlet boundary conditions for this elliptic solution are not satisfactory since the air flow rate is not known in practice. Therefore it was modified to be solved when no velocity is given at the channel inlet and pressure at the channel inlet is equal to the atmospheric plus the static head pressure (ρgl) and the channel exit pressure is atmospheric. This gave positive air flow and correct pressure defect along the channel from the inlet to the outlet. Convergence was only achieved after many iterations. The results obtained were in qualitative agreement with experiment. The elliptic procedure used required large computer time to achieve the required convergence. It was decided to run the PHOENICS in its transient mode where setting of initial and boundary conditions were considerably simplified. This resulted in predictions in close agreement with the elliptic steady state solution and the computation time required was considerably less.

The Q1 file and the special GROUND subroutine which were used in this theoretical solution, are presented in Appendices B and C.

3.3. 2 Initial and Boundary Conditions - Transient Solution

To complete the specification of the mathematical formulation, both initial and boundary conditions are needed. The values of variables at the start of the computation must be specified for the whole domain - some variables are given initial guessed values which helps to speed up the convergence towards the final steady state solution. Typical initial and boundary conditions were used in the set up in the Q1-file to simulate the fluid flow as sketched in Figure 3.5.

Initial Conditions

The following values were applied to initialize the solution for the whole field at time equal to zero as listed in Q1 file.

Atmospheric pressure		P1	= 0.0
Air temperature	T_{in}	(H1)	= 293.30 (K)
z velocity		W1	= 0.1 (m/sec)
y velocity		V1	= 0.0 (m/sec)
Air density		DEN1	= 1.187 (kg/m^3)

Boundary Conditions

Figure 3.5 illustrates the configuration of the flow and system co-ordinates.

At y = 0 Glass temperature T_G (H1) = 298.20 (K)

Velocity at the Glass = 0

y = b Wall temperature T_W (H1) = 347.70 (K)

Velocity at the wall = 0

z = 0 Inlet temperature T_{in} (H1) = 293.30 (K)

Inlet static pressure =

ρgl + outlet pressure = 34.947 (N/m^2)

z = 1 Outlet temperature T_{out} equal to the temperature at the last cell which is equal to the temperature of air flow in from the top of the channel.

Outlet pressure = atmospheric (used as zero datum in PHOENICS solution).

Density Calculation

The density of the fluid is assumed to be independent of the pressure but to vary with temperature according to the law of ideal gases, i.e.

$$\rho = \frac{p_a}{RT}$$

where R = gas constant for air = 287 (J/kg.K)

p_a = constant = 1 atmosphere = 10^5 (N/m^2)

T = temperature of the fluid (K)

3.4 Theoretical Results and Discussion

As explained in the previous sections, the theoretical results were obtained by numerical procedures using the PHOENICS Code program.

The results shown in this section are for a range of test conditions, some of which reproduce those in the experimental work and some of which were simply chosen to obtain a range of theoretical heat transfer correlation parameters.

The first set of results shown are those for the ISOTHERMAL wall boundary condition which will allow comparison later in this Chapter with the theoretical results obtained by other workers. However, in practice the channel walls would increase in temperature from the bottom to the top and so additional runs were made using PHOENICS to compare with the experimental tests run under variable wall temperature conditions.

It was also anticipated that the atmospheric pressure and temperature might have an influence on heat transfer and flow rates in the duct because the pressure difference across the channel (ρgl) depends on the ambient density. A number of runs were therefore made to test for this effect.

Basically the output from PHOENICS consists of velocities, pressures, densities and temperatures throughout the field. Using the GROUND subroutine further calculations may then be made using these parameters to calculate heat transfer coefficients and the dimensionless groups as already outlined in Section 2.3.

In PHOENICS and experimental calculations, the film temperature T_{film} at which the air transport properties were evaluated, for the calculation of the dimensionless groups (Nu and Gr) and heat transfer coefficients, was determined at fluid film temperature using the following equation:

$$T_{film} = [(Tw + Tg)/2 + T_{in}]/2 \qquad (3.21)$$

Figures 3.7 to 3.15 show the velocity and temperature profiles at different locations throughout the channel height for the same constant wall temperature conditions of [illegible] 74.7[illegible]°C, channel heights of 1, 2 and 3 metres and channel width of 50, 100 and 150 mm. These plots were made using the standard graphic subroutine of PHOENICS, Malin (71).

The assumed uniform velocity profile at channel inlet is seen to change gradually as the flow develops

under the influence of the drag of the walls and the buoyancy forcing term. Similar development is seen for all cases studied. The higher velocity region is seen to be close to the hot wall while the velocity over the remainder of the duct is, on average, near to the inlet value. It is also seen that the average velocity at exit is higher for the 3m length as compared with the 1m length.

The velocity profile is flat at the centre region between the plate and the glass and becomes even flatter as the channel width increases. Figures 3.13 to 3.15 show isothermal lines within the channels.

These diagrams are useful as a qualitative measure of the velocity and temperature profiles but because of the increased computation time involved with using small grid sizes close to the wall more detailed profiles were not obtained. The heat transfer to the air and hence the heat transfer coefficients had therefore to be obtained from the integration of the profiles across the channel as outlined earlier in Section 2.3.

3.4.1 Theoretical Results Plotted in Dimensionless Form

The PHOENICS output in the form of velocities, pressures and temperatures throughout the field was used in further calculations performed in the GROUND

subroutine to obtain the dimensionless heat transfer coefficients in terms of the important dimensionless parameters such as the Grashof and Prandtl numbers and b/x, the aspect ratio of the channel. The theoretical justification for these dimensionless groups can be found in Section 2.3. To integrate over the channel width in the calculation of the mass flow rate, 20 grids were used for the 100mm and 150mm widths, and 10 grids for the 50mm width, in a subroutine similar to Simpson's Rule in the GROUND subroutine.

Figure 3.16 shows the results plotted as Nu against GrPr b/x for three different atmospheric pressures. The range of pressures correspond roughly with the highest and lowest barometric pressures observed throughout a typical year. To cover the range of (GrPr b/x) shown, the runs were made with the wall temperatures and inlet air temperature kept at fixed values while the height and width of the duct was varied.

Accordingly the three values of the ambient density were calculated from the ideal gas equation:

$$\rho = p_a/RT \qquad (3.22)$$

Therefore the head pressure (i.e. ρgl) values were calculated and set for the pressure value in Group 13, e.g. COVAL (INLET, P1, FIXP, 34.947), in the Q1 file.

The results for any one pressure are seen to lie on a straight line to a confidence limit of 99.6% as shown in Figure 3.16 and the correlating equations for the three pressures are:

$$Nu = 0.874\ (GrPr\ b/x)^{0.186} \quad \text{for } p_a = 0.950 \text{ bar} \qquad (3.23)$$

$$Nu = 0.734\ (GrPr\ b/x)^{0.238} \quad \text{for } p_a = 1.000 \text{ bar} \qquad (3.24)$$

$$Nu = 0.816\ (GrPr\ b/x)^{0.241} \quad \text{for } p_a = 1.050 \text{ bar} \qquad (3.25)$$

Also, for the above series of conditions the dimensionless volume flow rate $\dot{Q}$ against the dimensionless channel length L were obtained and are shown plotted in Figure 3.17. The correlating equations are as follows:

$$\dot{Q} = 0.830\ (L)^{0.703} \quad \text{for } p_a = 0.950 \text{ bar} \qquad (3.26)$$

$$\dot{Q} = 0.803\ (L)^{0.604} \quad \text{for } p_a = 1.000 \text{ bar} \qquad (3.27)$$

$$\dot{Q} = 0.955\ (L)^{0.564} \quad \text{for } p_a = 1.050 \text{ bar} \qquad (3.28)$$

These results show that the atmospheric pressure, which influences the ambient density, has a very significant effect on the fluid flow and heat transfer in the channel. The larger the pressure difference across the channel the larger the air flow rate and heat transfer.

For example, for a channel of 3m height and 100mm wide with wall temperatures of 347.7 K and 298.2 K, which corresponds to a GrPr b/x product of 4.091×10^5, the increases in mass flow rate is of the order of 48.02% for a pressure of 1.05 bar compared to a pressure of 1 bar. Thus the ambient pressure effect would be of significance in the application of those results to Trombe wall design.

Figure 3.18 presents the variation of the static pressure defect $(p-p_a)$ with distance along the channel height. Inspection of this figure shows that the pressure at the channel inlet is equal to the static head pressure (ρgl). The pressure reduces almost linearly from the inlet to the channel and reaches atmospheric at the channel exit. The static pressure is very significant as a boundary conditions at the channel inlet. As may be seen from Figures 3.16 and 3.17 the pressure conditions have an appreciable effect on the dimensionless volume flow rate and Nusselt number because of the influence of pressure on density in the ρgl term in Equation 3.3. If the pressures at channel inlet and outlet are made equal, runs on PHOENICS have shown that the change in the buoyancy term as a result of heat transfer from the walls is insufficient to overcome the fluid resistance in the channel and recirculation effects within the channel were obtained. Therefore, the fluid needs a pressure difference across the working domain to enable it to move

with the existing fluid buoyancy force. In the PHOENICS solutions the pressure across the channel width at inlet was taken as uniform despite the temperature difference between the hot wall and cold glass which in practice affects the density values near the wall and the glass.

3.4.2 Non-Isothermal Walls

All the results discussed above have been for isothermal wall conditions. In a practical situation, however, where the heating may occur as a result of incident radiant energy being stored in a concrete wall, the wall temperature will inevitably increase towards the channel outlet. To establish the correct mean temperature on which to base the Gr and Nu number calculations, further runs were made using wall temperature variations corresponding to those obtained in the experimental work.

Figure 3.19 shows the comparison between the isothermal and non-isothermal cases. The figures in brackets for the non-isothermal case correspond to plate temperatures in a real experimental situation. The aluminium plate and the glass plate temperatures were variable along their lengths. The temperature variation along the length was introduced by using a suitable straight line equation as follows:

for the aluminium plate $T_w = 378 + 6.65Z$ (3.29)

for the glass sheet $T_g = 319 + 2.89Z$ (3.30)

These equations were used in the GROUND subroutines which are called by the Q1 file to give the temperature at any location on the plate and glass walls. All other boundary conditions were as used for the isothermal cases. The Q1 file and GROUND subroutine are shown in Appendices E and F, respectively. The non-isothermal PHOENICS results for Nusselt number and dimensionless volume flow rate show an increase of 9.45% and 22.8% respectively over the isothermal case. Figures 3.20 and 3.21 show comparison between two channels of the same size, one channel with uniform average plate and glass temperature and the other a channel with non-isothermal plate and glass as explained above. Development of the velocity and temperature profiles along the channels are shown in these figures.

The increase in mass flow rate and Nusselt number for non-isothermal conditions can be explained by examining Figure 3.20 and Figure 3.21. From the velocity distributions it can be seen that the velocity in the centre of the channel is greater for the non-isothermal case than for the isothermal case, while close to the hot wall it is evident that the maximum velocity is actually slightly less. The temperature profiles seem to show that

the temperature boundary layer is smaller for the non-isothermal case.

In the cases just discussed it must be remembered that the linear temperature profile chosen is unlikely to occur in practice. For uniformly heated storage walls cooled by air, the wall temperature variation depends on many parameters and so the equation of the wall temperature variation is difficult to predict. However, by considering the non-uniform wall temperature case, it is clear that the usual isothermal correlating equations for Nu and $\dot{Q}$ cannot be used with a simple arithmetic mean temperature.

Figure 3.22 shows the comparison of the PHOENICS solution with the results of Elenbaas (3), Bodoia and Osterle (13), Miyatake and Fukii (26), Ofi and Hetherington (25), Aung (28), and Aihara (32) for air. It is apparent from the figure that the PHOENICS solution compares favourably with the other results. The PHOENICS solution uses the static head pressure at the channel inlet as a boundary condition. In the calculation procedure, the average Nusselt number was based on the difference between the average of the wall and glass temperatures and the inlet temperature as used by Aung (28).
Also, the fluid properties were evaluated at film temperature as given in equation 3.21. The calculation of

the average Nusselt number was based on the warmer wall temperature and the fluid properties were evaluated on the film temperature which is given by the equation T_{film} = (Tw+Tin)/2. In Aung's (28) theoretical investigation the pressure drop due to the flow acceleration at the channel inlet and the inlet velocity profiles were considered. Aihara's theoretical results of Nusselt number are lower than the other results as shown in Figure 3.22. The above comparison between the PHOENICS solution and other available results indicates that the use of the PHOENICS code can be justified for the solution of natural convection in a vertical parallel heated wall channel and the results used with reasonable confidence.

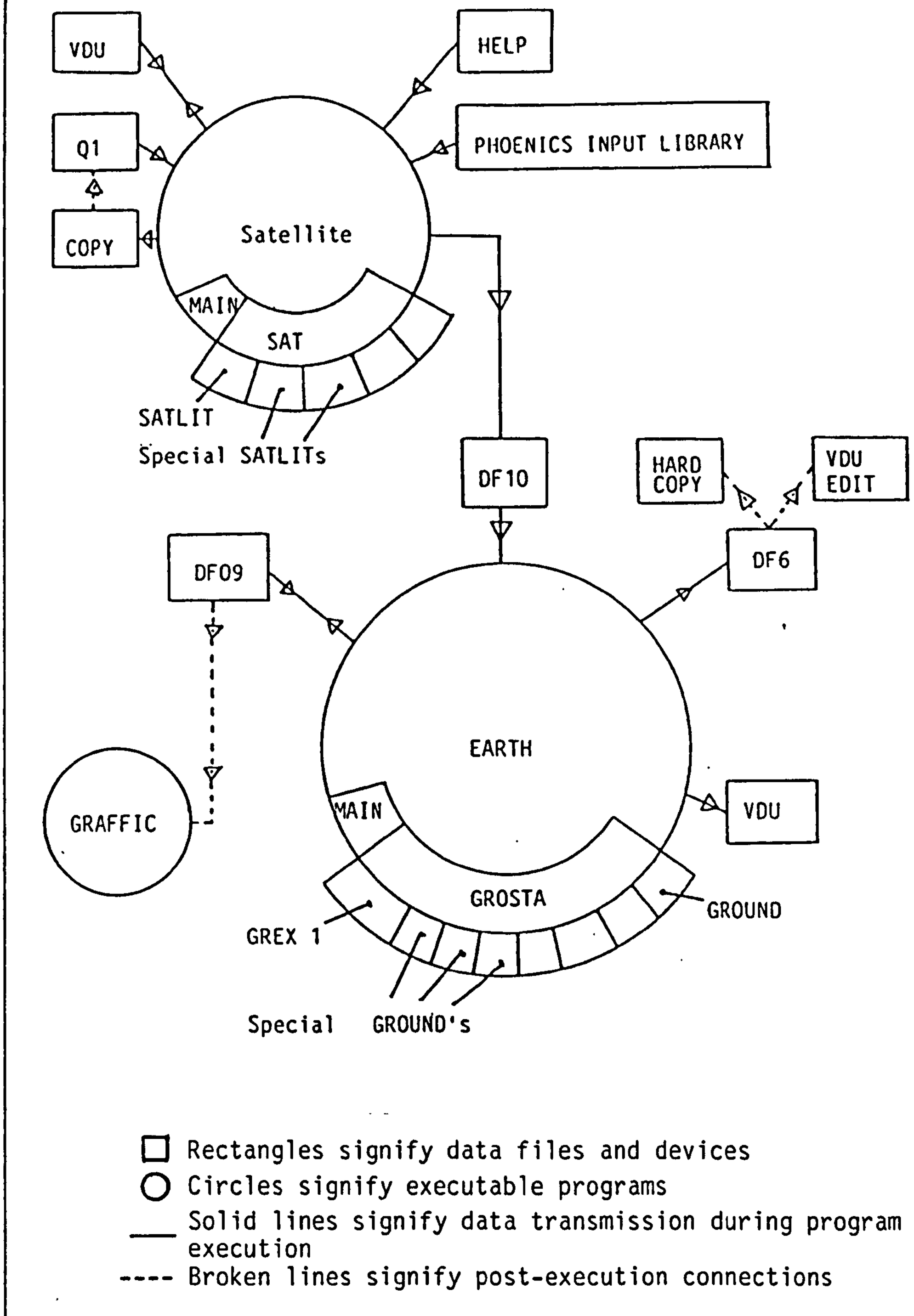

Figure 3.1 PHOENICS-84 Flow Chart

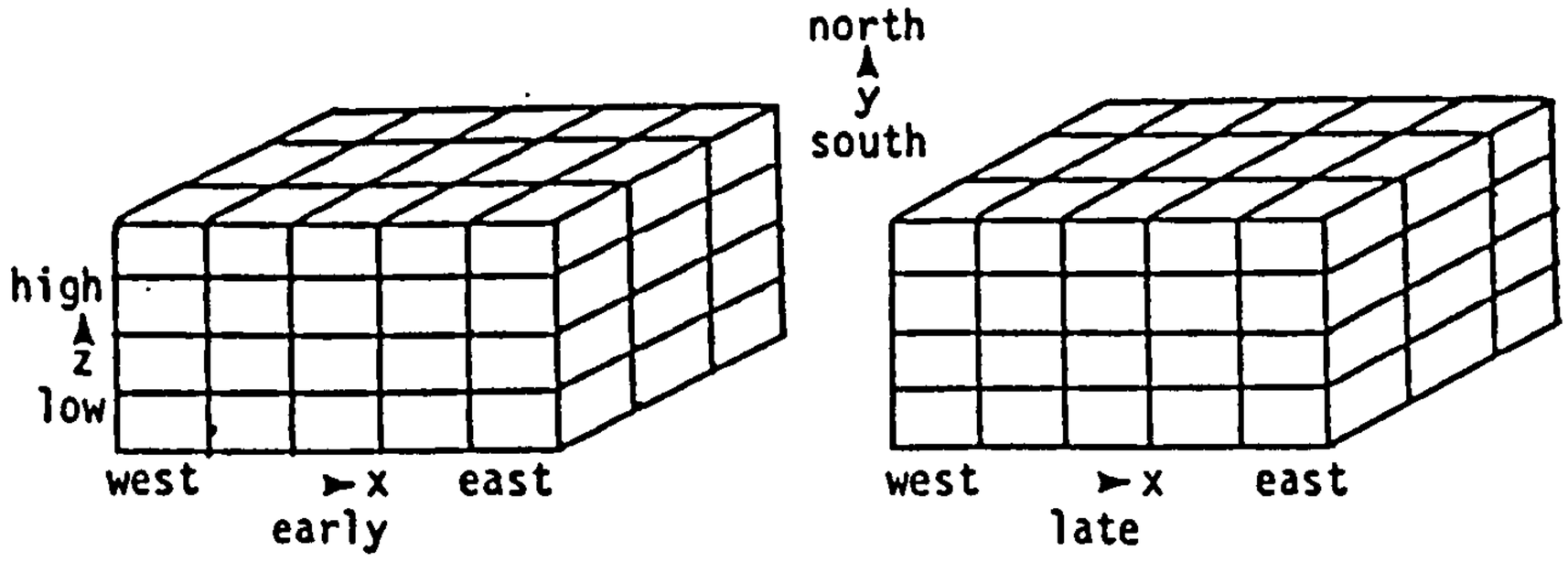

(a) Space-time domain

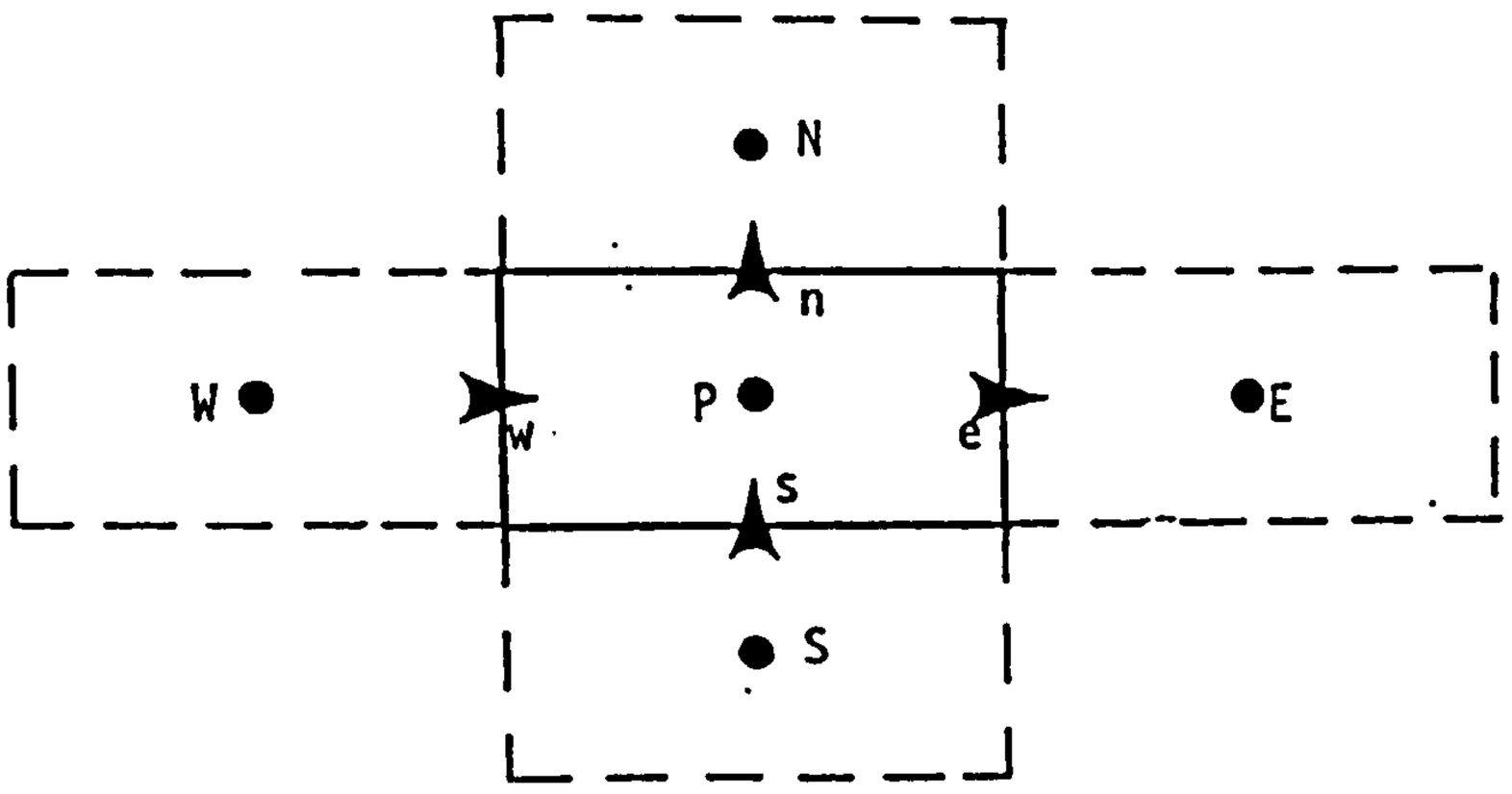

(b) Two-dimensional Control Cell

Figure 3.2 Cartesian Coordinates

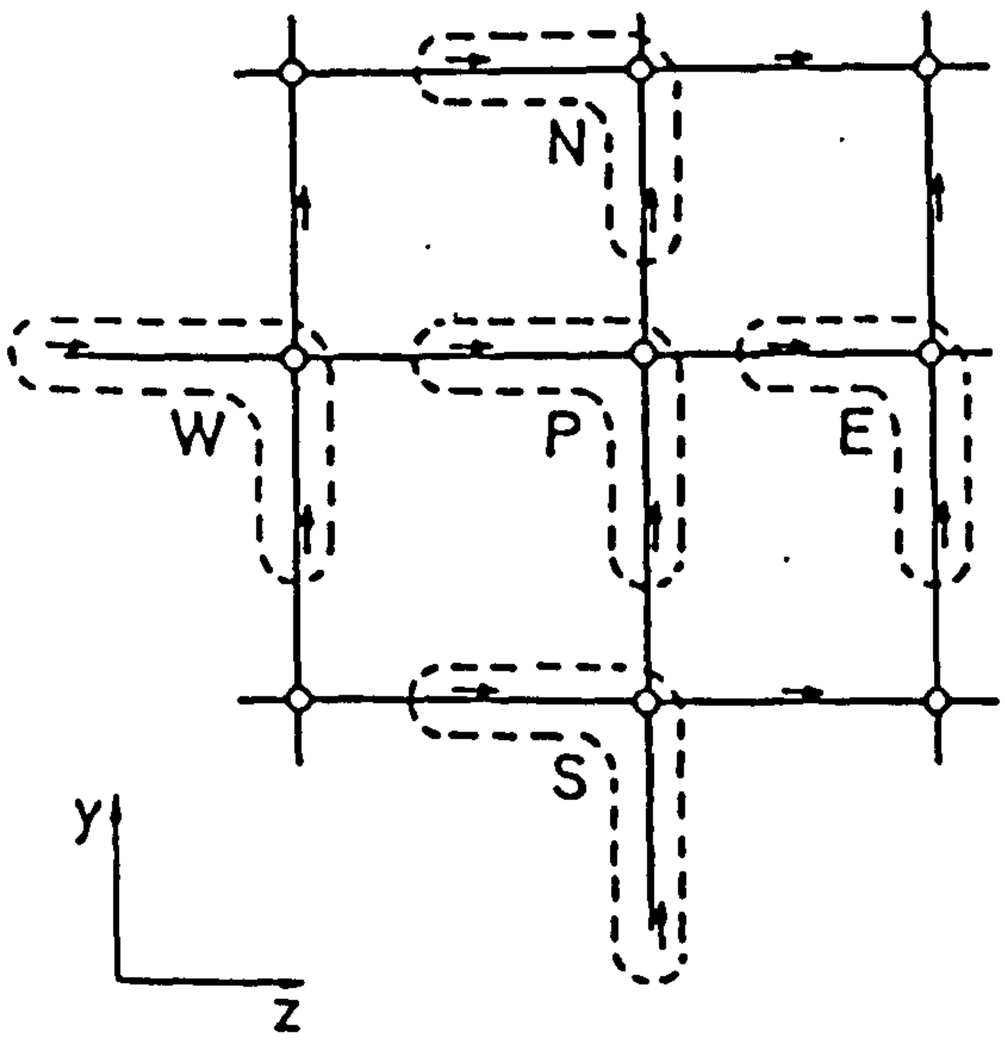

location	variable stored
o	p.u.ø
– –	w
1 –	v

Figure 3.3 The Staggered Grid

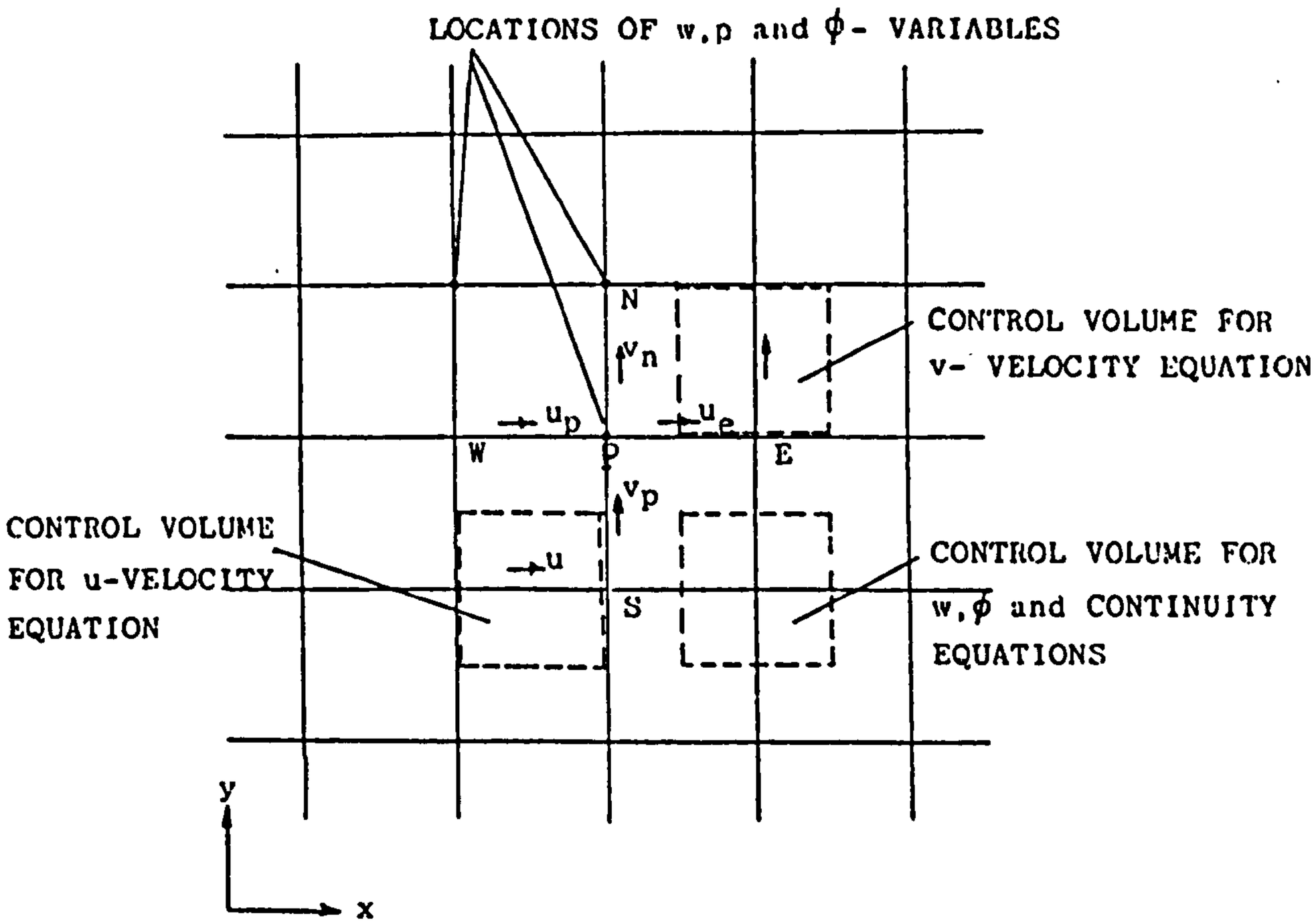

x-y PLANE

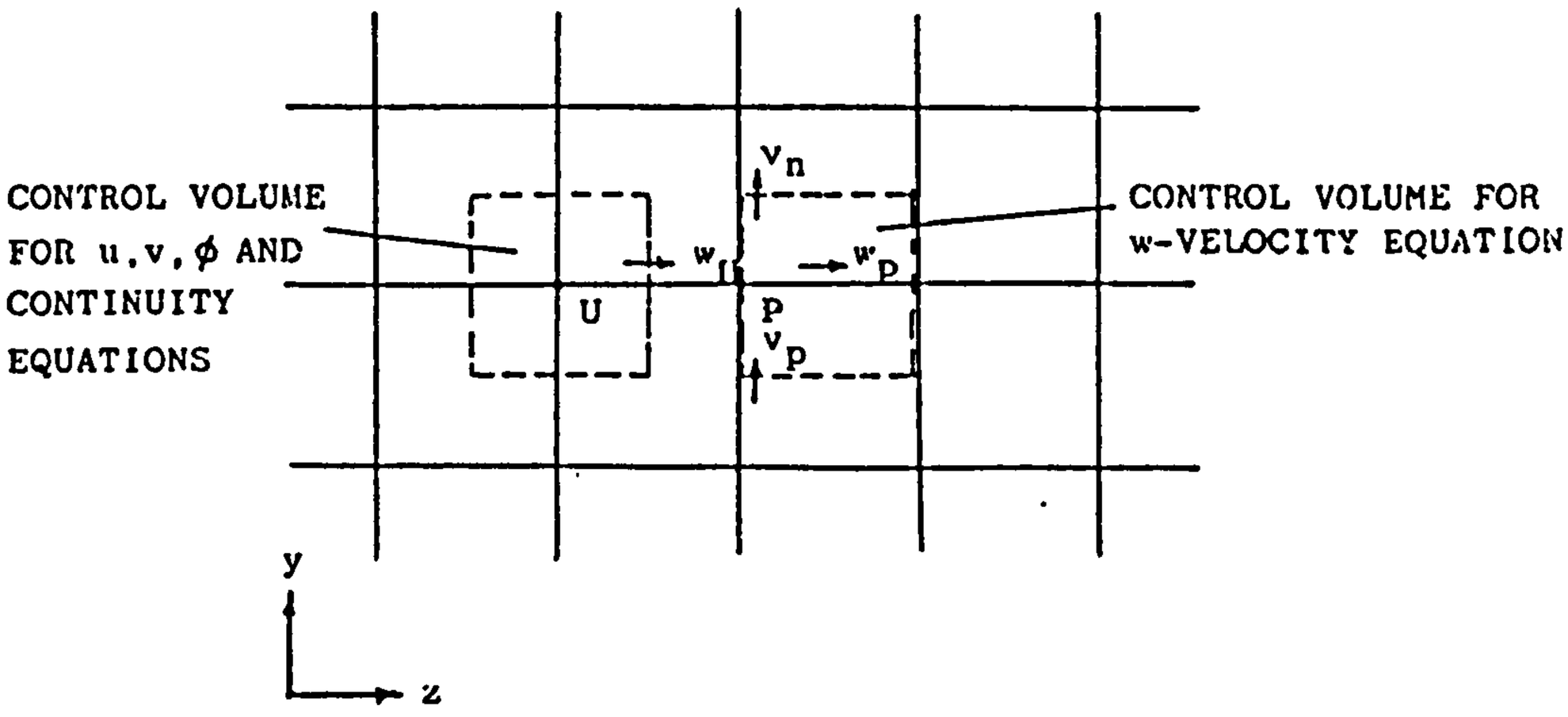

y-z PLANE

Figure 3.4 Storage Locations and Control Volumes for dependent variables

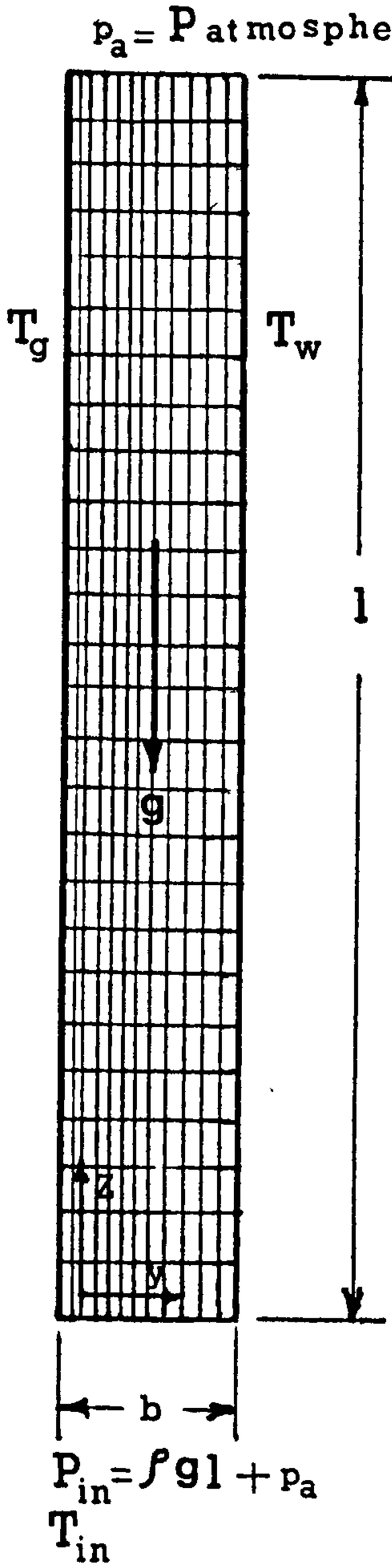

N.B. The fluid flow is in z-axis

Figure 3.5 Configuration of the Flow

Figure 3.6 Space Coordinate

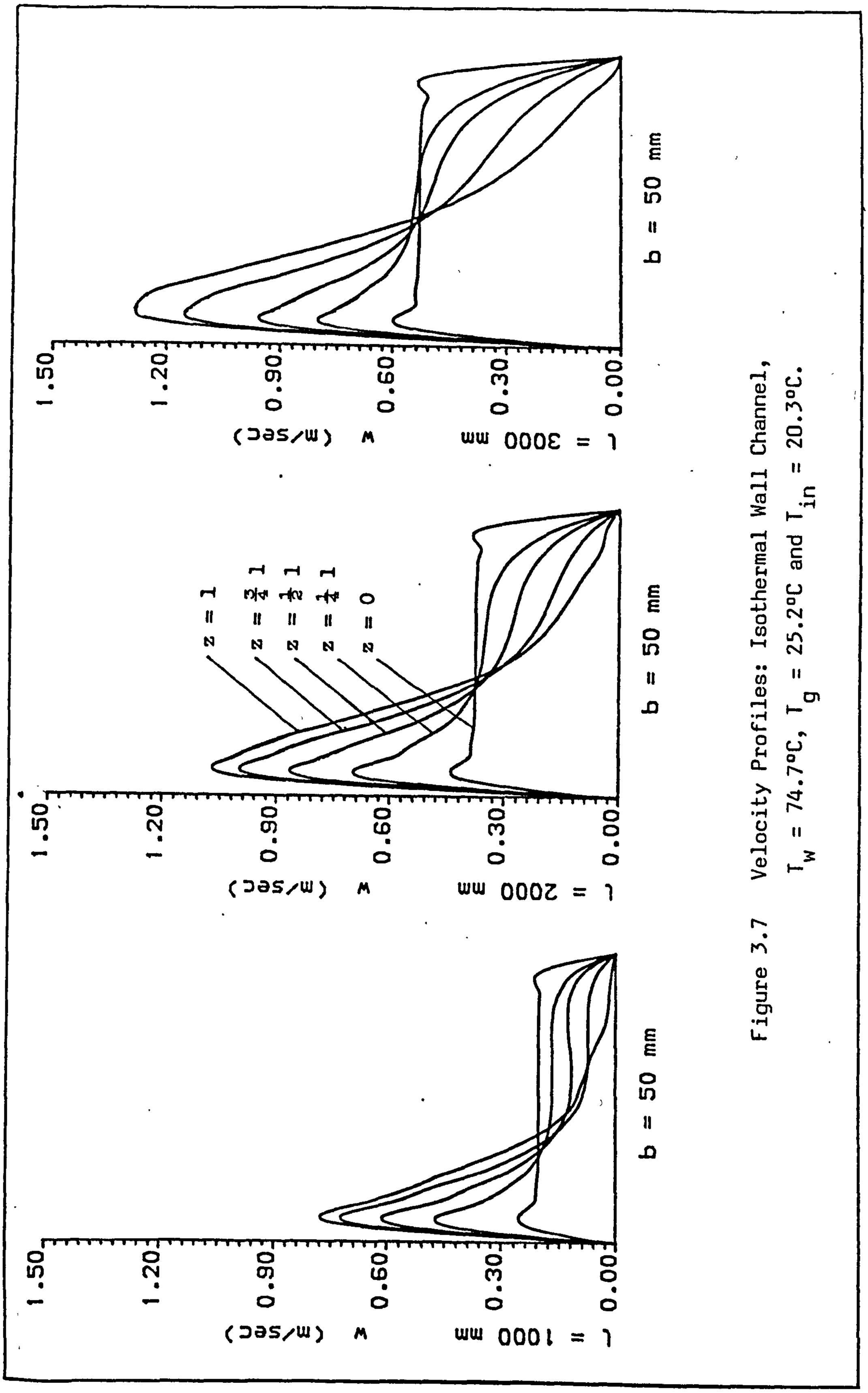

Figure 3.7 Velocity Profiles: Isothermal Wall Channel, T_w = 74.7°C, T_g = 25.2°C and T_{in} = 20.3°C.

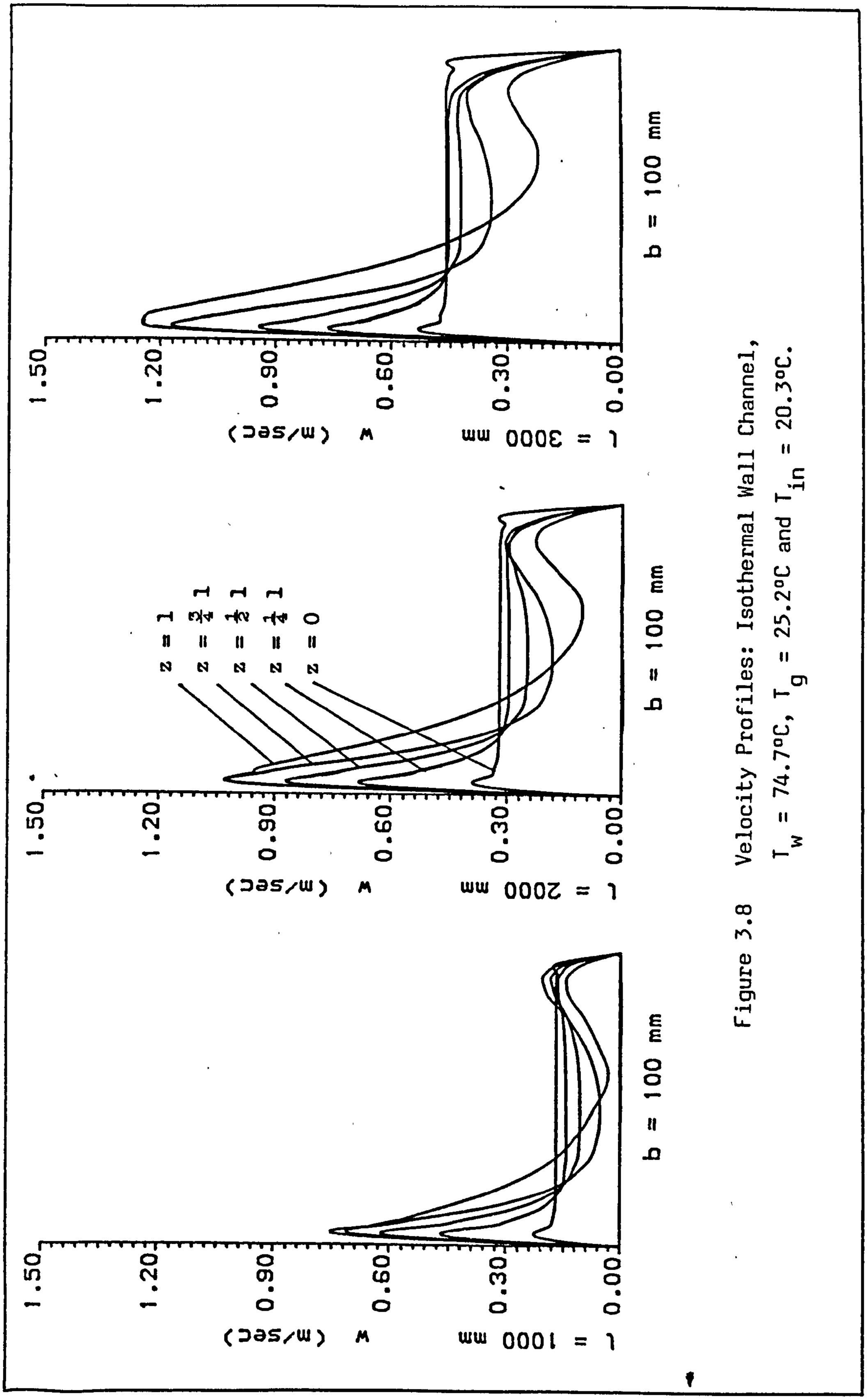

Figure 3.8 Velocity Profiles: Isothermal Wall Channel, T_w = 74.7°C, T_g = 25.2°C and T_{in} = 20.3°C.

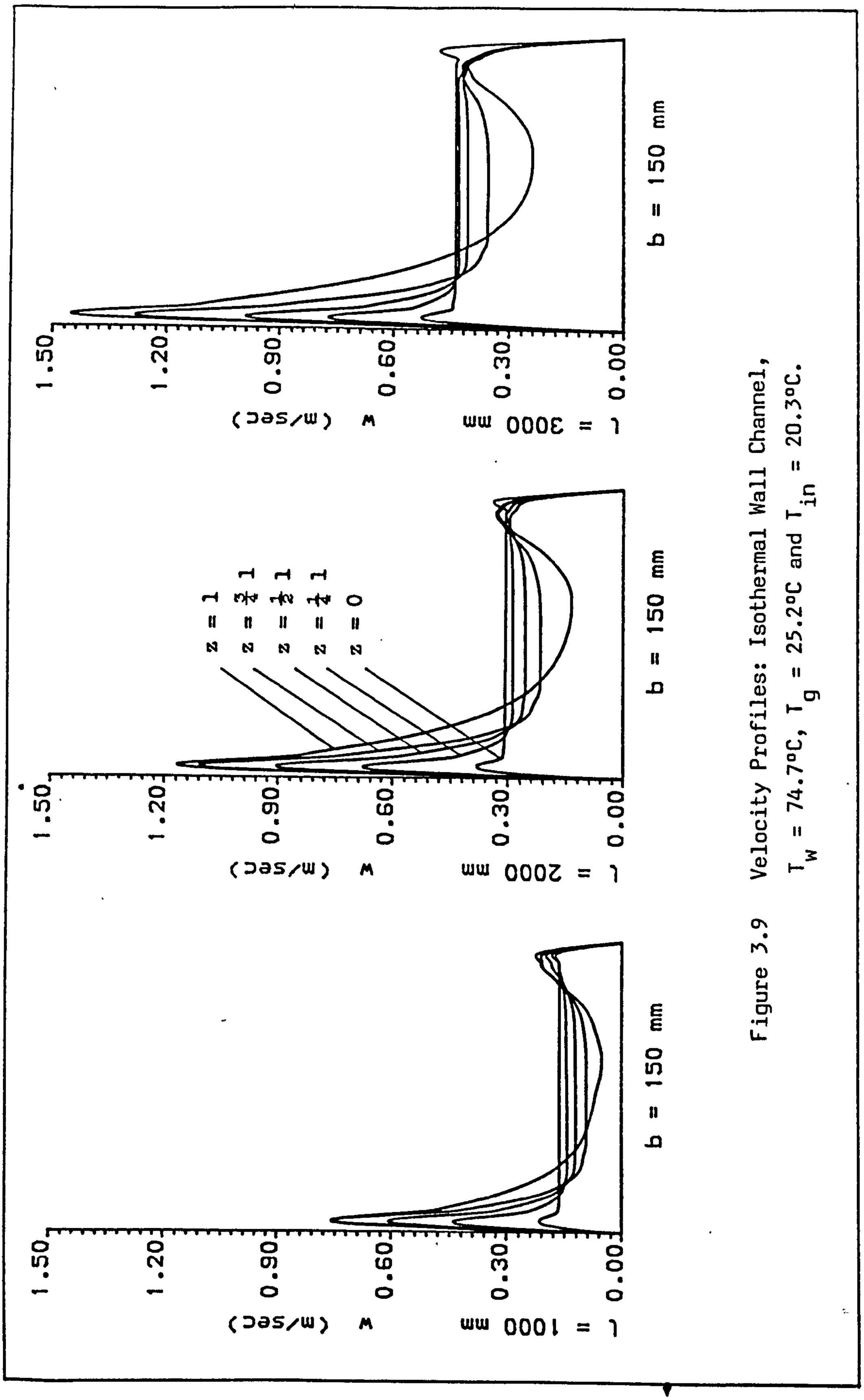

Figure 3.9 Velocity Profiles: Isothermal Wall Channel, T_w = 74.7°C, T_g = 25.2°C and T_{in} = 20.3°C.

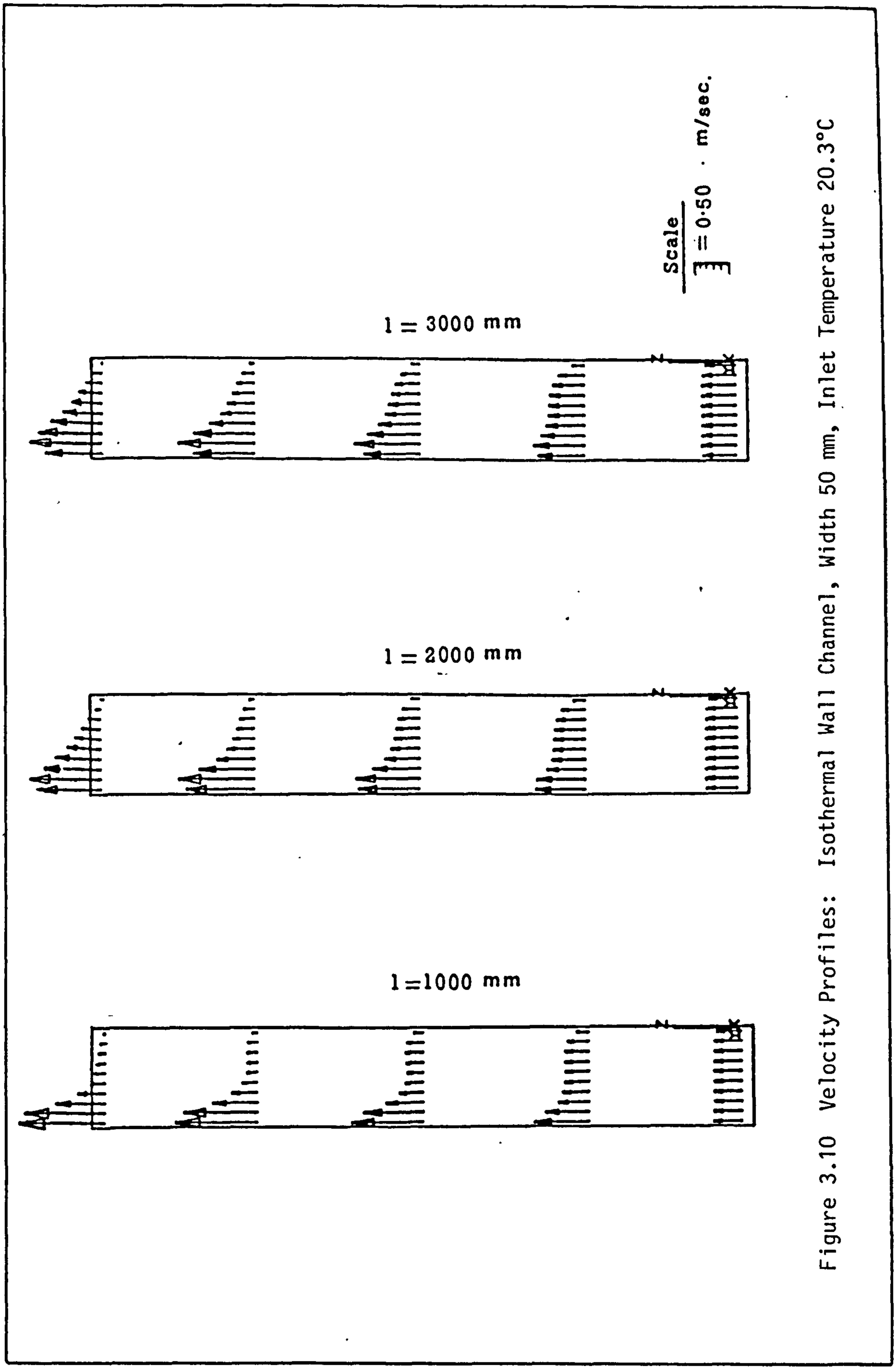

Figure 3.10 Velocity Profiles: Isothermal Wall Channel, Width 50 mm, Inlet T

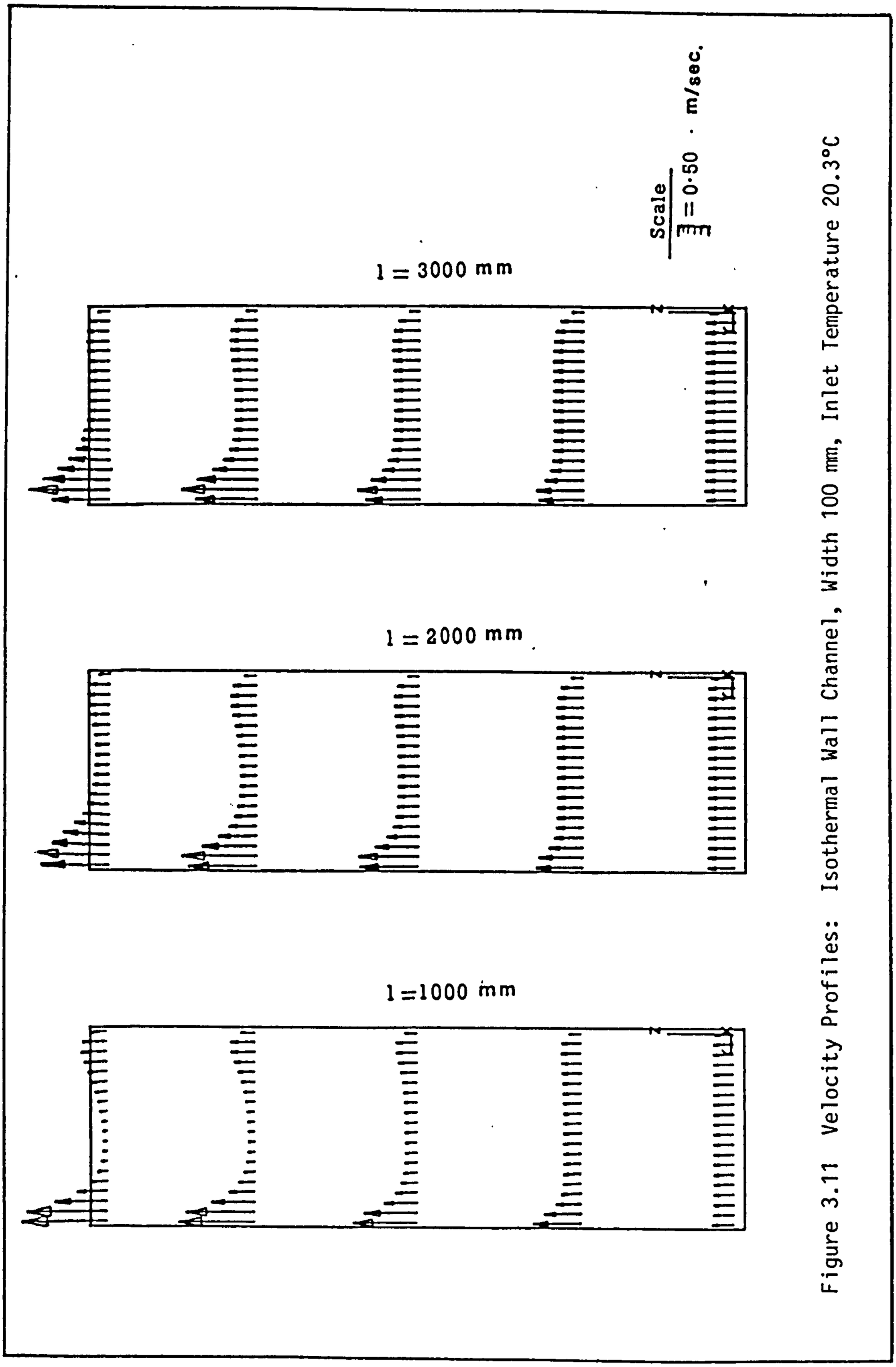

Figure 3.11 Velocity Profiles: Isothermal

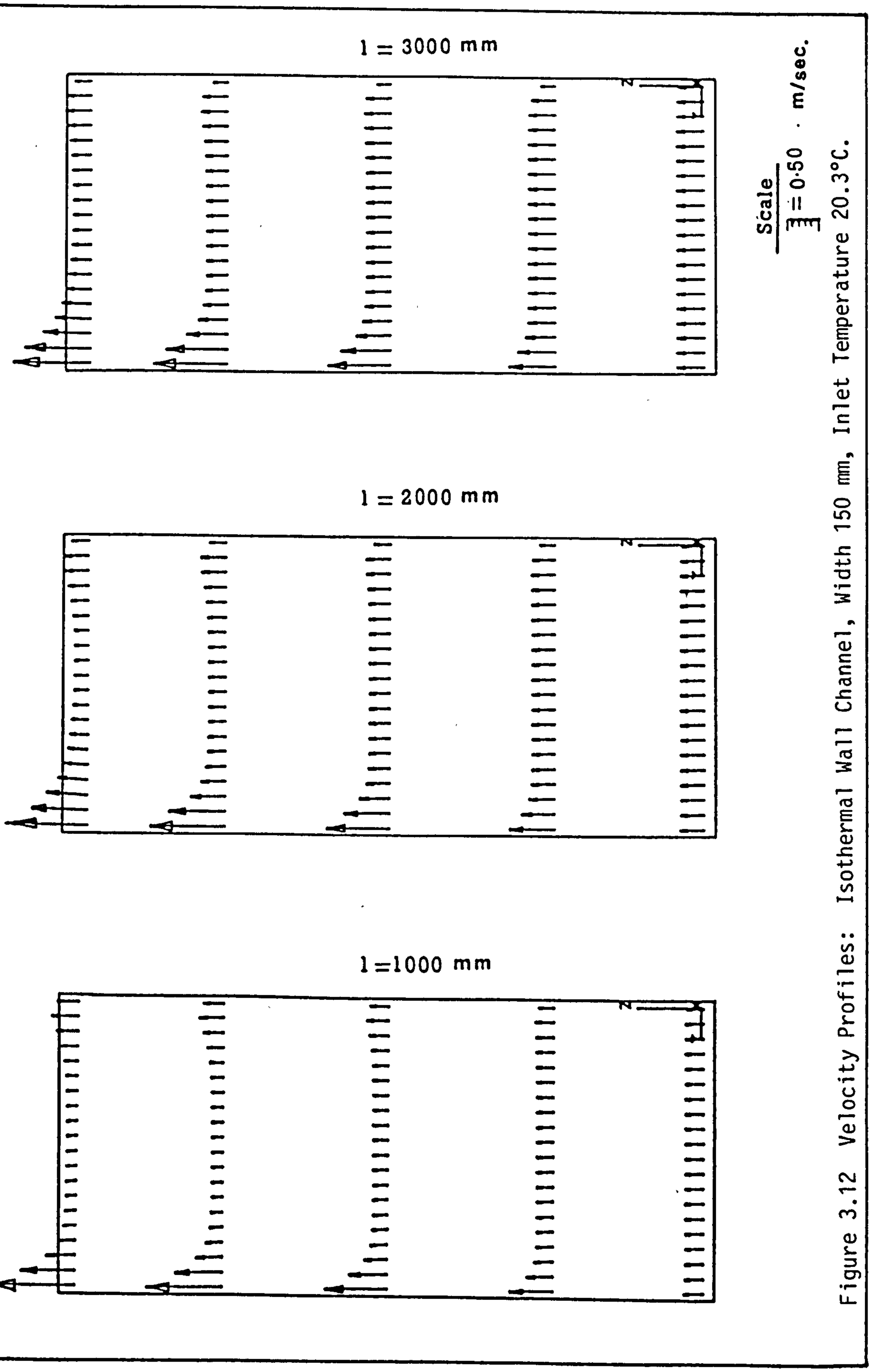
l = 3000 mm
l = 2000 mm
l =1000 mm
Scale
1 = 0·50 · m/sec.
Channel, Width 150 mm, Inlet Temperature 20.3°C.
Velocity Profiles: Isothermal Wall C

Figure 3.12 V

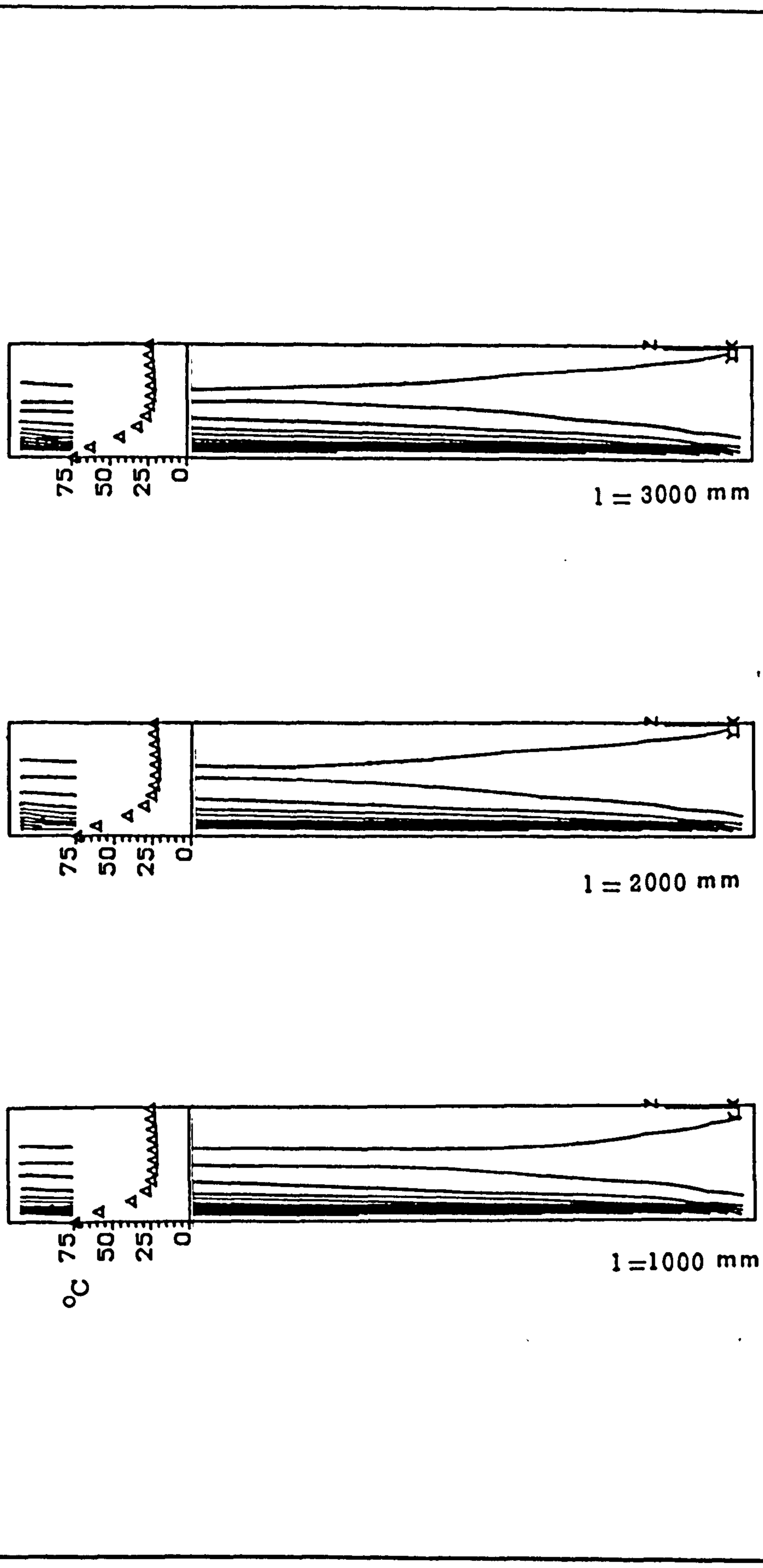

Figure 3.13 Isothermal lines: Isothermal Wall Channel, Width 50 mm, Inlet Temperature 20.3°C

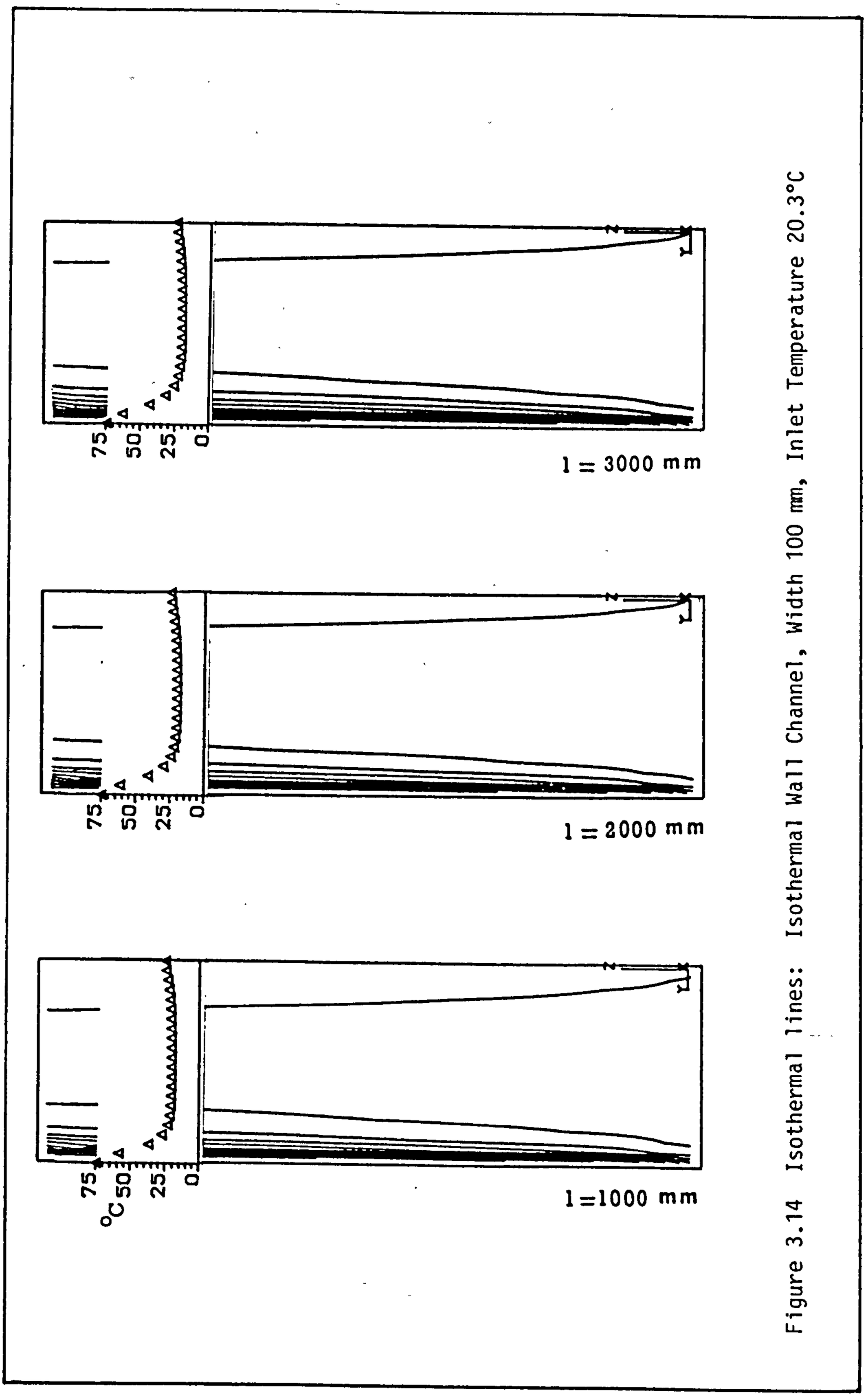

Figure 3.14 Isothermal lines: Isothermal Wall Channel, Width 100 mm, Inlet Temperature 20.3°C

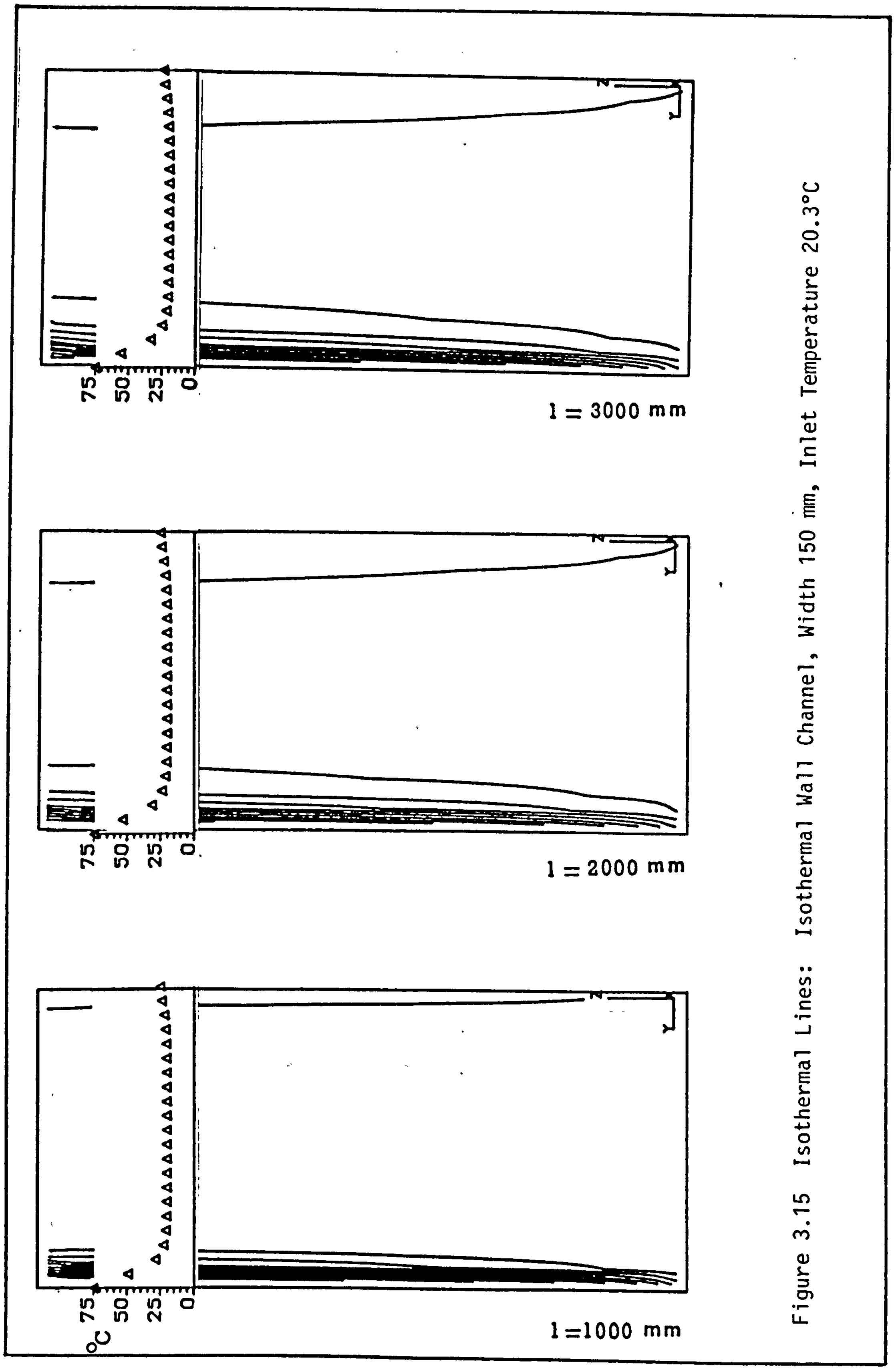
°C
75
50
25
0
l = 3000 mm
l = 2000 mm
l=1000 mm
Figure 3.15 Isothermal Lines: Isothermal Wall Channel, Width 150 mm, Inlet Temperature 20.3°C

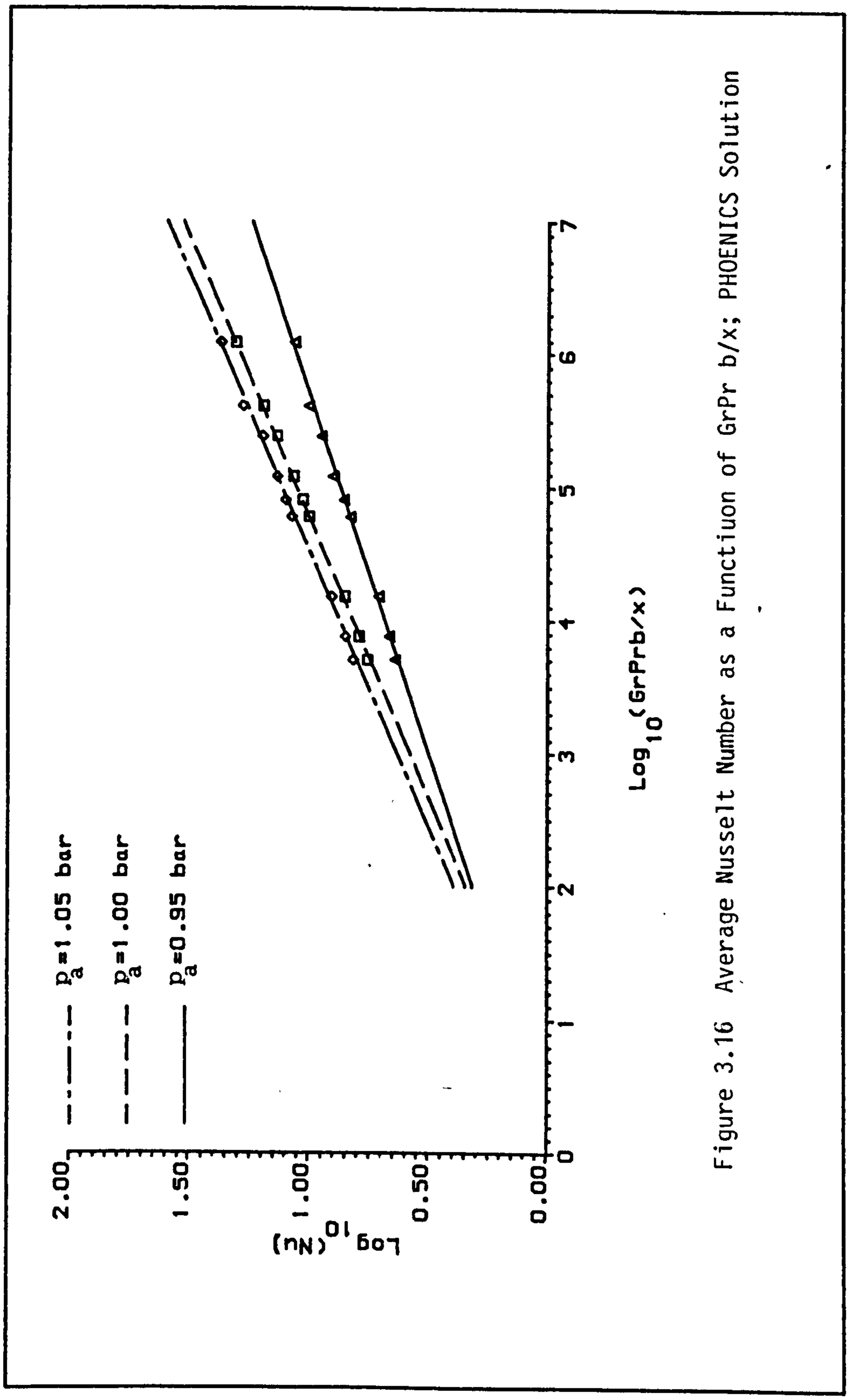

Figure 3.16 Average Nusse

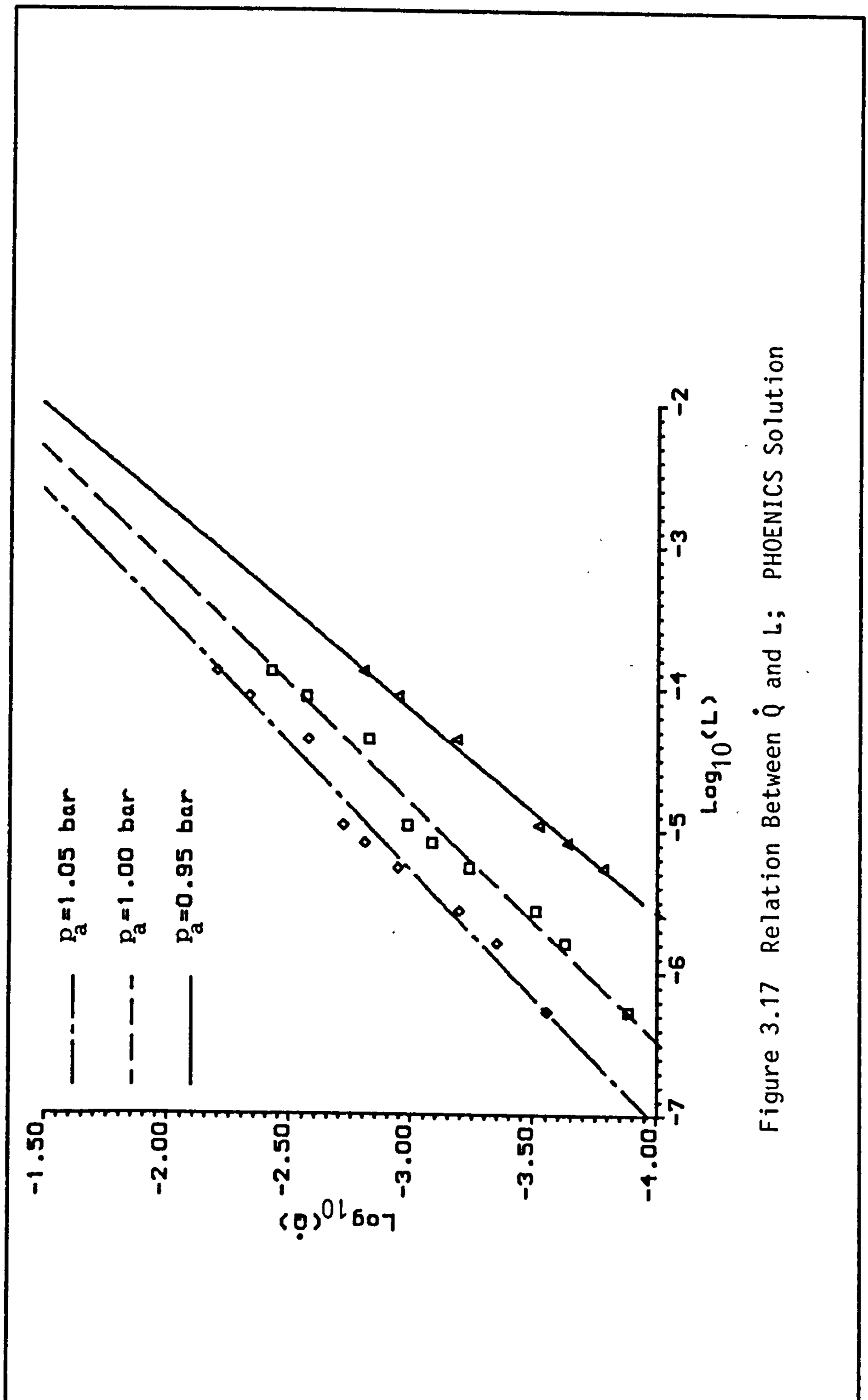

Figure 3.17 Relation Between $\dot{Q}$ and L; PHOENICS Solution

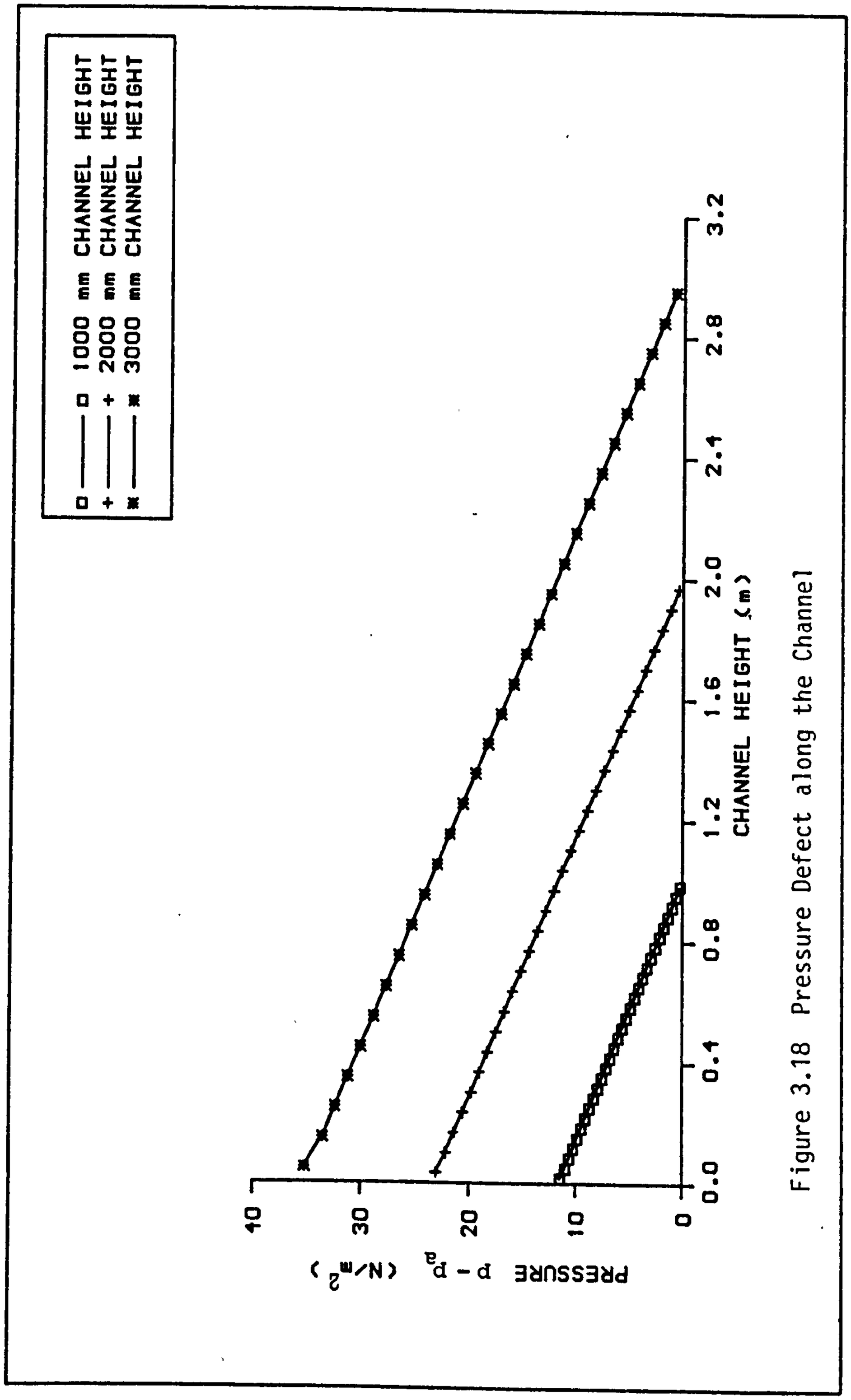

Figure 3.18 Pressure Defect along the Channel

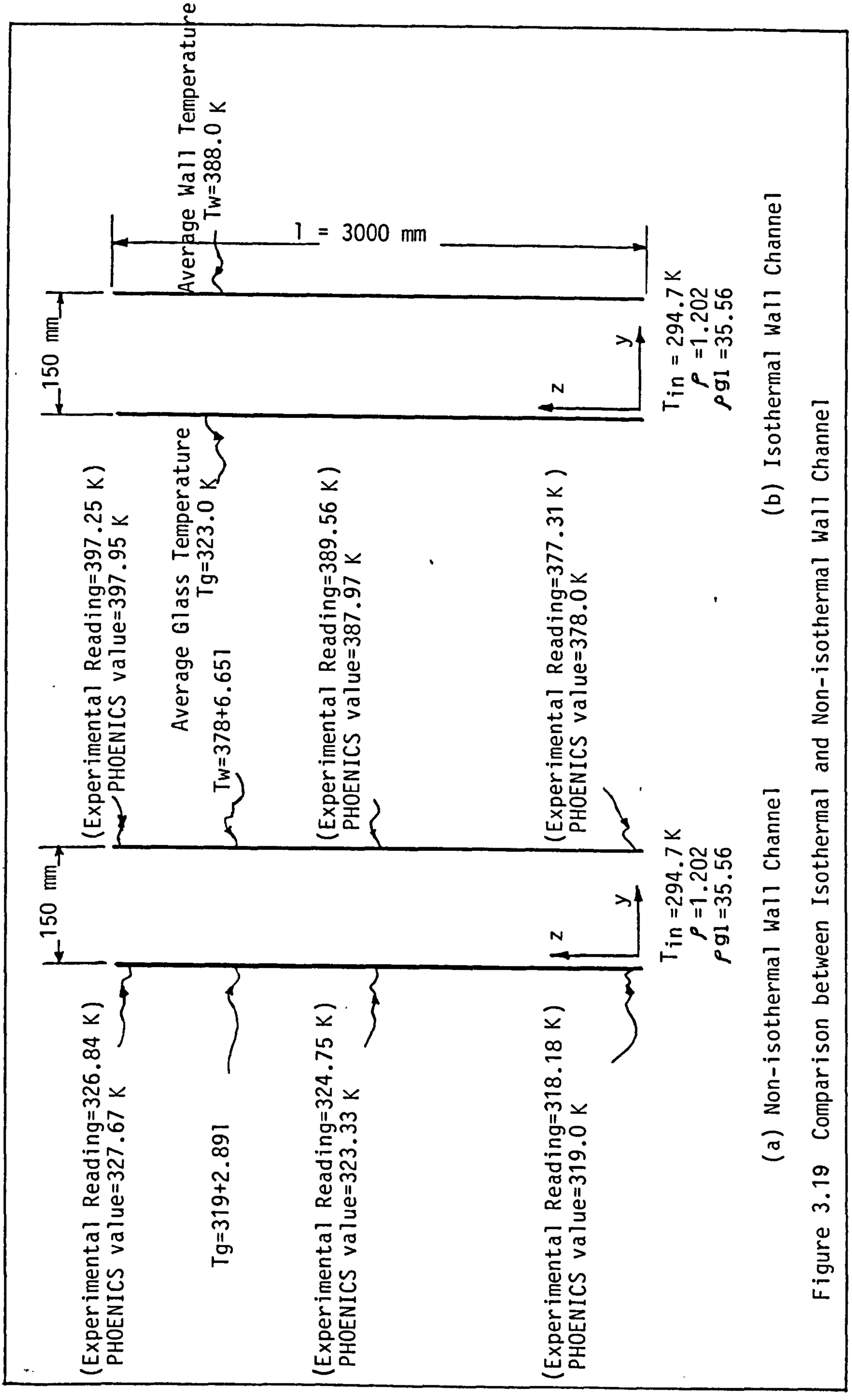
Average Wall Temperature
Tw=388.0 K
l = 3000 mm
150 mm
(Experimental Reading=397.25 K)
PHOENICS value=397.95 K
Average Glass Temperature
Tg=323.0 K
78+6.651
(Experimental Reading=389.56 K)
PHOENICS value=387.97 K
(Experimental Reading=377.31 K)
PHOENICS value=378.0K
z
y
Tin = 294.7 K
ρ =1.202
ρgl =35.56
(b) Isothermal Wall Channel
d Non-isothermal Wall Channel
150 mm
(Experimen
PHOENI
Tw=378
(Experimen
PHOENICS
(Experimen
PHOENICS
(Experimental Reading=326.84 K)
PHOENICS value=327.67 K
Tg=31
319+2.891
(Experimental Reading=324.75 K)
PHOENICS value=323.33 K
(Experimental Reading=318.18 K)
PHOENICS value=319.0 K
z
y
Tin =294.7 K
ρ =1.202
ρgl =35.56
(a) Non-isothermal Wall Channel
e 3.19 Comparison between Isothermal and N

Figure 3

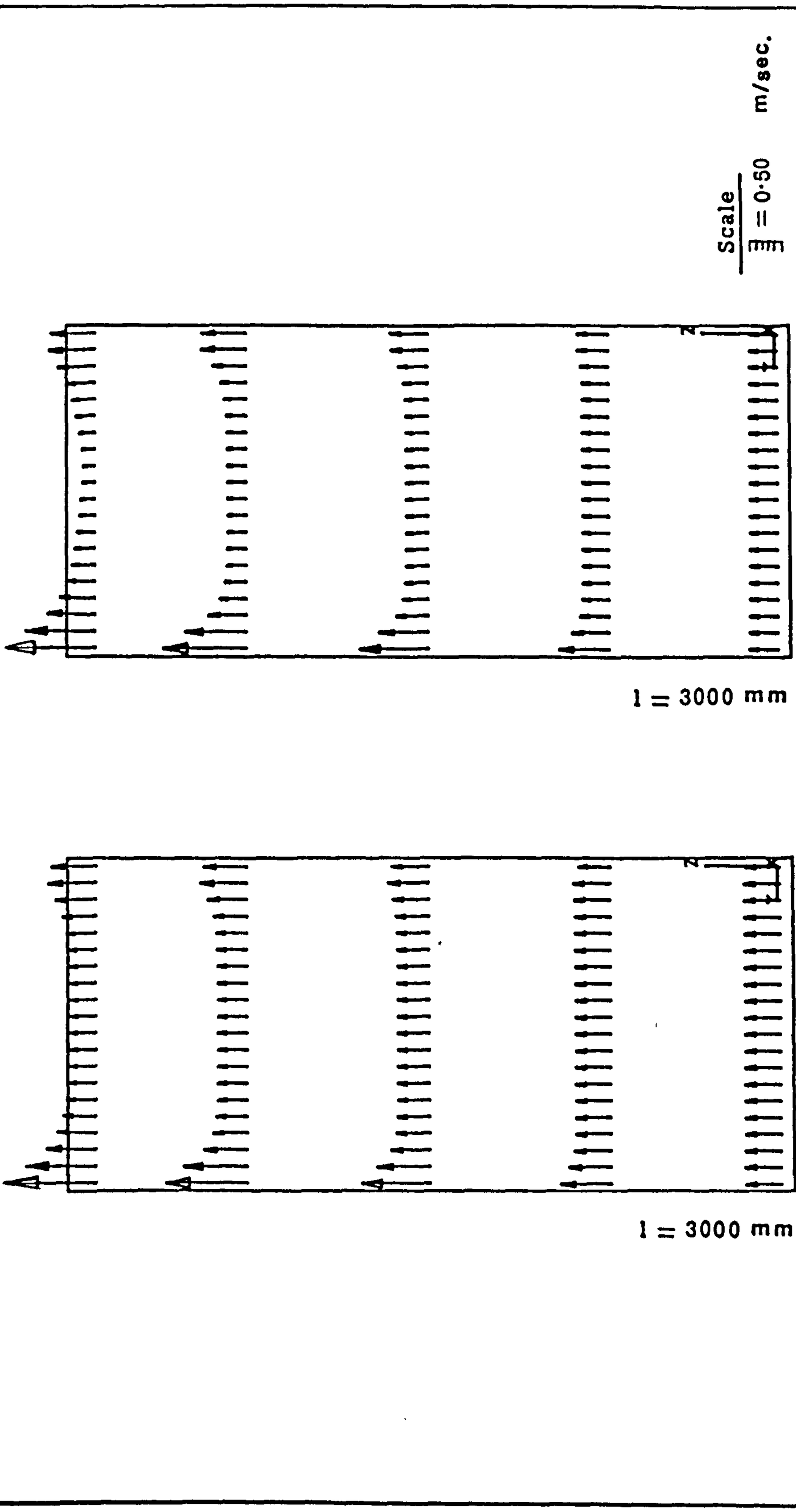

Figure 3.20 Comparison Between the Velocity Profiles of the Isothermal and Non-isothermal Wall Channel at 150 mm Width.

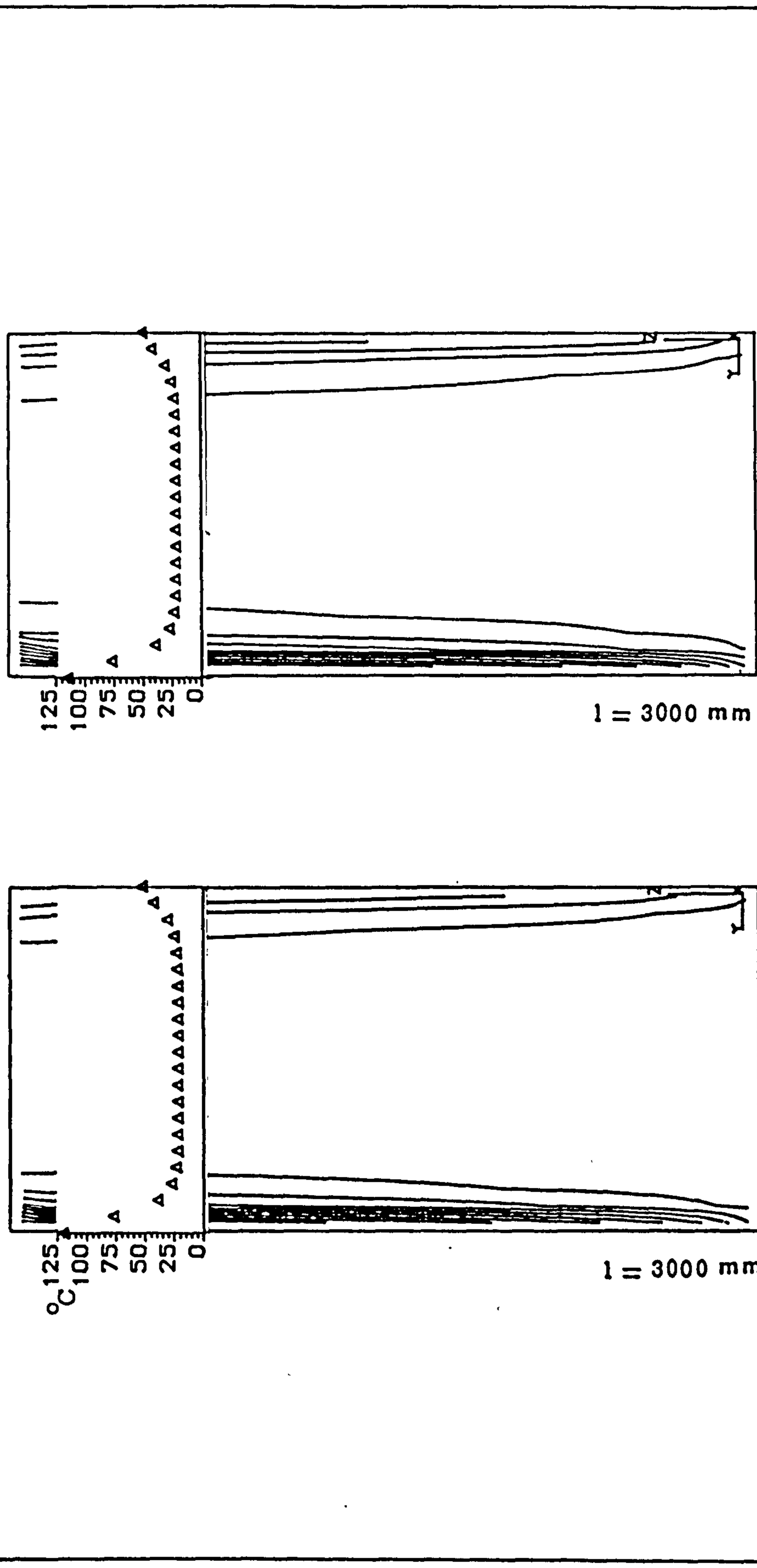

Figure 3.21 Comparison Between Isothermal and Non-isothermal Wall at 150 mm Width Channel

USER: CLCR07 FILE: REFALLGNEWA PLOT NO: 1 DATE: 19-AUG-87

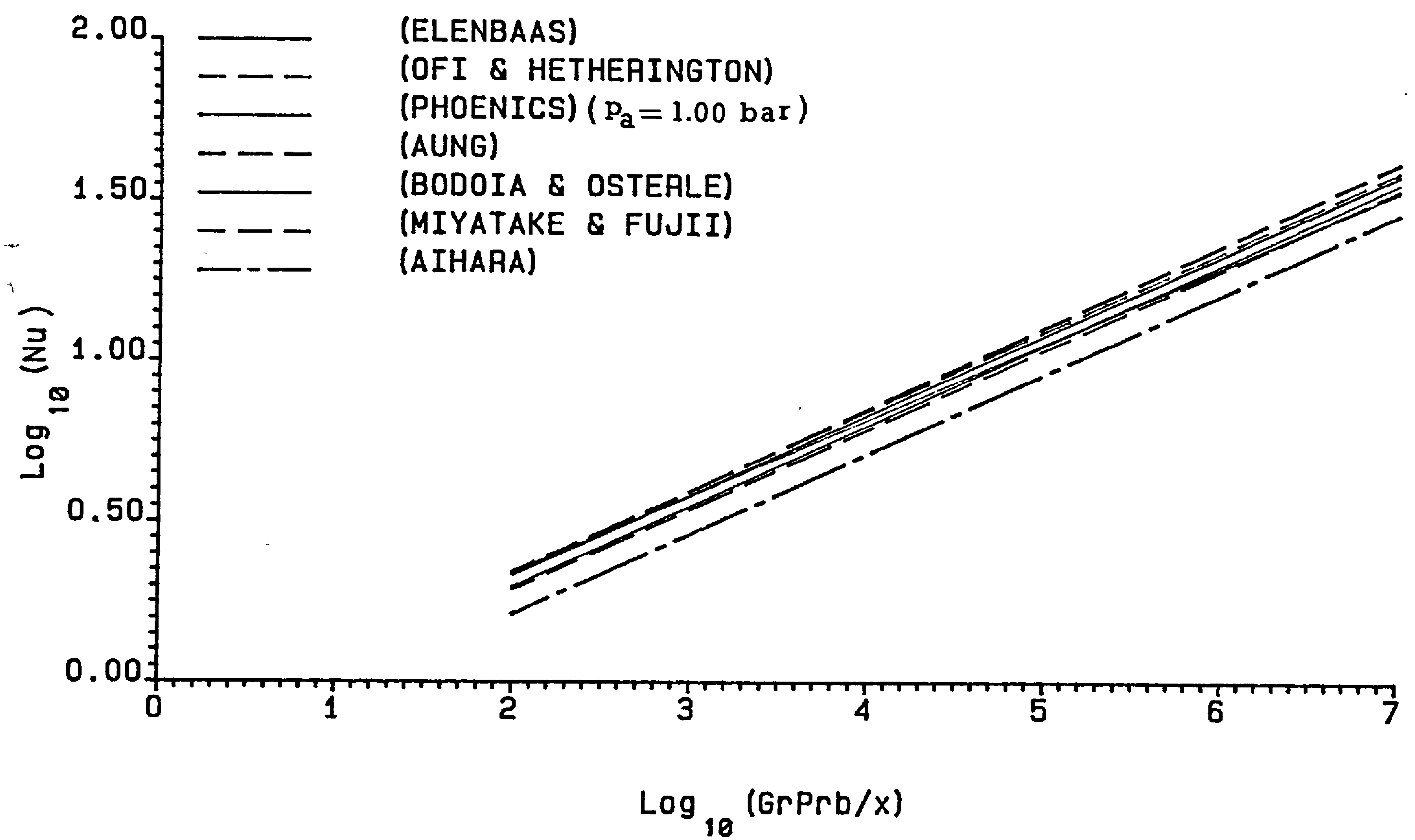

Figure 3.22 Comparison between PHOENICS Solution and Existing Results for Air .

CHAPTER 4

Experimental Apparatus, Procedures and Measurements

4.1 Introduction

In order to make logical comparisons between experimental and theoretical results it was essential to design the experimental apparatus to conform closely with the assumptions required for the theoretical analysis. This Chapter describes the experimental apparatus and procedures used to obtain data for analysis and comparison with the theoretical solution discussed in Chapter 3.

The description of the experimental rig is given in detail in Section 4.2.

The experimental work was performed in six parts.

The first part was the measurement of the heat loss through the rear of the heater plate assembly.

The second part was the determination of the variation of the incident radiation over the test plate at fixed distances from the solar simulator.

The third part formed the major portion of the experimental work. Tests were performed to determine the

air flow rates and heat transfer coefficients for different constant wall temperatures and ranges of the channel width and height. Tests were also performed with the solar simulator lamps operating at full and half power and with the wall temperature controls adjusted as for the constant wall temperature tests. Tests were also conducted using the solar simulator as the sole source of energy input.

The fourth part involved repeating some of the above tests but with diffuser sections at the channel inlet and outlet.

The fifth part was a study of transient conditions in the channel.

Finally, the sixth part was concerned with the effects of the ambient humidity and pressure on the fluid flow in the channel.

The objectives of the experimental work may be summarised as follows:

(a) To obtain experimental data regarding flow in vertical parallel wall ducts over ranges of the variable parameters.

(b) To obtain data for comparison with results obtained using the computational procedure presented in Chapter 3.

(c) To provide data for use in the design of heated vertical parallel wall ducts.

(d) To obtain results for comparison with those of other workers.

4.2 Description of Apparatus

The location of the experimental rig was of importance in order to eliminate extraneous draught effects which could affect the accuracy of measurements since it was anticipated that the air velocities in the channel would be very small. The required area, height, air draught effects and power supply were considered when choosing a suitable site within the laboratory. The test rig was erected within an enclosure surrounded by four wooden side walls and open at the top. The dimensions of the enclosure were 3.64 m x 4.17 m and height 3.675 m. A sliding door was arranged on one wall of the enclosure to allow access. Figure 4.1 shows a view of the enclosure within the laboratory.

The experimental rig is shown in Figure 4.2 and consisted of the following major components:

(a) Heater plate assembly

(b) Velocity probe and thermocouple assembly and positioner

(c) Power supply and control system

(d) Glass wall assembly

(e) Side walls

(f) Supporting structure, and

(g) Solar simulator system.

Each of the above items are described in the following Section.

4.2.1 Heater Plates

Two heater plates, one 1 m long and one 2 m long and each 1 m wide were used. The heater plate assemblies consisted of aluminium plates (6.35 mm thick), resistance heater elements, insulation material and a plywood support board. It was ensured that the plates were flat and studs were fitted on the rear side to permit attachment of the plate to a 19 mm thick plywood support board. The side of the plates in contact with the air flow was carefully polished to remove any scratches.

Heater Elements

The electrical resistance heating elements were cut from 0.35 mm thick sheets of a graphite material, trade name SIGRAFLEX F2010, details of which are given in Appendix G. To determine the best shape and dimensions for the heater element, small scale tests were carried out using various element geometries. Eventually a design was obtained which gave the required temperature levels with uniform temperature distribution over the plates. The geometry of the full size elements is shown in Figure 4.3. The elements were cut from the SIGRAFLEX sheeting with the

aid of an accurately made template. For the 1 m and 2 m plates three and six separate heater elements respectively were used.

Insulation Material

The insulation material used was thin sheets of TRITON KAOWOOL ceramic fibre paper 0.5 mm thick and also 25 mm thick board of the same material. This material has good electrical insulation properties as listed in Appendix H. Two layers of the insulation paper sheets were placed on the back of the aluminium plate. The insulation sheets were placed between the aluminium plates and the resistance heater elements to provide electrical insulation between the plates and the elements. The insulation board was also cut and accurately placed over the heater elements to minimise heat losses from the heater elements to the environment. Strips of insulation, 25 mm thick, were cut and fitted to cover the sides of the aluminium plates to minimise side heat losses. Insulating mastic was used to join and the fill up any gaps in the insulation assembly. Holes were cut in the insulation board to match the position of the tufnol blocks fitted over the studs, (see Figure 4.3).

Support Boards

These boards were of 19 mm thick plywood board measuring 1 m and 2 m respectively in length and 1012 mm width as shown in Figure 4.4. The plywood board was not completely flat and provision had to be made to ensure that it would be flat at all times. This was achieved by using

a 25 mm square section channel to make a frame which was then securely attached to the plywood board. This then formed the main support for the heating plate. Holes were drilled in the plywood board to accommodate the studs attached to the heater plate.

The electrical terminal blocks for the heating elements were made from tufnol of 25 mm thick with a central hole. The blocks were positioned under the heater element ends and secured to the plywood board by means of two screws. A brass bolt with a relatively large washer was placed through the heater element ends and the terminal block holes and tightened onto the heating element using a washer and nut. The input power supply leads were firmly attached to the bolts of the terminal blocks.

The construction of the support steel frame for the heater plates consisted of a simple angle iron frame of the required length to take the three metres maximum length required. A frame made of angle iron was used to hold the complete heater plate assemblies and this frame was used for mounting the assembly on to the tubular steel supporting structure (see Figure 4.2). It was ensured that the surface of the heater plates were truly vertical when attached to the supporting framework. The steel frame was mounted on to the scaffolding structure at a level of 555 mm from the floor. The heater frame assembly is shown in Figure 4.2.

4.2.2 Power Supply and Control System

There were three separate heater elements, which could be controlled individually, for each metre height of plate. This was done for the 1 metre height experiments only and thereafter groups of elements were combined in series and controlled through one variac per group of elements. Each variac was connected to a suitably arranged electric circuit consisting of ammeter, voltmeter and terminals installed in a box which allowed for both direct and continuous current and voltage readings. Also current and voltage could be read by a portable, high accuracy, ammeter and digital voltmeter which could be plugged into the terminals as desired so that the meter readings could be frequently checked as shown in Figure 4.5.

4.2.3 Heater Plate Back Losses

The object of these experiments was to measure the heat loss through the back of the heater plate assembly. To calculate this value, the temperature distribution through the insulation board and plywood had to be obtained. The actual temperature values were measured at the inside and outside surface of the insulating board and also at the back surface of the plywood board. At six different locations on the back of the heater plate assembly, holes were drilled to the required depths and thermocouples were inserted as shown in Figure 4.6. The thermocouples were then connected to a HP Multiprogrammer / Interface Unit which could feed the temperature readings directly into the HP-9845B computer. The same input power supply for each heater element, i.e. input power = I*V, was set using the

ammeters and voltmeters in the power supply control assembly box and fine adjustments were carried out from time to time to maintain constant input power supply. The system was then allowed to stabilise for two hours and a set of readings taken. The input power was then increased and the procedure repeated.

It was assumed for simplicity that heat conduction through the heater plate assembly materials was one-dimensional steady-state and the heat losses from the edges were negligible in comparison with those from the back. The thermal loss through from the back of the assembly was then calculated by using Fourier's Law for heat conduction in a one-dimensional composite slab, as shown in Figure 4.7, i.e.

$$Q_{cond.} = \frac{T_A - T_C}{\frac{x_A}{k_A} + \frac{x_B}{k_B}} \qquad (4.1)$$

where $Q_{cond.}$ = Heat conduction in the x-direction (W/m^2)

k_A = Thermal conductivity of the insulation = 0.07 (W/m.C)

k_B = Thermal conductivity of the plywood = 0.08 (W/m.C)

T_A = Temperature at the insulation surface (°C)

T_C = Temperature at the back of the plywood board (°C)

x_A = Thickness of the insulation = 0.025 (m)

x_B = Thickness of the plywood board = 0.019 (m)

The locations where measurements were taken are shown in Figure 4.6.

The temperature data obtained from the experimental tests are tabulated in Tables 4.1 to 4.5. Readings for point 3 are shown separately in Figure 4.8.

Figure 4.9 shows the variation of overall back heat loss against heater input power supply at each of the six measuring points. This figure also shows that the heat loss increased with increase in input power supply in a similar manner at each point. The heat loss at points 3 and 6, as shown in Figure 4.6, is always at a higher value than for the other points because locations 3 and 6 are at the bottom of the heater plate near the horizontal working platform, which reduced the circulation of air in this region, resulting in higher surface temperature readings. The heat losses at points 2 and 5 are less than the losses from points 1 and 4 because the back plate assembly, despite having a strengthening member projecting from it, acts mainly as a heated vertical flat plate and hence the natural convection heat transfer coefficient reduces with height.

The losses through the back of the insulation are seen to be a considerable percentage of the input power, varying from 26% to 49% for input powers of 60 W and 160 W respectively as presented in Table 4.6 and shown plotted in Figure 4.10. In assessing these losses it was appreciated

Table 4.1 Temperature Readings and Calculations at Heater Input Power = 60.0 Watts

HEATER INPUT POWER = 60.0 WATTS

AMBIENT TEMPRATURE = 20.3 C

POINT	TA	TB	TC	QLOSS
1	35.33	26.85	22.93	20.85
2	33.64	26.12	22.20	19.24
3	39.65	27.35	24.17	26.03
4	37.74	26.13	23.93	23.23
5	31.47	25.63	20.96	17.68
6	41.54	26.61	23.92	29.63

Table 4.2 Temperature Readings and Calculations at Heater Input Power = 100.0 Watts

HEATER INPUT POWER = 100.0 WATTS

AMBIENT TEMPRATURE = 21.3 C

POINT	TA	TB	TC	QLOSS
1	45.87	32.51	26.79	32.09
2	43.11	30.81	25.21	30.10
3	53.67	34.04	28.71	41.98
4	50.64	32.11	27:98	38.11
5	40.18	29.84	23.74	27.65
6	56.61	32.75	27.65	48.71

Table 4.3 Temperature Readings and Calculations at Heater Input Power = 120.0 Watts

HEATER INPUT POWER = 120.0 WATTS

AMBIENT TEMPRATURE = 22.2 C

POINT	TA	TB	TC	QLOSS
1	50.99	36.07	28.58	37.69
2	47.91	34.15	27.37	34.54
3	60.61	37.17	30.90	49.97
4	56.46	35.01	30.18	44.20
5	44.41	33.49	25.41	31.95
6	63.23	35.35	30.04	55.82

Table 4.4 Temperature Readings and Calculations at Heater Input Power = 140.0 Watts

HEATER INPUT POWER = 140.0 WATTS

AMBIENT TEMPRATURE = 22.5 C

POINT	TA	TB	TC	QLOSS
1	55.23	38.28	29.86	42.67
2	52.40	35.65	28.88	39.56
3	66.61	39.86	32.43	57.48
4	62.28	37.24	31.70	51.43
5	48.27	34.44	26.43	36.73
6	68.06	38.04	31.31	61.81

Table 4.5 Temperature Readings and Calculations at Heater Input Power = 160.0 Watts

HEATER INPUT POWER = 160.0 WATTS

AMBIENT TEMPRATURE = 23.2 C

POINT	TA	TB	TC	QLOSS
1	59.10	39.42	30.04	48.87
2	55.64	36.79	28.83	45.09
3	71.83	41.78	33.41	64.61
4	66.86	39.17	32.93	57.06
5	51.51	37.10	27.67	40.09
6	73.26	39.72	32.04	69.32

Table 4.6 Heater Plate Assembly Percentage Heat Loss

POWER	POINT 1	POINT 2	POINT 3	POINT 4	POINT 5	POINT 6
60.0	34.75	32.06	43.38	38.70	29.46	49.38
100.0	33.08	30.10	41.98	38.11	27.65	48.71
120.0	31.40	28.78	41.64	36.83	26.62	46.51
140.0	30.47	28.25	41.05	36.73	26.23	44.14
160.0	30.54	28.18	40.38	35.66	25.05	43.33

that edge effects were present and probably contributed to an error in the calculated values.

The thermocouple located closest to the heater element might have been in a region where two-dimensional conduction existed and, in addition, contact between the wood and insulation was probably not perfect, which would also result in an under prediction of the losses. However, since uniform working plate temperatures could be achieved even with those losses, no further refinement of the insulation at the back was considered necessary.

4.2.4 Glass Wall Assembly

The glass wall was formed by two clear glass sheets of 4 mm thickness and 1010 mm x 1006 mm with 12 mm air gap between them. The glazing frame was manufactured using 40 mm square section mild steel tube. This was made into a 1024 mm x 3100 mm rectangular frame as shown in Figure 4.2. An important feature of the glazing support frame was the adjusting screws on each side which allowed the frame to be accurately moved in and out at the required distance of 6 to 300 mm from the aluminium plate.

Side Walls

The sides of the channel were sealed with hardwood side walls to prevent entrainment of air. Six sizes of the hardwood side walls of 25, 50, 75, 100, 125 and 150 mm width and approximate length were used corresponding to the required channel width.

Supporting Structure

This was made from steel scaffolding tubing of 48 mm diameter fitted together by elbows and T-fittings to take a channel size of 1280 x 4530 mm. It was made level horizontally, and plumbed vertically. The structure was screwed to the floor at the bases with rawl bolts. A tubular structure was erected on which to hang the solar simulator as shown in Figure 4.2. The power supply and control assembly were placed on a platform behind the heater plate assembly. The data acquisition system, the selector switches and the digital thermometer were also placed on a platform behind the heater plate assembly.

4.3 Temperature and Velocity Measurements

The velocity probe and three thermocouples for air velocity and temperature measurements in the channel are supported by a brass tube of 11 mm diameter which was attached to a carriage, the movement of which was controlled by a fine - threaded screwed - rod, with an attached vernier scale. During a test run, lateral movement across the channel could thus be obtained easily, while the whole assembly had to be moved to measure air temperatures and velocities at different vertical locations. The probe and thermocouples were located 153 mm upstream of the brass support tube.

Figure 4.11(a) shows the air velocity probe, thermocouples and carriage and Figure 4.11(b) shows the scale positioner.

The temperatures were measured by T-type (copper-constantan) thermocouples. All thermocouples were connected to two multipoint selector switch boxes to enable different banks of thermocouples to be read. Some thermocouples were connected by jumper connections between the boxes and a digital electronic thermometer via a multipoint selector box for direct reading and observation. The thermocouple outputs were connected to two HP 69432A Scanner and Analogue/Digital convertor cards in the HP 6940B Multiprogrammer. The multiprogrammer controls the bi-directional multiprogram system, i.e. output data distribution/input data multiplexing. However, the initiation of data collection is from the programmed computer HP 9845B via HP Multiprogrammer. The collected data is then transmitted to the computer for processing, display and storing on a casette.

Temperatures of the glass, the heated plate and the air were determined at a number of different vertical locations. To obtain good average values, three thermocouples were installed at fixed heights across the plate and glass while air temperatures were determined using the air velocity and temperature probe, which could be adjusted to any height.

The air flow velocity in the channel was measured using a hot-wire anemometer, (PSI AVM 502 Prosser Scientific Instruments Ltd) low flow air velocity meter with calibration board PCB incorporated. This device employed the principle of constant temperature operation

and incorporated a temperature compensating device which maintained the hot-wire at a constant temperature above that of the air stream. The measurement probe of the AVM consists of a thermistor which is sensitive to heat transfer between the element and the ambient environment. The electrical control system maintains the heated element at a constant temperature by utilising a feedback bridge circuit. The power required to keep the temperature constant is an analogue indication of the air velocity being measured where the rate at which heat is lost from the thermistor is proportional to the velocity of the air passing over it. The working velocity range at 0 - 3 m/sec, ambient temperature between 0 - 50°C.

A TA 400 (Airflow Developments Ltd) thermal anemometer was used to measure airstream velocity in the channel when the air temperature was higher than 50°C. The thermal anemometer covers the range 0 - 2 m/sec at ambient working temperatures 0 - 80°C. When the probe is held in the airstream an instantaneous and direct temperature or air velocity reading is obtained. The velocity sensitive element is a tiny thermistor bead mounted in the probe head. Air velocity is measured by metering the amount of electrical energy required to maintain the bead at a constant 150°C. To compensate for variation in airstream temperature the anemometer has a second, unheated thermistor incorporated in the probe.

4.4 Solar Simulator System

The solar simulator, in the experiments, only increased the temperature of the glass, the plate and nothing else. So in that sense was just another source of heat and really no different from the heating at the back of the plate.

The investigation of air flow in a heated duct is related to solar induced air flows in Trombe wall systems. To reproduce this kind of heating i.e. solar heating, it was decided to provide additional heating capability by installing a bank of lamps simulating solar intensities of about 1200 W/m^2 at 100 cm. This had the merit of not only simulating solar heating if only the lights were used but of providing additional heat, enabling higher plate temperatures to be obtained, if run in conjunction with the heated plate.

The solar simulator is a device which produces the same intensity and distribution of irradiance as that of the natural sunlight, Geisheker (81). Solar simulation is a useful method of testing a solar collection system because all the performance characteristics can be determined by varying each parameter independently, Ragsdale (82) and Duffie (83).

The solar simulator test facility was constructed so that the system could be tested under known, controllable and variable conditions. A photograph of the solar simulator is shown in Figure 4.12. The simulator uses 50 Tungsten Halogen Lamps, 150 W each, type 27 PAR 38 (manufactured by Thorn Lighting Ltd). This layout provided short-wave irradiance (0.3 to 3.0μm), Othieno (84), Grainger (85).

The lamps were distributed and fixed to a Dexion Steel frame 1200 x 3400 mm which was hung vertically from the overhead scaffolding frame and clamped in position parallel to the aluminium plate. The lamps were in three independent groups and connected in parallel. Each group was connected to a separate variac transformer the intensity of which was varied by adjusting the lamp input voltage to give the desired light intensity level. Experiments were carried out on full and half power with different channel gap widths, heights and plate temperatures.

4.4.1 Radiation Measurement Instruments

The equipment used to take the radiation readings was a tube solarimeter, type TSM 803 (manufactured by Delta-T Devices) which was linked to a chart recorder, SERVOSCRIBE type RE 511 (manufactured by GOERZ ELECTRO). This Solarimeter produces a millivolt output which is recorded directly by a chart recorder to give the solar energy received by the surface over a period of time. The most important feature of the solarimeter is the detector which

is enclosed in a tube of PYREX glass which is transparent to visible radiation. The detector consists of alternate matt black and white sections which reach different equilibrium temperatures when exposed to radiation. The junctions of a thermopile embedded in the black and white sections respond to the temperature difference and generate a millivolt output which is directly proportional to the irradiance.

The tube solarimeter is supplied calibrated at 15 mV per kW/m^2.

A Kipp and Zonen solarimeter type CM 10 was also used to measure the radiation level and check the readings against the tube solarimeter readings. The solarimeter was connected to an integrator display unit type TI-1750 (manufactured by Delta-T Devices). This solarimeter produces a millivolt output which was displayed directly by an integrator display unit. The solarimeter consists of three parts: (a) the detector consists of 100 thermocouples imprinted on a ceramic substrate using thick film techniques responding to the temperature difference and generates a millivolt output which is directly proportional to the radiation incidence level. The arrangement of the thermocouples is circular, resulting in a low azimuth error, (b) the detector is enclosed in two hemispheres of clear glass which are transparent to radiation, and (c) a white circular disk. The solarimeter and the integrator display unit are calibrated at 5.78 mV per kW/m^2 and 1 count = 10 mV.second respectively:

4.4.2 Irradiance Test Procedure

The radiation reaching a plane at a fixed distance from the lamps was measured using the tube solarimeter. As a check on the accuracy of the tube solarimeter, a number of readings were taken at selected positions using the Kipp and Zonen solarimeter.

A frame of 1 m width x 3 m length using Dexion of 40 x 40 mm which was hung vertically from the overhead scaffolding of the supporting structure and clamped in position. The support for the tube solarimeter consisted of two metal clips to which it was fixed by adhesive and these clips were then bolted to the flat face of another piece of Dexion. It was important to ensure that the detector surface of the tube solarimeter was parallel with the lamps. This piece of Dexion could be clamped horizontally to the frame at all the required levels. The vertical length of the working plane was divided into 18 levels. To obtain the required overall variation readings were taken with the tube solarimeter at three positions on each level (i.e. left, right and centre of the plane). This arrangement is due to the length of the tube solarimeter. This was done by unbolting the clips and moving it across the horizontal piece of Dexion. The position of the readings at different levels of the plane and the distance from the lamps are shown in Figure 4.13. Also, two metal clamps were made to hold the Kipp and Zonen solarimeter to the centre of the horizontal piece of Dexion.

Once the frame had been clamped with the tube solarimeter at the first required distance of 0.58 metre from the lamps, all the lamps were switched on. The system was then allowed to stabilise with the tube solarimeter and support clamped at left hand position. Once the reading had been taken on the chart recorder, the tube solarimeter was moved to the centre position, then onto the right hand position. At this point the piece of horizontal Dexion was moved and bolted at the next level, checking that it was still horizontal by means of spirit level. The same procedure was then carried out at each level through out the length of the working plane. Measurement data are presented in Subsection 4.4.3.

4.4.3 Irradiance Test Results

The measurement data are listed in Tables 4.7 to 4.11 and are shown plotted in Figures 4.14 to 4.18. The Figures show the variation of the incident radiation on the working plane at different positions for the plane at different distances from the lamps. They show, as expected, that the intensity reduces as the distance from the lamps is increased and that it is not directly proportional to the distance. The Figures show that for each case the radiation flux is greater in the middle than at the edges. In Figure 4.14 it is seen that when the lamps were at their closest hot spots were generated by the light rays intersecting at the working plane and that a non-uniform radiation distribution is incident on the working plane.

Table 4.7 Incident Radiation on a Plane at a Distance 580 mm from the Lamps

LEVEL	HEIGHT (cm)	POSITION A	POSITION B	POSITION C	AVERAGE
18	283.323	983.33	1433.33	1133.33	1183.33
17	266.657	803.33	1266.66	1000.00	1023.33
16	249.991	900.00	1506.66	1213.33	1206.66
15	233.325	813.33	1300.00	1233.33	1115.55
14	216.659	1016.66	1406.66	1333.33	1252.22
13	199.993	960.00	1310.00	1106.66	1125.55
12	183.327	966.66	1523.33	1210.00	1233.33
11	166.661	826.66	1456.66	1140.00	1141.11
10	149.995	960.00	1323.33	1240.00	1174.44
9	133.329	993.33	1233.33	1266.66	1164.44
8	116.663	966.66	1240.00	1100.00	1102.22
7	99.997	866.66	1306.66	1023.33	1065.55
6	83.331	1123.33	1340.00	1200.00	1221.11
5	66.665	1306.66	1406.66	1260.00	1324.44
4	49.999	1233.33	1400.00	1310.00	1314.44
3	33.333	1076.66	1186.66	1166.66	1143.33
2	16.666	926.66	1116.66	1100.00	1047.77
1	0.000	870.00	1000.00	960.00	945.55

Table 4.8 Incident Radiation on a Plane at a Distance 1050 mm from the Lamps

LEVEL	HEIGHT (cm)	POISTION A	POSITION B	POSITION C	AVERAGE
18	283.323	600.00	693.33	590.00	627.77
17	266.657	793.33	993.33	740.00	842.22
16	249.991	866.66	1033.33	936.66	945.55
15	233.325	900.00	1193.33	893.33	995.55
14	216.659	953.33	1220.00	1106.66	1093.33
13	199.993	946.66	1236.66	960.00	1047.77
12	183.327	966.66	1216.66	943.33	1042.22
11	166.661	906.66	1246.66	1000.00	1051.11
10	149.995	883.33	1203.33	1006.66	1031.11
9	133.329	873.33	1160.00	1033.33	1022.22
8	116.663	883.33	1100.00	970.00	984.44
7	99.997	893.33	1126.66	963.33	994.44
6	83.331	890.00	1136.66	956.66	994.44
5	66.665	940.00	1170.00	1010.00	1040.00
4	49.999	950.00	1136.66	966.66	1017.77
3	33.333	900.00	1076.66	990.00	988.88
2	16.666	926.66	933.33	830.00	896.66
1	0.000	616.66	776.66	710.00	701.11

Table 4.9 Incident Radiation on a Plane at a Distance 1275 mm from the Lamps

LEVEL	HEIGHT (cm)	POSITION A	POSITION B	POSITION C	AVERAGE
18	283.323	510.00	583.33	483.33	528.88
17	266.657	726.66	800.00	680.00	735.55
16	249.991	733.33	900.00	736.66	790.00
15	233.325	840.00	1000.00	860.00	900.00
14	216.659	823.33	1033.33	800.00	885.55
13	199.993	903.33	1066.66	866.66	945.55
12	183.327	860.00	1066.66	826.66	917.77
11	166.661	876.66	1083.33	896.66	952.22
10	149.995	826.66	1050.00	940.00	938.88
9	133.329	843.33	1013.33	900.00	918.88
8	116.663	850.00	993.33	900.00	914.44
7	99.997	850.00	1003.33	886.66	913.33
6	83.331	860.00	1016.66	886.66	921.11
5	66.665	866.66	1013.33	893.33	924.44
4	49.999	833.33	973.33	860.00	913.33
3	33.333	760.00	890.00	776.66	808.88
2	16.666	693.33	810.00	713.33	738.88
1	0.000	566.66	700.00	626.66	631.11

Table 4.10 Incident Radiation on a Plane with the Lamps at Full Power

CHANNEL WIDTH (cm)	DISTANCE FROM LAMPS (cm)	HEIGHT 100 (cm)	HEIGHT 50 (cm)	AVERAGE
15.0	99.00	1.1293E+3	1.2050E+3	1.167E+3
12.5	101.50	1.1190E+3	1.1866E+3	1.152E+3
10.0	104.00	1.0866E+3	1.1960E+3	1.129E+3
7.5	106.50	1.0853E+3	1.1733E+3	1.129E+3
5.0	109.00	1.0741E+3	1.1973E+3	1.135E+3
2.5	111.50	1.0679E+3	1.1800E+3	1.123E+3
0.0	114.00	1.0350E+3	1.1400E+3	1.087E+3

Table 4.11 Incident Radiation on a Plane with the Lamps at Half Power

CHANNEL WIDTH (cm)	DISTANCE FROM LAMPS (cm)	HEIGHT 100 (cm)	HEIGHT 50 (cm)	AVERAGE
15.0	99.00	0.2870E+3	0.3100E+3	0.299E+3
12.5	101.50	0.2770E+3	0.3060E+3	0.291E+3
10.0	104.00	0.2720E+3	0.3040E+3	0.288E+3
7.5	106.50	0.2710E+3	0.3040E+3	0.287E+3
5.0	109.00	0.2700E+3	0.2970E+3	0.283E+3
2.5	111.50	0.2640E+3	0.2860E+3	0.275E+3
0.0	114.00	0.2550E+3	0.2770E+3	0.266E+3

However, as the lamps are moved to a distance of 1050 mm from the working plane, the curves become smoother as shown in Figure 4.15. When the distance is increased to 1275 mm the curves then become fairly flat and show a uniform incident radiation distribution over the working plane, as shown in Figure 4.16.

Figures 4.17 and 4.18 show the relationship between the average intensity and distance from the lamps at full and half power.

Some additional tests were made using the Kipp and Zonen solarimeter to check the intensity results and it was observed that close agreement existed between the methods. There were slight differences as a result of the global nature of the Kipp and Zonen solarimeter compared to the more directional response of the tube solarimeter.

4.5 Main Test Procedure

The test procedure was designed to obtain both uniform wall temperatures along the length of the channel, so that comparison with the theory for this case could be made, and also to simulate the more realistic wall temperature conditions which might exist in a solar induced convective flow.

The procedure was carried out to obtain air velocity and temperature readings at different elevations and with different gap widths. The main test procedure was conducted in three stages (a) using only the lamps at half

and full power (b) constant wall temperature obtained using the heating elements and (c) constant wall temperature power input as for (b) but with the lamps at half and full power.

Results were obtained using the following experimental procedure. The brass tube carriages were fixed on each side of the system at a pre-determined height. The wooden side walls were fixed between the heater plate and the double glazing to form a channel. After recording data the carriage position was changed and more data recorded. When tests were completed for one gap size the gap was increased and the procedure repeated.

For the cases with only the lights providing the heating, with the system in a steady state condition, the temperature and air velocity were measured at 5, 10 and 13 locations across air gaps of 25, 50, 75, 100, 125 and 150 mm respectively using the carriage to determine the precise location of each measurements. At the same time other temperature measurements at various locations on the system (i.e. on the plate, inner and outer glass plates, inlet and outlet air, front and back ambient temperatures, and back heater plate assembly) were taken. The air velocity was measured by a hot-wire anemometer PSI AVM 502 low flow air velocity meter. For each elevation, the AVM was first calibrated against the air temperature at the centre of the channel with no air flow and the zero velocity calibration was set accordingly. The air velocity was recorded by simply inputing the reading from the scale of the

anemometer into the HP computer. The temperature data collection was initiated from the HP computer by running the program as given in Appendix I.

The same procedure was adopted for the constant wall temperature tests. The power supply to the three variacs was switched on, using time clocks, at 4.00 am. The system temperature was allowed to stabilise over a period of 5 hours and then plate temperature readings checked for uniform plate temperature distribution. Continuous observation and fine adjustment was carried out until a steady state condition was established with the desired uniform plate temperature distribution.

A series of tests were carried out by using the one metre heater plate, with the corresponding one metre length of double glazing. In the second test series, the two metres heater plate was used with the two metres length of the double glazing. The final test series involved the use of the combination of the one metre and two metres lengths of heater plates with the corresponding double glazing to give an overall total length of three metres. All the above series of tests, a, b and c were performed with the three different overall lengths and varying gap widths. Experimental data are analysed and are presented in detail in Chapter 5.

4.6 Testing with Inlet and Outlet Diffusers

The objective of this section of the experimental work was to find out the effects on the fluid flow of diffusers

fitted to both ends of the channel to reduce the entry and exit losses as shown in Figure 4.19. Tests with the entry and exit diffusers were made only using the 3 metres long channel and the experimental procedure was the same as described previously.

The calculation to determine a suitable diffuser radius was carried out in conjunction with the table for standard size bellmouth diffusers given in ASHRAE [86].

Since the losses at entry and exit reduce asymptotically with radius, the radius of the diffusers was chosen so that a representative low loss coefficient was obtained without having to go to extremely large radii. By taking an average of the results, a final diffuser radius could be calculated.

$$D = 2HW/(H+W) \qquad (4.2)$$

where D = equivalent of rectangular diameter (cm)

W = channel width (b) (cm)

H = channel breadth = 100 (cm)

Using Equation 4.2 gives:

		W	2.500	5.000	7.500	10.000	12.500	15.000
Co	r/D	D	4.878	9.524	13.954	18.182	22.222	26.087
0.03	0.2	r	0.976	1.905	2.791	3.636	4.444	5.217

The average value of diffuser radius r = 3.161 cm and the size chosen was 4 cm radius which corresponds to 8 cm diameter pipe. The value of the average radius was rounded

up to correspond with the nearest standard pipe available which was 7.62 cm (3 inch) inside diameter, and 8 cm outside diameter.

The choice of the plastic pipe simplified greatly the manufacture of the curved inlet and outlet sections for the diffuser. By quartering the pipe longitudinally, the four sections of correct radius could be obtained from the one pipe.

The machining of the pipe into the four sections was the most difficult part of the work because of the nature of the material used. Plastic materials when being cut in the manner which was required for this test have the tendency to spring open on themselves and, therefore, a method had to be found of securing the material whilst the four longitudinal axial cuts were being made. This was done by first making a wooden spindle of length 1100 mm and diameter equal to inside pipe diameter on a centre lathe machine. The plastic pipe was then fitted on the wooden spindle and was securely held in place by woodscrews through the holes which were made in the pipe. The longitudinal axis was cut on a milling machine. The woodscrews were removed, the holes were filled with epoxy resin, and smoothed flush with the surface. Wooden splints were used to make the securing of the diffuser sections easier. Epoxy resin was used to secure the sections in position on the entry and exit of the channel.

The test was carried out as in the main test procedure which was explained in detail in Section 4.5. Readings for the temperatures and air velocity were taken across the channel widths of 50, 100 and 150 mm at channel heights of 2.5 and 3 metres. This procedure was repeated for wall temperatures of 35, 50, 75 and 100°C. The data was analysed and is presented in Section 5.3.

4.7 Transient Tests

During the experiments every effort was made to ensure that steady state conditions existed. However, because of the situation in the laboratory of the test cell, draughts and to a certain extent, air temperature increases were inevitably present. To estimate the effect of some of these influences on the heat transfer coefficients in the channel a series of 'transient' tests were run. The intention behind these tests was to check the vulnerability of the test procedure to those outside influences which were largely uncontrolled during the duration of the experiments.

The test was carried out as in the main test procedure which was explained in detail in Section 4.5. Readings for the temperatures and air velocity were taken across the channel widths of 50, 100 and 150 mm at a channel height of 3 metres and wall temperature of 75°C. Three tests were conducted for each channel width with intervals of 5 minutes. The first test was carried out with the wall at 75°C and the solar simulator on with full light intensity. The second and third tests were carried out when the power

supply and the solar simulator were off and the temperatures were falling. The data was analysed and is presented in Section 5.4.

4.8 Ambient Pressure and Humidity Effects-Experimental Work

The objective of this section of the experimental work was to determine the effects of the atmospheric pressure and humidity conditions on the fluid flow in the channel. These tests were made only on days selected when the pressure and humidity were unusually high or low. Tests were carried out using a channel width of 100 mm at a channel height of 3 metres and constant wall temperature of 75°C. Another set of tests were carried out with the above conditions when the solar simulator was on with full light intensity. The experimental results are presented in Section 5.5.

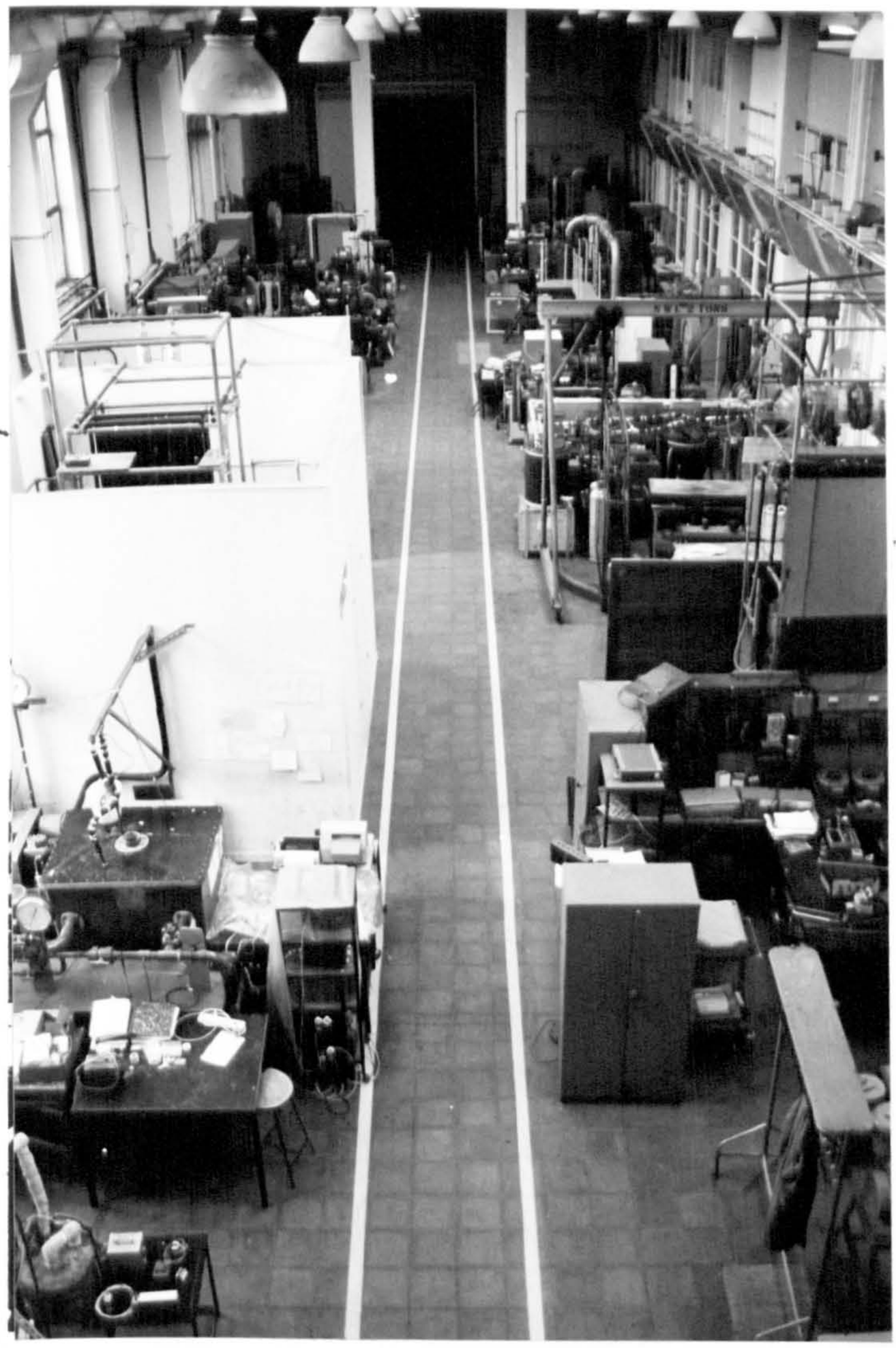

Figure 4.1 View of the Enclosure within the Laboratory

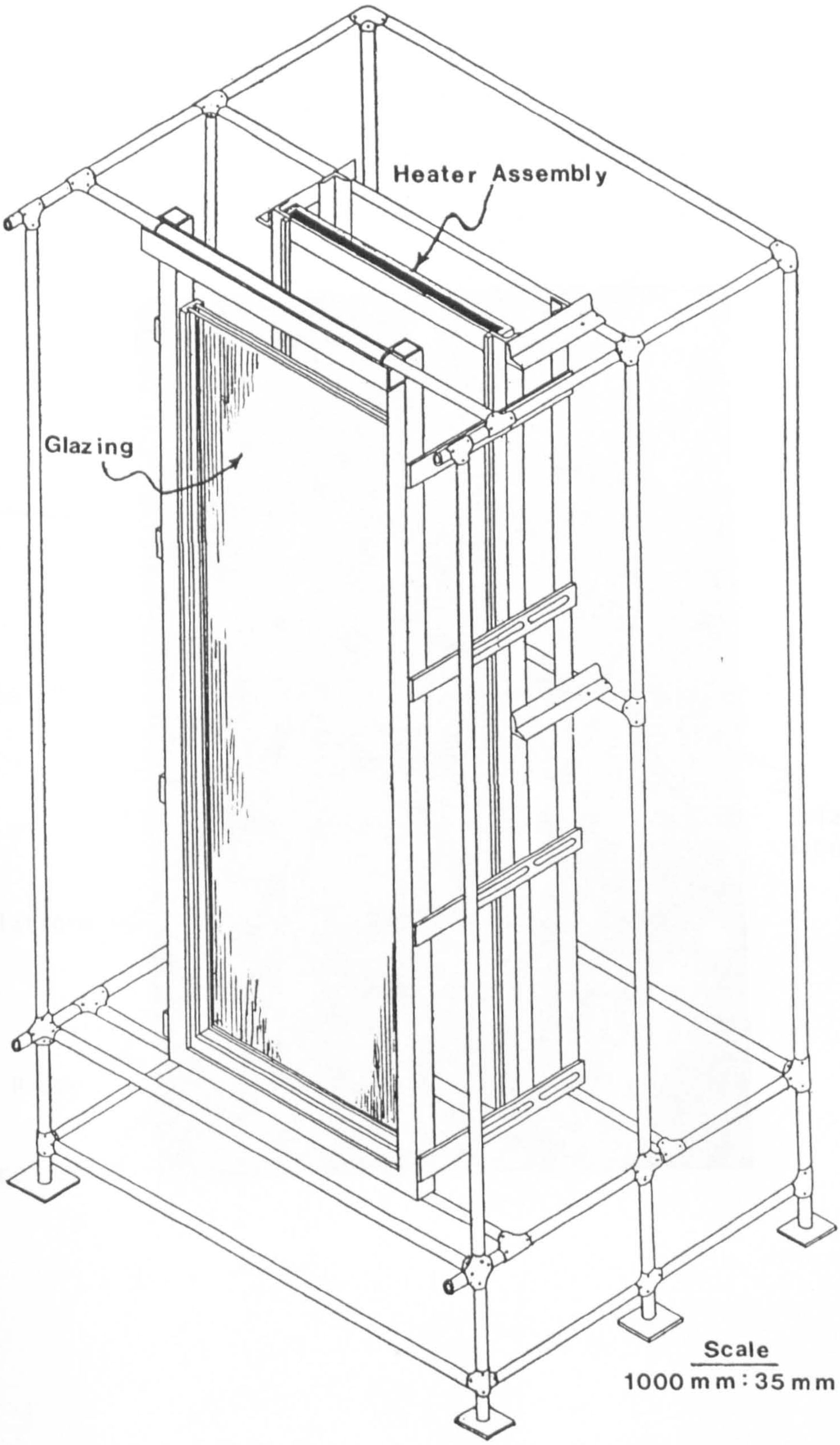

(a) Sketch of the Experimental Rig

Figure 4.2 Experimental Rig

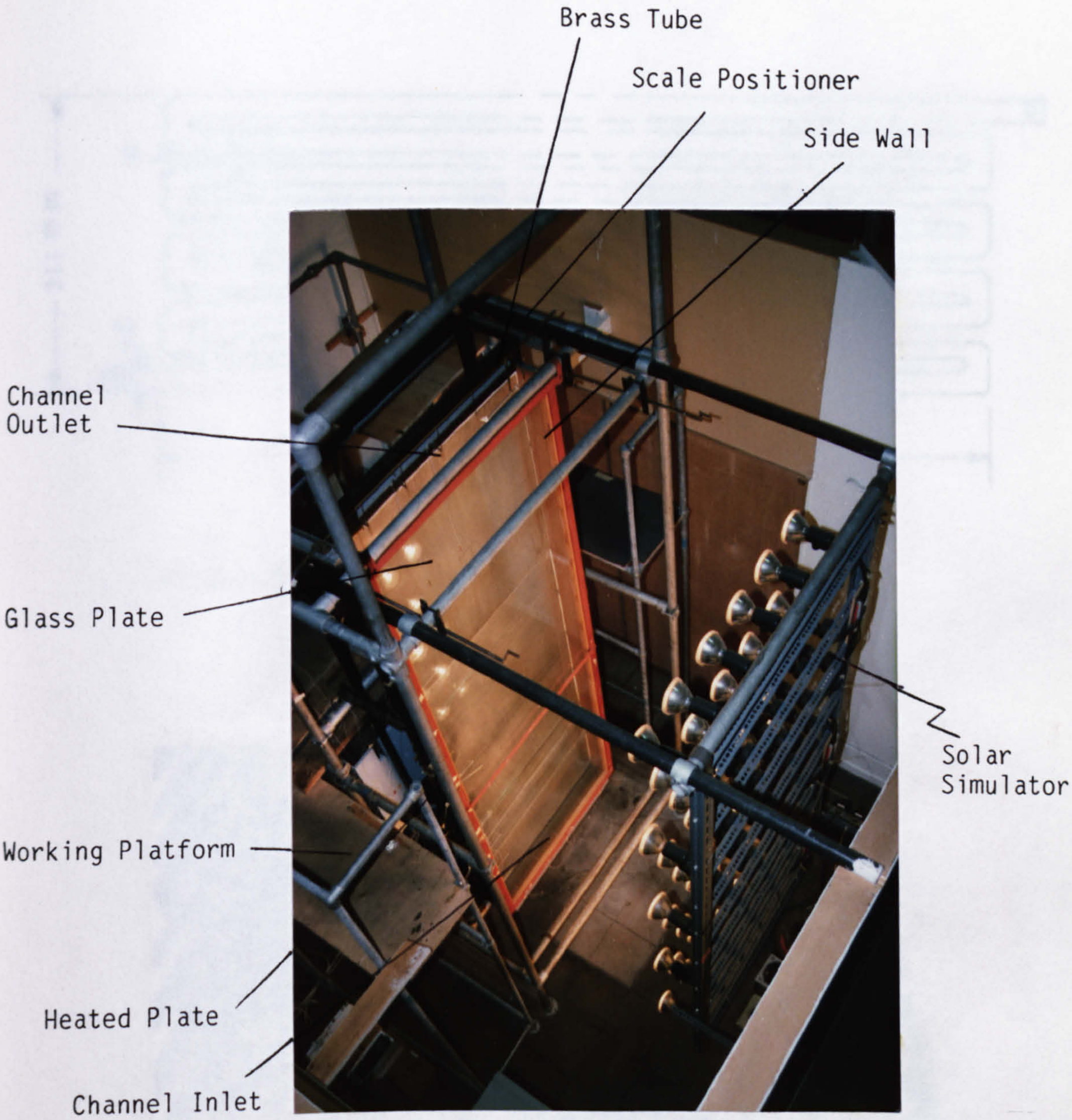

(b) Photograph of the Experimental Rig

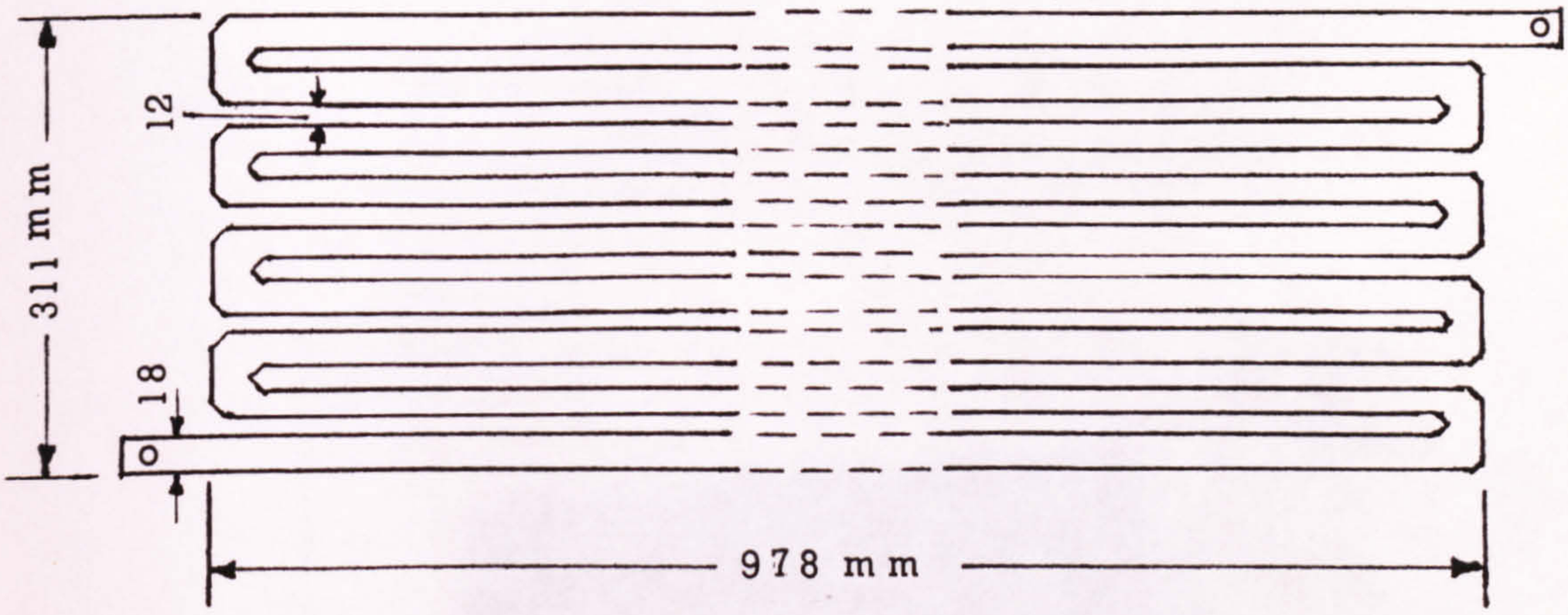

(a) Sketch Diagram of the Heater Element

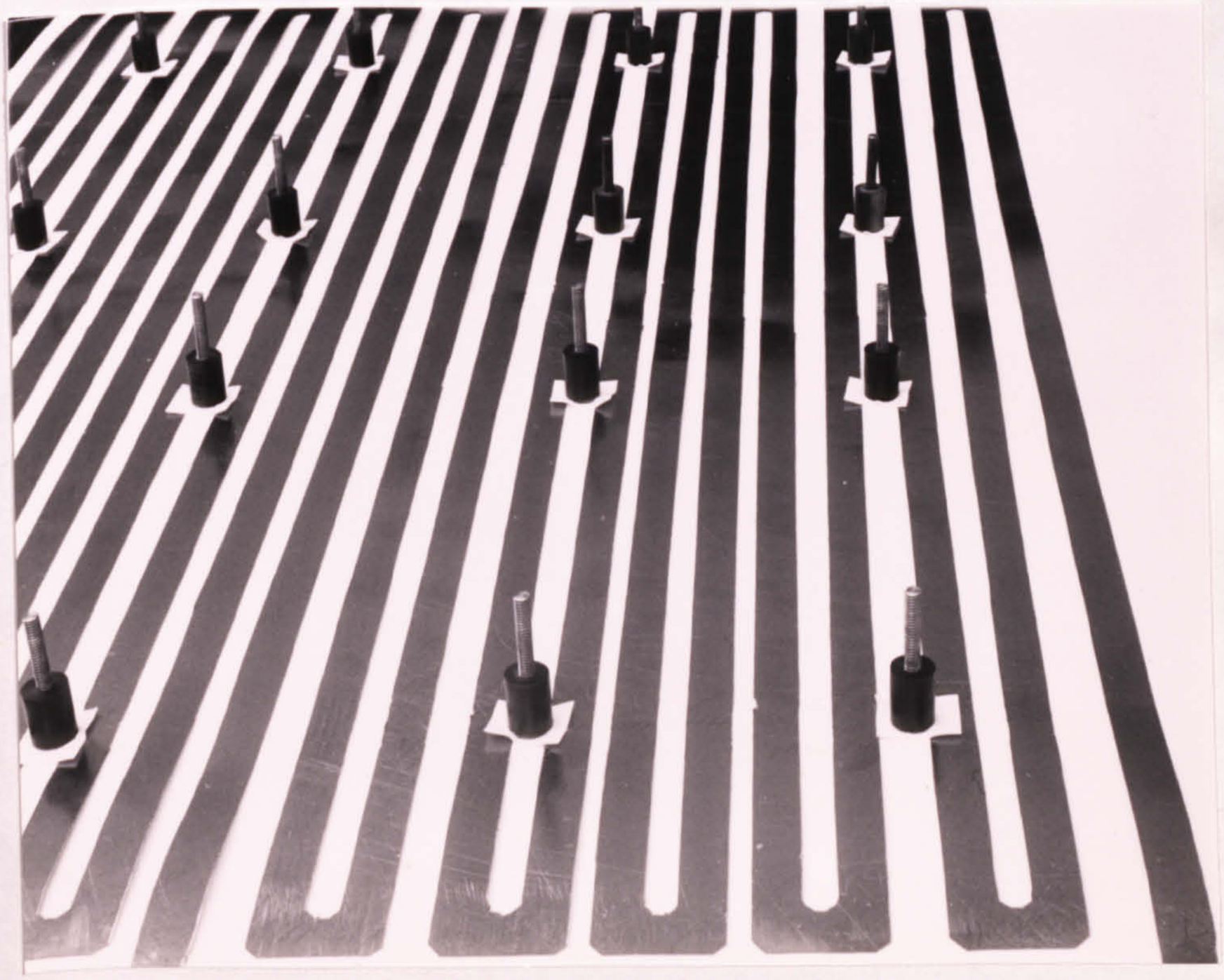

(b) Photograph of the Heater Elements

Figure 4.3 Heater Elements

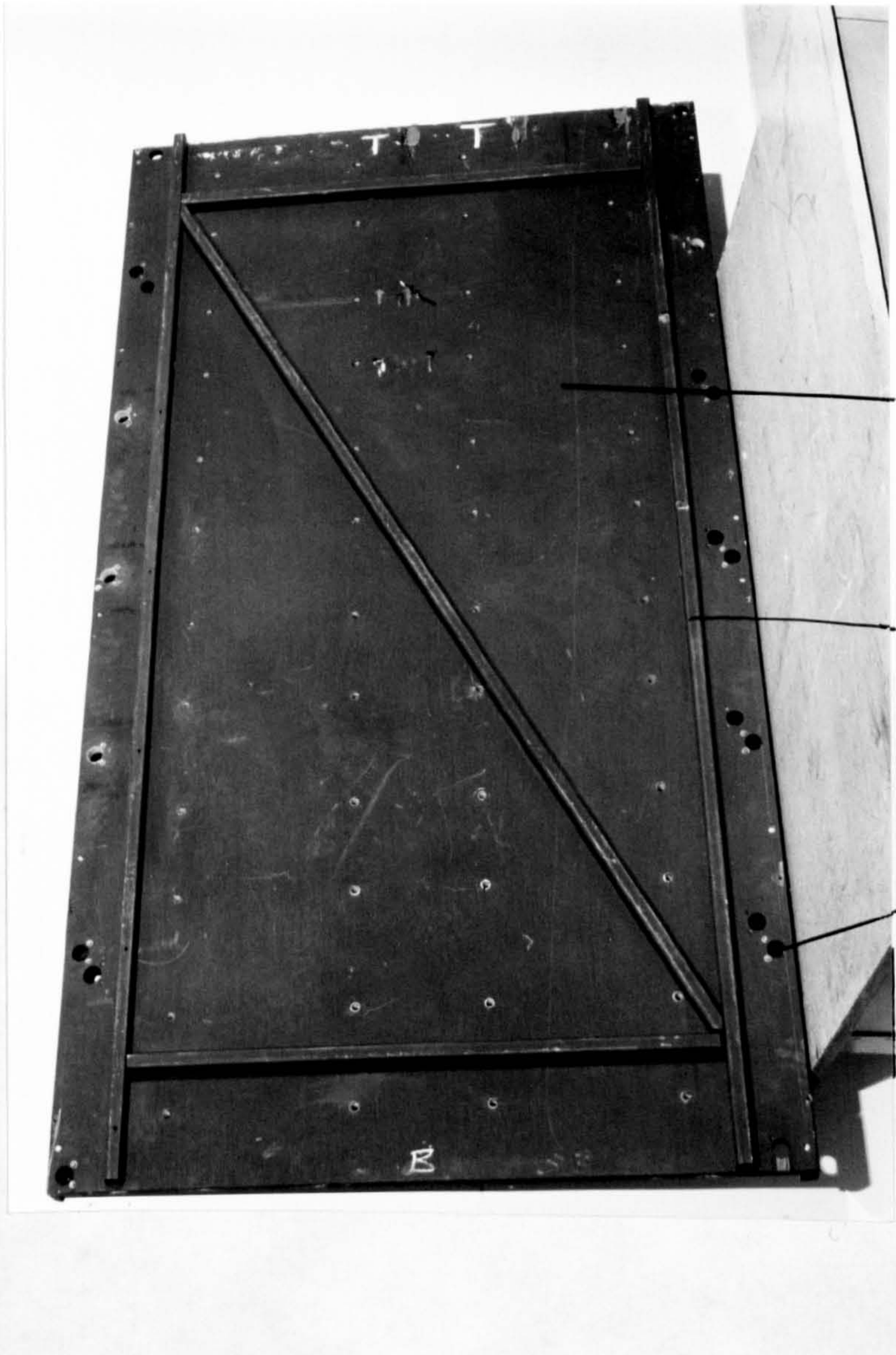

Figure 4.4 Plywood Support Board for the 2 meter Heater Plate Assembly

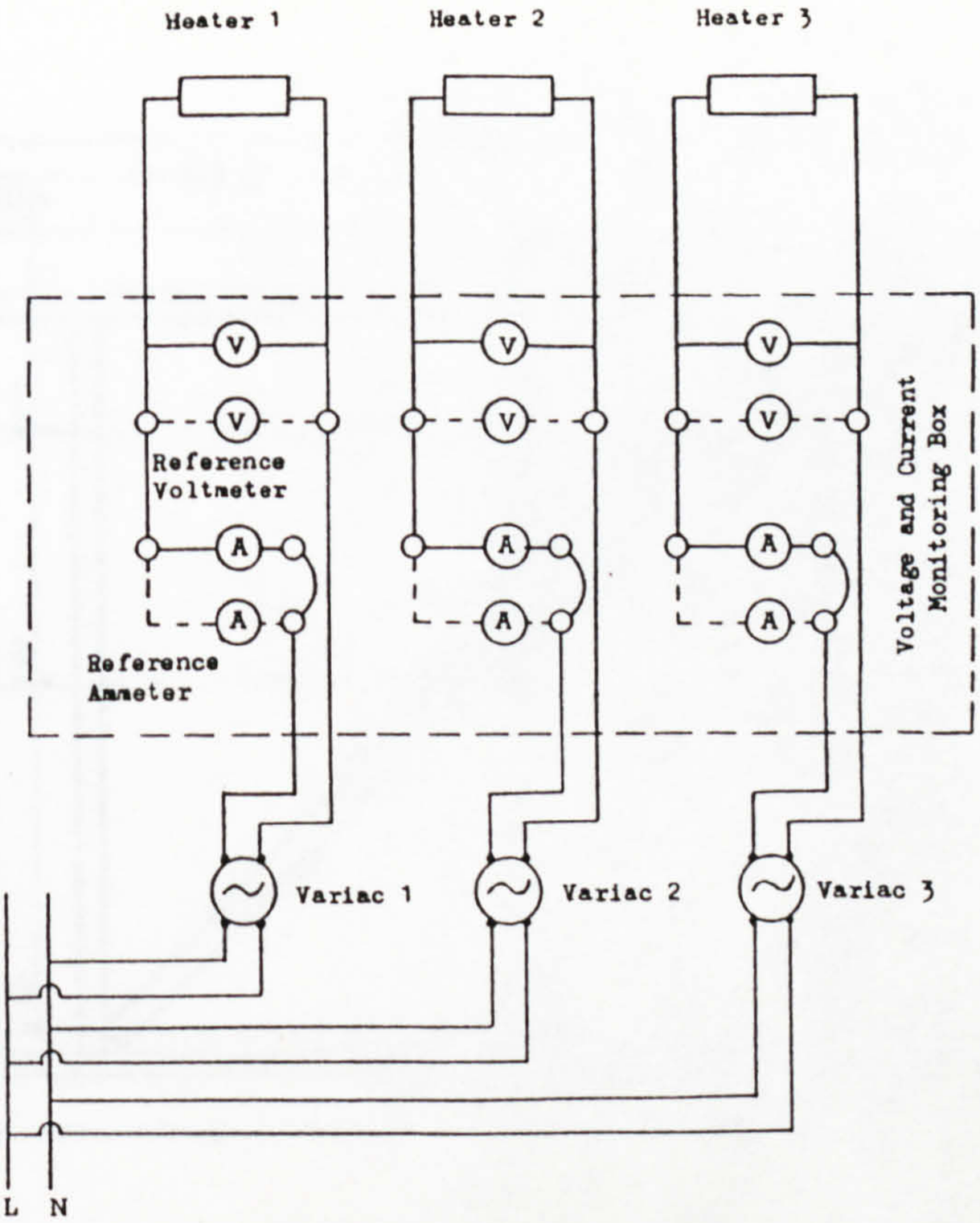

(a) Power Supply and Control Assembly Diagram

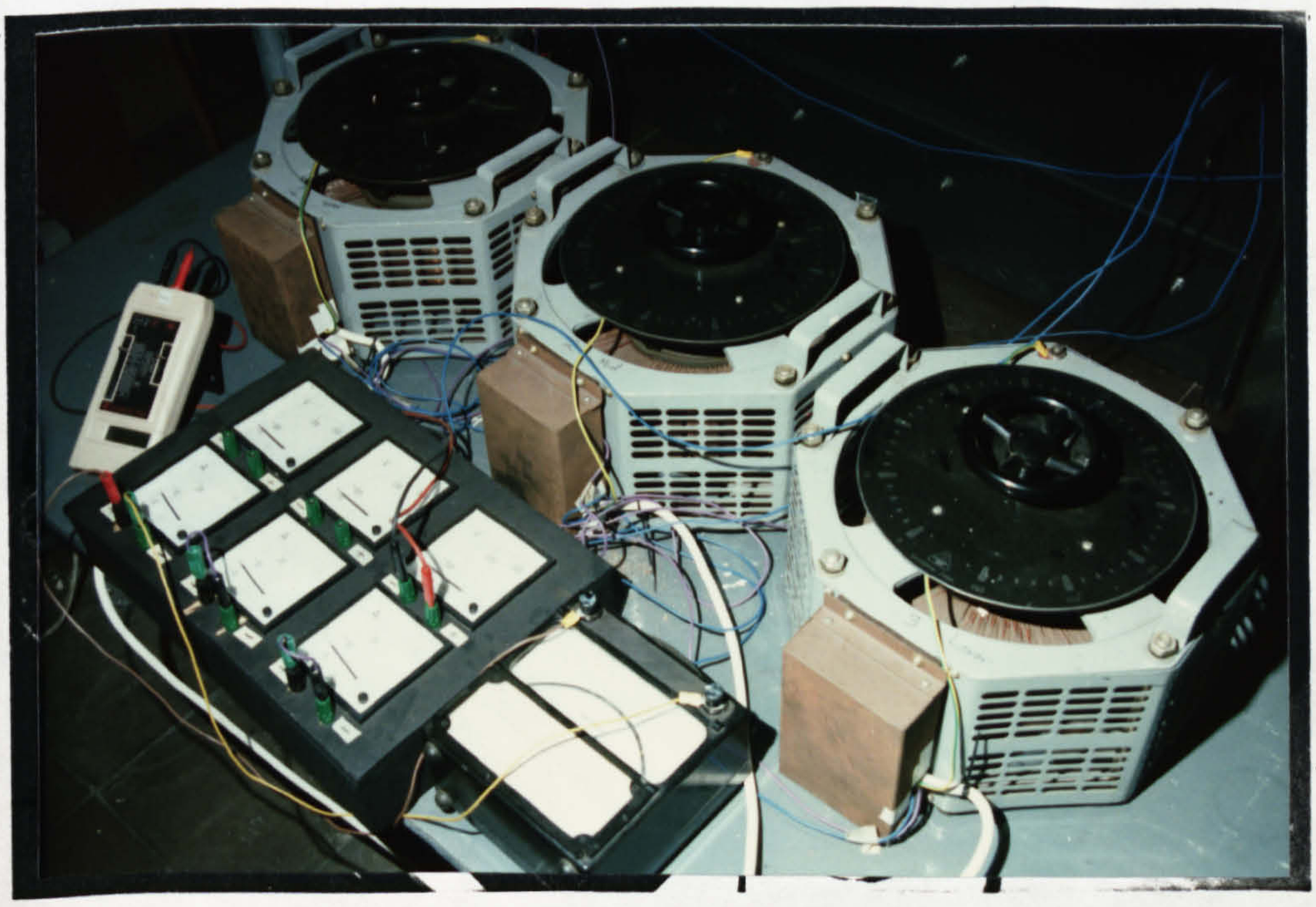

(b) Photograph of the Power Supply and Control Assembly

Figure 4.5 Power Supply and Control Assembly

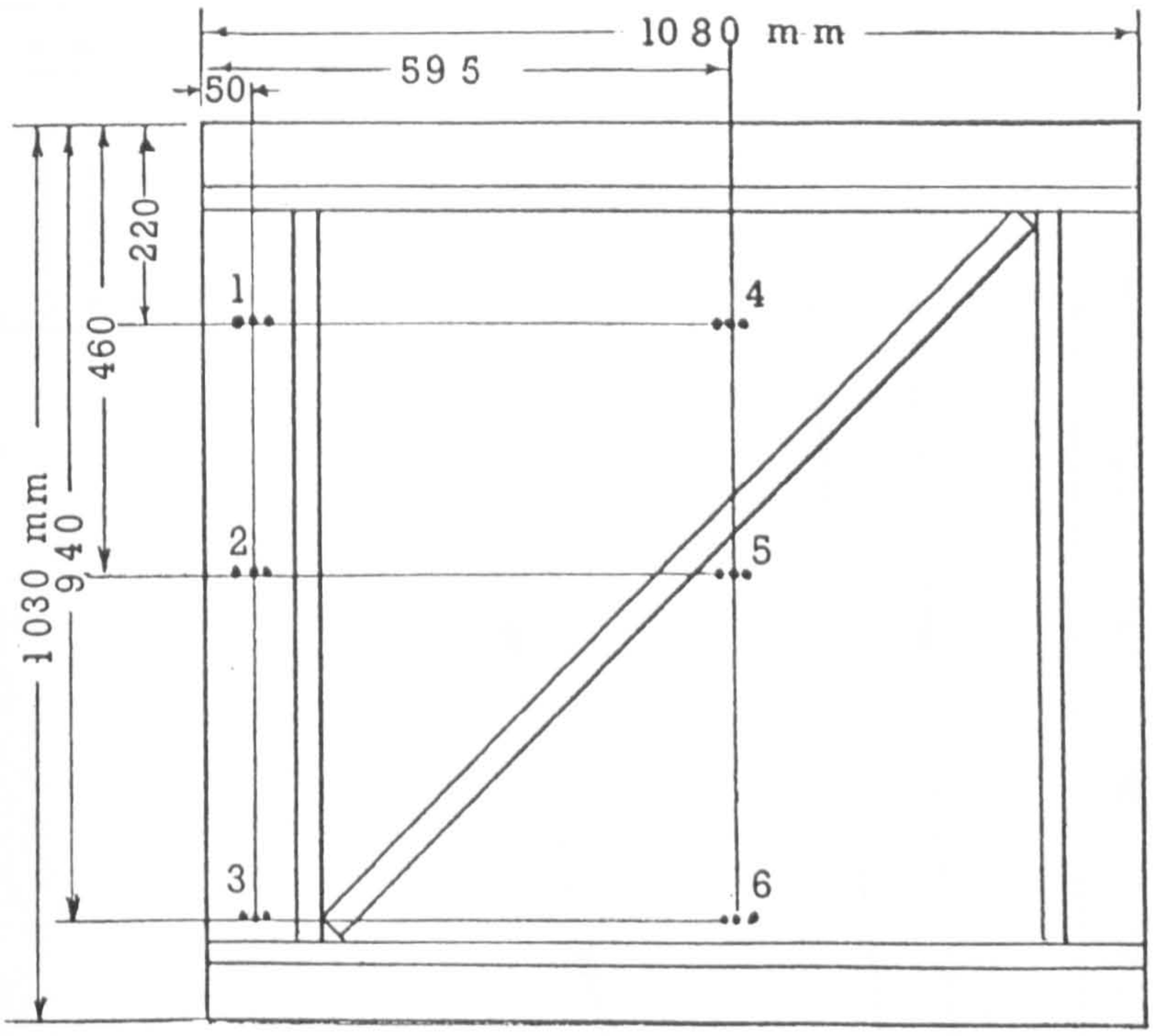

Figure 4.6 Thermocouple Locations on the Back of the One Meter Heater Plate Assembly

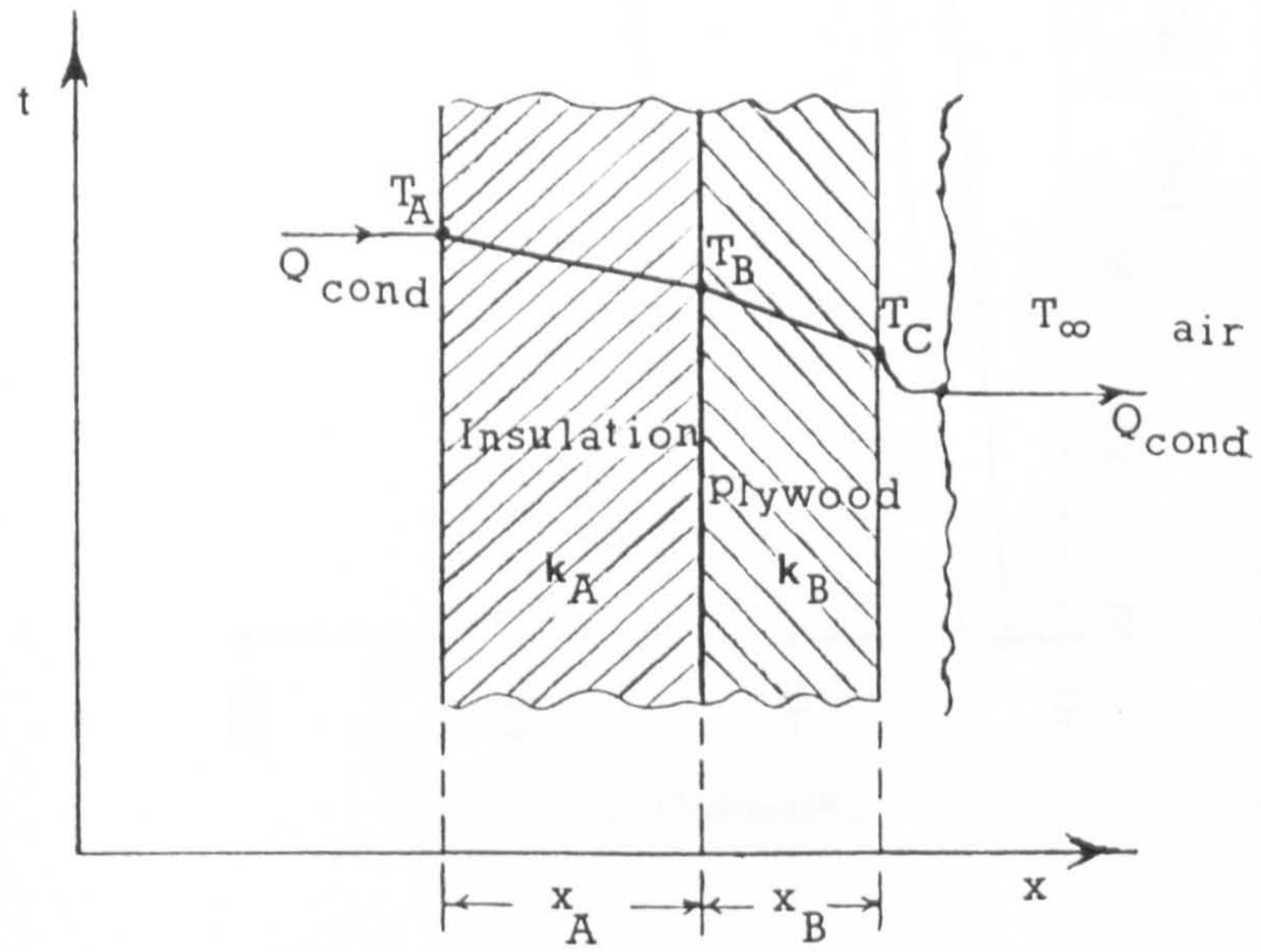

Figure 4.7 Heat Conduction through the Heater Plate Assembly

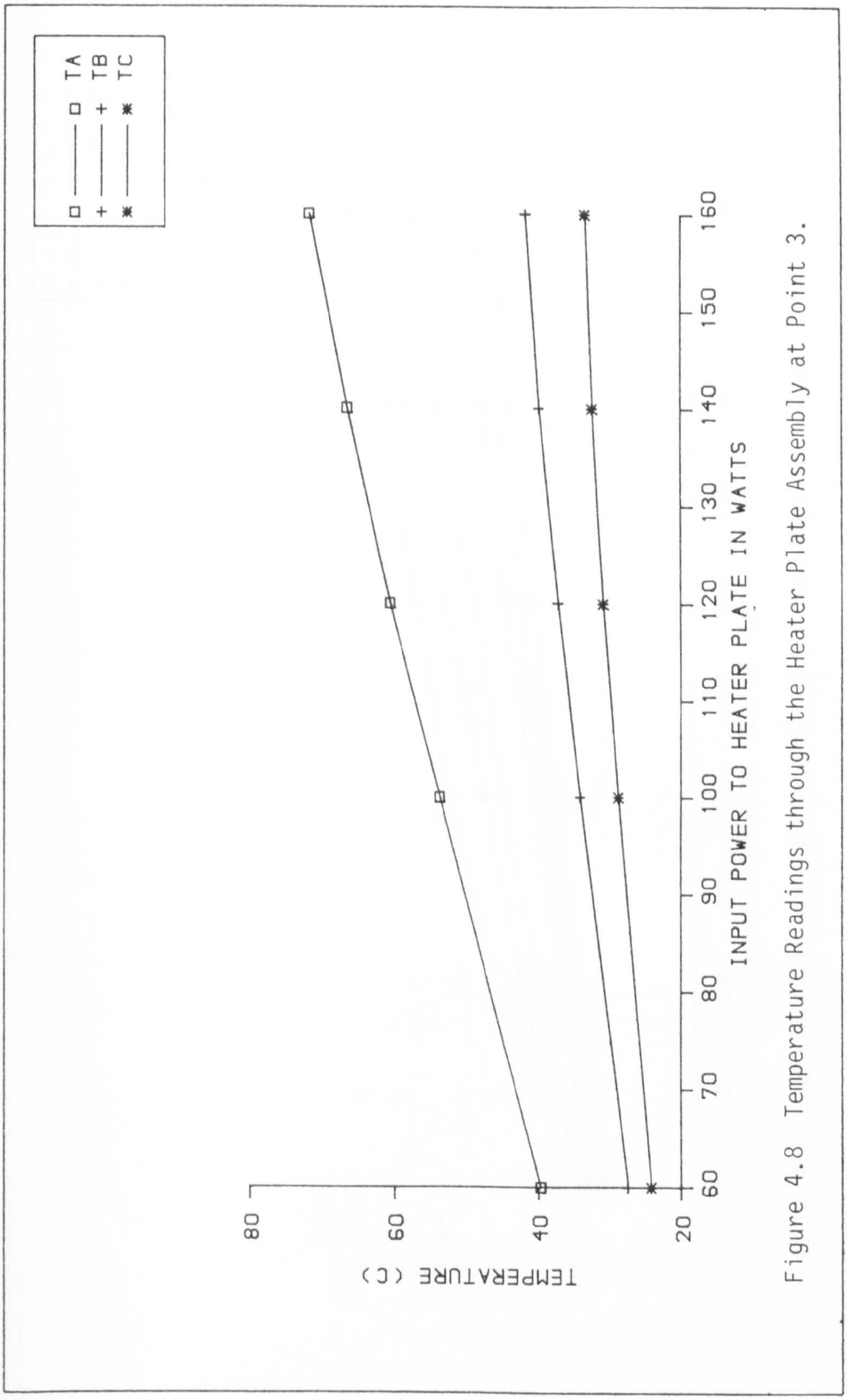

Figure 4.8 Temperature Readings through the Heater Plate Assembly at Point 3.

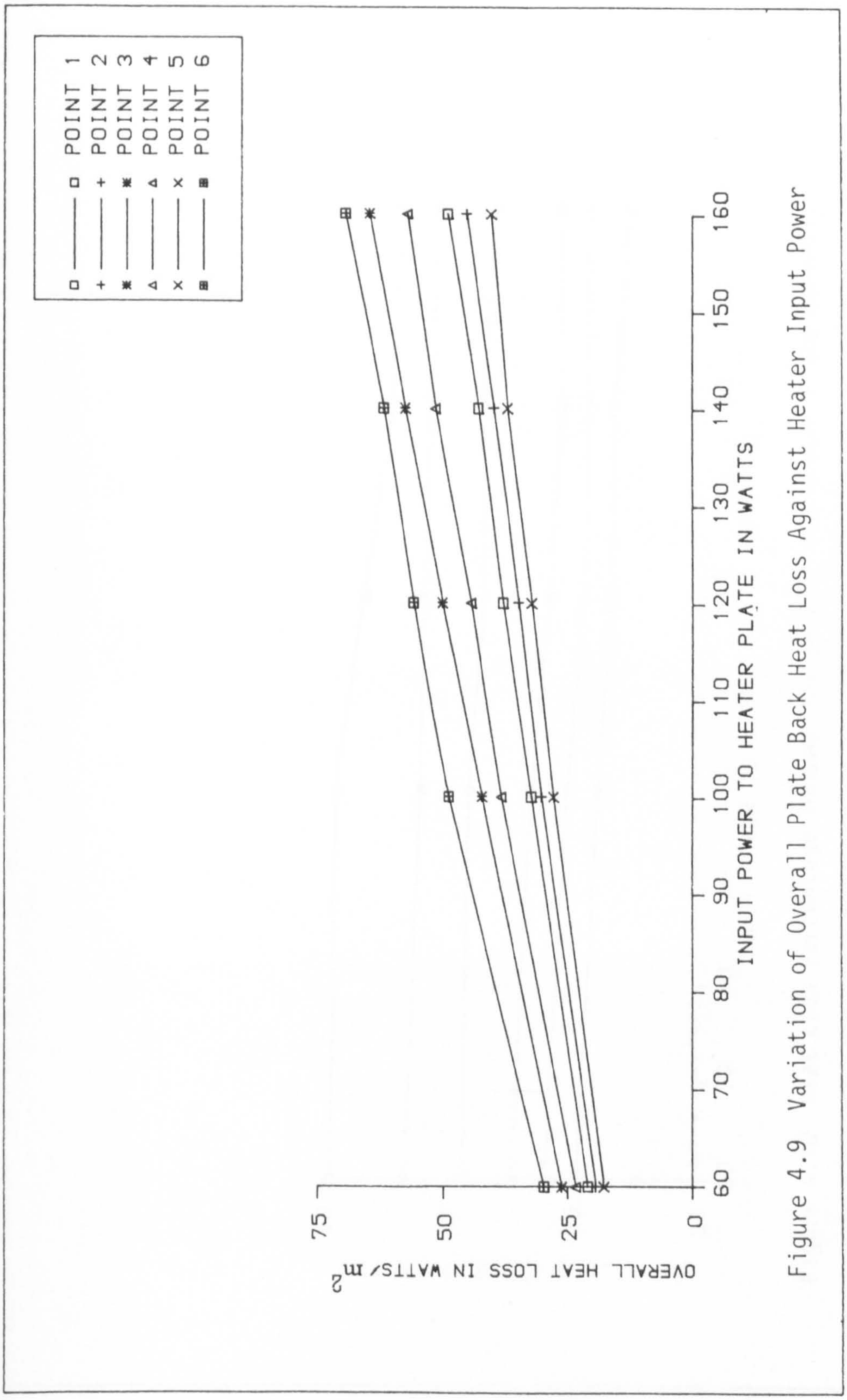

Figure 4.9 Variation of Overall Plate Back Heat Loss Against Heater Input Power

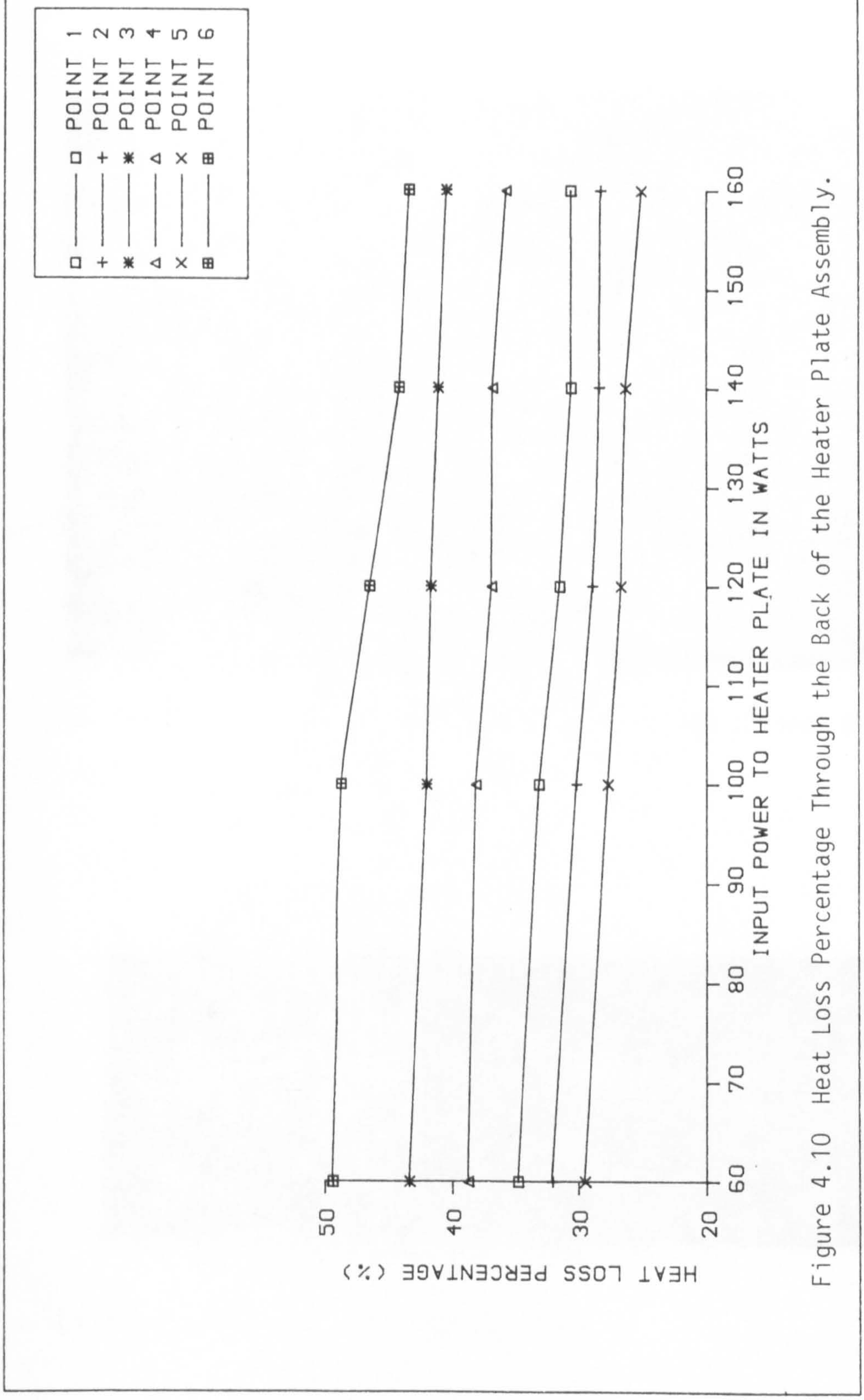

Figure 4.10 Heat Loss Percentage Through the Back of the Heater Plate Assembly.

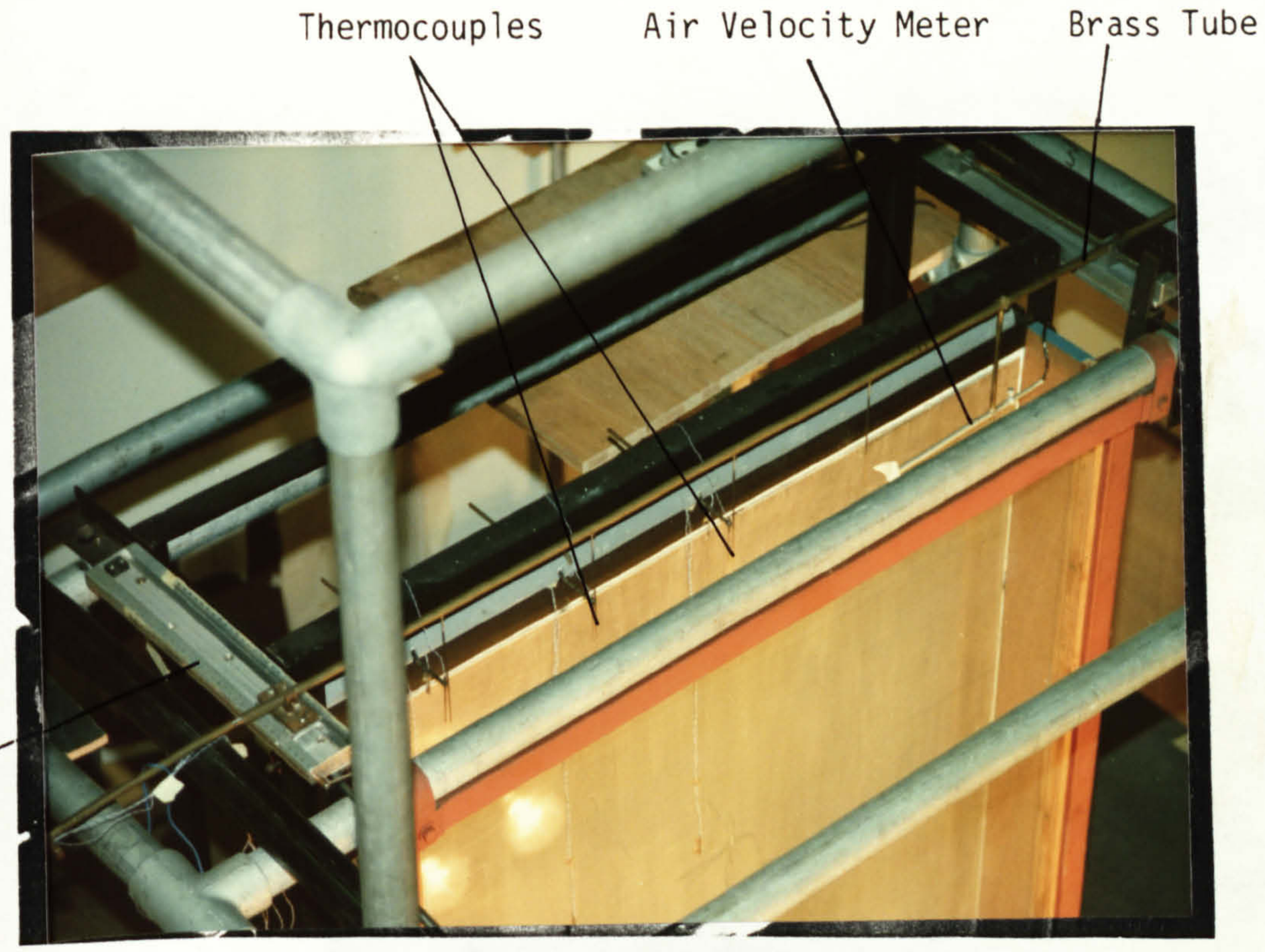

(a) Photograph of the Brass Tube Mounted on the Channel Exit

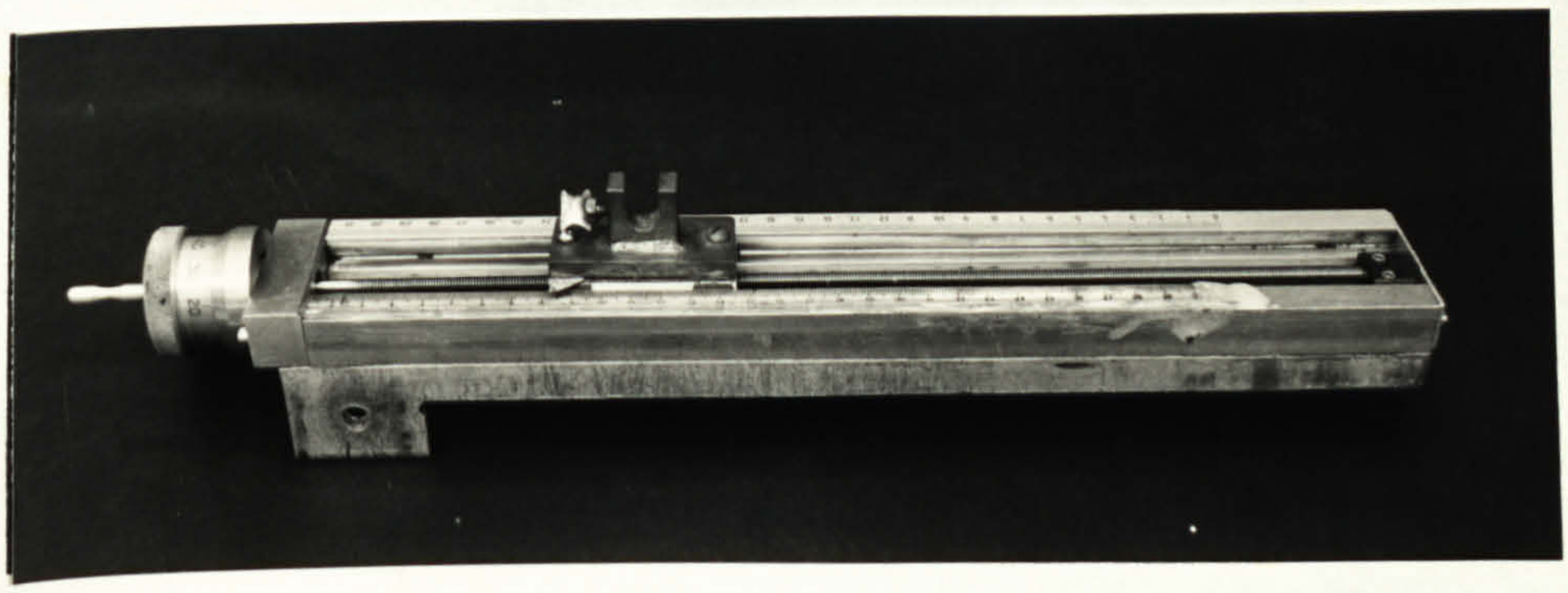

(b) Photograph of the Scale Positioner

Figure 4.11 Air Velocity Probe, Thermocouple Carriage and Positioner

Figure 4.12 Solar Simulator

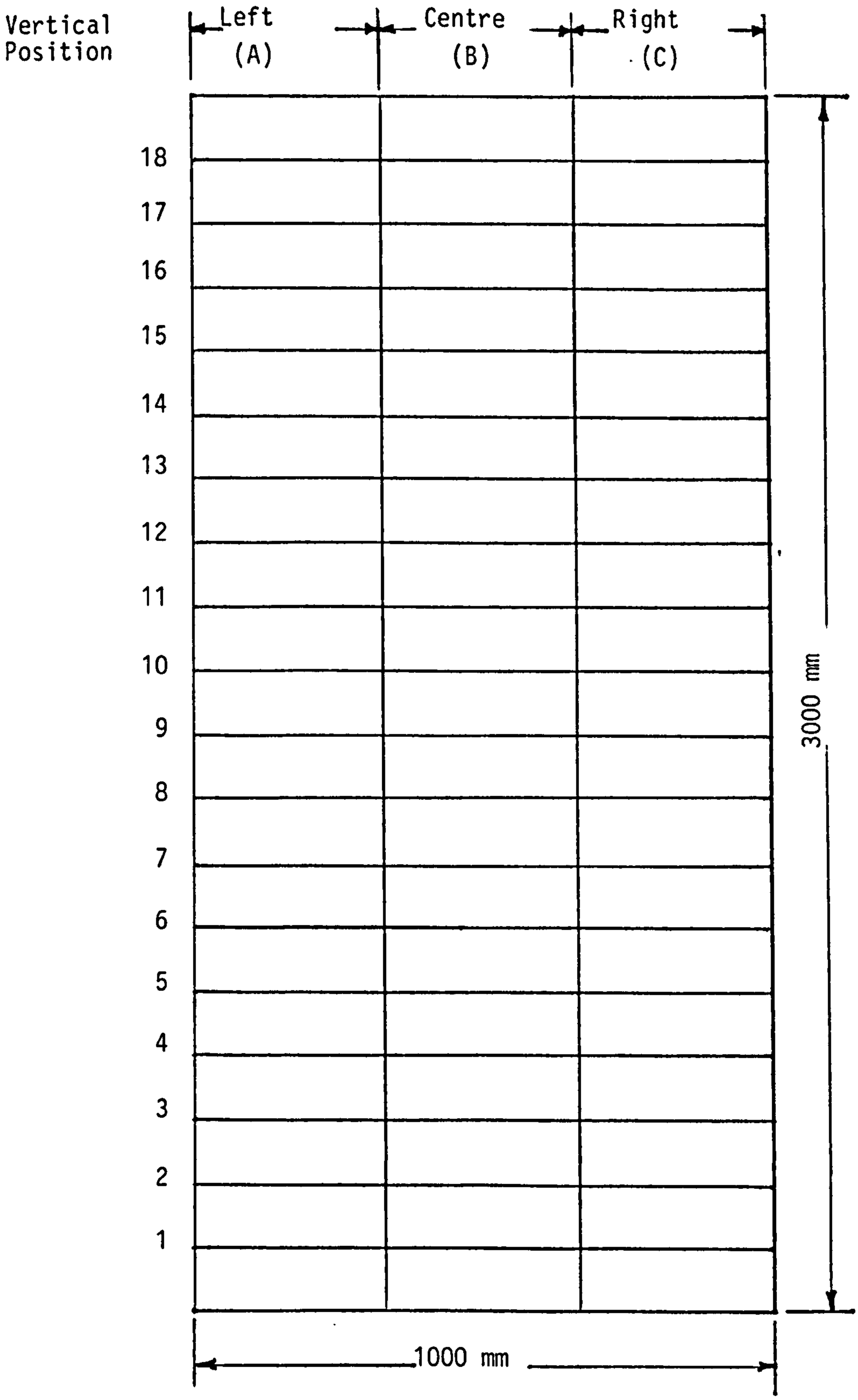

Figure 4.13 Solariometer Positions

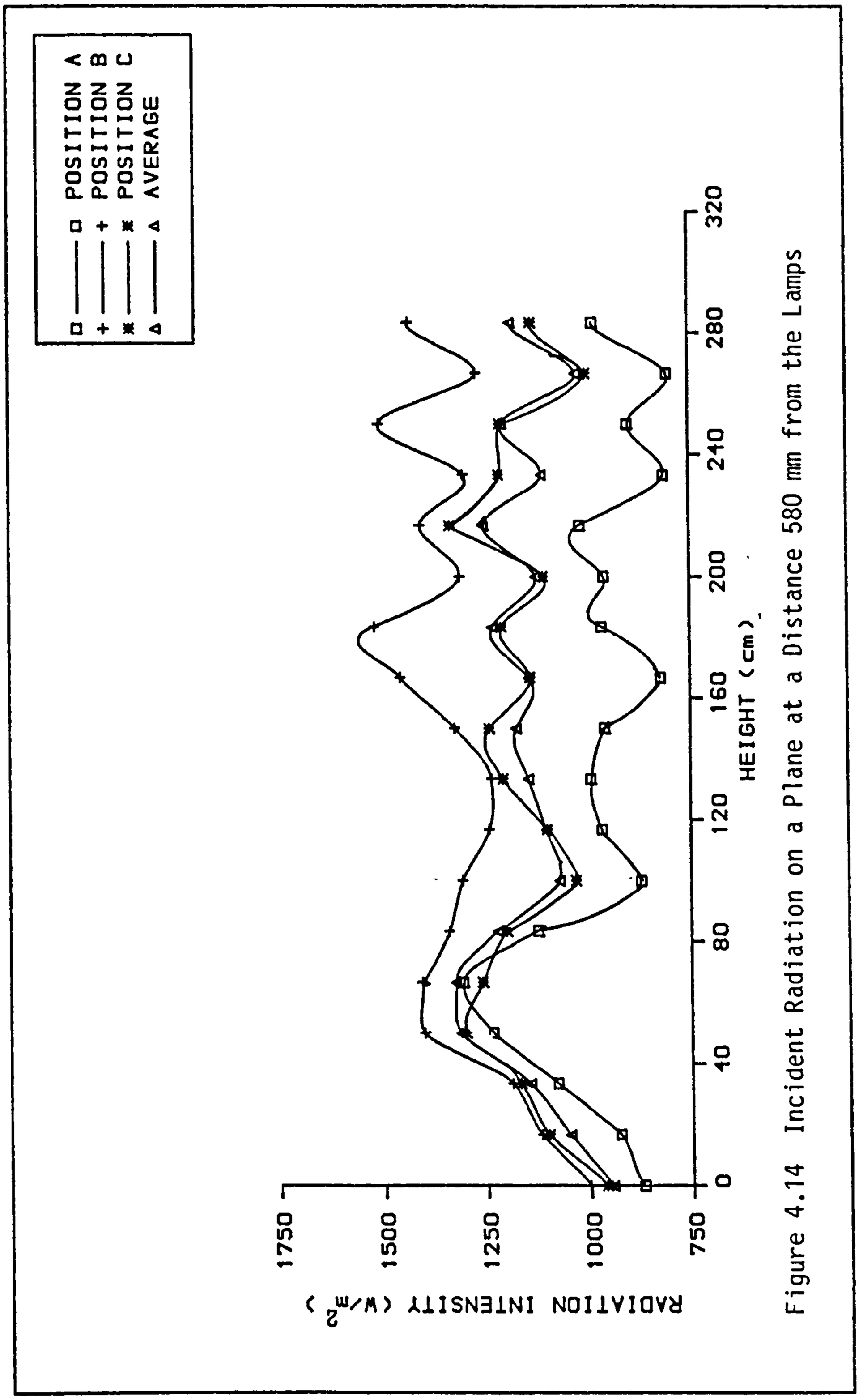

Figure 4.14 Incident Ra

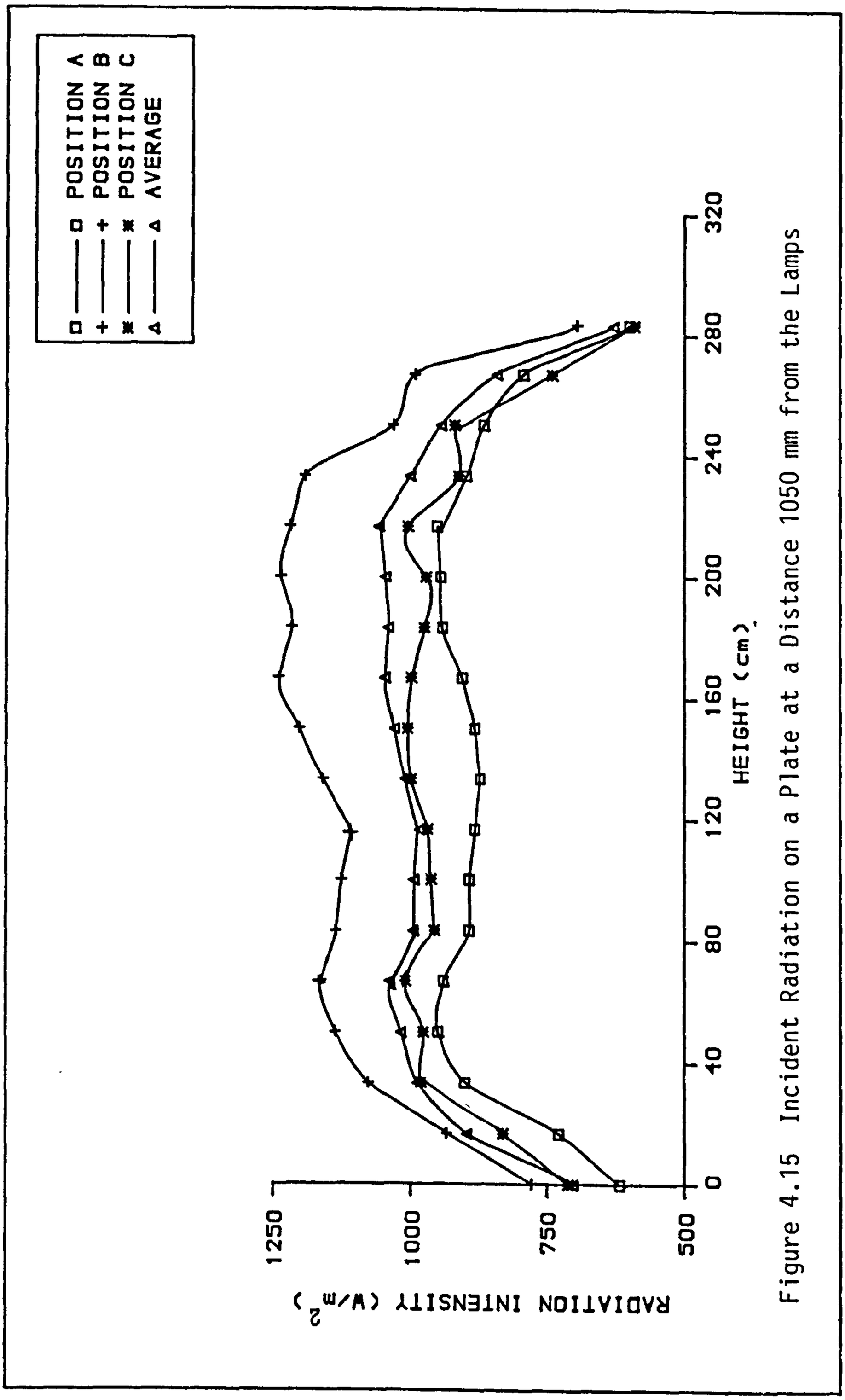

Figure 4.15 Incident Radiation on a Plate at a Distance 1050 mm from the Lamps

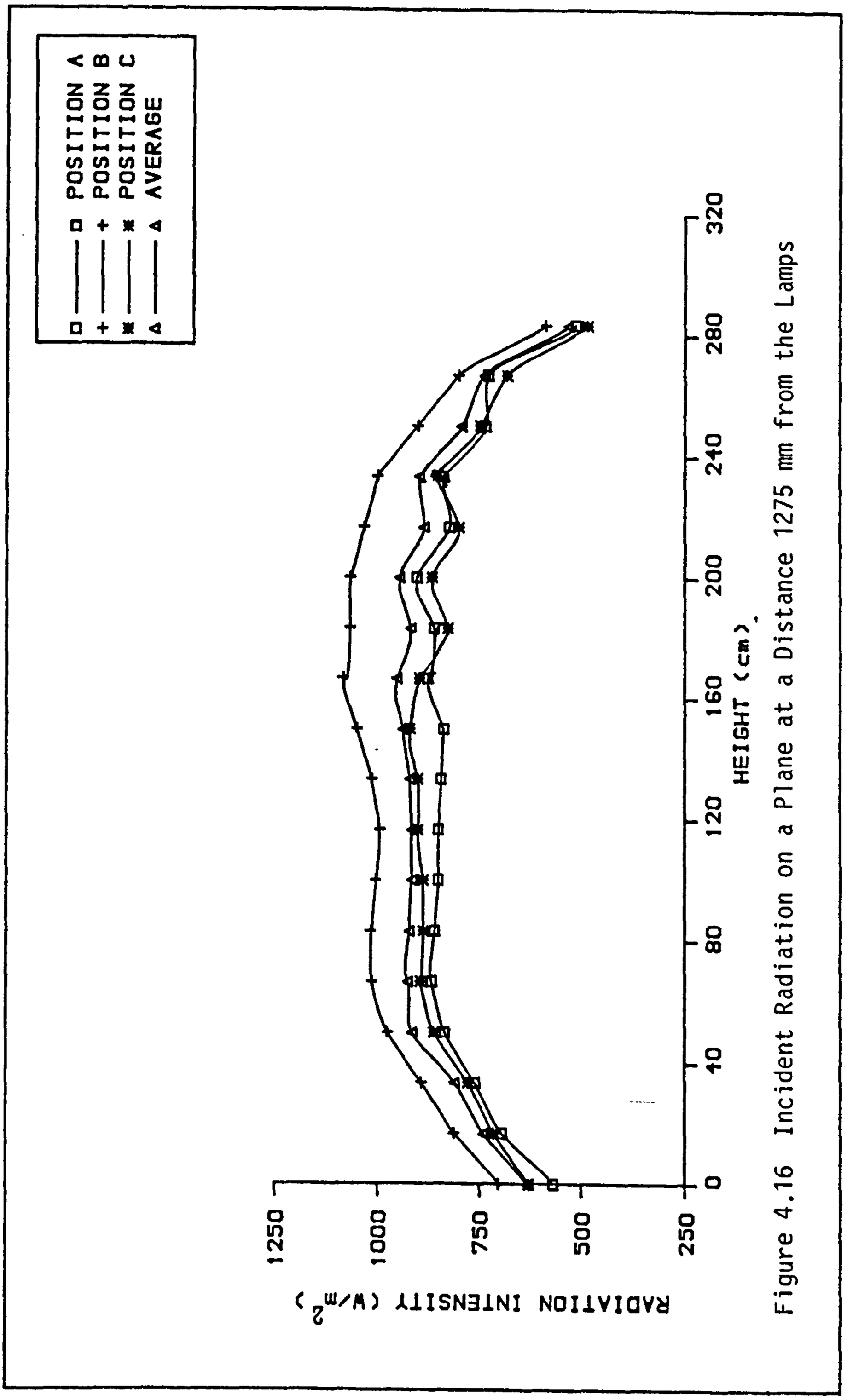

Figure 4.16 Incident Radiation on a Pl

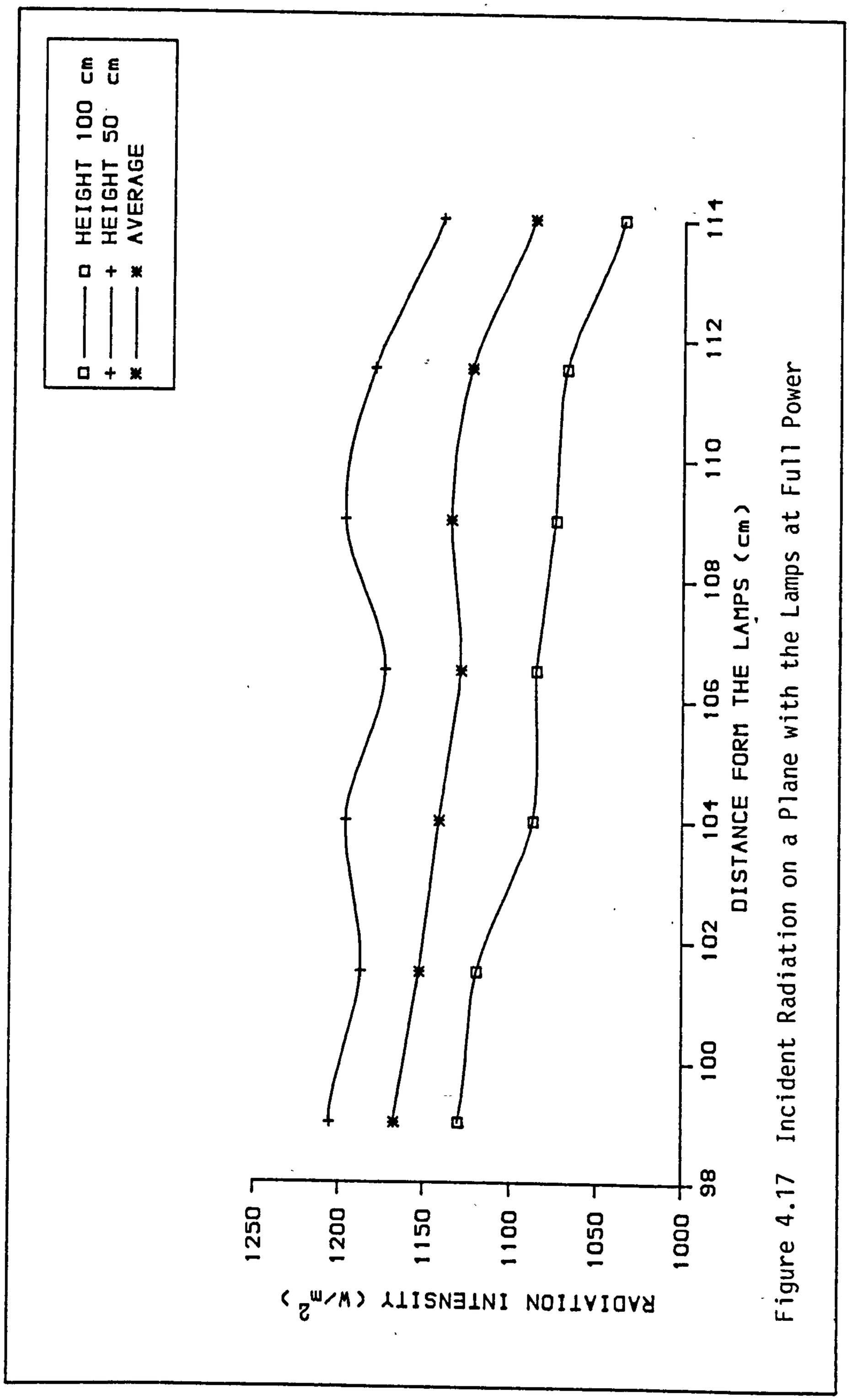

Figure 4.17 Incident Radiation on a Plane with the Lamps at Full P

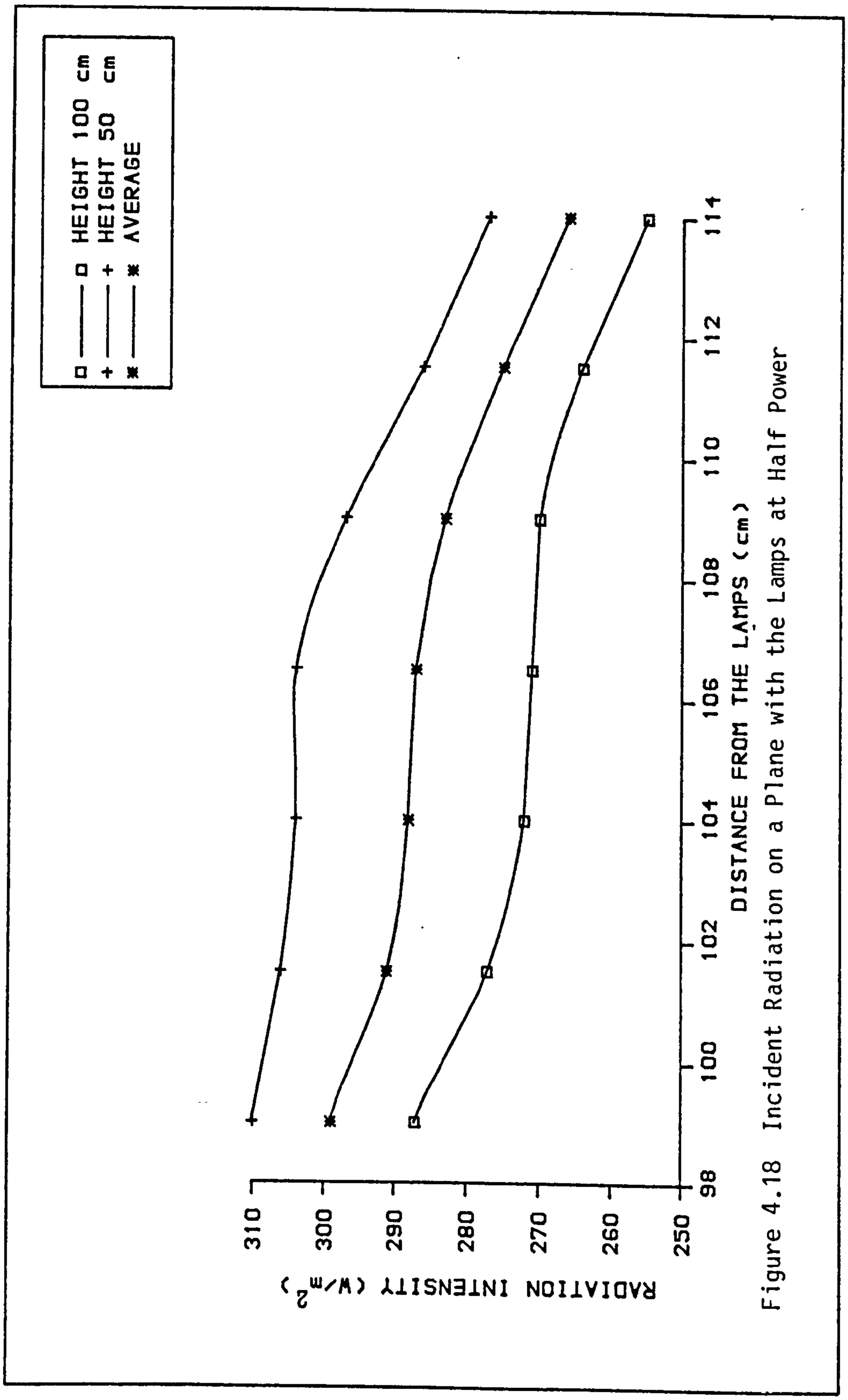

Figure 4.18 Incident Radiation on a Plane with the Lamps at Half Power

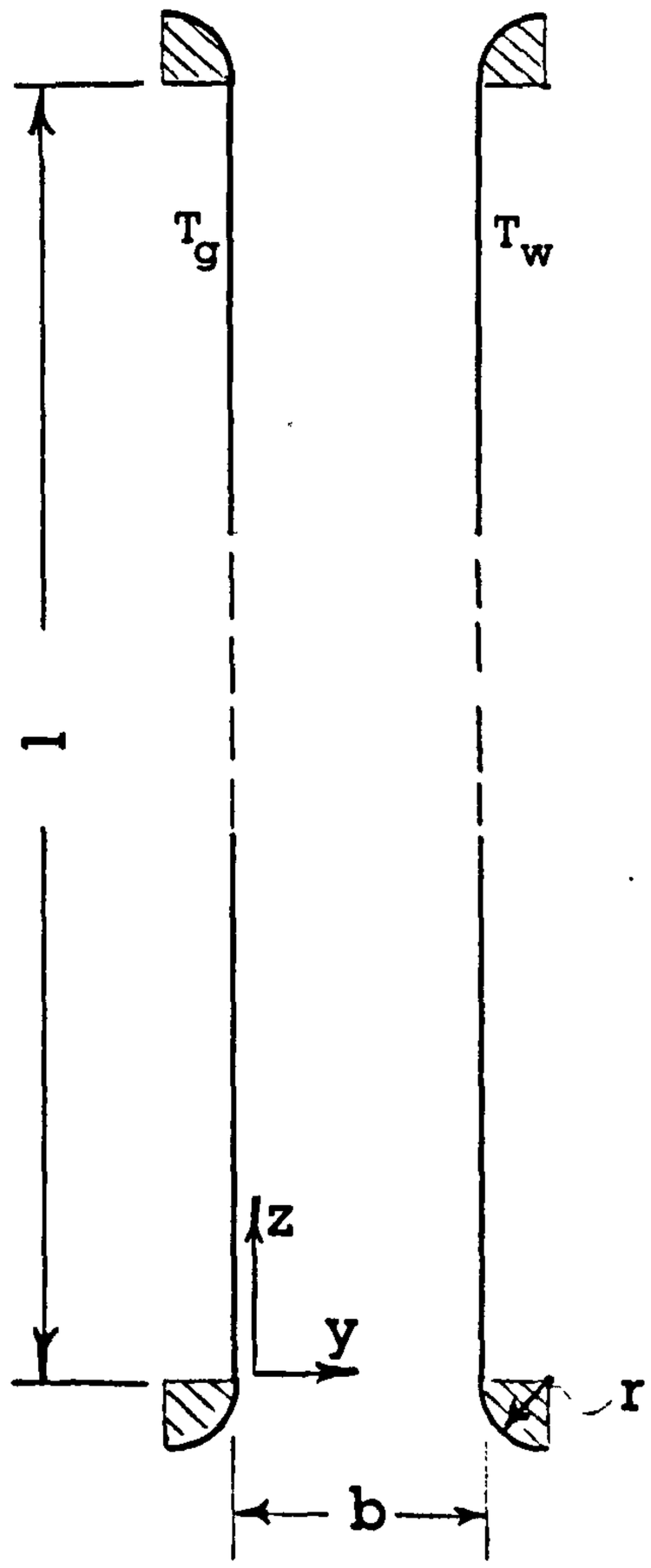

Figure 4.19 Three Metres Channel fitted with Diffuser Sections

CHAPTER 5

EXPERIMENTAL RESULTS AND DISCUSSION

5.1 Introduction

This Chapter presents the results of the main experimental tests, as well as additional tests on the effects of diffuser sections at inlet and outlet, transient cooling tests and tests made on specially selected days to investigate the effects of humidity and atmospheric pressure. The HP-computer program was used to analyse the experimental data. The results of each of the above tests are displayed in the Figures and discussed individually. Several correlations between the Nusselt number and dimensionless volume flow rate as a function of GrPr b/x and dimensionless channel length are drawn. Comparisons between the experimental results, the PHOENICS solutions and existing data are presented. Considering the present system as a basic Trombe wall, solar collector efficiencies and induced air flow have also been plotted for a range of channel heights, widths and light intensities.

5.2 Main Experimental Results

As explained in Section 4.5, experimental results were obtained for air flow in a vertical channel for the

following range of variables. For the main tests the heated wall temperature was adjusted to constant values of 35, 50, 75, 100 and 125°C, the aspect ratio, channel height to channel width, was varied as shown in the Table 5.1. Further tests with the lamps at full and half power and the wall temperature controls adjusted as if for constant wall temperature were also made as were tests with the lighting used as the only heat source.

Table 5.1 Aspect Ratio

l \ b	25	50	75	100	125	150
1000	40	20	13.33	10	8	6.66
2000	80	40	26.66	20	16	13.33
3000	120	60	40	30	24	20

Figures 5.1 to 5.6 show details of the dimensional and dimensionless velocity and temperature profiles at different levels in the channel up to a height of 3 m for a constant plate temperature of 75 °C and channel widths of 50, 100 and 150 mm. The flat part of the temperature profile is more extensive for larger channel widths.

All the figures for all widths show gradually developing velocity and temperature profiles. For larger channel heights, the warmer faster moving regions of the

air seem to be nearer the hot aluminium plate and for "developed" flow the velocity and temperature gradients are much greater at the hot wall than at the colder glass wall. It should be appreciated that 'fully developed' flow would take a much longer channel than used in these tests.

For narrow channel widths, the velocity profile is nearly parabolic as shown in Figure 5.1 but as the width increases, the velocity profile changes shape and the maximum value moves nearer the heated plate. This is shown in Figures 5.3 and 5.5. It is also noticeable that even at inlet the velocity profile is slightly assymetric with slightly higher velocities occurring near the hot wall which conflicts to a certain extent with the assumption of a uniform velocity profile as used in the PHOENICS solution.

The temperature profiles of Figures 5.2, 5.4 and 5.6 develop similarly with height and are seen to be flat in the centre of the channel. The flat part of the temperature profile is more extensive for larger channel widths. As expected the temperature profile at inlet is uniform at the ambient temperature.

Results were also obtained for higher plate temperatures of up to 125°C and Figures 5.7 to 5.10 present

profiles for plate temperatures of 100°C and 125°C for channel width 100 mm.

The experimental results presented above were obtained using the HP-computer program listed in Appendix J and this program also computed the total heat transfer to the air by using the velocity and temperature distributions in the integral form of Equation 2.39. Heat transfer coefficients, Nusselt numbers and other relevant dimensionless parameters such as Grashof Number, dimensionless air flowrate, referred to in Chapter 2, were also calculated at this stage. These data, when plotted in the traditional manner as functions of Nu against GrPr b/x and dimensionless flowrate against dimensionless channel height were then correlated using standard computer library subroutines on the VAX computer.

Figures 5.11 and 5.12 show the average Nusselt number Nu plotted against GrPr b/x for the following cases:

(a) for constant wall temperature.

Correlation of the data gives the following equation

$$Nu = 0.632\ (GrPr\ b/x)^{0.258} \qquad (5.1)$$

(b) for the lamps at half and full power with and without wall heating

$$Nu = 0.429\ (GrPr\ b/x)^{0.313} \qquad (5.2)$$

Figure 5.13 shows a comparison between cases (a) and (b).

It can be seen from these graphs that the scatter of the points from the correlating line is greatest for high values of GrPr b/x. Since the value of the abscissa GrPr b/x reduces as the channel aspect ratio b/x decreases, i.e. as channel length increases for a fixed width , . the results for (GrPr b/x) values greater than 10^4 are for relatively undeveloped channel flow. These results are liable to be subject to inlet air condition disturbances and the low values of air velocity are more likely to be subject to instrumentation errors. Furthermore the low plate temperature results, i.e. those for plate temperature of say 35°C, which results in low flowrates,are also more suspect than the high temperature results.

Figure 5.12 shows the results where heating was provided by using only the lights at half and full power and also where additional heater power was used as if for constant wall temperature. Again the scatter reduces as GrPr b/x decreases, and the slope of the correlating line

this time is seen to be slightly different than for the previous result. The difference is quite marked as shown in Figure 5.13 and is attributed to the fact that the wall and glass temperatures are no longer isothermal. As was demonstrated in the PHOENICS runs for a linearly varying wall temperature more heat was transferred to the air than for the isothermal case with the same average temperature. This conclusion appears to be justified by the present experimental results where more heat than expected is transferred to the air on the upper half of the plate. It must be pointed out however that the plate mean temperature was based on the simple average of three temperature readings at evenly spaced locations along the channel.

The relationship between dimensionless channel length L and the dimensionless volume flow rate Q is shown plotted in Figures 5.14 and 5.15. For the following cases the correlations obtained are

(a) for constant wall temperature

$$\dot{Q} = 0.591(L)^{0.559} \qquad (5.3)$$

(b) for the lamps at half and full power with and without wall heating

$$\dot{Q} = 0.535(L)^{0.522} \qquad (5.4)$$

Figure 5.16 shows comparison between cases (a) and (b).

Here it can be seen that the scatter of the points is less than before for both constant wall temperature and additional radiant heating from the lights. The correlating line for the additional heating cases lies above that for constant wall temperature heating case. In these figures the dimensionless flowrate $\dot{Q}$, is plotted against the dimensionless channel length which is given by, x/b Gr. These results depend mainly on the measurements of flowrate, or velocity across the channel, and are less sensitive to the temperature profile measurements, which of course has a strong influence on the previously presented heat transfer results. There is still however a marked difference in slope between the constant temperature case and the cases where radiant heating was provided i.e. the non-isothermal cases. This is shown in Figure 5.16.

An attempt was made to bring the Nusselt number values for these cases into line with the constant wall temperature curve by introducing a modified average wall temperature ($\overline{T}_{ave}$). From the results of the two previous correlations, the modified values of $\overline{T}_{ave}$ are given by the following equation and this is shown plotted against

GrPr b/x in Figure 5.17.

$$\frac{\bar{T}_{ave}}{T_{ave}} = 0.944 + 0.0186\ (\log_{10} \text{GrPr b/x}) \qquad (5.5)$$

This "correction" factor will give a weighting to the average wall and glass temperatures toward the hot section of the wall and the glass to make its contribution greater in the Nusselt number calculations. The modified value for T_{ave} would give a designer the choice of using the isothermal wall correlating equation for the non-isothermal case provided all the wall temperature data were available.

Finally, Figures 5.18 and 5.19 show all the points plotted on one curve for heat transfer and the other for flowrate. The Nusselt Number for the non-isothermal cases has been modified by the temperature "correction" factor equation while the flow rates for the non-isothermal cases have not. Modification of the flow rate seems to be unnecessary since the flow rate calculation is less dependent on wall temperature variation whereas the Nusselt Number is. For the non-isothermal cases a slight increase in flowrate over the range of GrPr b/x was however observed.

Figures 5.11 and 5.14 show results for the Nusselt Number and dimensionless volume flow rate scattered about the best fit line. Although it was felt that these results were acceptable consideration was given to the

various factors, other than experimental error, which might possibly influence these results. As explained in the PHOENICS results the pressure boundary condition at the channel inlet and outlet was a major factor affecting the solution for such a flow. The atmospheric pressure value affects the ambient fluid density and hence the imposed pressure drop along the channel. Ambient humidity could also have an effect. Thus further experimental tests were made on days of high and low pressure and also high and low humidity.

Since even the so-called isothermal tests were invariably subjected to draughts and slow transients, tests were run and readings taken for a period of time after the heater was switched off, so that the extent of the influence of transients on any of the main readings could be assessed. Another aspect which may have an effect on the fluid flow in the channel was also considered. This was the use of diffuser sections at the channel inlet and outlet. This aspect was also investigated experimentally.

5.3 Diffuser Experimental Results

Experimental tests were carried out as explained in Section 4.6. The results of Nu against GrPr b/x and $\dot{Q}$ against L are plotted in Figures 5.20 and 5.21,

respectively. These figures also show the data for the constant wall temperature condition without the diffusers corresponding to the same conditions of the constant wall temperature with diffusers fitted. The results show that the diffusers have a very small effect on the fluid flow in the channel. The scatter of points is much the same as before which demonstrates that smoothing the inlet flow has little effect. However it cannot be stated conclusively that the inlet conditions do not affect in some way the results obtained. Therefore the diffuser tests were largely inconclusive.

However from Figure 5.21 it is seen that the air flow does appear to be marginally increased when the diffusers are fitted as a result of the altered conditions at inlet and outlet. This is also reflected in Figure 5.20 where the Nusselt Number is seen to be slightly less than that obtained without the diffuser.

5.4 Transient Experimental Results

During these tests, the apparatus was first of all heated and brought up to a steady state with the plate temperature at 75°C. All sources of heating were then switched off and readings of temperature were taken as the apparatus cooled down. The cooling rate of the hot wall

was of the order of 2.74°C per min. and this figure could not be altered as it depends on the thermal properties of the plate assembly. Because of the difficulty and time involved in making temperature and velocity traverses there was an interval of about 2 minutes between the start and finish of taking the readings. However as this was also the case during the main tests, it was thought that if the test on the influence of a deliberate transient was to be meaningful, readings should be taken in the usual way.

The Nu and $\dot{Q}$ were calculated for a set of three tests with an interval of 5 minutes between them, as explained in the experimental procedure Section 4.7. The experimental results of Nu against GrPr b/x and $\dot{Q}$ against L are plotted in Figures 5.22 and 5.23 respectively. The calculation procedure, as explained in Section 2.3, was based on the lengthwise averaged wall and glass temperatures.

The above figures show that all the results lie close to the curve of the main test results. As expected from the results, the GrPr b/x values reduced with time because of the drop in the average wall and glass temperatures.

The conclusion to be reached from these tests is that even for a transient as rapid as that introduced in

the tests the disposition of the points relative to the correlating line is still good and well within the overall scatter of the other points from the main tests. Thus the response of the apparatus and experimental readings to the less severe transients normally encountered was not thought to be a main contribution to the experimental error already noted.

5.5 Ambient Pressure and Relative Humidity Effects Results

The test results used in this section are intended to highlight the influence of the related atmospheric variables, pressure and relative humidity, which, during the main tests had been observed in a qualitative way to influence the flow rates etc. in the channel when other conditions were ostensibly the same. In other words this section investigates the effects of pressure and humidity on the results with a view to explaining some of the scatter noticed.

From the main tests some results have been taken for days of very high, P_{atm} = 1.032 bar, and very low, P_{atm} ≈ 0.995 bar, atmospheric pressures, and some additional tests were run on days when the humidity varied, but the pressures were approximately the same. To consider the theoretical effect of moisture content, calculations have been made to assess the influence of

taking a mean value for the properties of the air-water vapour mixture, and this calculated value is then compared with the result of the same tests where the air has been assumed to be dry.

Relative humidity is defined as the ratio of the partial pressure of the water vapour in moist air at a given temperature t, to the partial pressure of the water vapour in saturated air, at the same temperature t. Hence the relative humidity of the moist air can be written by the equation, Jones (87):

$$\phi = \frac{P_s}{P_{ss}} \tag{5.6}$$

The moisture content is defined as the mass of water vapour in kilograms which is associated with one kilogram of dry air in an air-water vapour mixture. Hence it may be written as:

$$g_s = 0.622 \frac{P_s}{(P_{at} - P_s)} \quad \text{(kg/kg of dry air)} \tag{5.7}$$

The total moisture content is given as

$$g_{s_{total}} = \text{Mass} \times g_s \quad \text{(kg)} \tag{5.8}$$

Then the mass of dry air can be written as

$$Mass_{dry} = Mass - g_{s_{total}} \quad (kg) \tag{5.9}$$

The density of dry air can be calculated by using the air partial pressure, P_a,

$$\rho_a = \frac{P_a}{RT} \quad (kg/m^3) \tag{5.10}$$

where

P_a is the partial pressure of the dry air

= (Pat -Ps) (N/m^2)

R is the gas constant

= 287 (J/kgK)

T is the absolute temperature (K)

The mass of dry air and the mass of moisture was evaluated as above for all the tests. The properties, for the tests on humidity, were then calculated based on a weighted average i.e.

$$Value_{prop} = \frac{\text{mass air x air prop + mass of wet vapour x wet vapour prop}}{\text{mass of mixture}} \tag{5.11}$$

The results have been recalculated using these mean properties of the mixture and compared with the results calculated as if the air was dry.

Typical Calculation for ϕ = 47%, P=1.0027 bar.

l = 3000 mm, b=100 mm, Tw=343.73 K

Tg =300.13 K and T_{in}=293.33 K.

	Normal Calculation	Air-Water Vapour Mixture Calculation
Mass	5.902×10^{-2}	5.902×10^{-2}
$\dot{q}$	5.063×10^{-2}	5.224×10^{-2}
$\dot{Q}$	9.140×10^{-4}	9.362×10^{-4}
Heat	$5.894 \times 10^{+2}$	$6.260 \times 10^{+2}$
H	3.435	3.648
Nu	$1.281 \times 10^{+1}$	$1.178 \times 10^{+1}$
ρ	1.138	1.130
Cp	1.006	1.028
K	2.682×10^{-2}	3.098×10^{-2}
ν	1.646×10^{-5}	1.634×10^{-5}
L	8.911×10^{-6}	8.786×10^{-6}
GrPr b/x	$7.856 \times 10^{+4}$	$7.967 \times 10^{+4}$

Therefore, heat gain by the water vapour

= $6.260 \times 10^{+2} - 5.894 \times 10^{+2}$ = 36.6 Watts.

These calculations show that the influence of humidity is such that the Nusselt Number is reduced by 8.74% say for the conditions of the specimen calculation while the GrPr b/x product changes by only 1.41%,

therefore, previous main results for days on which the pressure and humidity have been high and low, respectively, will lie above the correlating line. If all of these results had been monitored for humidity, which was not the case, then it is possible that a considerable amount of scatter in the points could have been reduced. This has been done for certain results taken on days for which meteorological data was obtained from the Met. Office and the movement of these points is shown on the Figure 5.24.

The atmospheric pressure variation was looked at in the same way. Days of extreme pressures, high and low, about 1.020 bar to 0.968 bar were identified from recorded data in the Laboratory and tests made on these days were examined to see whether the points lay above or below the correlation as was suggested in the PHOENICS result.

Figures 5.25 and 5.26 identify the points with pressure and humidity readings.

5.6 Comparison Between Experimental Results, The PHOENICS Solution and Existing Data.

Comparison between the constant wall temperature experimental results and the PHOENICS code solution are plotted in Figures 5.27 and 5.28. These show good agreement between the experimental results and PHOENICS solution for Nusselt number and dimensionless volume flow rate against GrPr b/x and L respectively. However, it can be seen that a small difference in slopes of the lines exists in both cases. Figure 5.27 shows that the experimental results for Nusselt number are identical at a value of GrPr b/x of 10^3 and 5.2% higher at GrPr b/x of 10^7 than predicted by the PHOENICS solution. Figure 5.28 shows that the experimental results of dimensionless volume flow rate are identical and 14.1% higher than the PHOENICS solution for the values of dimensionless channel length of 10^{-3} and 3.16×10^{-7} respectively. Thus, the agreement between the theoretical and experimental results improves as the value of GrPr b/x decreases, i.e. as the flow develops. Large values of GrPr b/x infer either short channel lengths, or large channel widths, or low wall temperatures or a combination of all three.

Because agreement between the theoretical and experimental results improves as the flow develops then it seems reasonable to investigate factors which might

influence the rate at which the temperature and velocity profiles develop in the channel. Inlet effects must therefore be discussed. In the PHOENICS solution uniform velocity and temperature profiles at inlet were used, as indeed is the case with most other previous research work. However this ideal condition for the air flow at inlet will not exist in practice. The incoming air will be influenced by the presence of the surrounding structure, the enclosure and most of all by the entrance effect of the channel. There is thus a fundamental difference between the theoretical and experimental inlet conditions which one would expect to become less important as b/x becomes small. In the work by Aung (28,29), his theoretical result intersected with his data for developing flow at a value of GrPr b/x of about 10^3 and so all of the results in the present work are for developing flow. It is worth noting that Ofi and Hetherington (25) also observed that the slope was greater for wide channels and their results are referred to in Chapter 2.

Another factor contributing to the experimental points lying above the theoretical curve is the variation in temperature of the glass wall. No temperature control of the glass was possible, and so the glass temperature was determined by the radiation absorbed from the hot wall and by the radiation and convection from the glass to the surroundings. The glass temperature tended to vary from

inlet to outlet and for the case of channel length 3000 mm, width 50 mm and 100°C wall temperature, the variation was from 27.66°C to 35.64°C. It has already been demonstrated in Chapter 3, that non-uniform wall temperatures give higher Nusselt numbers and so this glass temperature variation would also tend to raise the experimental results above the theoretical line. Since the glass wall did not provide the main convective driving force, it is considered that this effect would be much less significant than the entrance effect.

A further reason for the experimental results lying above the theoretical line, results from the difference in ambient pressure for the two cases. Most theoretical work was done using a pressure of 1 bar, whereas the experimental results were obtained for a variety of atmospheric pressures, normally above the value of 750 mm Hg which corresponds to 1 bar. As shown earlier for pressures of 0.95, 1.0 and 1.05 bar the atmosperic pressure has a significant influence on the pressure difference across the channel with the higher pressures giving rise to higher Nusselt numbers as shown in Figure 3.16.

Other more random influences on the experimental results, some of which have already been mentioned, include the following.

Even though the apparatus was enclosed the air flow and temperature was still influenced to some extent by conditions in the laboratory. Opening of external doors, overhead lighting, operating machinery all influenced the ambient air condition and so would have some effect on the results.

Tests were made, wherever possible, under favourable conditions but it must be acknowledged that these external influences were present, leading to a slight scatter in the results. From a qualitative observation, it was thought that the most detrimental external influence was that of induced draughts across the top of the enclosure.

There is very little relevant experimental data in the literature to which the present results can be compared in the range of GrPr b/x which was considered in this study. Also, the literature review shows that there are no theoretical or experimental correlations for the relationship between the dimensionless volume flow rate and the dimensionless channel length for developing flow in a channel. The only theoretical investigations available, Bodoia and Osterle (13) and Aung (28, 29), give the dimensionless flow rate for the case of fully developed flow in a channel as presented in Section 2.2.

Figure 5.29 shows comparison of the experimental results and PHOENICS solution (p_a=1 bar) with the results of Elenbaas (3), Bodoia and Osterle (13), Miyatake and Fujii (26), Ofi and Hetherington (25), Aung (28) and Aihara (32) for air. It is noticeable in this figure that the present experimental results and PHOENICS solution compares favourably with the other results. Possible reasons for the slight difference could be the value of atmospheric pressure used and the definition of film temperature and the associated pressure value used to define kinematic viscosity appearing in Grashof number.

5.7 Use of the Apparatus as a Trombe Wall System

5.7.1 Efficiency Studies

The present system design is similar to the Trombe wall system referred to in Chapter 2. As is well known, the Trombe wall system is a natural convection solar air heating collector. When the sun shines on the system, the glass and the wall absorb the solar energy which causes temperature rises of the two surfaces. Heat is only delivered by convection when the channel wall and glass temperatures are high enough to cause thermo-circulation of the fluid because of the buoyancy effect.

The convective thermo-syphoning efficiency η_c can be defined as:

$$\eta_C = \frac{Q_x}{I\ A} \qquad (5.12)$$

where

Q_x is the heat collected by the air up to a location x in the channel (w)

I is the average light intensity incident on the outside of the glass surface (w/m^2), and

A is the collection area (m^2).

The tests described in this section were made with the heating supplied by the solar simulator only with no attempt made to control the heightwise variation of wall temperature. It was felt that the wall temperatures, both plate and glass, varied so greatly, that these results could not reasonly be compared with the constant wall temperature cases and were better dealt with by considering them in the context of an actual Trombe wall. Clearly, the storage aspects of a real Trombe wall design have not been included here, but the main influences on the air flow in such a system i.e. plate height, channel width and wall temperature variation have been accounted for.

Figures 5.30 and 5.31 show the efficiency of the channel plotted against the channel widths for different channel heights with the lamps at half and full power. The convective efficiencies are low because a large portion of heat delivered by the lights is transferred through the

back of the heater plate assembly as discussed in Chapter 4. These figures show that an increase in the channel width gives an increase in the efficiency of the channel while an increase in height for a particular width gives a decrease in efficiency. These statements are valid for all channel widths except the 25 to 100 mm widths for the two and three metre channel heights with the lamps at half power. Also, the efficiency results indicate that the heat gain by the air is not directly proportional to the channel height. It can also be inferred that the increase in the heat gain by the air in the two and three metre channels is not proportional to the increase in the insolation for the two and three metre channels respectively. This was found to be true with the lamps at both half and full power.

5.7.2 Flowrate Experimental Results

Mass and volume flow rates are plotted in Figures 5.32 to 5.35 for different channel heights and widths for the lamps at half and full power. These Figures show increases in the mass and volume flow rate as the channel width and height increases. The mass and volume flowrates are also seen to be greater with the lamps at full power than at half power for the same height and width. For one metre channel height and the lamps at half power, the mass

and volume flowrate decreases when the channel width is over 125 mm. Therefore the channel width of 125 mm appears to be an optimum value for this case. Apart from the one case already discussed, all others showed the same trend of mass and volume flow rates tending to some asympotic value but the range of channel widths available did not permit investigation of optimum channel widths for these cases.

5.7.3 Application to Design of Convective Ventilating Systems.

Ideally, designers of buildings should be able to predict the convective performance of such architectural features as the Trombe wall, solar chimney or similar passive solar elements. Before any use can be made of the correlations referred to earlier in this thesis, the designer must consider further calculations to take account of thermal storage, radiant and convective exchanges between all the system components to obtain the wall temperature variation with height and probably also time. Each system design has to be considered individually and it is thought that the present work and resulting correlation equations could possibly be included in a computer simulation of such systems to describe the air flow behaviour in the channel. This problem is however outwith the scope of the present work and the following simplified

procedure for use by a designer is suggested.

If the designer is interested in predicting the laminar convective flow performance of a passive ventilation system it is necessary to know the geometry of the system, and the wall, glass and inlet temperatures. For a given value of GrPr b/x the Nusselt number can be obtained using equation 5.1 or Figure 5.11. Also, it is possible to predict the volume flow rate $\dot{Q}$, for a fixed channel height L, using equation 5.3 or Figure 5.14. Conversely, if a required flow rate must be obtained then the designer can vary the duct height and width but the assumed wall temperature must give the correct value of GrPr b/x.

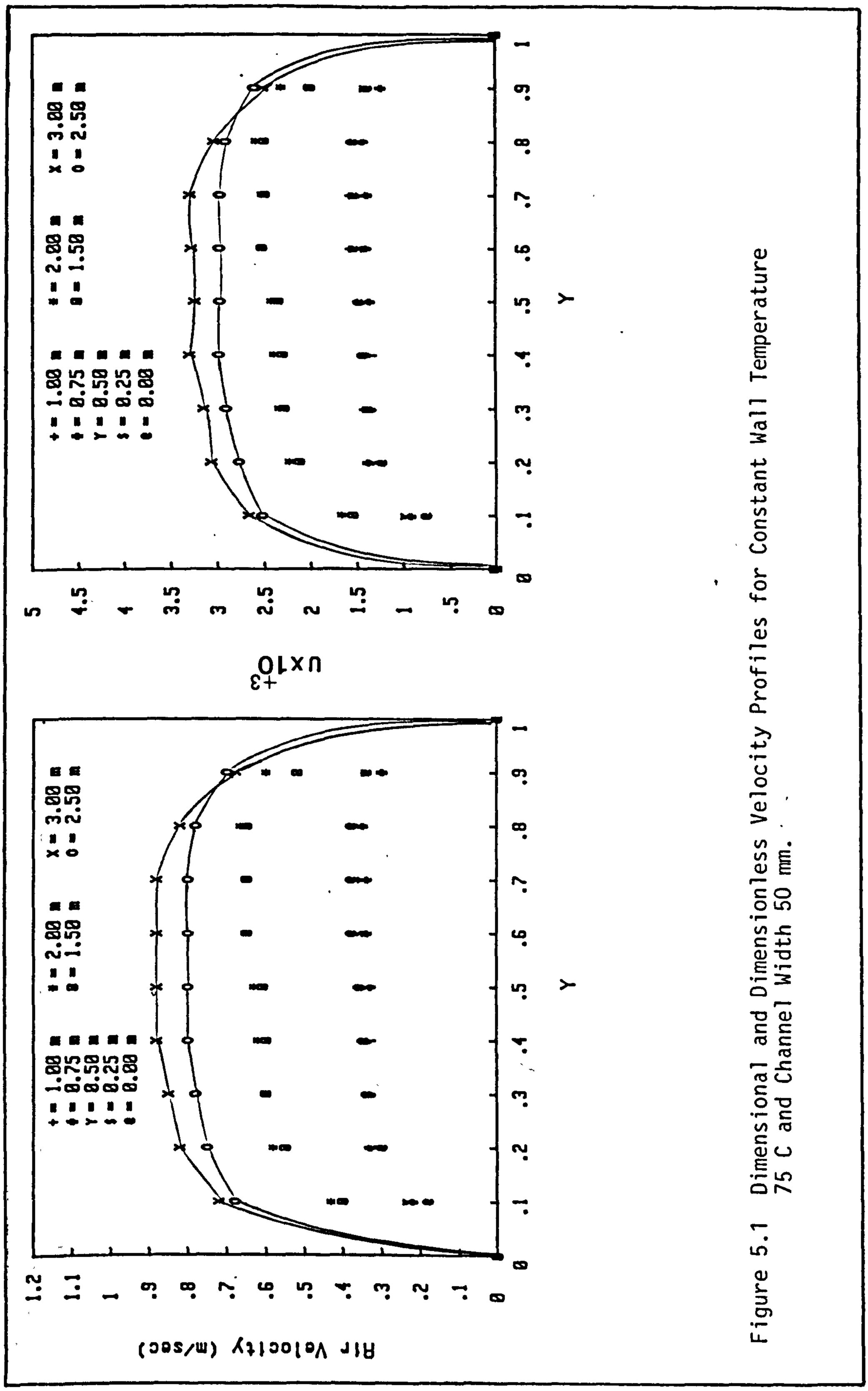

Figure 5.1 Dimensional and Dimensionless Velocity Profiles for Constant Wall Temperature 75 C and Channel Width 50 mm.

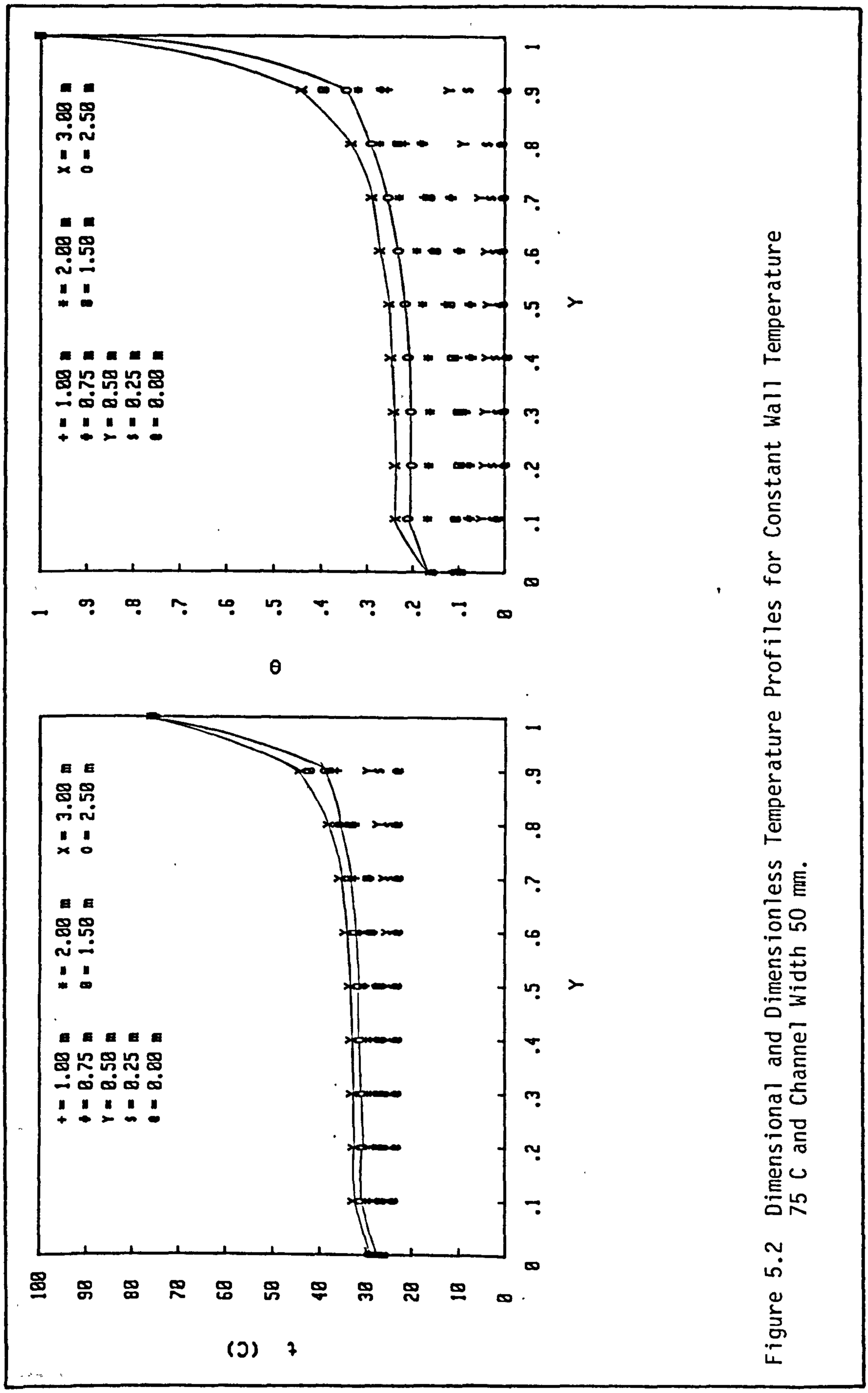

Figure 5.2 Dimensional and Dimensionless Temperature Profiles for Constant Wall Temperature 75 C and Channel Width 50 mm.

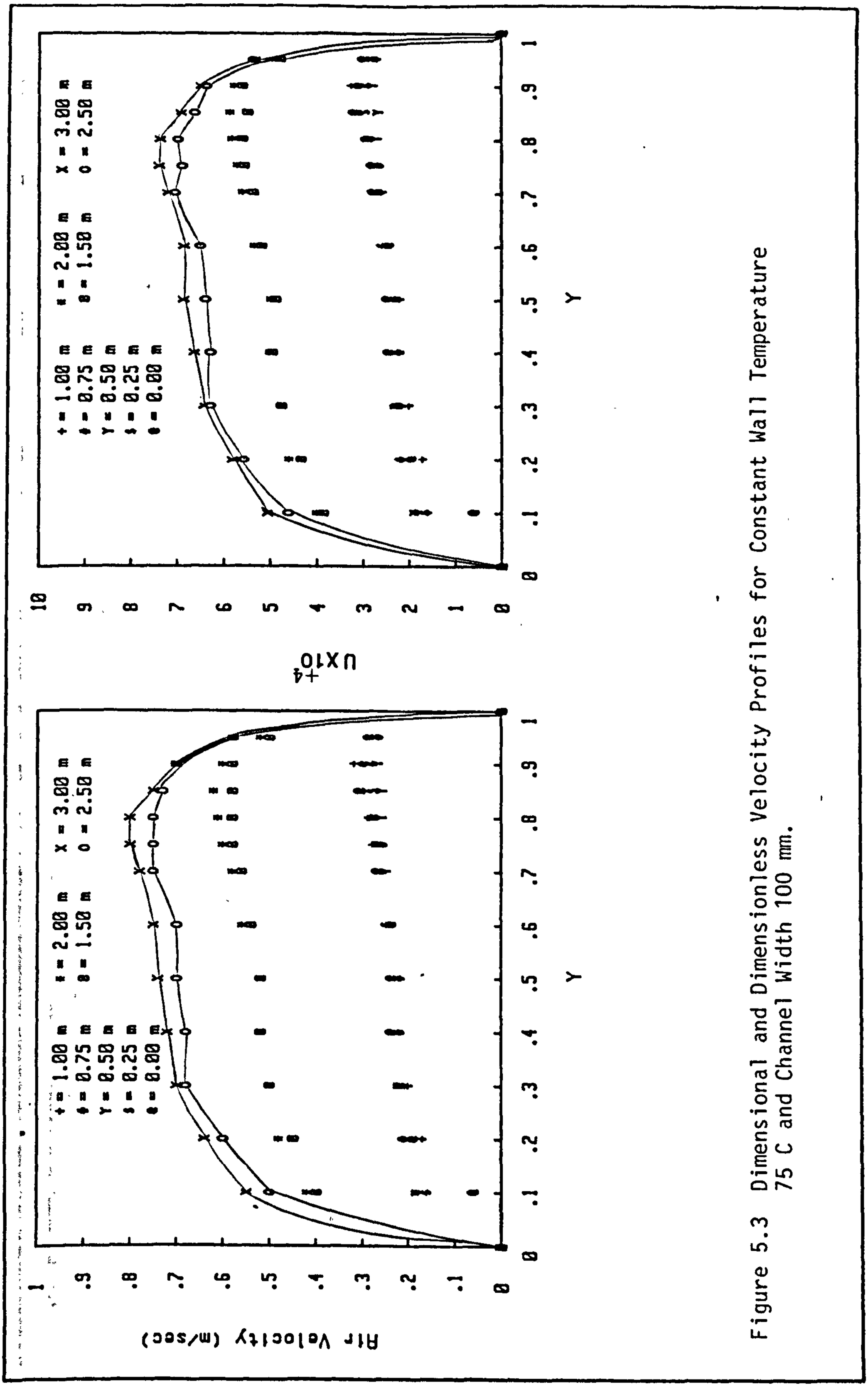

Figure 5.3 Dimensional and Dimensionless Velocity Profiles for Constant Wall Temperature 75 C and Channel Width 100 mm.

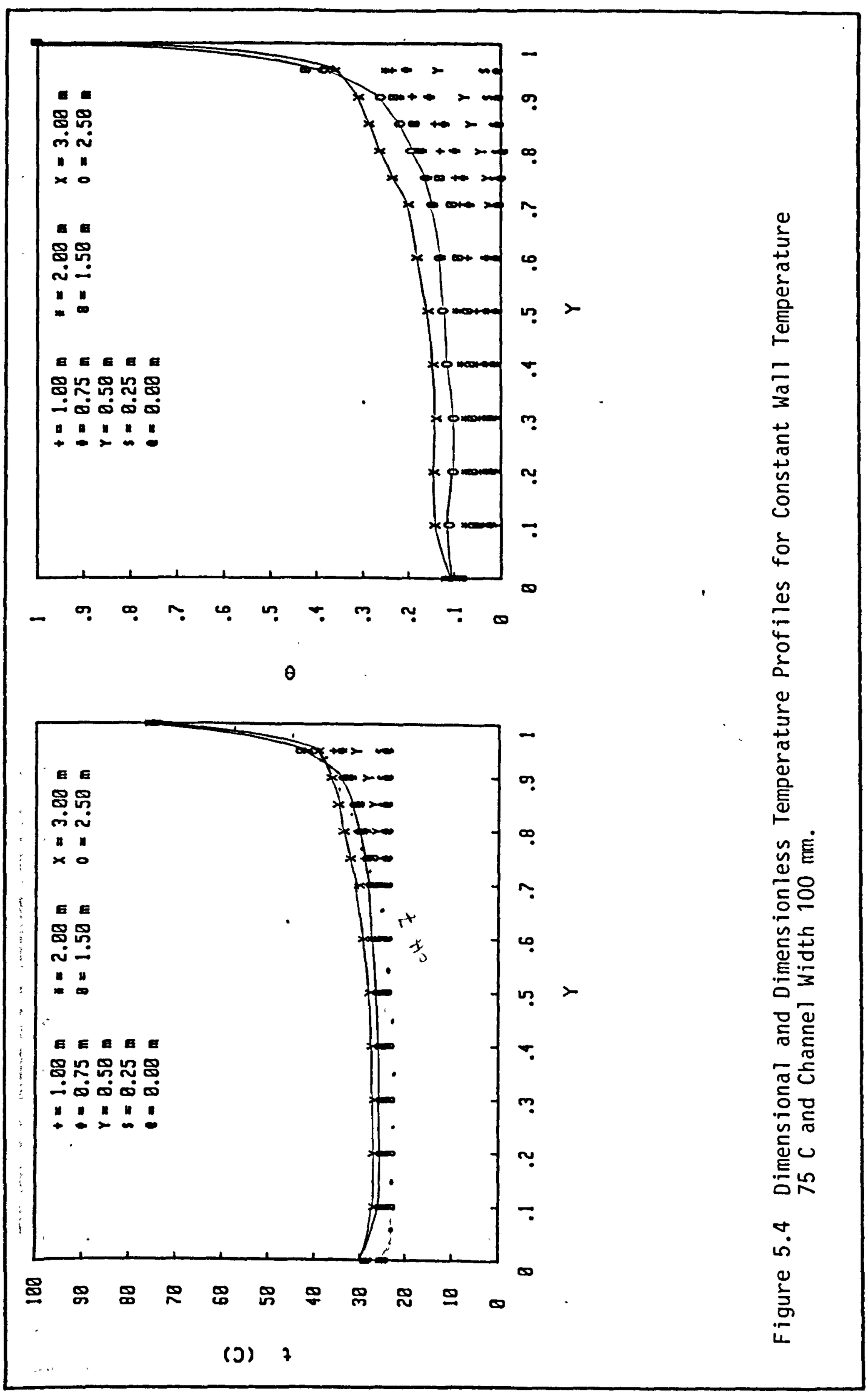
x = 2.00 m
o = 1.50 m
x = 3.00 m
o = 2.50 m
+ = 1.00 m
♦ = 0.75 m
Y = 0.50 m
s = 0.25 m
● = 0.00 m
Θ
Y
t (C)
Dimensional and Dimensionless Temperature Profiles for Constant Wall
75 C and Channel Width 100 mm.

Figure 5.4

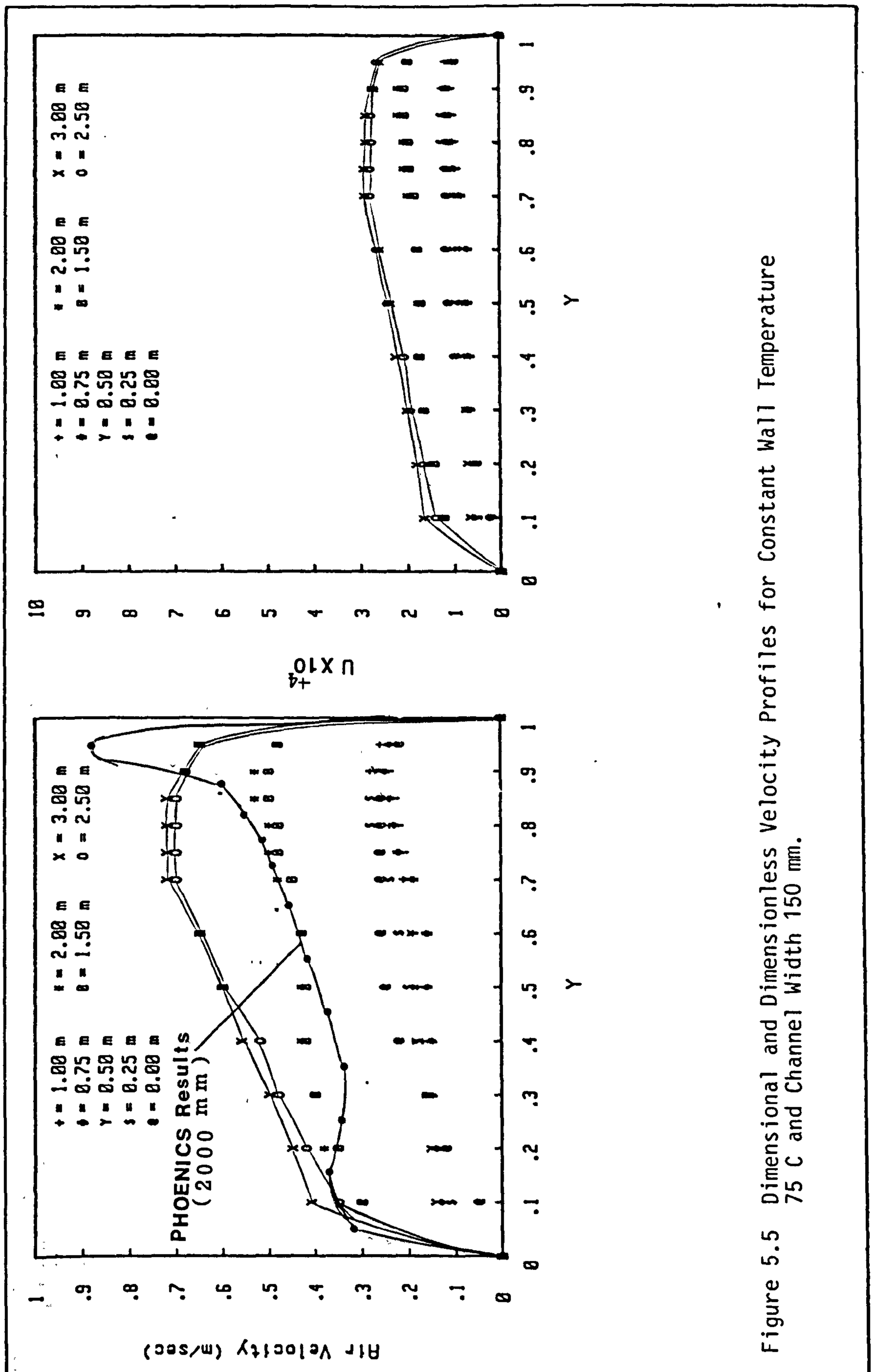

Figure 5.5 Dimensional and Dimensionless Velocity Profiles for Constant Wall Temperature 75 C and Channel Width 150 mm.

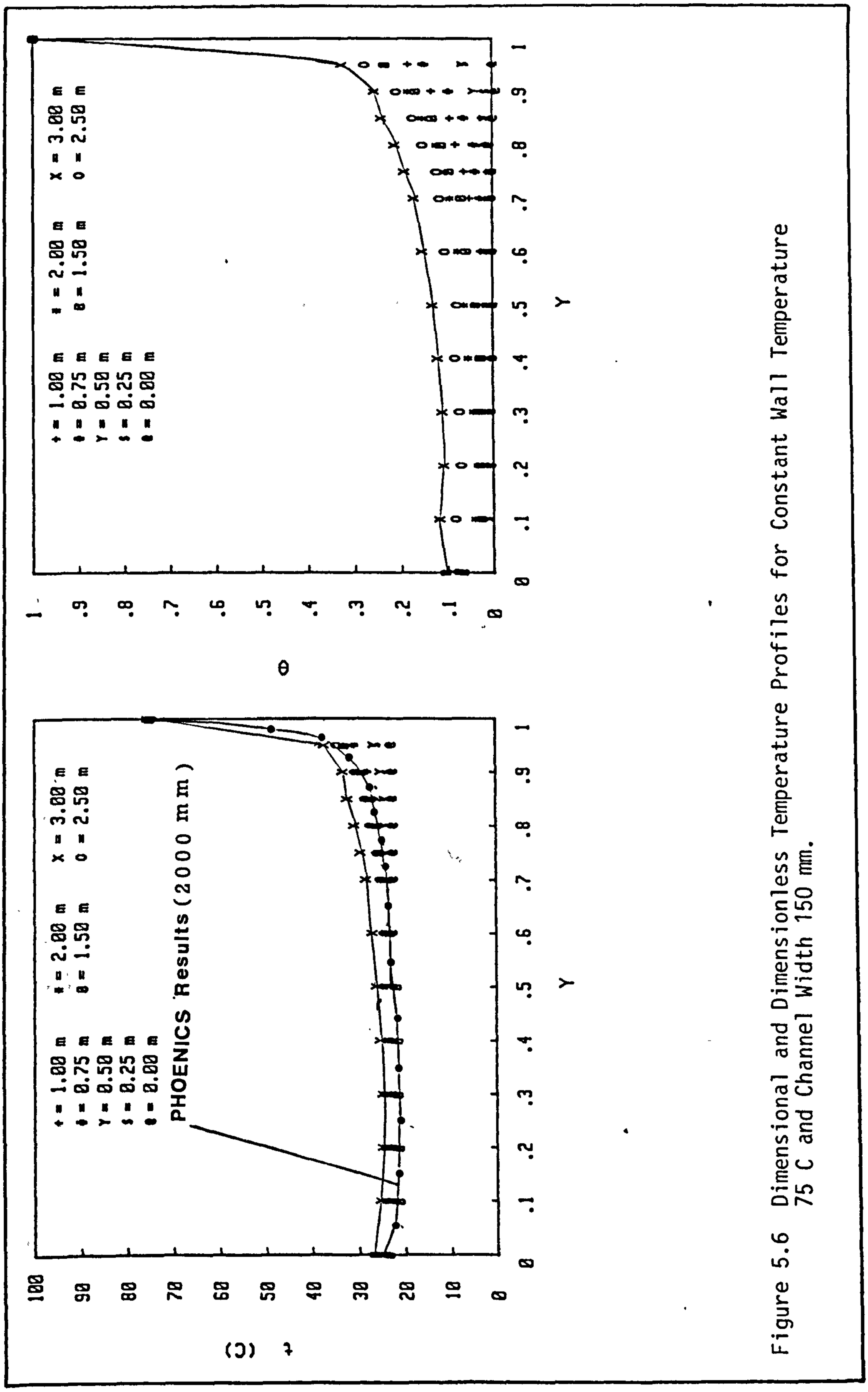

Figure 5.6 Dimensional and Dimensionless Temperature Profiles for Constant Wall Temperature 75 C and Channel Width 150 mm.

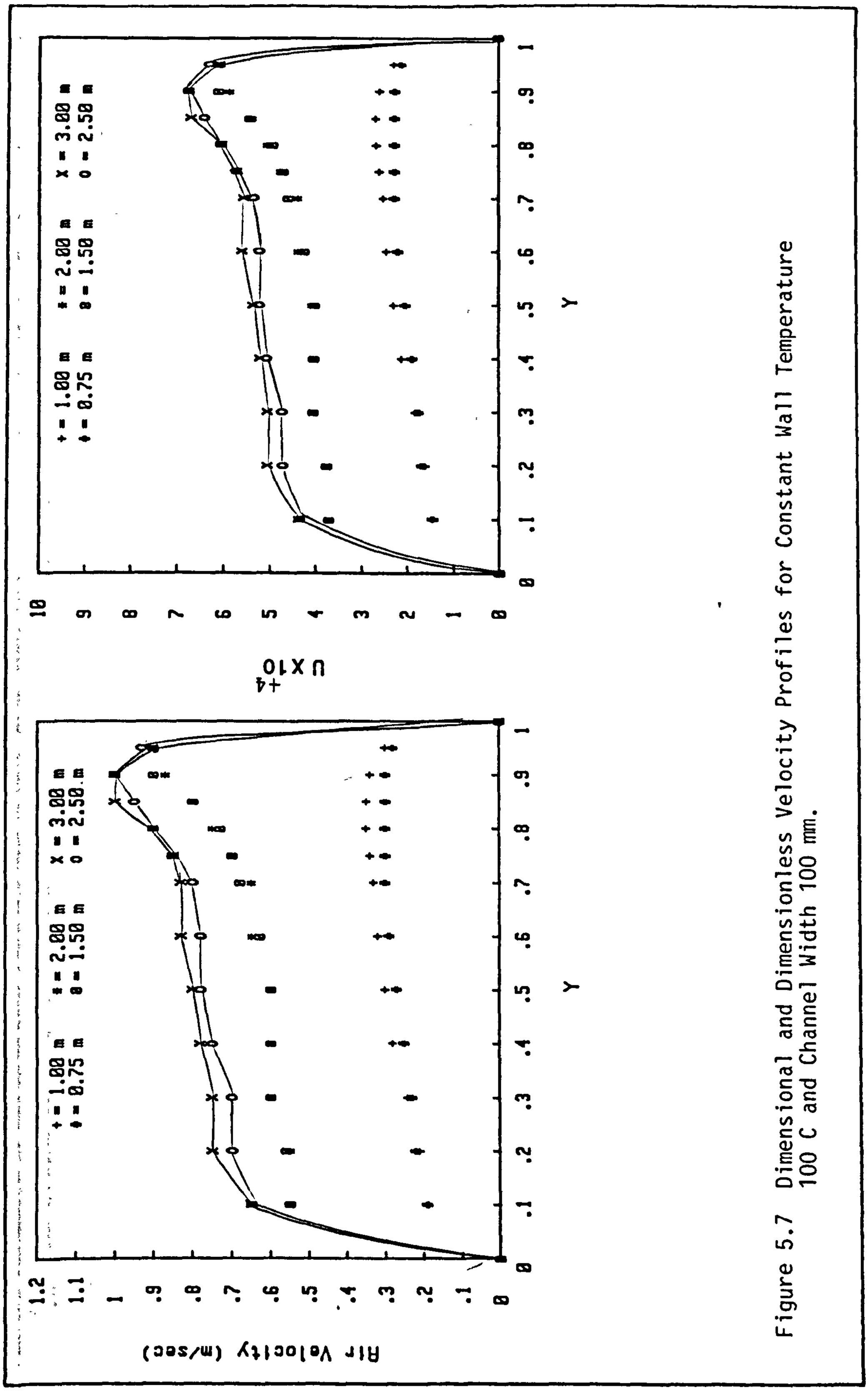

Figure 5.7 Dimensional and Dimensionless Velocity Profiles for Constant Wall Temperature 100 C and Channel Width 100 mm.

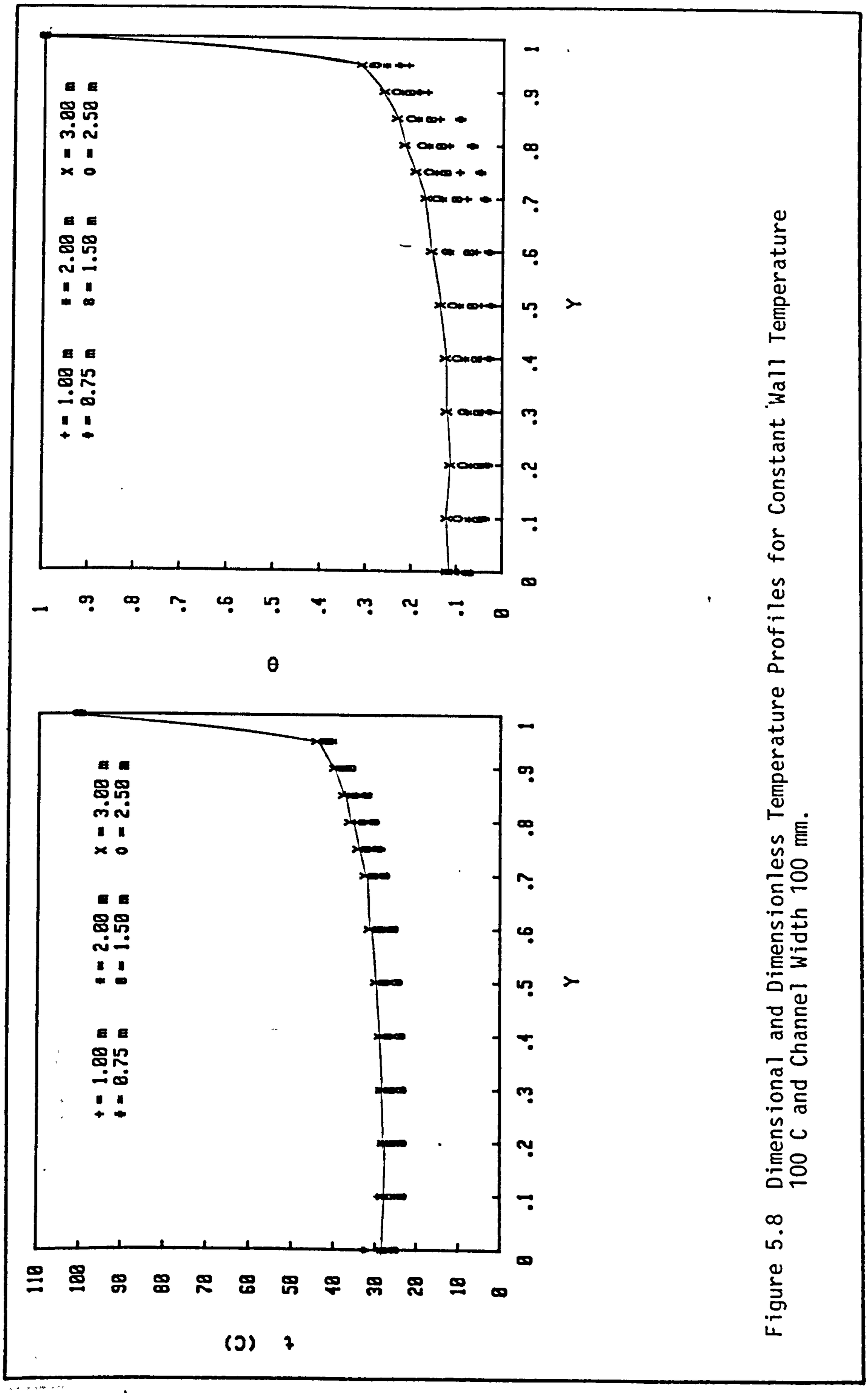

Figure 5.8 Dimensional and Dimensionless Temperature Profiles for Constant Wall Temperature 100 C and Channel Width 100 mm.

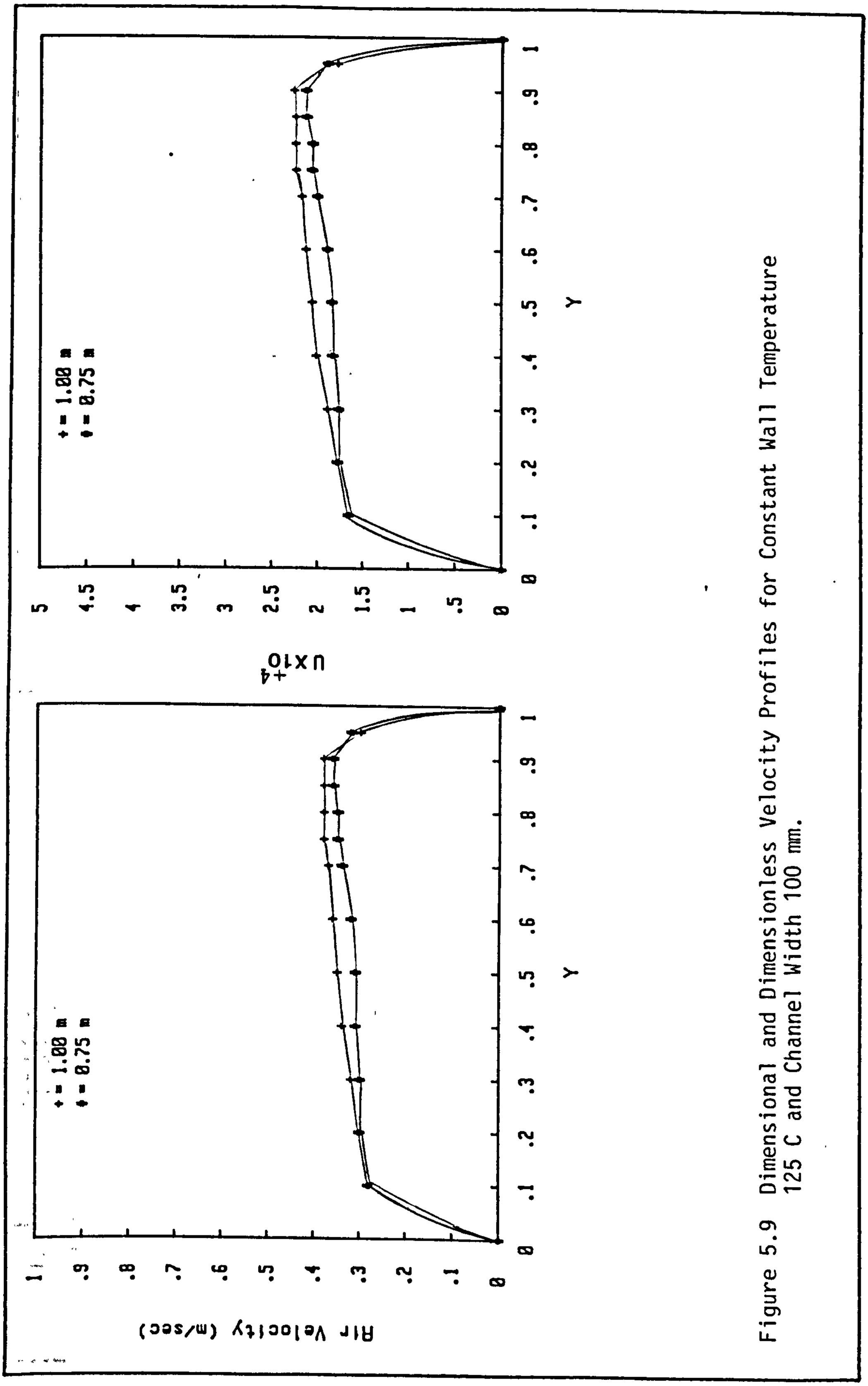

Figure 5.9 Dimensional and Dimensionless Velocity Profiles for Constant Wall Temperature 125 C and Channel Width 100 mm.

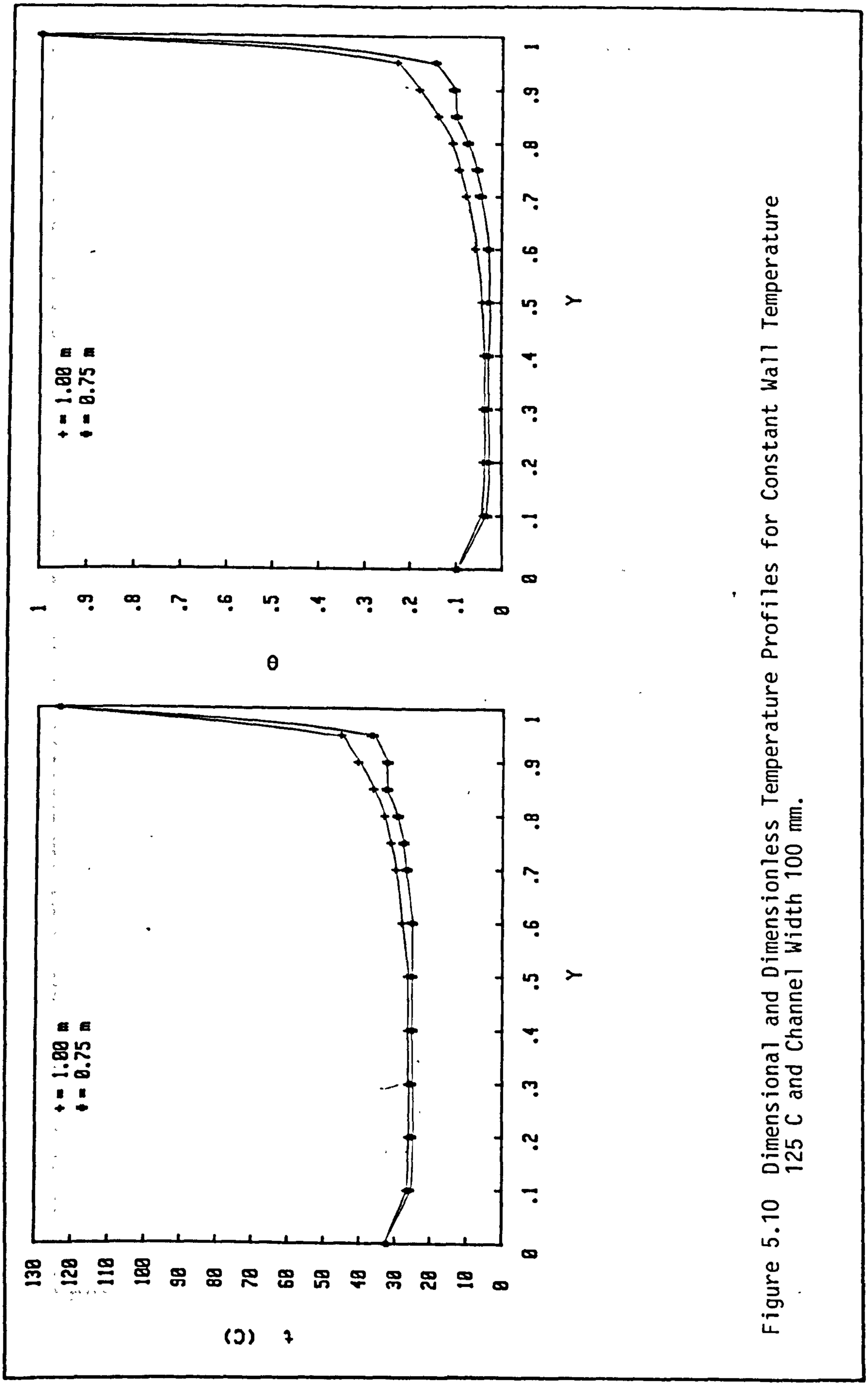

Figure 5.10 Dimensional and Dimensionless Temperature Profiles for Constant Wall Temperature 125 C and Channel Width 100 mm.

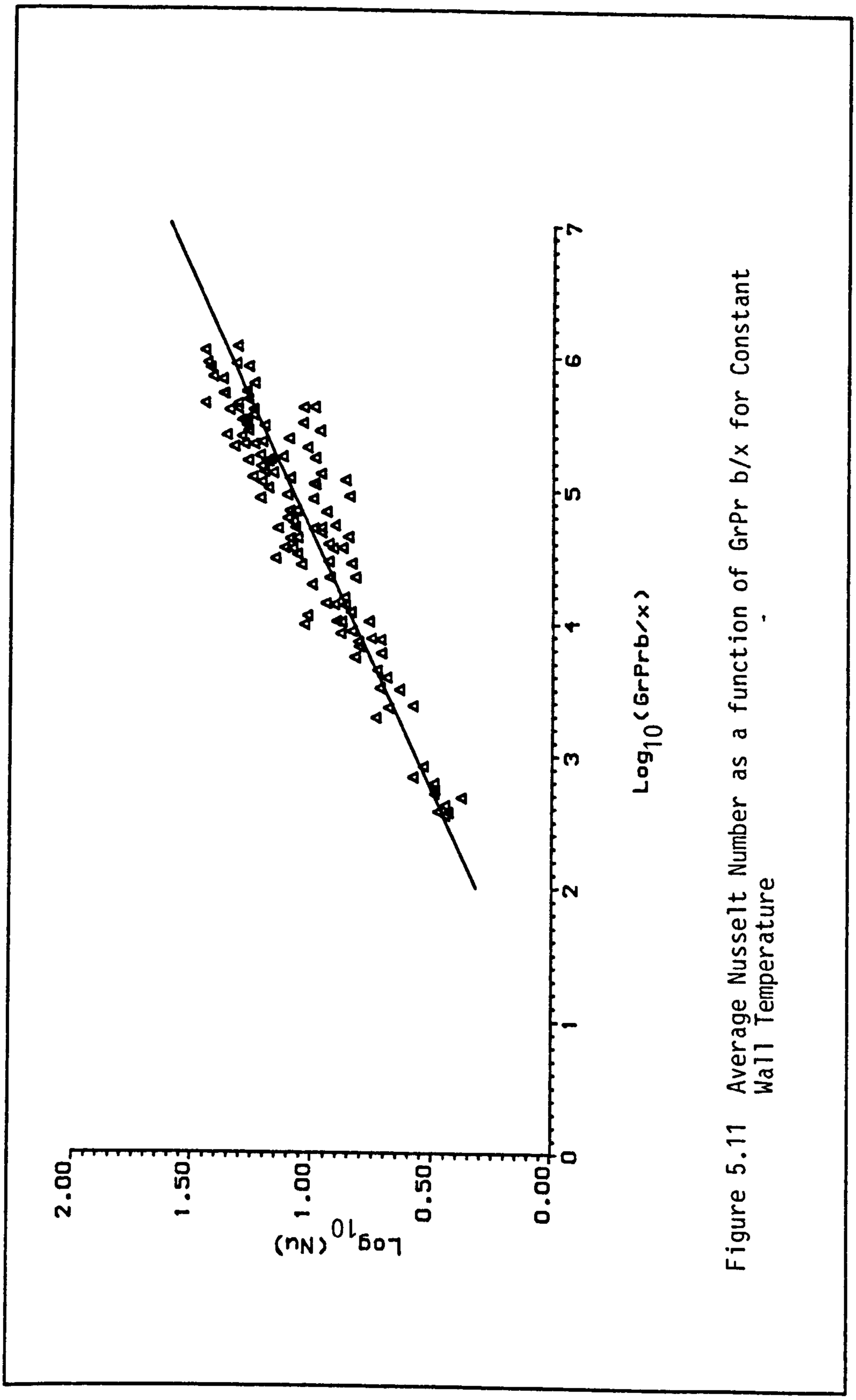

Figure 5.11 Average Nusselt Number as a function of GrPr b/x for Constant Wall Temperature

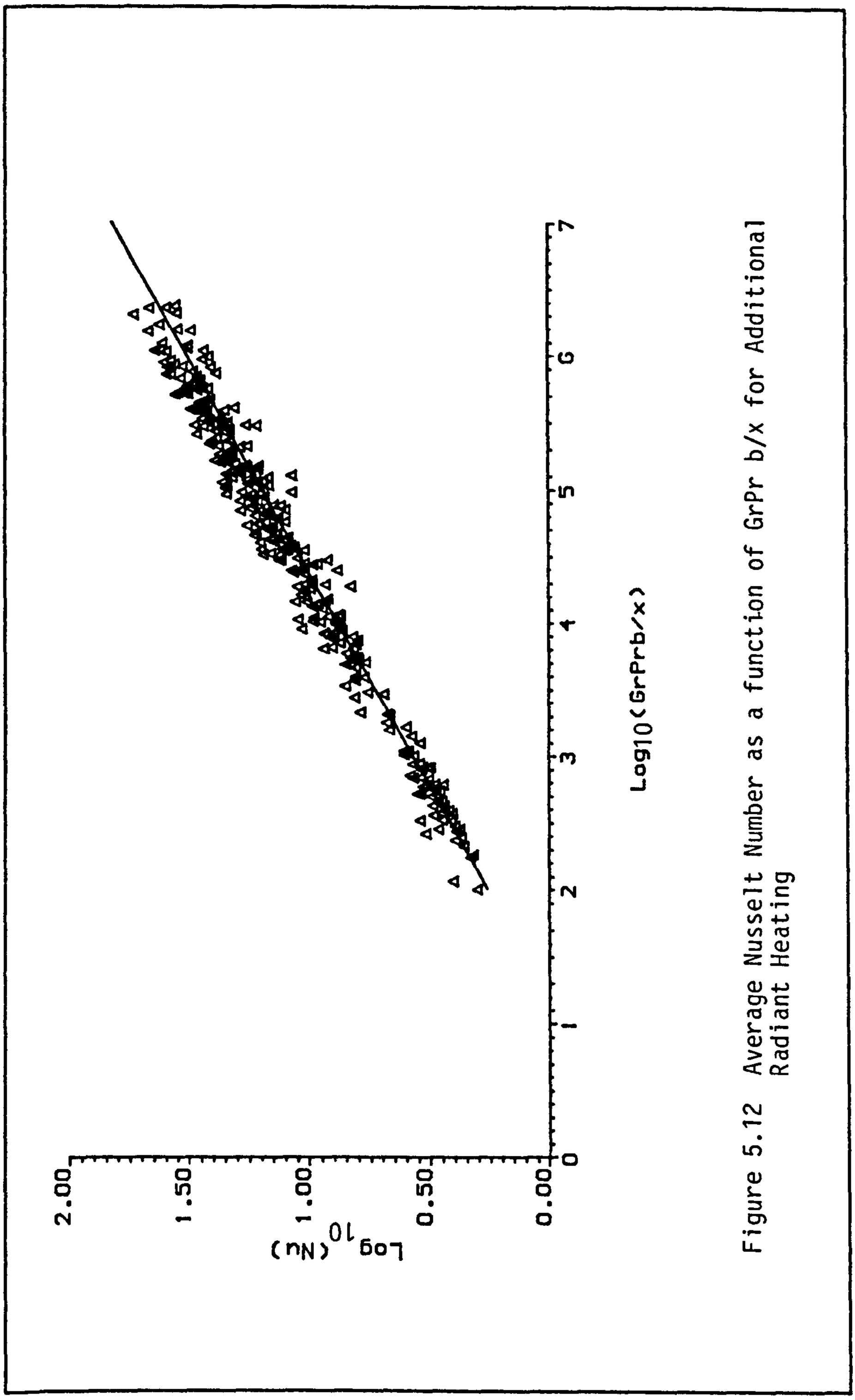

Figure 5.12 Average Nusselt Number as a function of GrPr b/x for Additional Radiant Heating

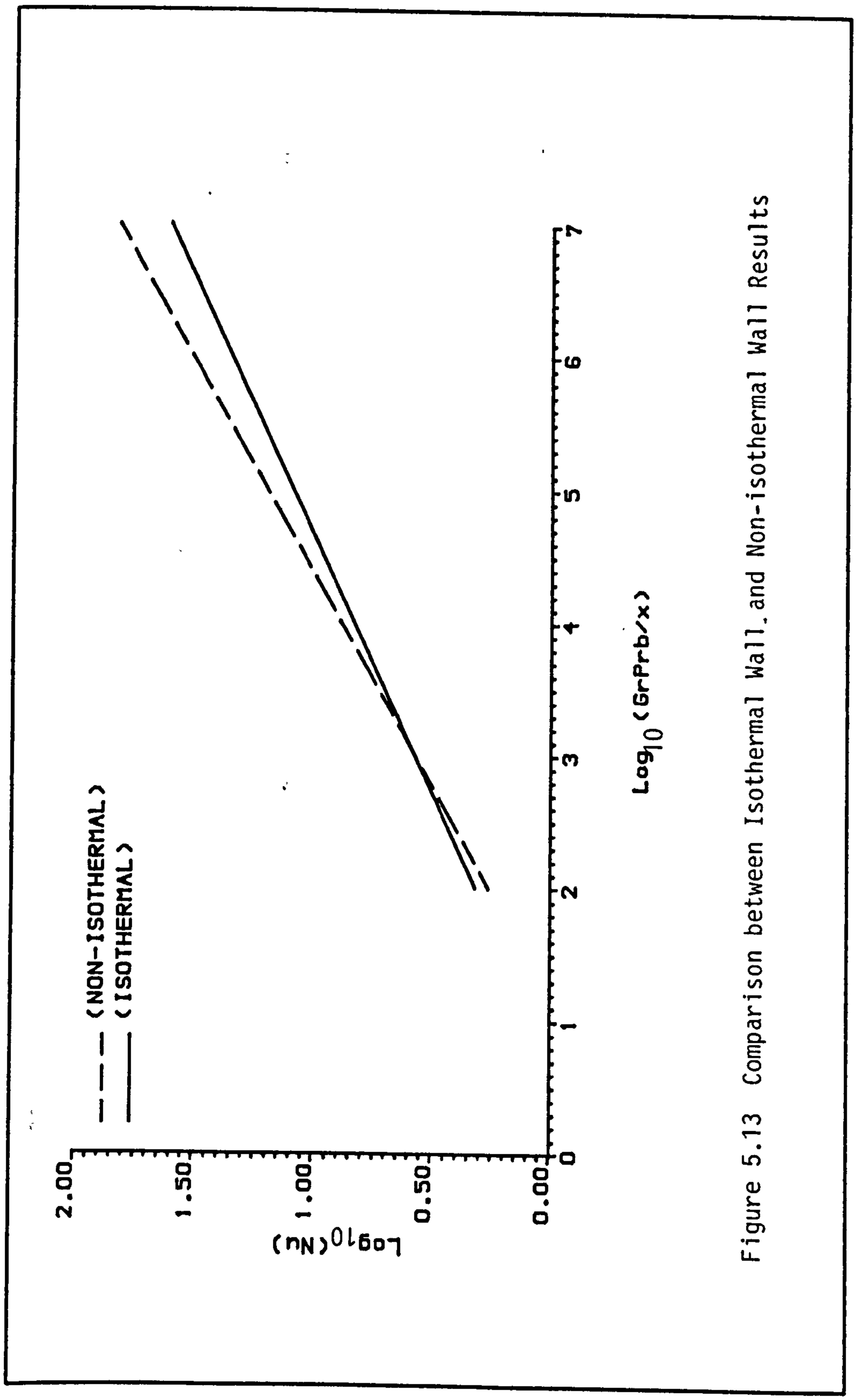

Figure 5.13 Comparison between Isothermal Wall and Non-isothermal Wall Results

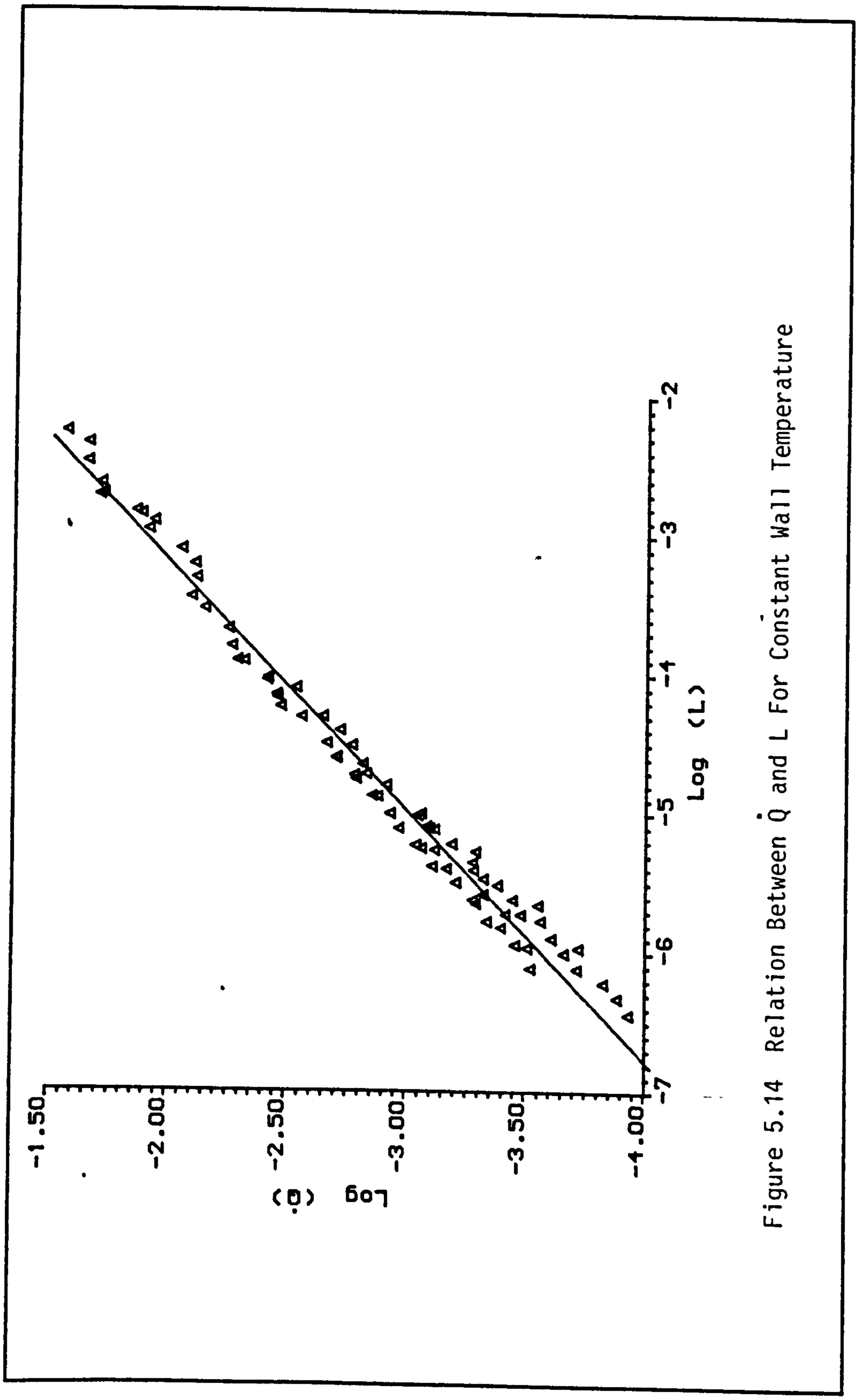

Figure 5.14 Relation Between Q̇ and L For Constant Wall Temperature

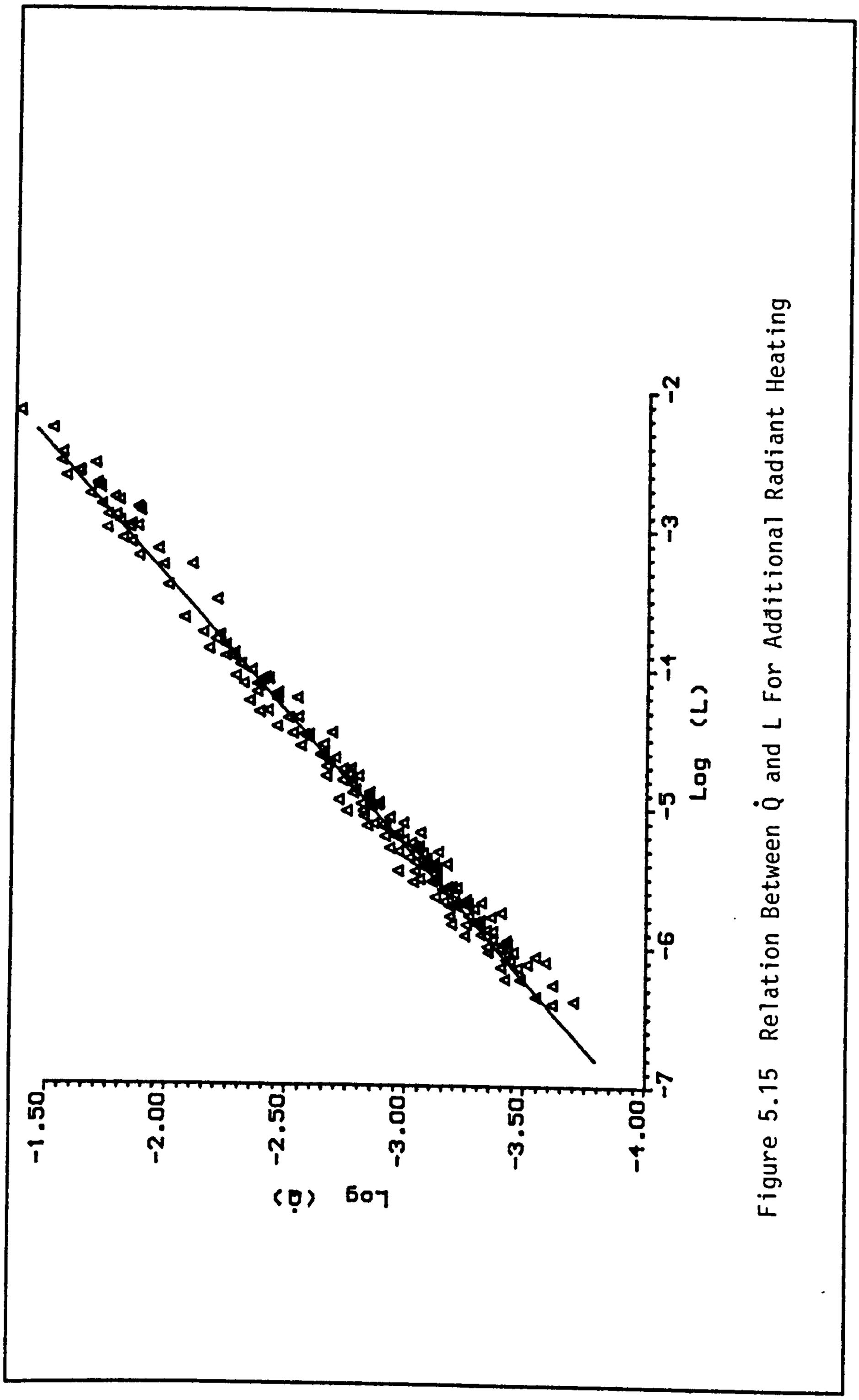

Figure 5.15 Relation Between $\dot{Q}$ and L For Additional Radiant Heating

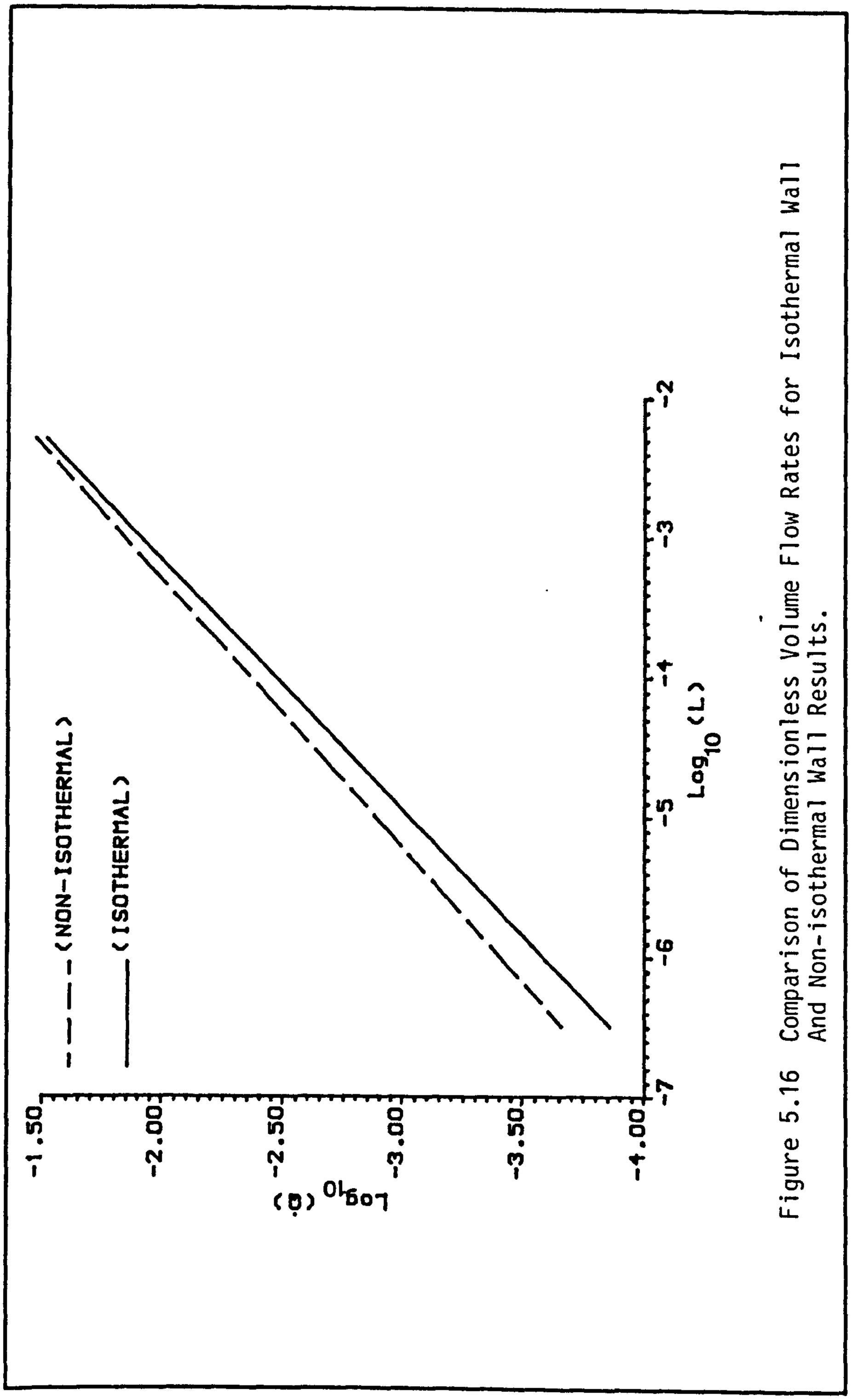

Figure 5.16 Comparison of Dimensionless Volume Flow Rates for Isothermal
And Non-isothermal Wall Results.

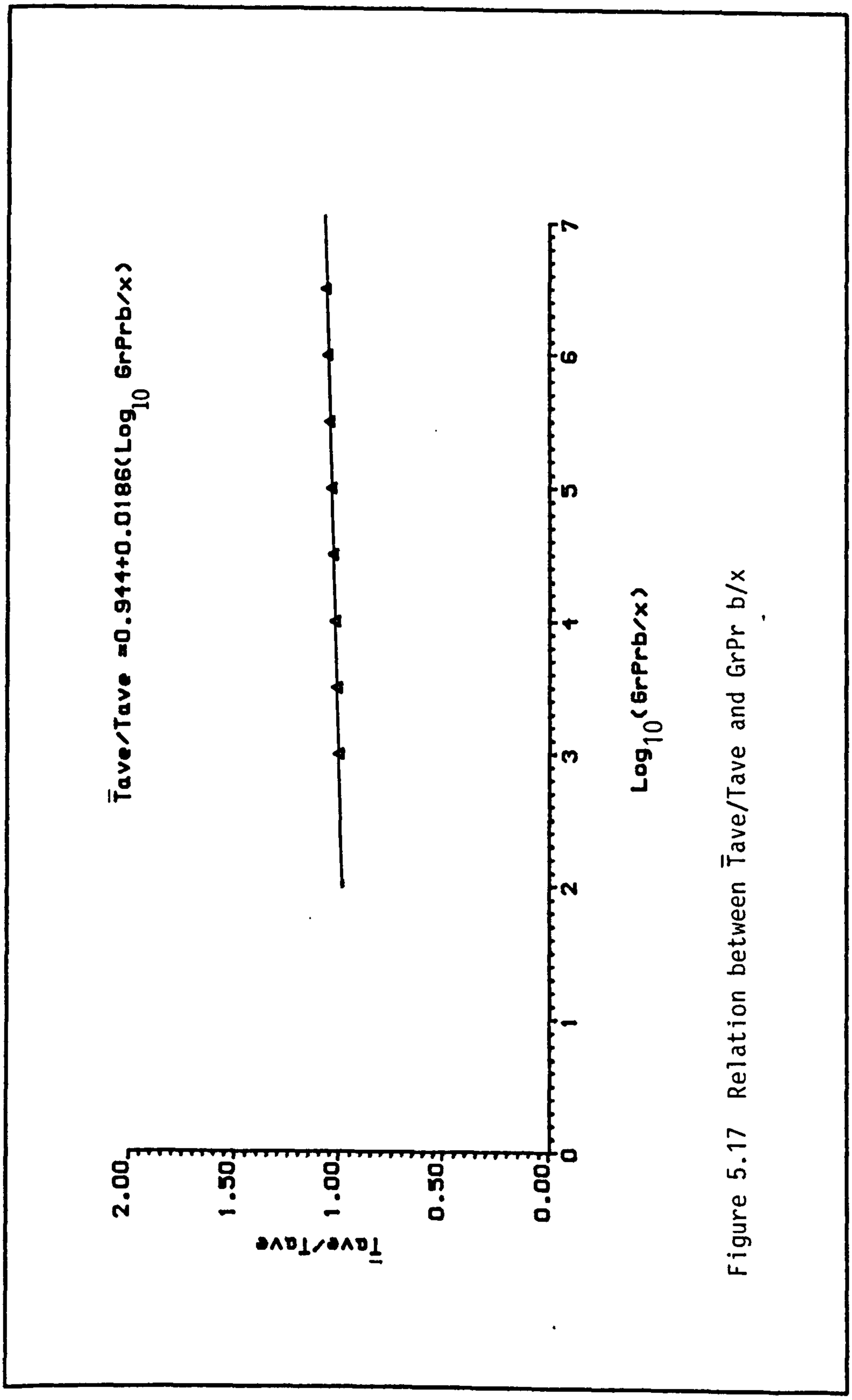

Figure 5.17 Relation between $\bar{T}ave/Tave$ and GrPr b/x

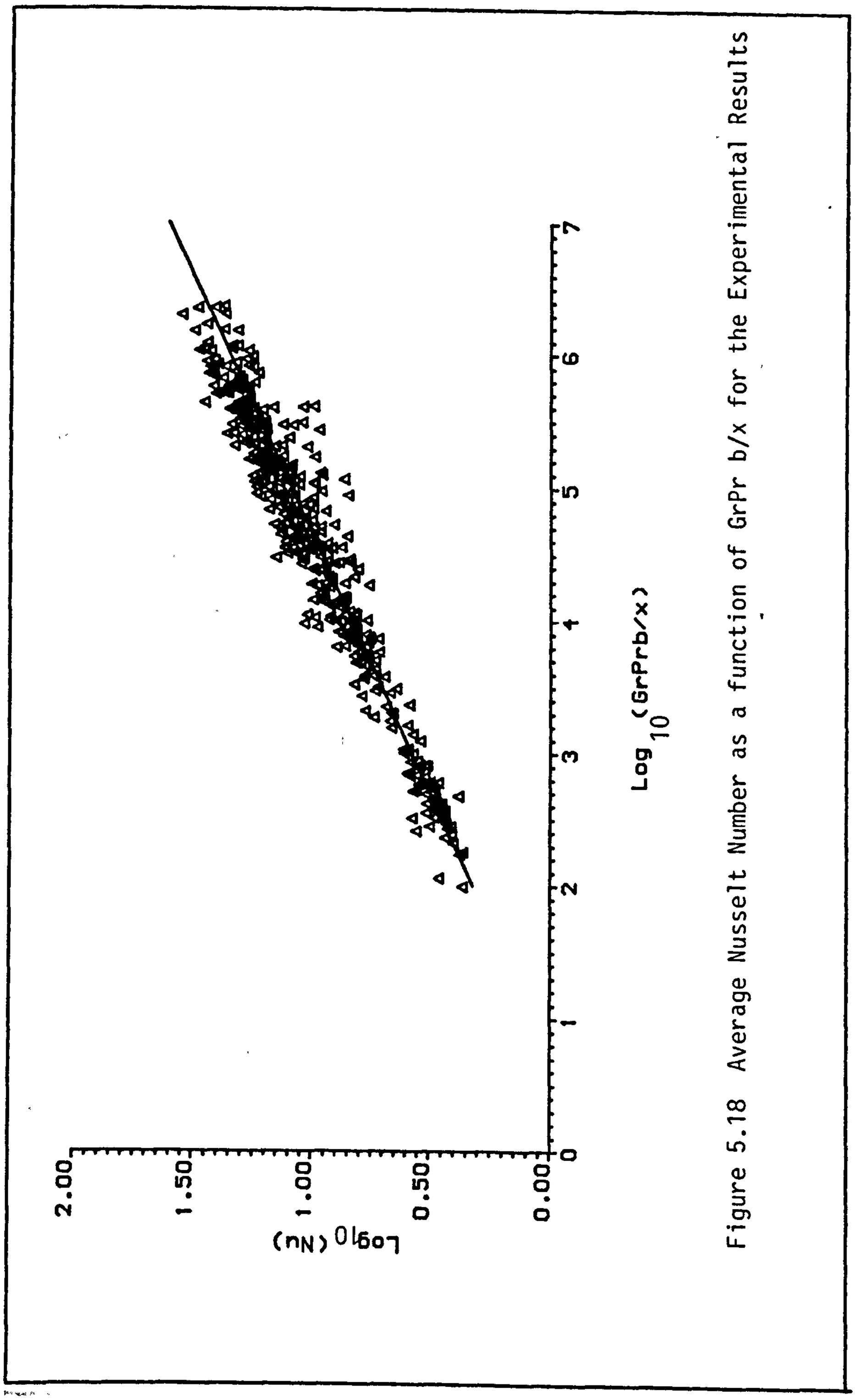

Figure 5.18 Average Nusselt Number as a function of GrPr b/x for the Experimental Results

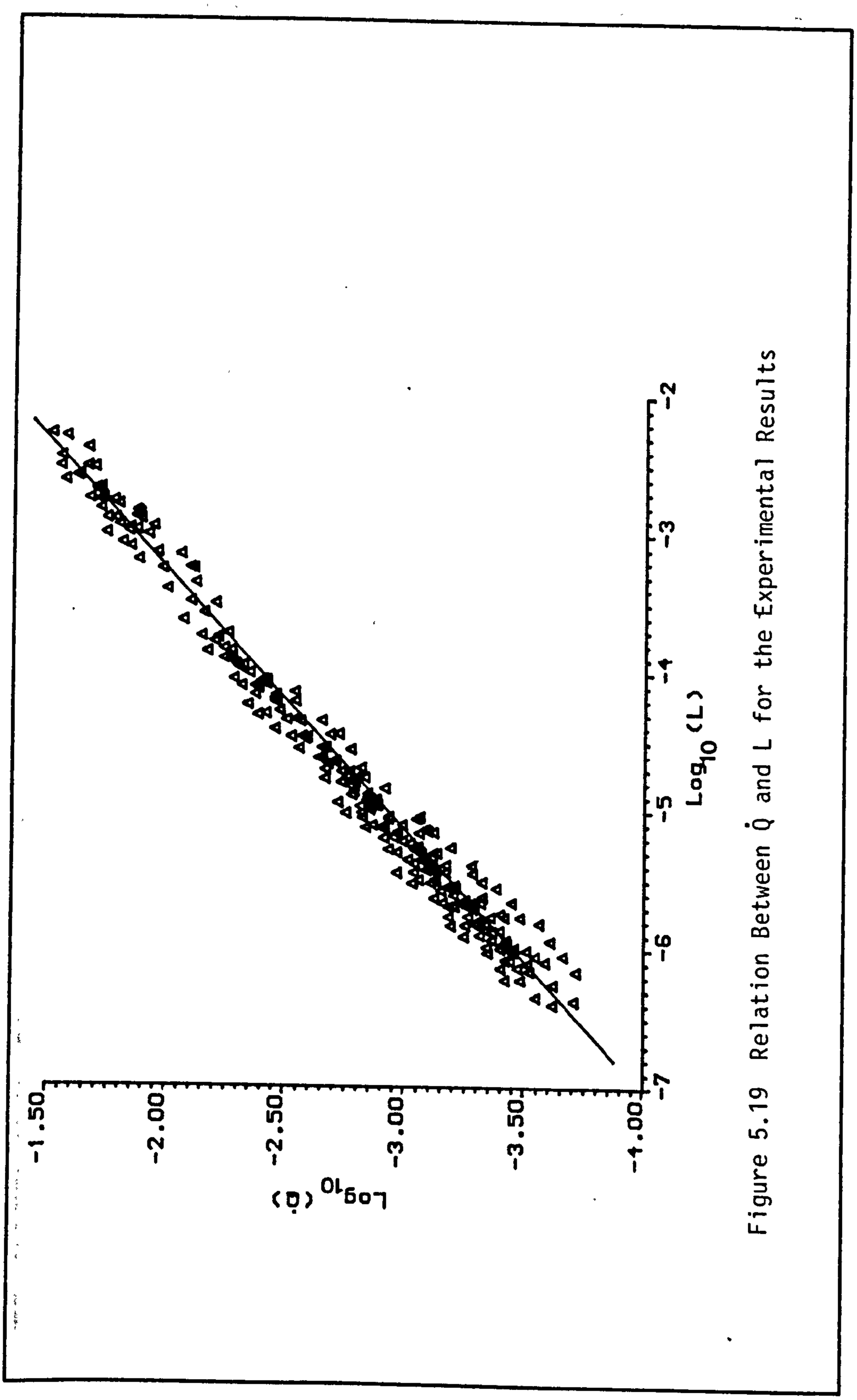

Figure 5.19 Relation Between $\dot{Q}$ and L for the Experimental Results

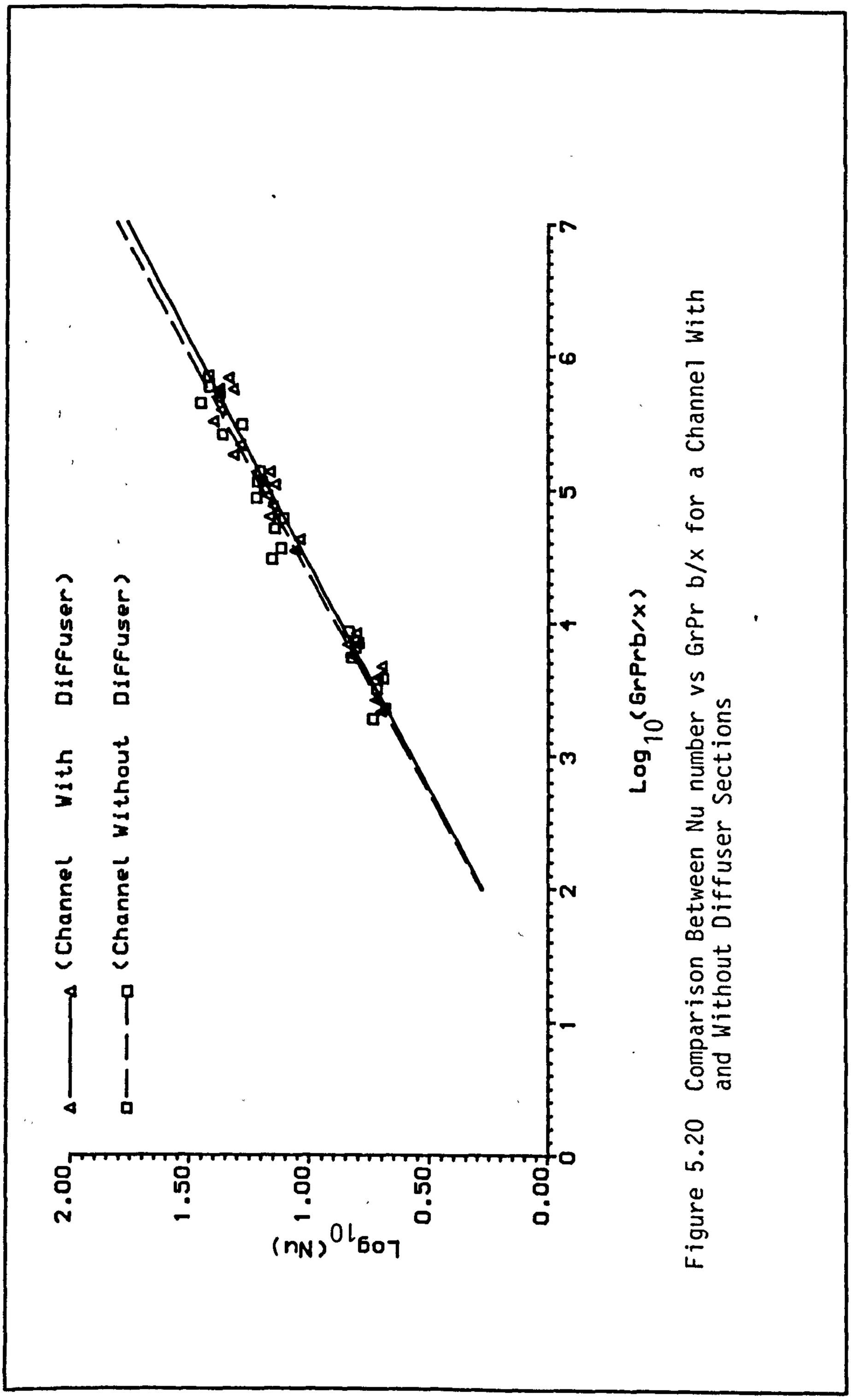

Figure 5.20 Comparison Between Nu number vs GrPr b/x for a Channel With and Without Diffuser Sections

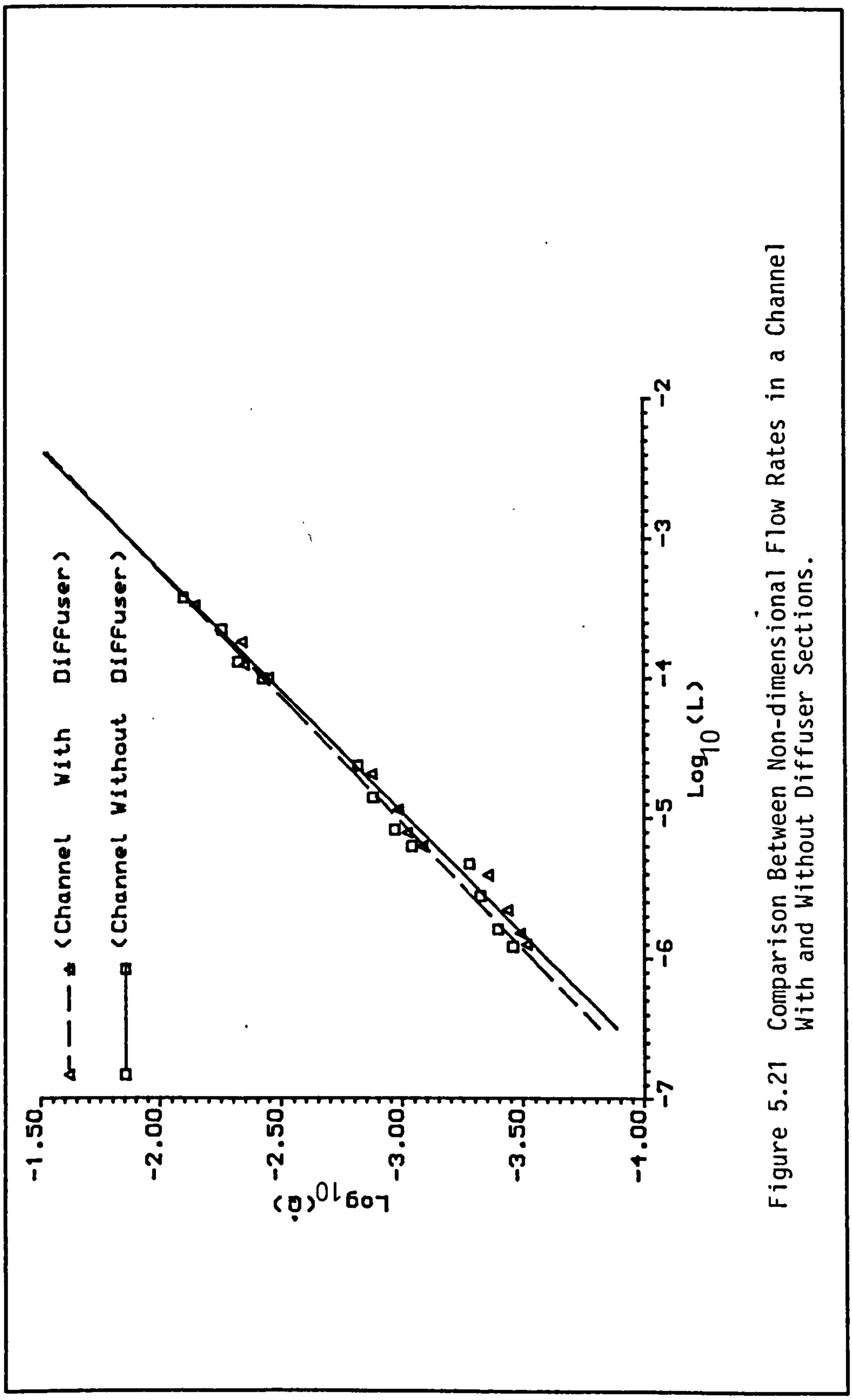

Comparison Between Non-dimensional Flow Rates in a Channel With and Without Diffuser Sections.

Figure 5.21

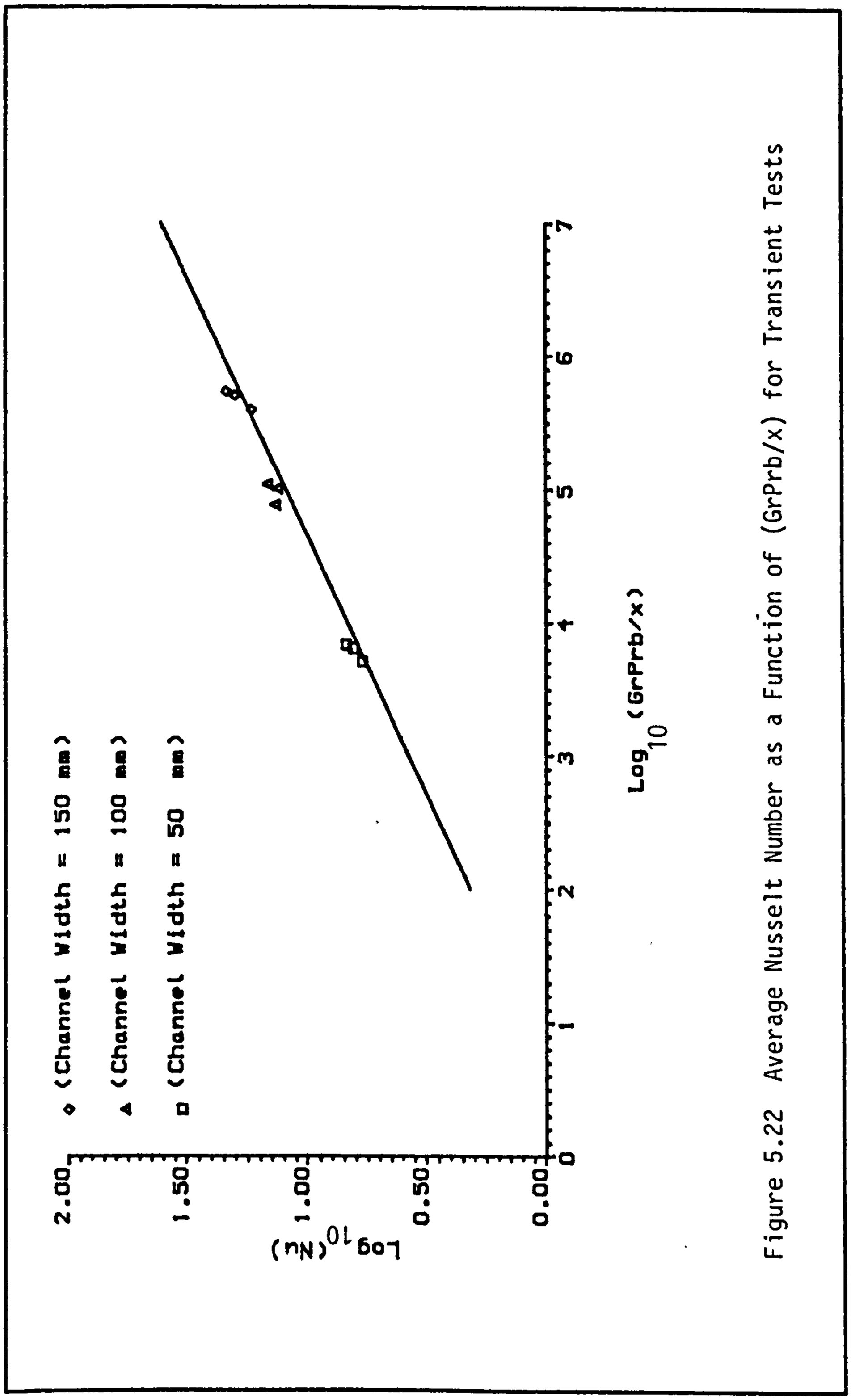

Figure 5.22 Average Nusselt Number as a Function of (GrPrb/x) for Transient Tests

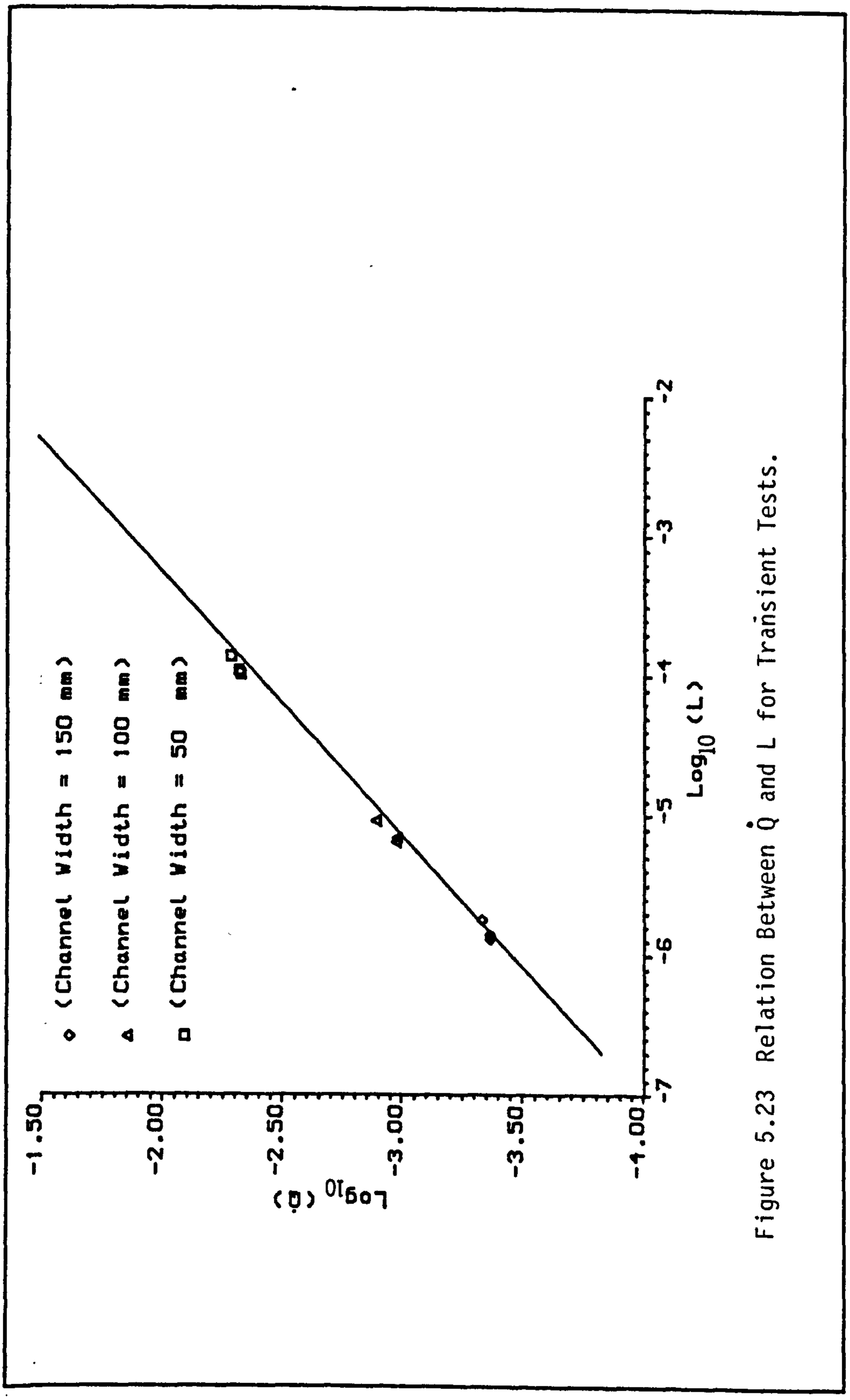

Figure 5.23 Relation Between $\dot{Q}$ and L for Transient Tests.

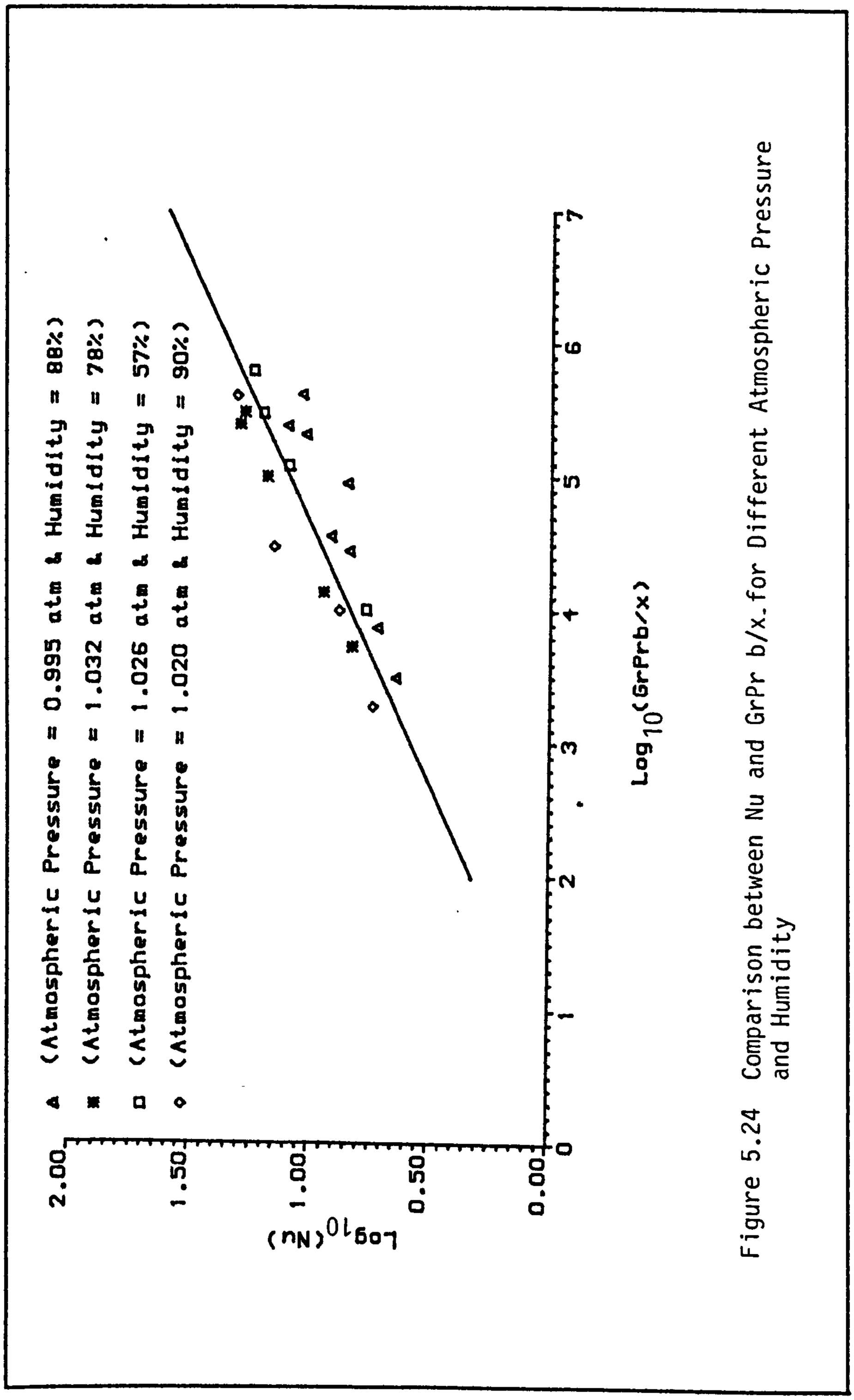

Figure 5.24 Comparison between Nu and GrPr b/x for Different Atmospheric Pressure and Humidity

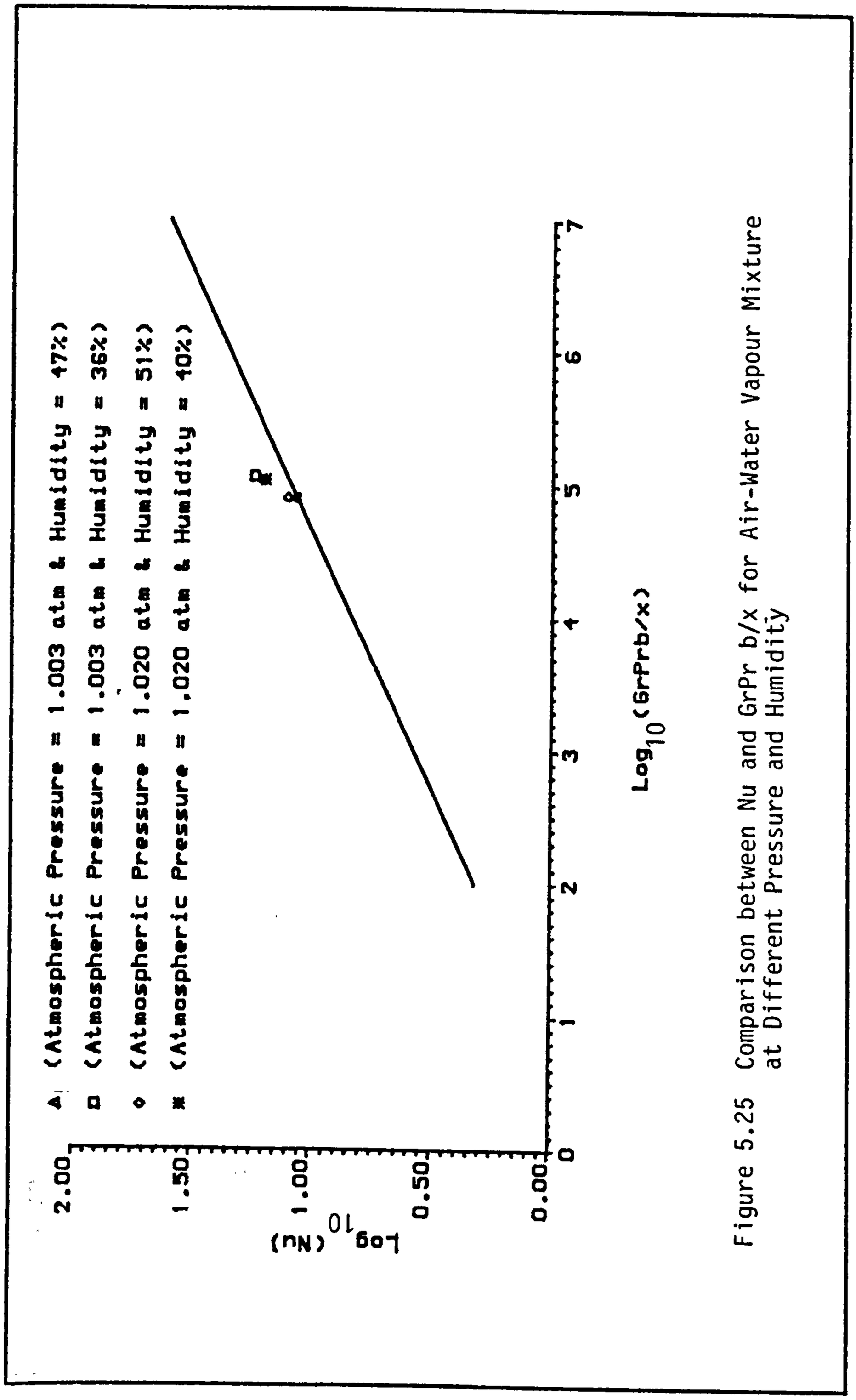

Figure 5.25 Comparison between Nu and GrPr b/x for Air-Water Vapour Mixture at Different Pressure and Humidity

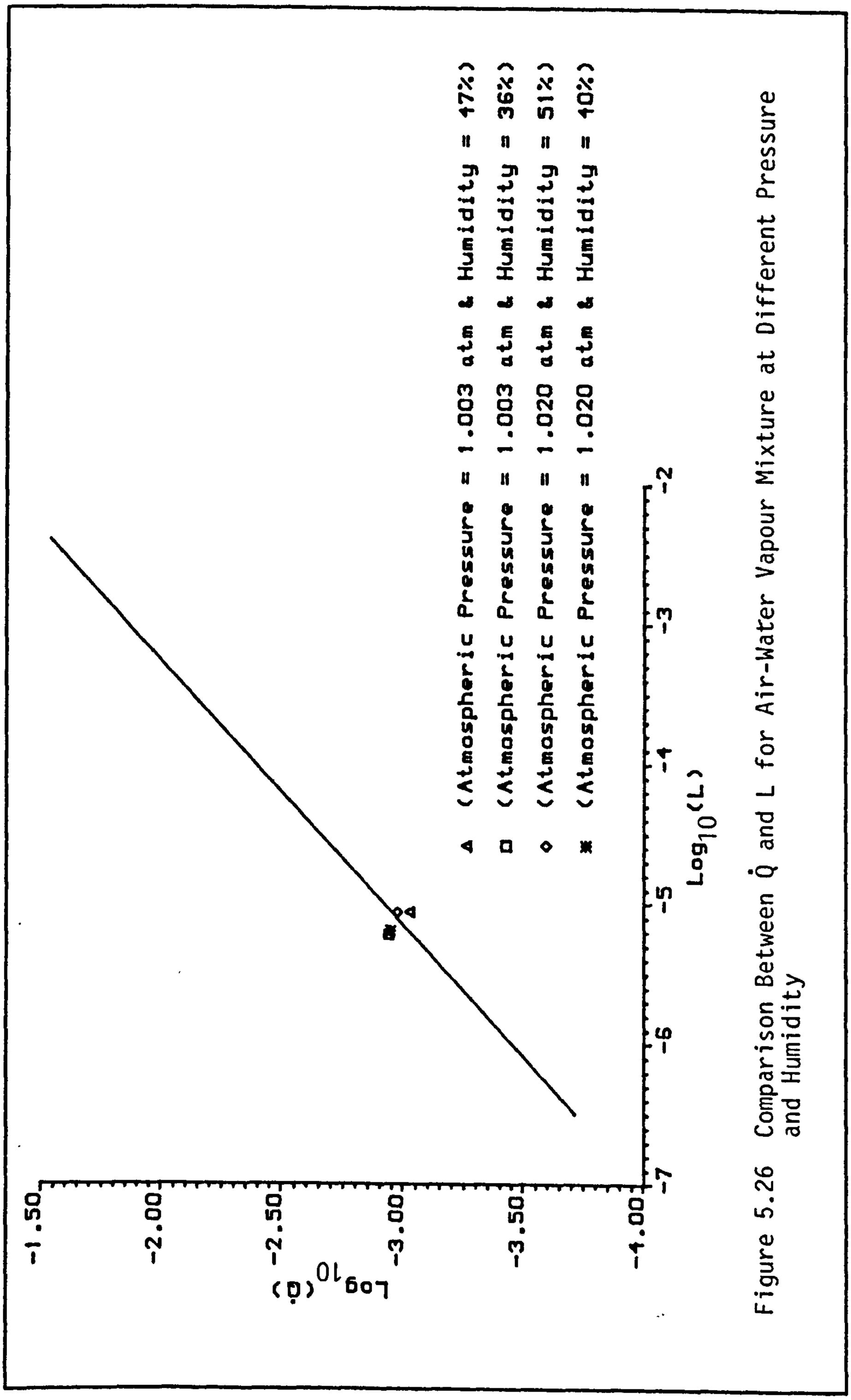

Figure 5.26 Comparison Between $\dot{Q}$ and L for Air-Water Vapour Mixture at Different Pressure and Humidity

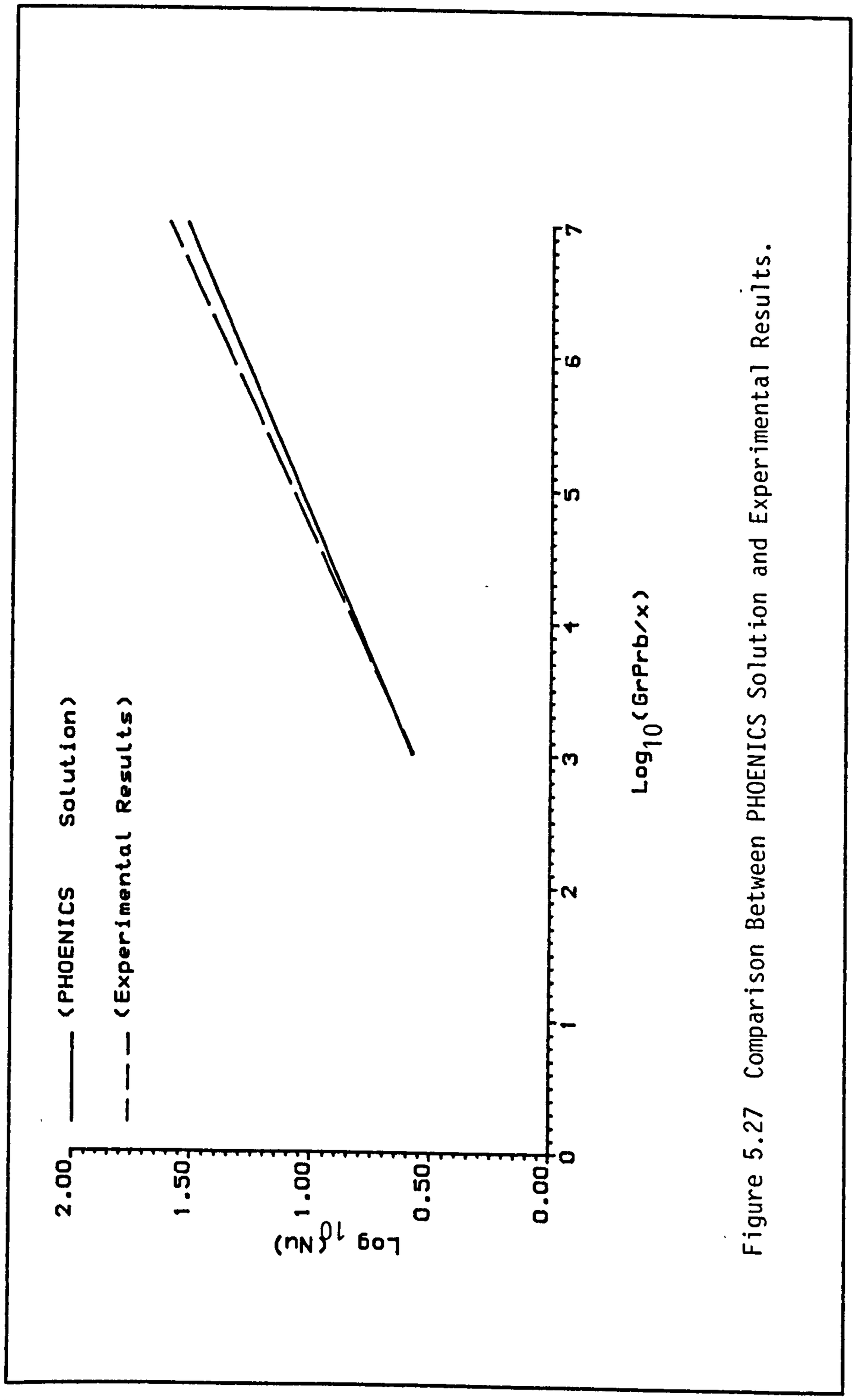

Figure 5.27 Comparison Between PHOENICS Solution and Experimental Results.

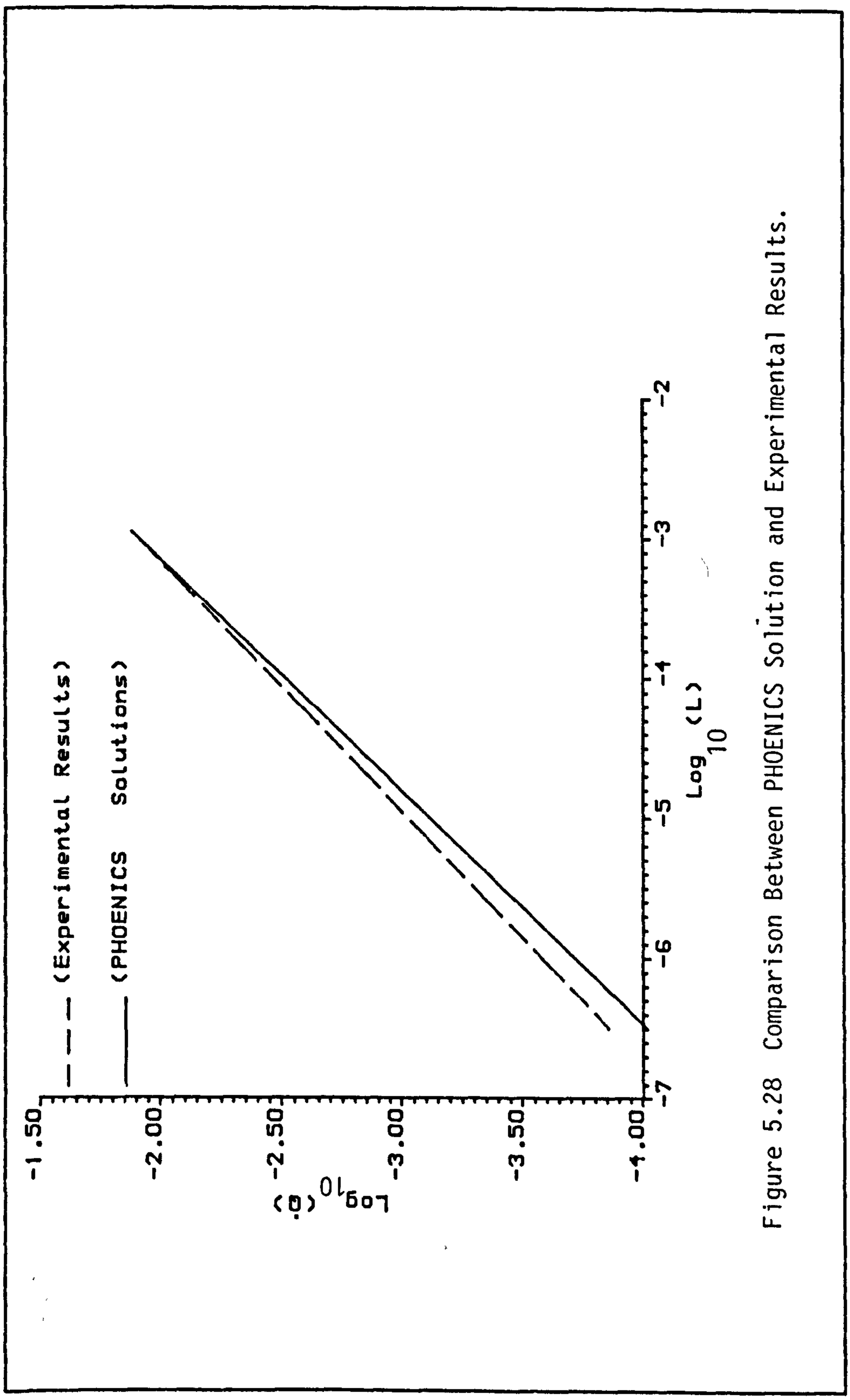

Figure 5.28 Comparison Between PHOENICS Solution and Experimental Results.

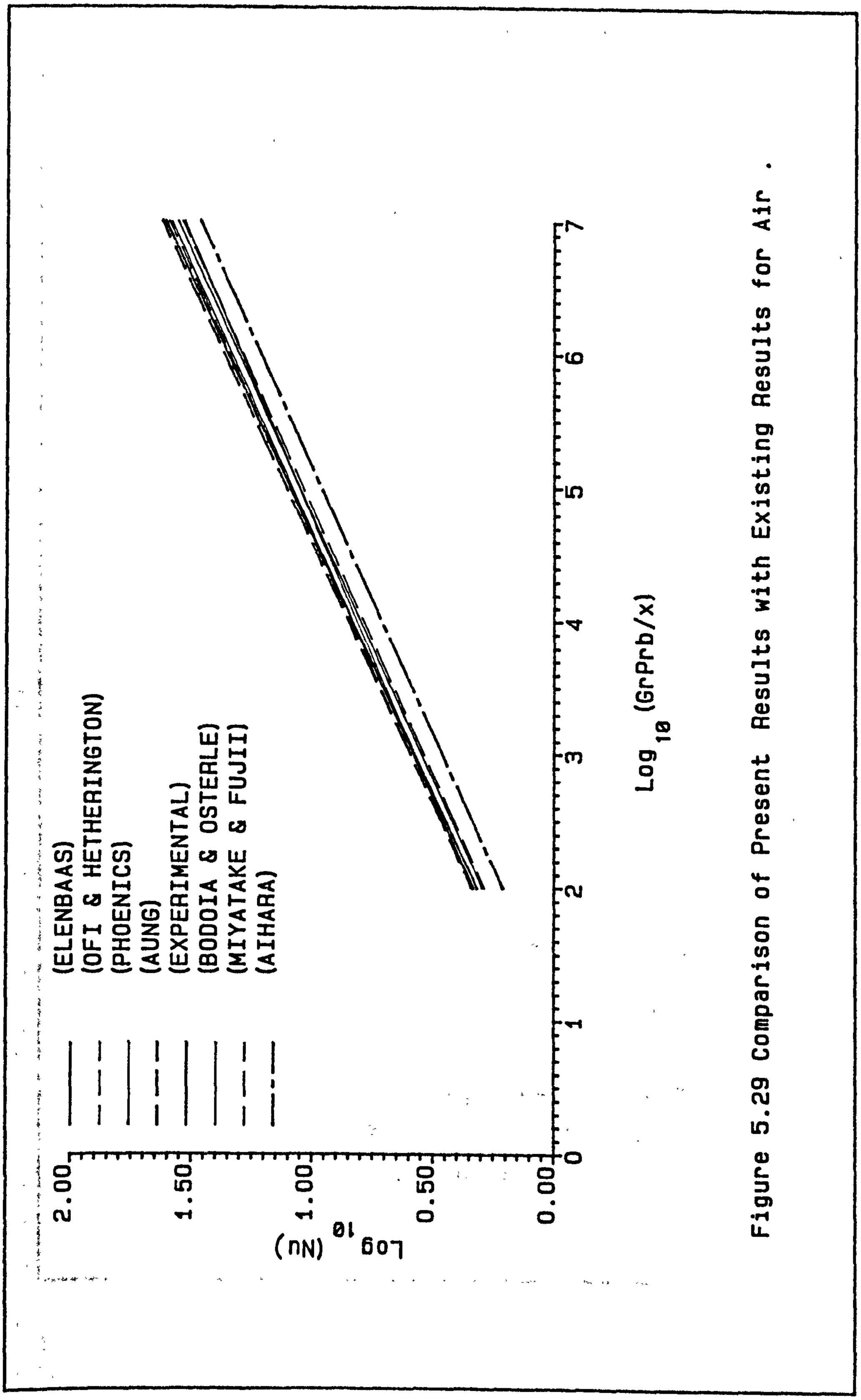

Figure 5.29 Comparison of Present Results with Existing Results for Air .

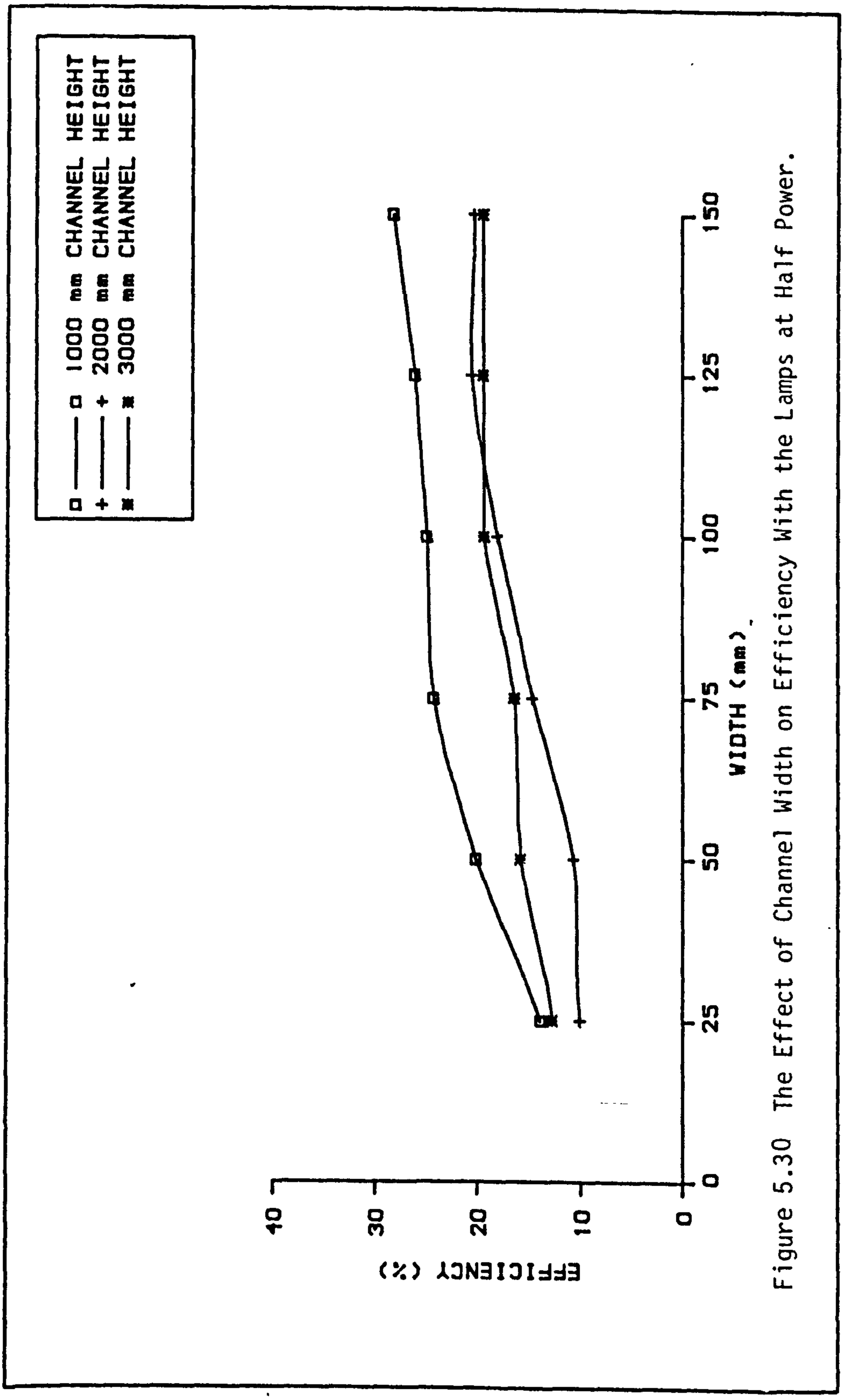

Figure 5.30 The Effect of Channel W

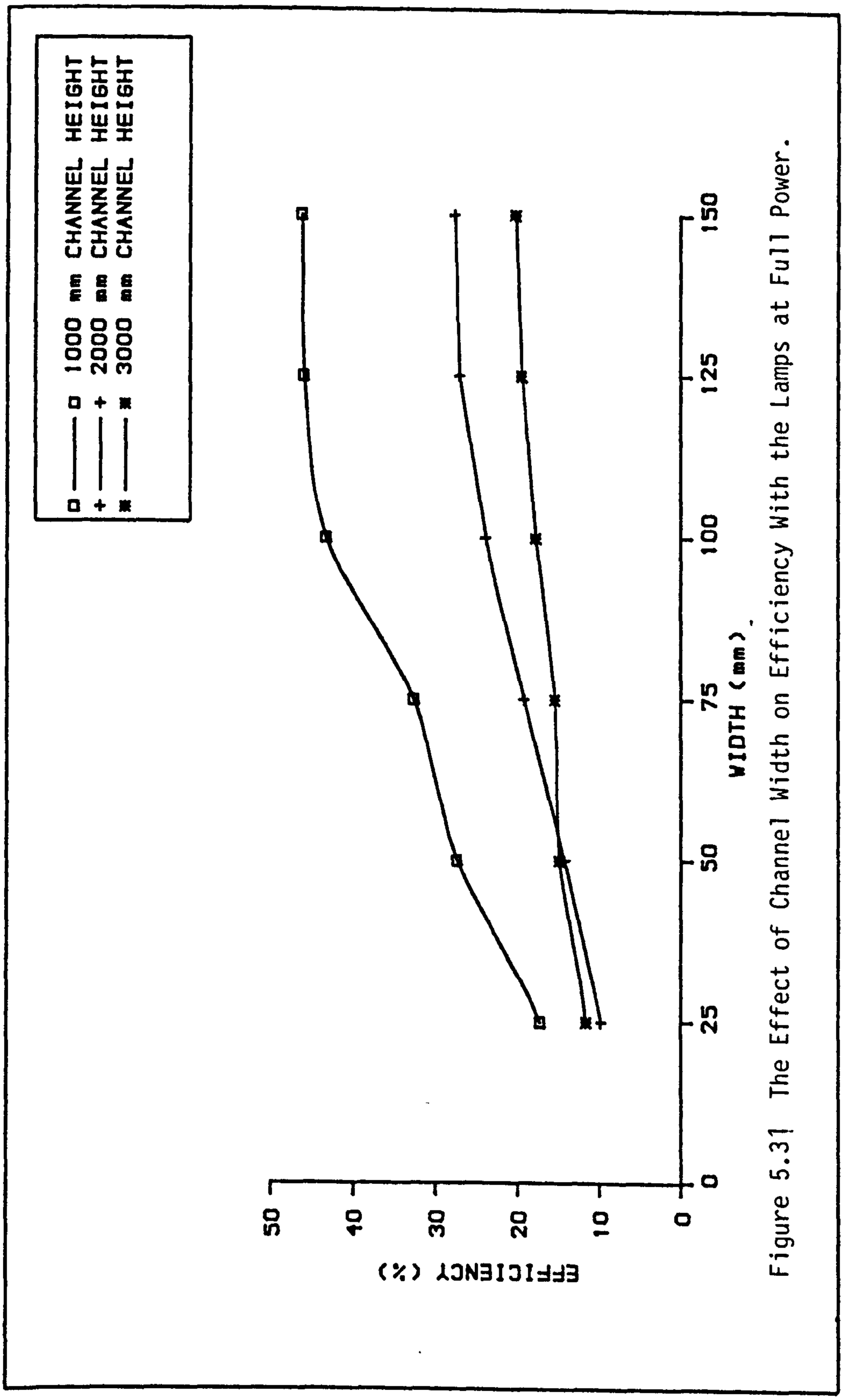

Figure 5.31 The Effect of Channel Width on Efficiency With the Lamps at Full Power.

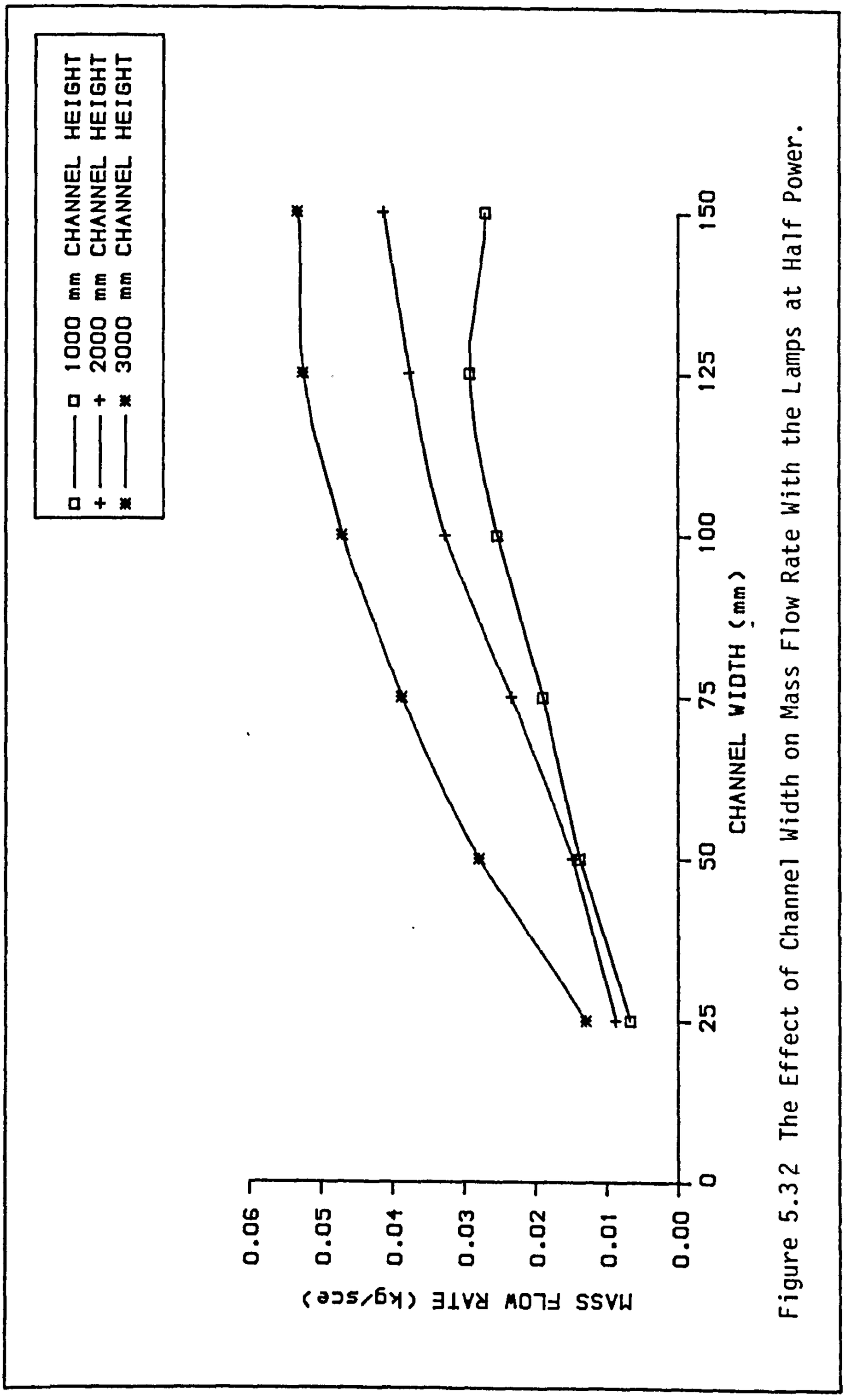

Figure 5.32 The Effect of Channel Width on Mass Flow Rate With the Lamps at Half Power.

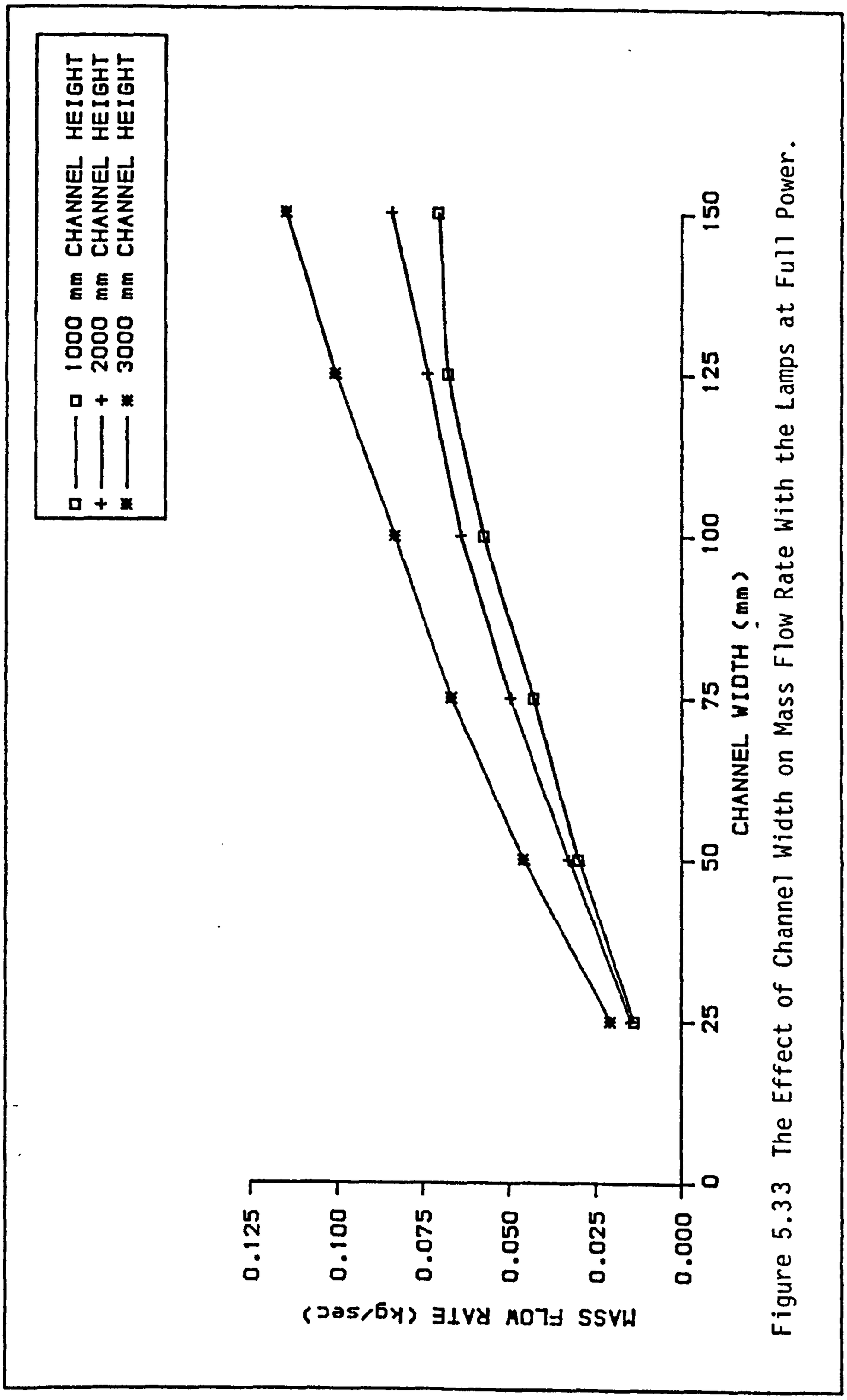

Figure 5.33 The Effect of Channel Width on Mass Flow Rate With the Lamps at Full Power.

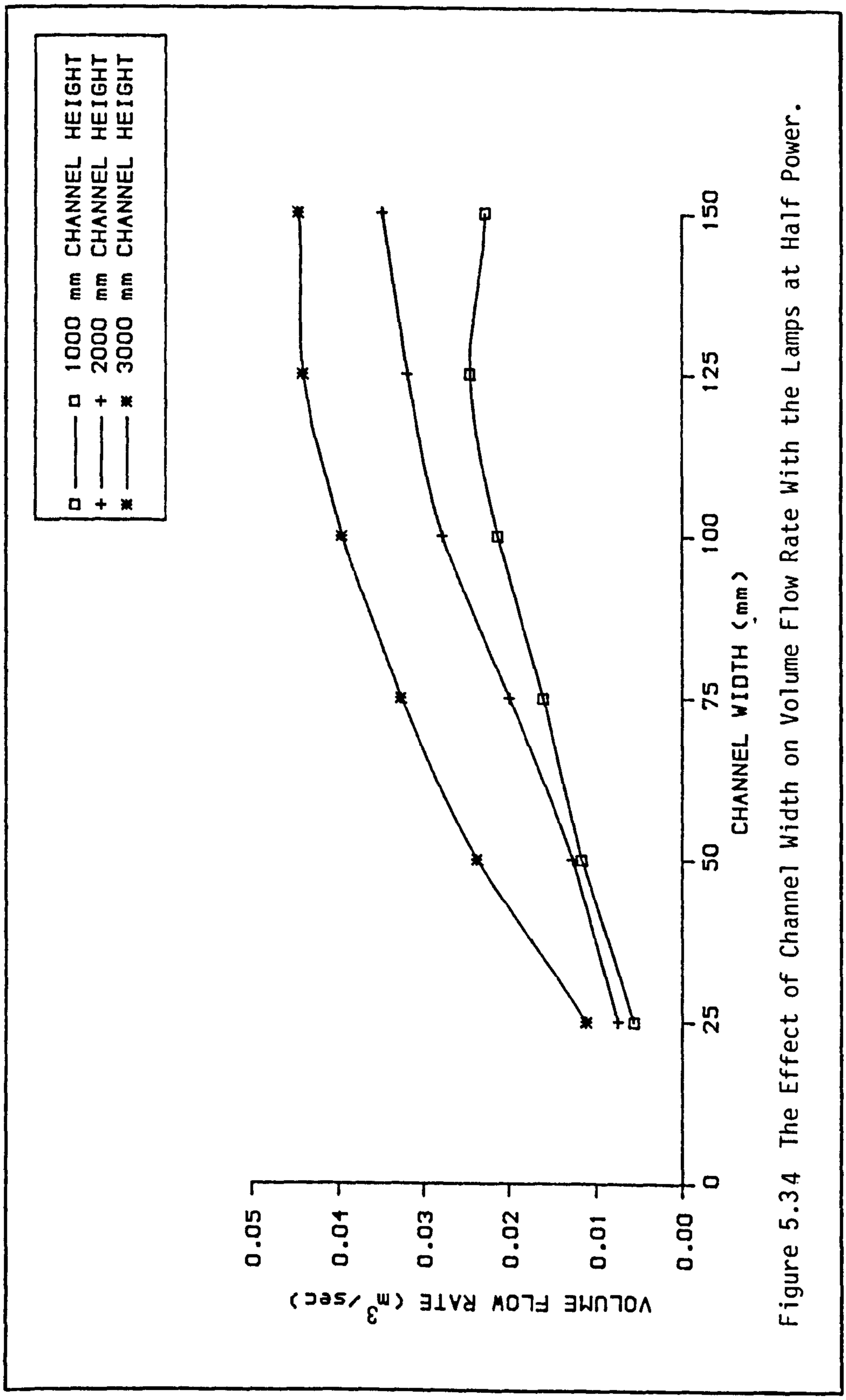

Figure 5.34 The Effect of Channel Width on Volume Flow Rate With the Lamps at Half Power.

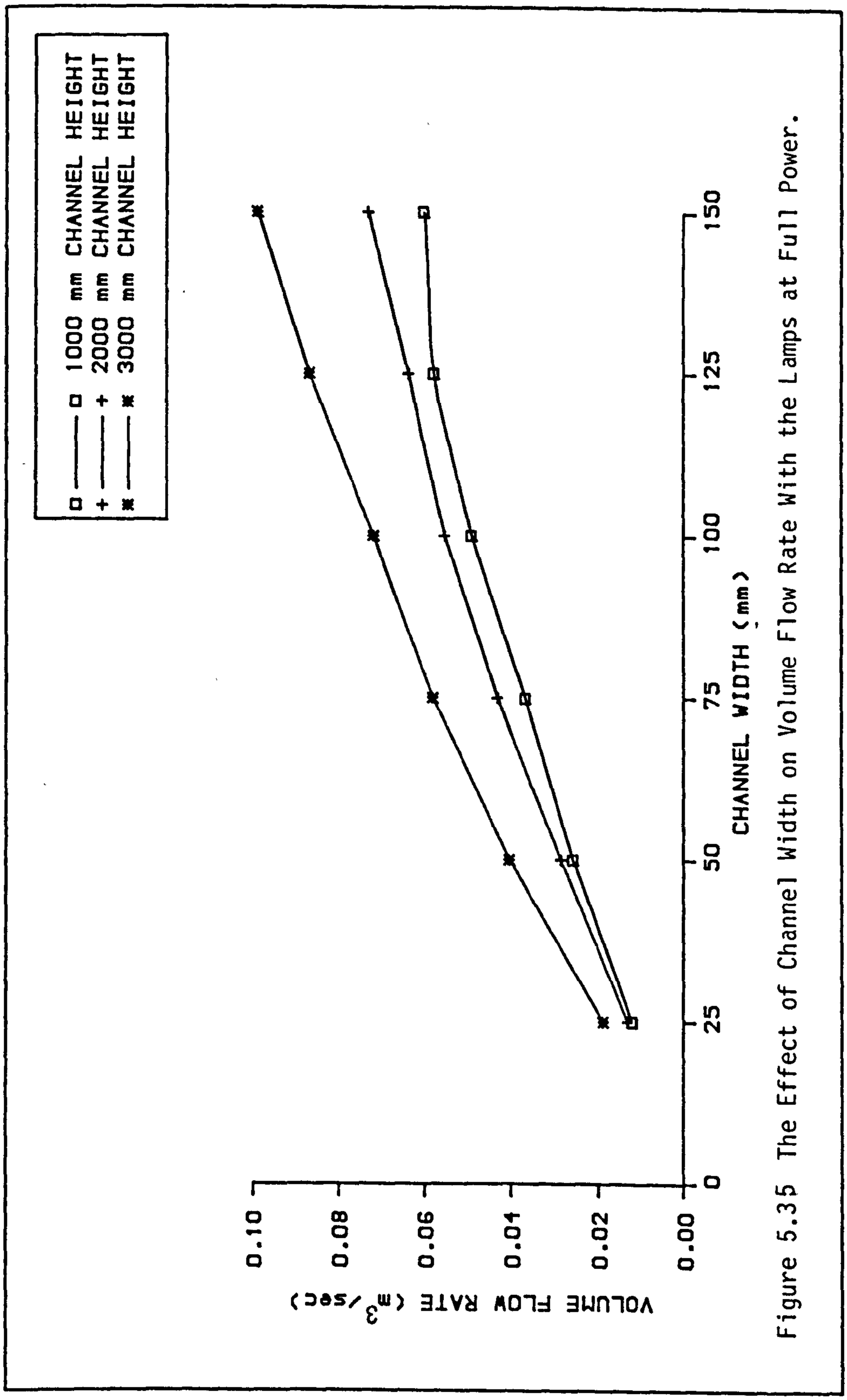

Figure 5.35 The Effect of Channel Width on Volume Flow Rate With the Lamps at Full Power.

CHAPTER 6

CONCLUSIONS AND SUGGESTIONS FOR FUTURE RESEARCH

6.1 Conclusions

Natural convection in a parallel vertical plate channel has been investigated both theoretically and experimentally. Both isothermal and non-isothermal wall conditions have been studied. Factors associated with the performance of the system, such as diffusers at inlet and outlet, transient operation, atmospheric pressure and humidity have also received some attention. The following conclusions have been drawn.

1. The PHOENICS results indicate that the solution procedure described in this study converges to the solution of the governing differential equations if the grid spacing and time-step used are suitably refined.

2. The flexibility of the PHOENICS procedure was successfully demonstrated by predicting the flow for different channel sizes and conditions.

3. The PHOENICS solutions for the average Nusselt number Nu as a function of GrPr b/x at atmospheric pressure led to the following correlation equation

$$Nu = 0.734\ (GrPr\ b/x)^{0.238} \qquad (6.1)$$

The value of Nusselt number increases or decreases as the atmospheric pressure is increased or decreased respectively. Equations for Nusselt number variation at different pressures are given in Chapter 3.

4. The relationship, obtained from the PHOENICS results, between dimensionless flow and dimensionless channel length L at atmospheric pressure is:

$$\dot{Q} = 0.803\ (L)^{0.604} \qquad (6.2)$$

$\dot{Q}$ increases or decreases as the atmospheric pressure is increased or decreased respectively. Equations for $\dot{Q}$ variation with L for different pressures are given in Chapter 3.

5. The constant wall temperature experimental results were correlated by

$$Nu = 0.632\ (GrPr\ b/x)^{0.258} \qquad (6.3)$$

for the range $10^2 < GrPr\ b/x < 2.25 \times 10^6$.

6. The non-isothermal wall temperature experimental results were correlated by

$$Nu = 0.429\ (GrPr\ b/x)^{0.313} \qquad (6.4)$$

This equation gives a higher Nusselt number than for the case of isothermal wall. This non-isothermal wall case can be treated as a uniform wall temperature case if the average wall temperature is modified using the following equation.

$$\frac{\bar{T}_{ave}}{T_{ave}} = 0.944 + 0.0186\ (\log_{10} GrPr\ b/x) \qquad (6.5)$$

The modified value, $\bar{T}_{ave}$, allows the use of the isothermal wall correlation equation to calculate the heat transfer coefficient for non-isothermal cases.

7. The dimensionless flow rate $\dot{Q}$ induced between the plates was shown to be a function of dimensionless channel length L. $\dot{Q}$ increases as L increases which indicates that $\dot{Q}$ increases as the actual height of the channel increases and as the width increases and the following equation was obtained using the experimental results:

$$\dot{Q} = 0.548\ (L)^{0.532} \qquad (6.6)$$

8. The actual mass flow rate increases as the channel height and/or the channel width increases and also as the wall temperature is increased.

9. The variation of pressure of the air in the flow direction was found to be almost linear for all conditions examined. The pressure term in the momentum equation has a very significant effect on the fluid flow in the channel. The PHOENICS solutions using the correct static head pressure at the channel inlet agree well with the experimental results.

10. In general, the simple diffuser sections tested have a very small effect on the fluid flow in the channel. The Nusselt number decreases slightly for high values of GrPr b/x when the diffuser is fitted.

11. Dry air was found to have a smaller volume flow rate and higher Nusselt number than moist air.

12. The efficiency of the system as a solar collector is sensitive to channel width and height. The efficiency increases as the channel height and/or width increases. Also, the efficiency increases when the radiation level increases.

13. The experimental results obtained in this study are in close agreement with the PHOENICS results.

6.2 Suggestions for Future Research

Arising from the experiences of the research described in this thesis, and taking account of the objective already achieved, the following recommendations are made:

1. The velocity and temperature profiles at the channel inlet were assumed uniform for the PHOENICS solutions. Actually, the fluid will enter the channel with a profile somewhat different from this uniform profile. It is therefore necessary to re-consider the assumption for inlet velocity and temperature profiles.

2. Further refinement of the grid size variation and the use of other time-step sizes and iteration numbers chosen for the PHOENICS solution could be made bearing in mind required computer time. Turbulent flow effects could be investigated using the k-ε turbulence model which is available in the PHOENICS code.

3. The PHOENICS program could be used to predict Nusselt numbers corresponding to developed flow by decreasing the (GrPr b/x) product. This would however take a considerable amount of computer time.

4. The successful two-dimensional PHOENICS solution procedure for the problem of natural convection between two vertical parallel walls could be extended to predict the real three dimensional flows which exist in a Trombe wall system.

5. An optical method, such as holographic interferometry, could possibly be used to examine the flow in a non-intrusive way.

6. The accuracy of the experimental procedure for controlling the plate temperature can be improved by using an automatically controlled power supply. This could be operated by means of temperature sensors installed on the aluminium plate which feed back and control the temperature level required by controlling the input power supply.

7. The method and technique of data collection could be improved. If a data acquisition system with more input points was available, the time lag between readings taken at different heights, experienced in the present system could be reduced considerably. More thermocouples could be installed permanently across the channel thus further reducing the time taken to complete one set of test readings. Consideration

could also be given to the use of a hot-wire anemometer in the determination of the velocity distributions.

8. This study should be extended to consider the more complex problem of transient radiation on to a Trombe wall system and the resulting transient variation in wall temperature and air flow rates in the vertical channel.

REFERENCES

1. CARPENTER, L.G. and WASSELL, H.C. "The Loss of Heat by National Convection from Parallel Vertical Plates in Air", Proceedings of the Institution of Mechanical Engineers, Vol. 128, pp.439-457, 1934.

2. KENNARD, R.B. "Temperature Distribution and Heat Flux in Air by Interferometry", Temperature, Its Measurement and Control in Science and Industry, 1941, American Inst. Phys. Ed., Reinbold Pub., pp. 685-706.

3. ELENBAAS, W. "Heat Dissipation of Parallel Plates by Free Convection", Physica, Holland, Vol. 9, pp 1-28, 1942.

4. ELENBAAS, W. "The Dissipation of Heat by Free Convection from the Inner Surface of Vertical Tubes of Different Shapes of Cross-section", Physica, Vol. 9, pp. 865-874, 1942.

5. ELENBAAS, W. "Dissipation of Heat by Free Convection", Philips Research Laboratories, Vol. 3, No.5, pp. 338-360, October 1948.

6. ELENBAAS, W. "Dissipation of Heat by Free Convection", Philips Research Laboratories, Vol. 3, No.6, pp.450-465, 1948.

7. OSTRACH, S. "Laminar Natural Convection Flow and Heat Transfer of Fluids With and Without Heat Sources in Channels with Constant Wall Temperatures", NACA Technical Note, 2863, 1952.

8. OSTRACH, S. "An Analysis of Laminar Free-Convection Flow and Heat Transfer about a Flat Plate Parallel to the Direction of the Generating Body Force", NACA, Report 1111, 1953.

9. KOBAYASHI, A. and FUJIMOTO, Y. "Study of Heat Dissipation by Natural Convection Between Parallel Vertical Plates", Trans. Japan Soc. Mech. Engrs., Vol.20, (1954), pp 233-237.

10. SIEGEL, R. and NORRIS, R.H. "Tests of Free Convection in a Partially Enclosed Space Between Two Heated Vertical Plates", Trans. ASME, Vol. 79, 1957, pp. 663-673.

11. JAKOB, M. "Heat Transfer", John Wiley & Sons, Inc., New York, N.Y., 1949, p.530.

12. SIEGEL, R. "Analysis of Laminar and Turbulent Free Convection from a Smooth Vertical Plate with Uniform Heat Dissipation per Unit Surface Area", General Electric Report, 54GL89, April 1954.

13. BODOIA, J.R. and OSTERLE, J.F. "The Development of Free Convection Between Heated Vertical Plates", ASME Journal of Heat Transfer, Vol. 84, 1962, pp. 40-44.

14. BODOIA, J.R. and OSTERLE, J.F. "Finite Difference Analysis of Plane Poiseuille and Couette Flow Developments", Applied Scientific Research, Vol. 10, Sec. A., 1961, pp. 265-276.

15. AIHARA, T. "Heat Transfer Due to Natural Convection from Parallel Vertical Plates", Trans, Japan Soc. Mech. Engrs., 29, (1963), pp. 903-909.

16. ENGEL, R.K. and MUELLER, W.K. "An analytical Investigation of Natural Convection in Vertical Channels", ASME Paper No. 67-HT-16 (1967).

17. RAO, T.L.S. and MORRIS, W.D. "Superimposed Laminar Forced and Free Convection between Vertical Parallel Plates When One Plate is Uniformly Heated and the Other is Thermally Insulated" , Proc. I. Mech. E., Vol. 182, Part 3H, 1967-1968.

18. AKBARZADEH, A., CHARTERS, W.W.S. and LESSLIE, D.A. "Thermocirculation Characteristics of a Trombe Wall Passive Test Cell", Solar Energy, Vol. 28, No.6, pp.461-468, 1982.

19. WARNER, C.Y. and ARPACI, V.S. "An Experimental Investigation of Turbulent Natural Convection in Air at Low Pressure Along a Vertical Heated Flat-Plate", Int. J. Heat, Mass Transfer, Vol. 11, pp. 397-406, 1968.

20. AIHARA, T. "Natural Convection Heat Transfer from Vertical Rectangular-Fin Arrays", Part 1, Rep. Inst. High. Sp. Mech., Japan, Vol. 21, No.213, 1969/1970.

21. AIHARA, T. "Natural Convection Heat Transfer from Vertical Rectangular-Fin Arrays", Part 2, Bulletin of the JSME, Vol. 13, No. 64, 1970.

22. AIHARA, T. "Natural Convection Heat Transfer from Vertical Rectangular-Fin Arrays", Part 3, Bulletin of JSME, Vol. 13, No. 64, 1970.

23. AIHARA, T. "Natural Convection Heat Transfer from Vertical Rectangular-Fin Arrays", Part 4, Bulletin of JSME, Vol. 14, No. 74, 1971.

24. CURRIE, I.G. and NEWMAN, W.A. "Natural Convection Between Isothermal Vertical Surfaces", Preprints 4th Ins. Heat Trans. Conf., Versailles, Vol. 4, pp. NC 2.7, 1970.

25. OFI, O. and HETHERINGTON, H.J. "Application of the Finite Element Method to Natural Convection", Int. J. of Heat and Mass Transfer, Vol. 20, pp.1195-1204, 1977.

26. MIYATAKE, O. and FUJII, T. "Free Convective Heat Transfer Between Vertical Parallel Plates, One Plate is Isothermally Heated and the Other is Thermally Insulated", KAGAKO KOGAKU, Soc. Chem. Engrs. Japan, 36, 405-412, 1972. Heat Transfer, Jap. Res. Vol.1, No. 3, Jul-Sept., 1972, pp.30-38.

27. NAKAMURA,H., ASAKO, Y. and NAITOU, T. "Free Convective Heat Transfer Between Parallel Isothermal Plates", Preprint of the 42nd National Meeting of JSME, No. 120, 5, 1964.

28. AUNG, W. "Fully Developed Laminar Free Convection Between Vertical Plates Heated Asymmetrically", International Journal of Heat and Mass Transfer, Vol. 15, 1972, pp. 1577-1580.

29. AUNG, W., FLETCHER, L.S. and SERNAS, V. "Developing Laminar Free Convection Between Vertical Plates and Asymmetric Heating", International Journal of Heat and Mass Transfer, Vol. 15, 1972, pp. 2293-2308.

30. SERNAS, V., FLETCHER, L.S. and AUNG, W. "Heat Transfer Measurements with a Wollaston Prism Schlieren Interferometer", ASME Paper 72-HT-9, 1972.

31. AUNG, W. and O'REGAN, R. "A unitized and portable holographic interferometer", Presented at the ASME/ AICHE Nat. Heat Transfer Conf., Denver, Colo., August 6-9, 1972, ASME Paper 72-HT-10.

32. AIHARA, T. "Effects of Inlet Boundary Condition on Numerical Solutions of Free Convection between Vertical Parallel Plates", Rep. Inst. High Speed Mech., Tohoku Univ., Vol. 28, pp. 1-27, 1973.

33. AKBARI, H. and BORGERS, T. "Free Convective Laminar Flow Within the Trombe Wall Channel", Solar Energy, Vol. 22, No. 2, pp. 165-174, 1979.

34. BORGERS, T.R. and AKBARI, H. "Free Convection Turbulent Flow Within The Trombe Wall Channel", Solar Energy, Vol. 33, No. 3/4, pp.253-264, 1984.

35. PRATT, R. and KARAKI, S. "Natural Convection Between Vertical Plates with External Frictional Losses - Application to Trombe Walls", Third National Passive Solar Conference Proceedings, Proceedings of AS ISES, Vol. 3, 1979, pp.61-66.

36. SPARROW, E.M. and BAHRAMI, P.A. "Experiments on Natural Convection from Vertical Parallel Plates With Either Open or Closed Edges", ASME Journal of Heat Transfer, Vol. 102, pp. 221-227, 1980.

37. TICHY, J. and QUINN, C. "Simualtion Analysis of Trombe Wall System Performance Based on the AKBARI-BORGERS Channel Flow Solution", ASME paper 82-WA/Sol-11.

38. MELHUS, OLE "Numerical Analysis of Natural Convection in Vertical Ducts. (Abstracts), Ph.D Thesis, University of Trondheim, NTH, Nov. (1981).

39. MELHUS, OLE and MAGNUSSEN, B.F. "Numerical Computation of Natural Convection in Vertical Ducts", Numerical Methods in Laminar and Turbulent Flow, Proceedings of the Third International Conference held in Seattle, 8-11 August, 1983, Pineridge Press, Swansea, U.K., pp.853-863.

40. NAKAMURA, H., ASAKO, Y. and NAITOU, T. "Heat Transfer by Free Convection between Two Parallel Flat Plates", Numerical Heat Transfer, Vol. 5, pp. 95-106, 1982.

41. KETTLEBOROUGH, C.F. "Transient Laminar Free Convection between Heated Vertical Plates including Entrance Effects", Int. J. Heat Mass Transfer, Vol. 15, pp. 883-896, 1972.

42. TICHY, J. "The Effect of Inlet and Exit Losses on Free Convective Laminar Flow In the Trombe Wall Channel", ASME Paper 82-WA/Sol-10.

43. BAR-COHEN, A. and ROHSENOW, W.M. "Thermally Optimum Spacing of Vertical, Natural Convection Cooled, Parallel Plates", Trans. of the ASME, Journal of Heat Transfer, Vol. 106, pp.116-123, Feb. 1984.

44. NAKAMURA, H., ASAKO, Y. and NAITOU, T. "Developing Combined Free and Forced Laminar Convection Between Vertical Parallel Plates with Constant Wall Temperature", J. Chem. Eng. Japan, Vol. 11, No. 1, pp.19-24, 1978.

45.CORDIER, A. and DUROU, C. "Visualization By Holographic Interferometry of Temperatures in Passive Components", Proceedings of the 6th National Passive Solar Conference, September 8-12, pp.205-209, 1981, Portland, Oregon, U.S.A.

46. BURCH, T., RHODES, T. and ACHARYA, S. "Laminar Natural Convection Between Finitely Conducting Vertical Plates", Int. J. Heat Mass Transfer, Vol. 28, No. 6, pp.1173-1186, 1985.

47. ORMISTON, S.J., RAITHBY, G.D. and HOLLAND, K.G.T. "Numerical Predictions of Natural Convection In a Trombe Wall System", Int. J. Heat Mass Transfer, Vol. 29, No. 6, pp.869-877, 1986.

48. KREIDER, J.F. and KREITH, F. "Solar Heating and Cooling, Engineering, Practical Design, and Economics", Revised First Edition, McGraw-Hill Book Company, 1977.

49. McVEIGH, J.C. "Sun Power, An Introduction to the Applications of Solar Energy", 1st Ed., Pergamon Press, 1977.

50. GREELEY, R.S., OUELLETTE, R.P. and CHEREMISINOFF, P.N. "Solar Heating and Cooling of Buildings", Ann Arbor Science Publishers, Inc., 1981.

51. OHANESSIAN, P. and CHARTERS, W.W.S. "Thermal Simulation of a Passive Solar House Using a Trombe-Michel Wall Structure", Solar Energy, Vol. 20, pp.275-281, 1978

52. WRIGHT, D. "Natural Solar Cooling" Proceedings of the 3rd National Passive Solar Conference, pp.512-517, San Jose, California, January 11-13, 1979.

53. HOLTZ, M.J. and PLACE, W. "A classification scheme for the Common Passive and Hybrid Heating and Cooling Systems", Proceedings of the 3rd National Passive Solar Conference, pp. 282-289, San Jose, California, January 11-13, 1979.

54. JÄGER, F. "Solar Energy Applications in Houses: Performance and Economics in Europe", Pergamon Press, Oxford, 1981.

55. TROMBE, F., ROBERT. J.F., CABANAT, M. and SESOLIS, B. Some Performance Characteristics of the, CNRS Solar House Collectors", Proceedings of the First Passive Solar Heating and Cooling Conference, and Workshop, pp. 201-222, Albuquerque, NM, Los Alamos Scientific Laboratory of University of California, Los Alamos, NM 87545, 18-19 May 1976.

56. LEBENS, R.M. "Passive Solar Heating Design", Applied Science Publishers Ltd., 1980.

57. UNIVERSITY of ARIZONA "The peakshaver solar collector" The Environmental Research Laboratory, 2nd National Passive Solar Conference Proc. Philadelphia, PA, U.S.A. Vol. III, pp. 910, March 1978.

58. BIER, I.J. "Vertical Solar Louvers: a system for tempering and storing solar energy", 2nd National Passive Solar Conference Proc., Philadelphia, PA, U.S.A. Vol I, pp.209, March 1978.

59. CASPERSON, R. and HOCEVAR, R.L. "Experimental Investigation of the Trombe Wall Passive Energy System", Third National Passive Solar Conference Proceedings, Proceedings of AS of ISES, Vol. 3, 1979, pp. 231-238.

60. BILGEN, E. and CHAABAN, M. "Solar Heating-Ventilating System Using a Solar Chimney", Solar Energy, Vol. 28, No.3, pp.227-233, 1982.

61. SPALDING, D.B. "Numerical Computation of Multi-phase Fluid Flow and Heat-Transfer", Recent Advance in Numerical Methods in Fluids, Vol.1, Ed. C. Taylor and K. Morgan, Pineridge Press, Swansea, 1980.

62. SPALDING, D.B. "PHOENICS A General-Purpose Computer Program for Multi-Dimensional One-and-Two-Phase Flow", HTS/81/11, October 1981.

63. CHAM LTD., "Lecture Panels for PHOENICS Basic User Course", CHAM, TR/121, July 1986.

64. ROSTEN, H.I. and SPALDING, D.B. "PHOENICS - Beginner's Guide and User Manual", CHAM, TR/100, April 1986.

65. PATANKAR, S.V. and SPALDING, D.B. "A Calculation Procedure for Heat Mass and Momentum Transfer in Three-dimensional Parabolic Flows", Int. J. of Heat and Mass Transfer, Vol.15, pp 1787-1806, 1972.

66. ROSTEN, H.I., SPALDING, D.B. and TATCHELL, D.G., "PHOENICS : A General-Purpose for Fluid-Flow, Heat Transfer and Chemical Reaction Processes" CHAM Ltd, Wimbledon, London, 1983/11.

67. CHAM LTD. "The PHOENICS Input Library". Vol.1, CHAM, TR/101/1, 21 March 1986.

68. EDWARDS, J.P. and ROSTEN, H.I. "Special GROUND and SATLIT Subroutines in Use in the PHOENICS Input Library", CHAM, TR/125, 27 March 1986.

69. MARKATOS, N.C. and PERICLEOUS, K.A. "Natural Convection in an Enclosed Cavity", PDR/CHAM UK/16, October 1982.

70. MARKATOS, N.C. and PERICLEOUS, K.A. "Laminar and Turbulent Natural Convection in an Enclosed Cavity", Int. J. Heat & Mass Transfer, Vol.27, No.5, pp.755-772, 1984.

71. MALIN, M.R. "GRAFFIC: AN INSTRUCTIONAL MANUAL", CHAM, TR/71a, September 1985.

72. HARLOW, F.H. and WELCH, J.E. "Numerical Calculation of Time-Dependent Viscous Incompressible Flow of Fluid with Free Surface", Physics Fluids, 8, 2182, 1965.

73. SCHLICHTING, H. "Boundary Layer Theory", McGraw-Hill Book Company, Inc. 1960.

74. ECKERT, E.R.G. and DRAKE, R.M. "Analysis of Heat and Mass Transfer", McGraw-Hill Book Company,Inc., 1972

75. PATANKAR, S.V. "Numerical Heat Transfer and Fluid Flow", McGraw-Hill Book Company, Inc. 1980.

76. BROYD, T.W., DEAN, R.B. and OLDFIELD, S.G. "The Use of a Computational Method to Assess the Safety and Quality of Ventilation in Industrial Buildings", I.Mech.E., C97/83, pp.65-74, 1983.

77. LAUNDER, B.E. and SPALDING, D.B. "The Numerical Computation of Turbulent Flows", Computer Methods in Applied Mechanics and Engineering, 3, pp.269-286, 1974.

78. SPALDING, D.B. "Numerical Computation of Multiphase Fluid Flow and Heat Transfer", Contribution to 'Report Advances in Numerical Methods in Fluids', Editors C. Taylor and T. Morgan, pp 139-167, 1980.

79. SPALDING, D.B. "Four Lectures on the PHOENICS Computer Code", Imperial College, CFD/82/5, 1982.

80. SPALDING, D.B. "A Novel Finite-Difference Formulation for Differential Equations Involving First and Second Derivatives", Int. J. Num. Mech. in Eng. Vol. 4, 1972.

81. GEISHEKER, P.J. and PUTMAN, W.J. "Development of Facilities and Methods for Thermal Performance Tests of Passive Domestic Hot Water System", Proceedings of the 6th National Passive Solar Conference, pp 200-204, September 8th-12th, 1981, Portland, Oregon, U.S.A.

82. RAGSDALE, R.G. and NAMKOONG, D. "The NASA-Langley Building Solar Project and the Supporting Lewis Solar Technology Program", Solar Energy, Vol. 18, No.1, pp 44-46, 1976.

83. DUFFIE, J.A. and BECKMAN, W.A. "Solar Energy Thermal Processes", John Wiley and Sons, Inc., 1974.

84. OTHIENO, H. "Multilayer Solar Air Heater and the Development of Small Scale Solar Maize Dryer for Village use in Kenya", Ph.D Thesis, Strathclyde University, 1983.

85. GRAINGER, W. "Small Scale Solar Crop Drives for Tropical Village Use", Ph.D Thesis, Strathclyde University, 1982.

86. ASHRAE HANDBOOK "Duct Design", 1981 Fundamentasls, American Society of Heating, Refrigerating and Air-Conditioning Engineers, Inc., Chapter 33, 3rd ed., 1982

87. JONES, W.P. "Air Conditioning Engineering", Edward Arnold, SI Units, 2nd ed., 1973.

88. BALCOMB, J.D., HEDSTROM. J.C. and McFARLAND, R.D. "Simulation as a Design Tool", Proceedings of First Passive Solar Heating and Cooling Conference Albuquerque, New Mexico, Los Alamos Scientific Laboratory Report LA-6637-C, May 1976, pp. 238-246.

89. BALCOMB, J.D., McFARLAND, R.D. and MOORE, S.W. "Simulation Analysis of Passive Solar Heated Buildings - Comaprison with Test Room Results", LA-UR-77-939, Los Alamos Scientific Laboratory, University of California, Los Alamos, New Mexico, U.S.A., 1977.

90. BALCOMB, J.D., HEDSTROM, J.C. and McFARLAND, R.D. "Passive Solar Heating of Buildings", Rep. LA-UR-77-1162, UNCLAS, Los Alamos Scientific Lab., N. Mex. U.S.A., 1977.

91. WRAY, W. and BALCOMB, J.D. "Trombe Wall vs. Direct Gain Comparison Analysis", Proceedings of the Third National Passive Solar Conference 1979, pp. 41-47.

92. BALCOMB, J.D., HEDSTROM, J.C. and McFARLAND, R.D. "Simulation Analysis of Passive Solar Heated Buildings Preliminary Results", Solar Energy, Vol. 19, pp. 277-282, 1977.

93. BALCOMB, J.D. and McFARLAND, R.D. "Simulation Analysis of Passive Solar Heated Buildings - The Influence of Climate and Geometry on Performance", LA-UR-77-938 Los Alamos, Scientific Lab., 1977.

94. BALCOMB, J.D., HEDSTROM, J.C. and McFARLAND, R.D. "Simulation Analysis of Passive Solar Heated Buildings - Comparison with Test Room Results", LA-UR-77-939, Los Alamos Scientific Laboratory, U.S.A., 1977.

95. BALCOMB, J.D. "State of Art in Passive Solar Heating and Cooling", LA-UR-78-774, UNCLAS, Los Alamos Scientific Lab., N. Mex., U.S.A., 1978.

96. BALCOMB, J.D. "Designing Passive Solar Building to Reduce Temperature Swings, LA-UR-78-1316, Los Alamos Scientific Laboratory, University of California, Los Alamos, New Mexico, 1978.

97. BALCOMB, J.D. and McFARLAND, R.D. "A Simple Empirical Method for Estimating the Performance of a Passive Solar Heated Building of the Thermal Storage Wall Type", Proc. 2nd National Passive Solar Conference, Philadelphia, 1978.

APPENDIX A

PHOENICS Computer Code

A.1 General

The name PHOENICS is an acronym standing for Parabolic, Hyperbolic or Elliptic Numerical Integration Code Series, Rosten et al (65).

A.2 Description of PHOENICS

This Appendix describes the PHOENICS computer code, the structure, contents and capabilities, for simulating single or two-phase flow, heat-transfer, and chemical-reaction processes. Steady or unsteady phenomena in one, two or three space dimensions are handled. The governing equations for conservation of matter, momentum, energy and chemical species are solved by a finite-domain method. Full viscous effects are included. The flow can be treated as laminar or the effects of turbulence can be accounted for via a two-equation model involving the solution of transport equations for the kinetic energy of turbulence and its dissipation rate. Variable fluid properties are allowed for, and compressibility effects can be included forsubsonic, supersonic and transonic flows.

The program is structured in a way which separates the central core program which embodies the general-purpose computational procedures, from the user-accessible input portions. Two levels of user input are provided. Straightforward setting of data-input variables can be used for the prescription of a wide range of problems involving only activation of built-in facilities. For more complex problems provision is made in a controlled way for the attachment of specially-provided programming sequences or subroutines.

The central part of the PHOENICS system is a single, general-purpose core program used for all applications, to which user access is provided at various levels to enable particular processes to be simulated. This single-general-purpose-code strategy has been found to be beneficial in several ways: it facilitates maintenance and systematic development; it enables improvements to be made available immediately to all users; and it allows users to concentrate attention on modelling aspects of their particular problem, without being concerned with the numerical solution of the fundamental governing equations.

PHOENICS is currently in use at a number of installations for a wide range of problems, including nuclear-power, aerospace, turbomachinery, defence, marine,

chemical-process, environmental and automotive applications.

A.3 Organisation

PHOENICS consists of three elements:

- The central 'EARTH' program, which is the common core program, used for all applications.
- A series of 'satellite' programs, each of which provides the specific, problem-defining input information which causes EARTH to simulate a particular process or item of equipment..
- A series of 'ground-stations', each associated with a particular satellite, each of which completes the problem-defining task.

The distinction between 'satellite' and 'ground-stations' is needed because the satellites are separate programs, which create data files to be read by EARTH, containing complete input specification. Because data transfer occurs only once it is impossible to provide, through the satellite, information which varies during the calculation, or which involves interaction with the calculation procedure. The ground-stations are therefore provided to perform this role.

The PHOENICS system is shown diagramatically in Figure A.1. The hexagonal satellites are shown communicating with EARTH through their own ground-stations (the 'blips' on the surface of EARTH).

A.4 Mathematical Details of the EARTH Program

The independent variables are x, y and z if a cartesian coordinate system is used, or θ, r and z if polar coordinates are used. For unsteady flows, time, t, is also an independent variable.

There are twenty-three dependent variables which can be selected by the user:

- o pressure p and the pressure correction p';
- o three first-phase velocities, u_1, v_1, w_1;
- o three second-phase velocities, u_2, v_2, w_2;
- o phase volume fractions, r_1 and r_2, and a 'shadow' volume fraction, r_2^*, used particularly for two-phase problems involving chemical reaction;
- o turbulence energy and dissipation rate, k and ε;
- o first- and second-phase enthalpies, h_1 and h_2; enthalpy of a third fluid, h_3;
- o four species concentrations, c_1, c_2, c_3, c_4;
- o three radiation-flux sums, R_x, R_y, R_z.

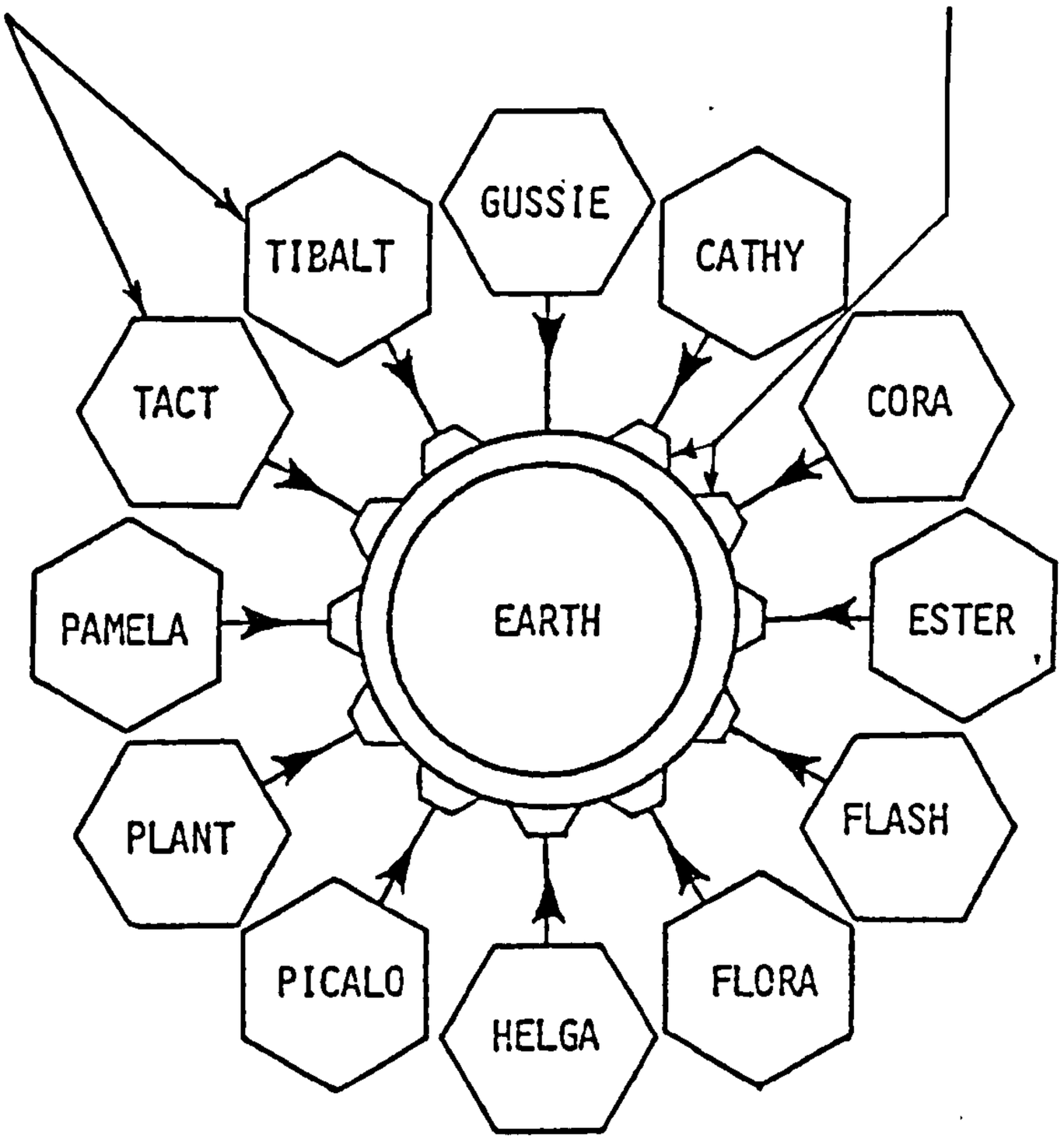

Figure A.1 Diagrammatic Representation of EARTH in PHOENICS System

The two quantities k and ε require some explanation. They represent local, time-averaged properties of the fluid turbulence, and are obtained from the modelled transport equations which constitute the two-equation k-ε model of turbulence, Launder and Spalding (77).

APPENDIX B

Q1 File for Isothermal Wall Channel

For this investigation the Q1 file was set up to simulate the fluid flow in a channel. The 24 groups for the Q1 file are described in detail and a listing of the file for a particular set of conditions is given in this Appendix.

Group 1. Run Title

The title of the program shows as "FREE CONVECTION FLOW IN RECTANGULAR DUCT".

Group 2. Transcience: time-step specification

STEADY = F, invokes the unsteady solution

GRDPWR (T, 10, 30.0, 1.0): Command for setting "Power-law" for time intervals is: (Time, number of time interval, total time, exponent in power law).

Group 3. X-direction grid specification

No entry is made here, because this is a two-dimensional simulation.

Group 4. Y-direction grid specification

GRDPWR (Y, 20, 0.1, 1.0) : Command for setting "power-law" for Y-interval is: (Y-axis, number of interval, total distance in Y-direction, exponent in power law). Also, Y-distances used were = 0.025, 0.05, 0.075, 0.01, 0.0125 and 0.015 (m).

Group 5. Z-direction grid specification

GRDPWR (Z, 30, 3.0, 1.0) calls for subroutine GRDPWR for (Z-direction, number of interval, total distance in Z-direction, exponent in power law). Also, Z-distances used were = 1.0, 2.0 and 3.0 (m).

Group 6. Body-fitted coordinates or grid distortion

No entry is made here, because the grid is regular.

Group 7. Variable stored, saved and named

SOLUTN(P1, Y, Y, Y, N, N, N)

SOLUTN(V1, Y, Y, N, N, N, N)

SOLUTN(W1, Y, Y, N, N, N, N)

SOLUTN(H1, Y, Y, N, N, N, N)

activates the solution for the first-phase pressure in a whole-field procedure, the Y component of the velocity, the Z component of the velocity, the enthalpy (temperature K in this case) in a slab-by-slab procedure. The NAME (DEN1) command gives the name DEN1 to variable index 15, and activates the solution for the density DEN1 in a slab-by-slab procedure.

Group 8. Terms (in differential equations) and devices

The command to determine the variable solution H1 (enthalpy) is active in the balance equation, and DIFCUT stands for diffusion/conversion cut-off. The diffusion contribution to the finite-domain-equation coefficient is diminished by DIFFCUT*ABS (convection contribution) but not allowed to become negative, in order to account approximately for diffusion-convection interactions. DIFCUT = 0.0, giving no diminution would correspond to the "upwind-interpolation" scheme.

Group 9. Properties of the medium (or media)

Group used to specify the properties of the fluid and Prandtl number.

RHO1 = GRND2 calls chapter 9/section 1 of ground example 1 (GREX1) Subroutine where the density of the fluid is

set to be independent of the pressure but to vary with temperature according to the law of ideal gases, i.e.

$$\rho = \frac{p}{RT} \quad \text{where } p = \text{constant} = 1 \text{ atm.}$$

The flow is laminar, the laminar viscosity is set at air inlet temperature. (See Subsection 3.2.5).

The Prandtl number for air is set to 0.7.

Group 10. Inter-phase-transfer processes and properties

No entry is made here. The default values suffice.

Group 11. Initialisation of variable or porosity fields

Group to specify the physical conditions existing at the start of the transient.

FIINIT(P1) = 0.0, sets initial values for pressure

FIINIT(H1) = 293.30, sets an initial uniform temperature in degree (K)

FIINIT(W1) = 0.1, sets the value for uniform z-velocity (m/sec)

FIINIT(V1) = 0.0, sets zero value for the y-velocity (m/sec)

FIINIT (DEN1) = 1.187 sets an initial value for density (kg/m^3).

Group 12. Convection and diffusion adjustments

No entry is needed here.

Group 13. Boundary conditions and special sources

Group to specify the regions over which boundary and internal conditions, and special sources are imposed:

PATCH (Patch name, type, first IX, last IX, first IY, last IY, first IZ, last IZ, first time step, last time step), commands to set the boundary or internal conditions or sources.

COVAL (Patch name, variable index, coefficient value).

Figure (3.5) shows region location and system coordinates. The boundary conditions that are required to specify the flow situation considered in the present study have been explained in section 3.3.

Wall boundary conditions

This patch sets the boundary conditions at the north (high-y) wall location. A coefficient of 1.0 and a value of 0.0 are set for the velocity at the wall. A coefficient of 1.428 (1.0/Prandtl number of air) and a value for the wall temperature are specified (for example 347.70 (K) in

the Q1 file listed).

Glass boundary conditions

This patch sets the boundary conditions at the south (low-y) wall location (glass plate). The coefficients and values for velocity and temperature are set as explained in the wall boundary conditions.

Inlet boundary conditions

This patch sets the boundary conditions at the low-z inlet location. A pressure coefficient of FIXP is set which corresponds to a pressure coefficient of numerical value of 1.0. A uniform static head pressure, relative to the outlet pressure, is specified at the inlet. This equals $\rho g l$ (for example 34.947 in the Q1 file listed).

Outlet boundary conditions

This patch sets the boundary conditions at high-z outlet location. A pressure coefficient of FIXP is set for outlet pressure as 0.0. The temperature (H1) at the outlet is set with the value as SAME which ensures that, if there is inflowing mass then this fluid has the same temperature as already prevails at the last cell.

Buoyancy source term by gravity

This patch sets to evaluate and add the source term due to buoyancy to the momentum equation according to the density effect. A FIXFLU velocity coefficient and -9.806 for the gravity acceleration in the z-direction are set.

Group 14. Downstream pressure for PARAB=.TRUE

No entry is needed here.

Group 15. Termination of sweeps

LSWEEP=25 number of iterative "sweeps" to be performed per time step.

The residual reference values for pressure, velocities and enthalpy are set to 1.E-6.

Group 16. Termination of iterations

No entry is needed here.

Group 17. Under-relaxation devices

The under-relaxation values for pressure, velocities, enthalpy and density are set to 0.3, 0.3, 0.3 and 0.5 respectively.

Group 18. Limits on variables or increments to them

No entry is needed here.

Group 19. Data communicated by satellite to GROUND

No entry is needed here.

Group 20. Preliminary print-out

NOHEAD = F sets the print-out of the Q1 file data at the beginning of the result file.

Group 21. Print-out of variables

The field print-out is provided for the pressure, velocity in z-direction, enthalpy and density.

Group 22. Spot-value print-out

Monitor output is elicited at every 5 sweeps and the NPRMON is set at each 10 sweeps. The monitor cell is chosen close to the wall by the settings IYMON = (NY-2) and IZMON = (NZ-2).

Group 23. Field print-out and plot control

The field print-out is provided after the final sweep at the last time step having been performed. Also a temperature and velocity profile are plotted at different z-locations.

Group 24. Dumps for restarts

SAVE=.T., if the results of the EARTH run are to be saved on DF09, for possible use in a subsequent restart or autopsy run.

Q1 File for Isothermal Wall Channel

```
TALK=F,RUN(1,1)
      ************************************************
     GROUP 1. RUN TITLE
TEXT(FREE CONVECTION FLOW IN RECTANGULAR DUCT)
      ************************************************
     GROUP 2. Transience: time-step specification
STEADY=F
GRDPWR(T,10,30.0,1.0)
     GROUP 3. X-direction grid specification
     GROUP 4. Y-direction grid specification
GRDPWR(Y,20,0.1,1.0)
     GROUP 5. Z-direction grid specification
GRDPWR(Z,30,3.0,1.0)
     GROUP 6. Body-fitted coordinates or grid distortion
     GROUP 7. Variable stored, solved & named
SOLUTN(P1,Y,Y,Y,N,N,N)
SOLUTN(V1,Y,Y,N,N,N,N)
SOLUTN(W1,Y,Y,N,N,N,N)
SOLUTN(H1,Y,Y,N,N,N,N)
DEN1=15
NAME(DEN1)=DEN1
SOLUTN(DEN1,Y,N,N,N,N,N)
     GROUP 8. Terms ( in differential equations ) & devices
TERMS(H1,N,Y,Y,Y,Y,N)
DIFCUT=0.0
     GROUP 9. Properties of the medium (or media)
RHO1=GRND2
RHO1A=0.0
RHO1B=2.87E-03
ENUL=1.91667E-5
PRNDTL(H1)=0.7
     GROUP 10. Inter-phase-transfer pricesses and properties
     GROUP 11. Initialization of variable or porosity fields
FIINIT(P1)=0.0
FIINIT(H1)=293.3
FIINIT(W1)=0.1
FIINIT(V1)=0.0
FIINIT(DEN1)=1.1879
      GROUP 12. Convection and diffusion adjustments
      GROUP 13. Boundary conditions and special sources
      *******   PLATE  WALL    ********
PATCH(WALL,NWALL,1,1,NY,NY,1,NZ,1,30)
COVAL(WALL,W1,1.0,0.0)
COVAL(WALL,H1,1.428,347.7)
      *******   GLASS -SOUTH WALL   *******
PATCH(GLASS,SWALL,1,1,1,1,1,NZ,1,30)
COVAL(GLASS,W1,1.0,0.0)
COVAL(GLASS,H1,1.428,298.2)
      *******   INLET          ********
PATCH(INLET,LOW,1,1,1,NY,1,1,1,30)
COVAL(INLET,P1,FIXP,34.947)
COVAL(INLET,H1,ONLYMS,293.3)
```

```
      ******  OUTLET    ********
PATCH(OUTLET,HIGH,1,1,1,NY,NZ,NZ,1,30)
COVAL(OUTLET,P1,FIXP,0.0)
COVAL(OUTLET,H1,ONLYMS,SAME)
      **BUOYANCY SOURCE TERM BY GRAVITY **
PATCH(BUOYANCY,PHASEM,1,1,1,NY,1,NZ,1,30)
COVAL(BUOYANCY,W1,FIXFLU,-9.806)
     GROUP 14. Downstream pressure for PARAB=.TRUE.
     GROUP 15. Termination of sweeps
LSWEEP=25
RESREF(P1)=1.E-6
RESREF(V1)=1.E-6
RESREF(W1)=1.E-6
RESREF(H1)=1.E-6
     GROUP 16. Termination of iterations
     GROUP 17. Under-relaxation devices
     ************************************
RELAX(P1,LINRLX,0.3)
RELAX(V1,FALSDT,0.3)
RELAX(W1,FALSDT,0.3)
RELAX(H1,FALSDT,0.3)
RELAX(DEN1,LINRLX,0.5)
     GROUP 18. Limits on variables or increments to them
     GROUP 19. Data communicated by satellite to GROUND
     GROUP 20. Preliminary print-out
NOHEAD=F
     GROUP 21. Print-out of variables
OUTPUT(P1,Y,Y,Y,Y,Y,Y)
OUTPUT(W1,Y,Y,N,Y,Y,Y)
OUTPUT(H1,Y,Y,Y,Y,Y,Y)
OUTPUT(DEN1,Y,N,N,N,N,N)
     GROUP 22. Spot-value print-out
TSTSWP=5
NPRMON=10
IYMON=(NY-2)
IZMON=(NZ-2)
     GROUP 23. Field print-out and plot control
NTPRIN=10
NPRINT=LSWEEP
IPLTL=LSWEEP
IPLTF=LSWEEP-30
     **** print Y-Z plane velocity and temprature prifile .
PATCH(PROFIL15,PROFIL,1,1,1,NY,1,1,1,1)
COVAL(PROFIL15,W1,-1.0,1.0)
PATCH(PROFIL110,PROFIL,1,1,1,NY,1,1,4,4)
COVAL(PROFIL110,W1,-1.0,1.0)
PATCH(PROFIL115,PROFIL,1,1,1,NY,1,1,6,6)
COVAL(PROFIL115,W1,-1.0,1.0)
PATCH(PROFIL120,PROFIL,1,1,1,NY,1,1,8,8)
COVAL(PROFIL120,W1,-1.0,1.0)
PATCH(PROFIL1,PROFIL,1,1,1,NY,1,1,30,30)
COVAL(PROFIL1,W1,-1.0,1.0)
COVAL(PROFIL1,H1,285.0,400.0)
PATCH(PROFIL2,PROFIL,1,1,1,NY,10,10,30,30)
COVAL(PROFIL2,W1,-1.0,1.0)
COVAL(PROFIL2,H1,285.0,400.0)
```

```
PATCH(PROFIL3,PROFIL,1,1,1,NY,15,15,30,30)
COVAL(PROFIL3,W1,-1.0,1.0)
COVAL(PROFIL3,H1,285.0,400.0)
PATCH(PROFIL4,PROFIL,1,1,1,NY,20,20,30,30)
COVAL(PROFIL4,W1,-1.0,1.0)
COVAL(PROFIL4,H1,285.0,400.0)
PATCH(PROFIL55,PROFIL,1,1,1,NY,NZ-1,NZ-1,1,1)
COVAL(PROFIL55,W1,-1.0,1.0)
PATCH(PROFIL510,PROFIL,1,1,1,NY,NZ-1,NZ-1,4,4)
COVAL(PROFIL510,W1,-1.0,1.0)
PATCH(PROFIL515,PROFIL,1,1,1,NY,NZ-1,NZ-1,6,6)
COVAL(PROFIL515,W1,-1.0,1.0)
PATCH(PROFIL520,PROFIL,1,1,1,NY,NZ-1,NZ-1,8,8)
COVAL(PROFIL520,W1,-1.0,1.0)
PATCH(PROFIL5,PROFIL,1,1,1,NY,NZ-1,NZ-1,30,30)
COVAL(PROFIL5,W1,-1.0,1.0)
PATCH(PROFIL6,FROFIL,1,1,1,NY,NZ,NZ,30,30)
COVAL(PROFIL6,H1,285.0,400.0)
    **************************
    GROUP 24. Dumps for restarts
SAVE=.T.
STOP
```

APPENDIX C

GROUND Subroutine for Isothermal Wall Channel

Subroutine GROUND is subdivided into 24 groups according to the 24 data groups which appear in the Q1 file. This subroutine consists of comments, statements, computed GOTO, CONTINUE and RETURN statements and GROUND's subroutines, but there are no statements activating changes in any variable. Thus GROUND consists of empty shells into which the user can insert his coding in FORTRAN language as necessary. For further details see PHONEICS User's Manual CHAM TR/121 (63), Rosten and Spalding (64). A list of the GROUND subroutine used in this study is presented at the end of this Appendix. This Appendix presents the calculations performed in subroutine GROUND as explained in Section 2.3. DIMENSION statements were used in the main block area for the array to be used in the calculations. Also DATA statements were placed for fluid properties and the dimensions involved. Section 6 of Group 19 were used to compute the required parameters. The parameters calculated were : average and film temperatures, aspect ratio, Grashof and Rayleigh numbers, Nusselt numbers and heat transfer coefficients at the wall and glass, average inlet temperature, volume and mass flow rates, dimensionless z-velocity, air flow and length, total heat transferred, average Nusselt numbers and average heat

transfer coefficient. A print-out of all the above parameters could be obtained.

GROUND Subroutine for Isothermal Wall Channel

```
C$DIR**MAIN
      PROGRAM MAIN
C FILE NAME GROUND.FTN----------------------------------090985
C
C     PROGRAM MAIN
C
C 1   The following two COMMON's, which appear identically in the
C     satellite MAIN program, allow up to 25 dependent variables to
C     be solved for (or their storage spaces to be occupied by
C     other variables, such as density). If a larger number is
C     required, the 25's should be replaced, in the next 8 lines,
C     by the required larger number; and the 100 in COMMON/F01/
C     should be replaced by 4 times the required number. Numbers
C     less than 25 are not permitted.
C
      COMMON/LGE1/L1(25)/LGE2/L2(25)/LGE3/L3(25)/LGE4/L4(25)
     1/LDB1/L5(25)/IDA1/I1(25)/IDA2/I2(25)/IDA3/I3(25)/IDA4/I4(25)
     1/IDA5/I5(25)/IDA6/I6(25)/GI1/I7(25)/GI2/I8(25)/HDA1/IH1(25)
     1/GH1/IH2(25)/RDA1/R1(25)/RDA2/R2(25)/RDA3/R3(25)/RDA4/R4(25)
     1/RDA5/R5(25)/RDA6/R6(25)/RDA7/R7(25)/RDA8/R8(25)/RDA9/R9(25)
     1/RDA10/R10(25)/RDA11/R11(25)
     1/GR1/R12(25)/GR2/R13(25)/GR3/R14(25)/GR4/R15(25)
     1/IPIP1/IP1(25)/HPIP2/IHP2(25)/RPIP1/RVAL(25)/LPIP1/LVAL(25)
      LOGICAL L1,L2,L3,L4,L5,DBGFIL,LVAL
      CHARACTER*4 IH1,IH2,IHP2,NSDA
C
      COMMON/F01/I9(100)
      COMMON/DISC/DBGFIL
      EXTERNAL WAYOUT
C
C 2   Set dimensions of data-for-GROUND arrays here.
      COMMON/LGRND/LG(10)/IGRND/IG(10)/RGRND/RG(10)/CGRND/CG(10)
      LOGICAL LG
      CHARACTER*4 CG
C
C 3   Set dimensions of data-for-GREX1 arrays here.
      COMMON/LSG/LSGD(20)/ISG/ISGD(20)/RSG/RSGD(100)/CSG/CSGD(10)
      LOGICAL LSGD
      CHARACTER*4 CSGD
C
C 4   Set dimension of patch-name array here.
      COMMON/NPAT/NAMPAT(100)
      CHARACTER*8 NAMPAT
C
C 5   The numbers in the next two statements (which must be ident-
C     ical) indicate how much computer memory is to be set aside
C     for storing the main and auxiliary variables. The user may
C     alter them if he wishes, to accord with the number of
C     grid nodes and dependent variables he is concerned with.
      COMMON F(150000)
      NFDIM=150000
```

```
C
C 6    Logical-unit numbers and file names, not to be changed.
       DBGFIL=.FALSE.
       CALL SUB4(LUSDA,10,LUPR1,14,LUPR3,14,LUDST,21)
       CALL SUB1H(NSDA,'DF10')
       CALL DSCFLS(LUPR3,'CON:',-11,16)
       CALL DSCFLS(6,'DF6 ',9,33)
       CALL DSCFLS(LUDST,'DSTL',9,33)
C
C      User may here change message transmitted to logical unit
C      LUPR3
       CALL WRIT40('GROUND STATION IS MYGROUND.FOR 250786      ')
       CALL MAIN1(NFDIM,LUPR1,LUPR3,LUSDA,NSDA)
       CALL WAYOUT(0)
       STOP
       END
C*************************************************************
       SUBROUTINE GROUND
       INCLUDE'SATEAR'
       INCLUDE'GRDLOC'
       INCLUDE'GRDEAR'
       INTEGER HIGH,OLD,AUX
CXXXXXXXXXXXXXXXXXXXXXXXXXXXXXXXXXXXXXX USER SECTION STARTS:
C
C 1    Set dimensions of satellite-to-GROUND data arrays to those
C      of the satellite.
       COMMON/LGRND/LG(10)/IGRND/IG(10)/RGRND/RG(10)/CGRND/CG(10)
       LOGICAL LG
       CHARACTER*4 CG
C
C 2    User dimensions own arrays here, for example:
C      DIMENSION UUH(10,10),UUC(10,10),UUX(10,10),UUZ(10)
C
       DIMENSION GH1(50,50),GW1(50,50)
       DIMENSION GDYV2D(50,1),GDEN1(50,1)
       DIMENSION GZ1(50),GH2(50,50)
C
C 3    User places his data statements here, for example:
C      DATA NXDIM,NYDIM/10,10/
C
       DATA CON,VIS/2.6855E-2,16.5055E-6/
       DATA CPF/1006.23/
       DATA TW,TG,TIN/347.7,298.2,293.3/
       DATA WID,LEN/0.1,3.0/
C
C 4    Index functions for GROUND-EARTH variable references.
       LOW(I)=NPHI+I
       HIGH(I)=2*NPHI+I
       OLD(I)=3*NPHI+I
       IN(I)=4*NPHI+I
       INDPHI(I,IZDASH)=-KF(I)+(IZ-IZDASH)*(KF(I)-KF(LOW(I)))

C
C 5    Set USEGRX=F in Q1 to deactivate subroutine GREX1.
            IF(USEGRX) CALL GREX1
C
C 6    Set USEGRD=F in Q1 to deactivate sequences below.
            IF(.NOT.USEGRD) RETURN
```

```
C
C 7   Insert own coding below as desired, guided by GREX1 examples.
C     Note that the satellite-to-GREX1 special data in the labelled
C     COMMONs /RSG/, /ISG/, /LSG/ and /CSG/ can be included and
C     used below but the user must check GREX1 for any conflicting
C     uses. The same comment applies to the EARTH-spare working
C     arrays EASP1, EASP2,....EASP10. If the call to GREX1 has been
C     deactivated then they can all be used without reservation.
C
          IF(IGR.EQ.13) GO TO 13
          IF(IGR.EQ.19) GO TO 19
       GO TO (1,2,3,4,5,6,7,8,9,10,11,12,13,14,15,16,17,18,19,20,21,
     122,23,24),IGR
C*************************************************************
C
C--- GROUP 1. Run title
C
     1 CONTINUE
       CALL MAKE(YG2D)
       CALL MAKE(DYV2D)
       RETURN
C*************************************************************
C
C--- GROUP 2. Transience; time-step specification
C
     2 CONTINUE
       RETURN
C*************************************************************
C
C--- GROUP 3. X-direction grid specification
C
     3 CONTINUE
       RETURN
C*************************************************************
C
C--- GROUP 4. Y-direction grid specification
C
     4 CONTINUE
       RETURN
C*************************************************************
C
C--- GROUP 5. Z-direction grid specification
C
     5 CONTINUE
       RETURN
C*************************************************************
C
C--- GROUP 6. Body-fitted coordinates or grid distortion
C
     6 CONTINUE
       RETURN
C*************************************************************
C
C--- GROUP 7. Variables stored, solved & named
     7 CONTINUE
       RETURN
C*************************************************************
C
```

```
C--- GROUP 8. Terms (in differential equations) & devices
C
      8 GO TO (81,82,83,84,85,86,87,88,89,810,811,812,813,814,815)
       1,ISC
     81 CONTINUE
C--- for U1AD.LE.GRND--- phase 1 additional velocity (VELAD).
        RETURN
     82 CONTINUE
C--- for U2AD.LE.GRND--- phase 2 additional velocity (VELAD).
        RETURN
     83 CONTINUE
C--- for V1AD.LE.GRND--- phase 1 additional velocity (VELAD).
        RETURN
     84 CONTINUE
C--- for V2AD.LE.GRND--- phase 2 additional velocity (VELAD).
        RETURN
     85 CONTINUE
C--- for W1AD.LE.GRND--- phase 1 additional velocity (VELAD).
        RETURN
     86 CONTINUE
C--- for W2AD.LE.GRND--- phase 2 additional velocity (VELAD).
        RETURN
C    * ---------------------- SECTION 7 ---- VOLUMETRIC SOURCE FOR GALA
     87 CONTINUE
        RETURN
C    * ---------------------- SECTION 8 --- CONVECTION FLUXES
     88 CONTINUE
        RETURN
C    * ---------------------- SECTION 9 --- DIFFUSION COEFFICIENTS
     89 CONTINUE
        RETURN
C    * ---------------------- SECTION 10 --- CONVECTION NEIGHBOURS
    810 CONTINUE
        RETURN
C    * ---------------------- SECTION 11 --- DIFFUSION NEIGHBOURS
    811 CONTINUE
        RETURN
C    * ---------------------- SECTION 12 --- LINEARISED SOURCES
    812 CONTINUE
        RETURN
C    * ---------------------- SECTION 13 --- CORRECTION COEFFICIENTS
    813 CONTINUE
        RETURN
C    * ---------------------- SECTION 14 --- USER'S SOLVER
    814 CONTINUE
        RETURN
C    * ---------------------- SECTION 15 --- CHANGE SOLUTION
    815 CONTINUE
        RETURN
C    * Make all other group-8 changes in group 19.
C*************************************************************************
C
C--- GROUP 9. Properties of the medium (or media)
C
      9 GO TO (91,92,93,94,95,96,97,98,99,900,901,902,903),ISC
C*************************************************************************
    900 CONTINUE
C--- for TMP1.LE.GRND---------- phase-1 temperature Index AUX(TEMP1)
        RETURN
    901 CONTINUE
```

```
C--- for TMP2.LE.GRND---------- phase-2 temperature Index AUX(TEMP2)
      RETURN
  902 CONTINUE
C--- for EL1.LE.GRND---------- phase-1 length scale Index AUX(LEN1)
      RETURN
  903 CONTINUE
C--- for EL2.LE.GRND---------- phase-2 length scale Index AUX(LEN2)
      RETURN
   91 CONTINUE
C--- for RHO1.LE.GRND--- density for phase 1 Index AUX(DEN1).
      RETURN
   92 CONTINUE
C--- for DRH1DP.LE.GRND--- D(LN(DEN))/DP for phase 1 (D1DP).
      RETURN
   93 CONTINUE
C--- for RHO2.LE.GRND--- density for phase 2 Index AUX(DEN2).
      RETURN
   94 CONTINUE
C--- for DRH2DP.LE.GRND--- D(LN(DEN))/DP for phase 2 (D2DP).
      RETURN
   95 CONTINUE
C--- for ENUT.LE.GRND--- reference turbulent kinematic viscosity.
      RETURN
   96 CONTINUE
C--- for ENUL.LE.GRND--- reference laminar kinematic viscosity.
      RETURN
   97 CONTINUE
C--- for PRNDTL( ).LE.GRND--- laminar PRANDTL nos., or diffusivity.
      RETURN
   98 CONTINUE
C--- for PHINT( ).LE.GRND--- interface value of first phase(FII1).
      RETURN
   99 CONTINUE
C--- for PHINT( ).LE.GRND--- interface value of second phase(FII2)
      RETURN
C*************************************************************
C
C--- GROUP 10. Inter-phase-transfer processes and properties
C
   10 GO TO (101,102,103,104),ISC
  101 CONTINUE
C--- for CFIPS.LE.GRND--- inter-phase friction coeff. AUX(INTFRC).
      RETURN
  102 CONTINUE
C--- for CMDOT.EQ.GRND- inter-phase mass transfer Index AUX(INTMDT).
      RETURN
  103 CONTINUE
C--- for CINT( ).EQ.GRND--- phase1-to-interface transfer
C                                                 coefficients (COI1)
      RETURN
  104 CONTINUE
C--- for CINT( ).EQ.GRND--- phase2-to-interface transfer
C                                                 coefficients (COI2)
      RETURN
C*************************************************************
C
C--- GROUP 11. Initialization of variable or porosity fields
C
   11 CONTINUE
      RETURN
```

```
C*************************************************************
C
C--- GROUP 12. Convection and diffusion adjustments
C
    12 CONTINUE
       RETURN
C*************************************************************
C
C--- GROUP 13. Boundary conditions and special sources
C
    13 CONTINUE
       GO TO (130,131,132,133,134,135,136,137,138,139,1310,
      11311,1312,1313,1314,1315,1316,1317,1318,1319,1320,1321),ISC
   130 CONTINUE
C------------------------------- coefficient = GRND
       RETURN
   131 CONTINUE
C------------------------------- coefficient = GRND1
       RETURN
   132 CONTINUE
C------------------------------- coefficient = GRND2
       RETURN
   133 CONTINUE
C------------------------------- coefficient = GRND3
       RETURN
   134 CONTINUE
C------------------------------- coefficient = GRND4
       RETURN
   135 CONTINUE
C------------------------------- coefficient = GRND5
       RETURN
   136 CONTINUE
C------------------------------- coefficient = GRND6
       RETURN
   137 CONTINUE
C------------------------------- coefficient = GRND7
       RETURN
   138 CONTINUE
C------------------------------- coefficient = GRND8
       RETURN
   139 CONTINUE
C------------------------------- coefficient = GRND9
       RETURN
  1310 CONTINUE
C------------------------------- coefficient = GRND10
       RETURN
  1311 CONTINUE
C------------------------------------------- value = GRND
       RETURN
  1312 CONTINUE
C------------------------------------------- value = GRND1
       RETURN
  1313 CONTINUE
C------------------------------------------- value = GRND2
       RETURN
  1314 CONTINUE
C------------------------------------------- value = GRND3
       RETURN
  1315 CONTINUE
C------------------------------------------- value = GRND4
```

```
      RETURN
 1316 CONTINUE
C------------------------------------- value = GRND5
      RETURN
 1317 CONTINUE
C------------------------------------- value = GRND6
      RETURN
 1318 CONTINUE
C------------------------------------- value = GRND7
      RETURN
 1319 CONTINUE
C------------------------------------- value = GRND8
      RETURN
 1320 CONTINUE
C------------------------------------- value = GRND9
      RETURN
 1321 CONTINUE
C------------------------------------- value = GRND10
      RETURN
C*****************************************************************
C
C--- GROUP 14. Downstream pressure for PARAB=.TRUE.
C
   14 CONTINUE
      RETURN
C*****************************************************************
C
C--- GROUP 15. Termination of sweeps
C
   15 CONTINUE
C    * Make changes for this group only in group 19.
      RETURN
C*****************************************************************
C
C--- GROUP 16. Termination of iterations
C
   16 CONTINUE
C    * Make changes for this group only in group 19.
      RETURN
C*****************************************************************
C
C--- GROUP 17. Under-relaxation devices
C
   17 CONTINUE
C    * Make changes for this group only in group 19.
      RETURN
C*****************************************************************
C
C--- GROUP 18. Limits on variables or increments to them
C
   18 CONTINUE
C    * Make changes for this group only in group 19.
      RETURN
C*****************************************************************
C
C--- GROUP 19. Special calls to GROUND from EARTH
C
   19 GO TO (191,192,193,194,195,196,197,198),I8C
  191 CONTINUE
```

```
C    * -------------------- SECTION 1 ---- START OF TIME STEP.
       RETURN
   192 CONTINUE
C    * -------------------- SECTION 2 ---- START OF SWEEP.
       RETURN
   193 CONTINUE
C    * -------------------- SECTION 3 ---- START OF IZ SLAB.
       RETURN
   194 CONTINUE
C    * -------------------- SECTION 4 ---- START OF ITERATION.
       RETURN
   195 CONTINUE
C    * -------------------- SECTION 5 ---- FINISH OF ITERATION.
       RETURN
   196 CONTINUE
C    * -------------------- SECTION 6 ---- FINISH OF IZ SLAB.
       IF(ISWEEP.NE.LSWEEP) RETURN
       IF(MOD(IZ,NZPRIN).NE.0.0) RETURN
  1961 CALL GETYX(W1,GW1,50,50)
       CALL GETYX(H1,GH1,50,50)
       TAVE=(TW+TG)/2.0
       TFILM=((TW+TG)/2.0)+TIN)/2.0
       ABUOY=1.0/TFILM
       GRASH=9.806*ABUOY*(TAVE-TIN)*(WID)**3.0/(VIS)**2.0
       RAYLGH=GRASH*0.7
       RASTAR=RAYLGH*WID/LEN
       ASP=LEN/WID
       DO 1962 I=1,NY
       TPG=GH1(3,1)-((GH1(3,1)-GH1(2,1))/2.0)
       ANUSG=15.0*(TG-TPG)/(TW-TIN)
       HGLAS=ANUSG*CON/WID
       TPW=GH1(20,1)-((GH1(20,1)-GH1(19,1))/2.0)
       ANUSW=30.0*(TW-TPW)/(TW-TIN)
  1962 HWALL=ANUSW*CON/WID
       IF(IZ.EQ.1.OR.IZ.EQ.11.OR.IZ.EQ.21.OR.IZ.EQ.25.OR.IZ.EQ.26.
      &OR.IZ.EQ.29.OR.IZ.EQ.30) THEN
       WRITE(6,*)'      IZ=',IZ,'      LSWEEP=',ISWEEP
C       PRINT *,'IZ=   ',IZ,'      ISWEEP  =',ISWEEP
C       PRINT *,'GH1(4,1)',GH1(4,1)
C       PRINT *,'GH1(21,1)=',GH1(21,1)
       WRITE(6,1963) GRASH,RAYLGH,RASTAR,ASP,ANUSG,HGLAS,ANUSW,HWALL
  1963 FORMAT(//,13X,'CROSS SEC. GRASHOF NUMBER =',1X,1PE10.3,/,13X,
      1'CROSS SEC. RAYLGH NUMBER  =',1X,1PE10.3,/,13X,
      2'MODIFYED  RAYLGH NUMBER   =',1X,1PE10.3,/,13X,
      3'ASPECT RATIO(HIGH/WIDTH)  =',1X,1PE10.3,/,13X,
      4'GLASS   NUSSELT  NUMBER   =',1X,1PE10.3,/,13X,
      5'HEAT COEFFICIENT AT GLASS =',1X,1PE10.3,/,13X,
      6'WALL    NUSSELT NUMBER    =',1X,1PE10.3,/,13X,
      7'HEAT COEFFICIENT AT WALL  =',1X,1PE10.3,//)
       ENDIF
       IF(IZ.EQ.1) THEN
 2000  TINBAR=0.0
       CALL GETYX(H1,GH1,50,50)
       DO 202 IX=1,NX
       DO 202 IY=1,NY
       TINBAR=TINBAR+GH1(IY,IX)
   202 CONTINUE
       TINBAR=TINBAR/FLOAT(NY)
       WRITE(6,203) TINBAR
   203 FORMAT(//,13X,'TINBAR=',1X,1PE10.3,/)
       ENDIF
```

```
      CALL GETYX(DYV2D,GDYV2D,50,1)
      CALL GETYX(W1,GW1,50,50)
      CALL GETYX(DEN1,GDEN1,50,1)
      AMDOT=0.0
      BMDOT=0.0
      CQDOT=0.0
      DO 1000 IX=1,NX
      DO 1000 IY=1,NY
      U=GW1(IY,IX)*WID/(VIS*GRASH)
      UXX=U*GDYV2D(IY,IX)/WID
C     **** GDY2D(IY,IX)/WID = Y DIMEINSIONLESS
      CQDOT=CQDOT+UXX
      AXX=GW1(IY,IX)*GDYV2D(IY,IX)
      AMDOT=AMDOT+AXX
      BMDOT=BMDOT+AXX*GDEN1(IY,IX)
 1000 CONTINUE
      IF(IZ.EQ.1.OR.IZ.EQ.11.OR.IZ.EQ.21.OR.IZ.EQ.25.OR.IZ.EQ.26.
     &OR.IZ.EQ.29) THEN
C       PRINT *,'IZ  =******',IZ
C       PRINT *,'AMDOT=',AMDOT
C       PRINT *,'BMDOT=',BMDOT
C       PRINT *,'CQDOT=',CQDOT
      WRITE(6,1001)AMDOT,BMDOT,CQDOT
 1001 FORMAT(//,13X,'AIR FLOW RATE=',1X,1PE10.3,/,13X,
     &'MASS AIR FLOW=',1X,1PE10.3,/,13X,
     &'DIM  AIR FLOW=',1X,1PE10.3,/)
      ENDIF
      IF(IZ.EQ.11.OR.IZ.EQ.21.OR.IZ.EQ.25.OR.IZ.EQ.26.OR.
     &IZ.EQ.29)THEN
      CALL GETYX(INDPHI(H1,1),GH1,50,50)
      QIN=0.0
      CALL GETYX(H1,GH2,50,50)
      CALL GETYX(W1,GW1,50,50)
      CALL GETYX(DEN1,GDEN1,50,1)
      CALL GETYX(DYV2D,GDYV2D,50,1)
      DO 3000 IX=1,NX
      DO 3000 IY=1,NY
      QIN=QIN+GW1(IY,IX)*GDEN1(IY,IX)*(GH2(IY,IX)-GH1(IY,IX))
     &*GDYV2D(IY,IX)
C       PRINT *,'QIN=',QIN
 3000 CONTINUE
C       PRINT *,'IZ =-------',IZ
      QZ=CPF*QIN
C       PRINT *,'QZ=',QZ
      CALL GETZ(ZGNZ,GZ1,50)
C       PRINT *,'GZ1=',GZ1
      HZ=QZ/(2.0*GZ1(IZ)*(TAVE-TINBAR))
      XZ=GZ1(IZ)/(WID*GRASH)
C       PRINT *,'HZ=',HZ
C       PRINT *,'GZ1(IZ)=',GZ1(IZ)
C       PRINT *,'XZ=',XZ
      ANUZ=HZ*WID/CON
C       PRINT *,'ANUZ=',ANUZ
      WRITE(6,3001)QZ,HZ,ANUZ,XZ
 3001 FORMAT(//,13X,'HEAT  AT  IZ  LOCATION   =',1X,1PE10.3,/,13X,
     &'HEAT COEFF AT IZ LOC.    =',1X,1PE10.3,/,13X,
     &'NUSSELT NUMBER AT IZ LOC.=',1X,1PE10.3,/,13X,
     &'DIMENSIONLESS X AT IZ LOC=',1X,1PE10.3,/)
      ENDIF
```

```
      RETURN
  197 CONTINUE
C   * ---------------------- SECTION 7 ---- FINISH OF SWEEP.
      RETURN
  198 CONTINUE
C   * ---------------------- SECTION 8 ---- FINISH OF TIME STEP.
      RETURN
C*************************************************************
C
C--- GROUP 20. Preliminary print-out
C
   20 CONTINUE
      RETURN
C*************************************************************
C
C--- GROUP 21. Print-out of variables
C
   21 CONTINUE
C   * Make changes for this group only in group 19.
      RETURN
C*************************************************************
C
C--- GROUP 22. Spot-value print-out
   22 CONTINUE
C   * Make changes for this group only in group 19.
      RETURN
C*************************************************************
C
C--- GROUP 23. Field print-out and plot control
   23 CONTINUE
      RETURN
C*************************************************************
C
C--- GROUP 24. Dumps for restarts
C
   24 CONTINUE
      RETURN
      END
```

APPENDIX D

PHOENICS operation

The PHOENICS operation is used in the following order:-

(1) The default values of all data item are set.

(2) The Q1 file (quick-input file) is read.

(3) The subroutine SATLIT is executed.

(4) A Q2 file is read (The Q2 file is not provided for general use, but is a device which is used in some of the tests made at time of installation).

(5) If TAKE = T, the program interacts with the user by way of the VDU.

(6) The data inputs, supplied by the user during the interaction session and recorded on the COPY file, are transferred to the Q1 file if the user so directs.

(7) A suitable-processed version of the data is written to a file called DF10 (i.e. disc file, logical unit 10), for transmission to EARTH.

(8) EARTH solves the problem specified by DF10, and outputs 3 files: (a) FOR014 which is a scratchpad file, deleted automatically if a successful run has been performed, (b) DF6 which is a text file containing the results of the run and which is overwritten at end of each run but if the user wishes to save its contents to

a permanent file he may do so, and (c) if the command SAVE=T in Q1 file (Group 24) is implemented then a file DF09 in a binary form is created. This last file is necessary and should be saved if the user wishes to perform a "Restart Run" and for "Autops Run" and/or a "GRAFFIC" run for plotting the results, CHAM (64).

Appendix E

Q1 File for Non-isothermal Wall Channel

```
TALK=F,RUN(1,1)
      ************************************************
     GROUP 1. RUN TITLE
TEXT(FREE CONVECTION FLOW IN RECTANGULAR DUCT)
      ************************************************
     GROUP 2. Transience: time-step specification
STEADY=F
GRDPWR(T,10,30.0,1.0)
     GROUP 3. X-direction grid specification
     GROUP 4. Y-direction grid specification
GRDPWR(Y,20,0.15,1.0)
     GROUP 5. Z-direction grid specification
GRDPWR(Z,30,3.0,1.0)
     GROUP 6. Body-fitted coordinates or grid distortion
     GROUP 7. Variable stored, solved & named
SOLUTN(P1,Y,Y,Y,N,N,N)
SOLUTN(V1,Y,Y,N,N,N,N)
SOLUTN(W1,Y,Y,N,N,N,N)
SOLUTN(H1,Y,Y,N,N,N,N)
DEN1=15
NAME(DEN1)=DEN1
SOLUTN(DEN1,Y,N,N,N,N,N)
     GROUP 8. Terms ( in differential equations ) & devices
TERMS(H1,N,Y,Y,Y,Y,N)
DIFCUT=0.0
     GROUP 9. Properties of the medium (or media)
RHO1=GRND2
RHO1A=0.0
RHO1B=2.87E-03
ENUL=1.930E-5
PRNDTL(H1)=0.7
     GROUP 10. Inter-phase-transfer pricesses and properties
     GROUP 11. Initialization of variable or porosity fields
FIINIT(P1)=0.0
FIINIT(H1)=294.7
FIINIT(W1)=0.1
FIINIT(V1)=0.0
FIINIT(DEN1)=1.202
      GROUP 12. Convection and diffusion adjustments
      GROUP 13. Boundary conditions and special sources
      *******    PLATE  WALL    ********
PATCH(WALL,NWALL,1,1,NY,NY,1,NZ,1,30)
COVAL(WALL,W1,1.0,0.0)
COVAL(WALL,H1,1.428,GRND7)
      *******    GLASS -SOUTH WALL   *******
PATCH(GLASS,SWALL,1,1,1,1,1,NZ,1,30)
COVAL(GLASS,W1,1.0,0.0)
COVAL(GLASS,H1,1.428,GRND8)
      *******    INLET          ********
PATCH(INLET,LOW,1,1,1,NY,1,1,1,30)
COVAL(INLET,P1,FIXP,35.56)
COVAL(INLET,H1,ONLYMS,294.7)
```

```
      ******    OUTLET    ********
PATCH(OUTLET,HIGH,1,1,1,NY,NZ,NZ,1,30)
COVAL(OUTLET,P1,FIXP,0.0)
COVAL(OUTLET,H1,ONLYMS,SAME)
      **BUOYANCY SOURCE TERM BY GRAVITY **
PATCH(BUOYANCY,PHASEM,1,1,1,NY,1,NZ,1,30)
COVAL(BUOYANCY,W1,FIXFLU,-9.806)
     GROUP 14. Downstream pressure for PARAB=.TRUE.
     GROUP 15. Termination of sweeps
LSWEEP=25
RESREF(P1)=1.E-6
RESREF(V1)=1.E-6
RESREF(W1)=1.E-6
RESREF(H1)=1.E-6
     GROUP 16. Termination of iterations
     GROUP 17. Under-relaxation devices
     ************************************
RELAX(P1,LINRLX,0.3)
RELAX(V1,FALSDT,0.3)
RELAX(W1,FALSDT,0.3)
RELAX(H1,FALSDT,0.3)
RELAX(DEN1,LINRLX,0.5)
     GROUP 18. Limits on variables or increments to them
     GROUP 19. Data communicated by satellite to GROUND
RG(6)=6.65
RG(7)=378.0
RG(8)=2.89
RG(9)=319.0
     GROUP 20. Preliminary print-out
NOHEAD=F
     GROUP 21. Print-out of variables
OUTPUT(P1,Y,Y,Y,Y,Y,Y)
OUTPUT(W1,Y,Y,N,Y,Y,Y)
OUTPUT(H1,Y,Y,Y,Y,Y,Y)
OUTPUT(DEN1,Y,N,N,N,N,N)
     GROUP 22. Spot-value print-out
TSTSWP=5
NPRMON=10
IYMON=(NY-2)
IZMON=(NZ-2)
     GROUP 23. Field print-out and plot control
NTPRIN=10
NPRINT=LSWEEP
IPLTL=LSWEEP
IPLTF=LSWEEP-30
     **** print Y-Z plane velocity and temprature prifile .
PATCH(PROFIL15,PROFIL,1,1,1,NY,1,1,1,1)
COVAL(PROFIL15,W1,-1.0,1.0)
PATCH(PROFIL110,PROFIL,1,1,1,NY,1,1,4,4)
COVAL(PROFIL110,W1,-1.0,1.0)
PATCH(PROFIL115,PROFIL,1,1,1,NY,1,1,6,6)
COVAL(PROFIL115,W1,-1.0,1.0)
PATCH(PROFIL120,PROFIL,1,1,1,NY,1,1,8,8)
COVAL(PROFIL120,W1,-1.0,1.0)
PATCH(PROFIL1,PROFIL,1,1,1,NY,1,1,30,30)
COVAL(PROFIL1,W1,-1.0,1.0)
COVAL(PROFIL1,H1,285.0,400.0)
```

```
PATCH(PROFIL2,PROFIL,1,1,1,NY,8,8,30,30)
COVAL(PROFIL2,W1,-1.0,1.0)
COVAL(PROFIL2,H1,285.0,400.0)
PATCH(PROFIL3,PROFIL,1,1,1,NY,15,15,30,30)
COVAL(PROFIL3,W1,-1.0,1.0)
COVAL(PROFIL3,H1,285.0,400.0)
PATCH(PROFIL31,PROFIL,1,1,1,NY,16,16,30,30)
COVAL(PROFIL31,W1,-1.0,1.0)
COVAL(PROFIL31,H1,285.0,400.0)
PATCH(PROFIL4,PROFIL,1,1,1,NY,23,23,30,30)
COVAL(PROFIL4,W1,-1.0,1.0)
COVAL(PROFIL4,H1,285.0,400.0)
PATCH(PROFIL55,PROFIL,1,1,1,NY,NZ-1,NZ-1,1,1)
COVAL(PROFIL55,W1,-1.0,1.0)
PATCH(PROFIL510,PROFIL,1,1,1,NY,NZ-1,NZ-1,4,4)
COVAL(PROFIL510,W1,-1.0,1.0)
PATCH(PROFIL515,PROFIL,1,1,1,NY,NZ-1,NZ-1,6,6)
COVAL(PROFIL515,W1,-1.0,1.0)
PATCH(PROFIL520,PROFIL,1,1,1,NY,NZ-1,NZ-1,8,8)
COVAL(PROFIL520,W1,-1.0,1.0)
PATCH(PROFIL5,PROFIL,1,1,1,NY,NZ-1,NZ-1,30,30)
COVAL(PROFIL5,W1,-1.0,1.0)
PATCH(PROFIL6,PROFIL,1,1,1,NY,NZ,NZ,30,30)
COVAL(PROFIL6,H1,285.0,400.0)
    **************************
    GROUP 24. Dumps for restarts
SAVE=.T.
STOP
```

Appendix F

GROUND Subroutine for Non-isothermal Wall Channel

The GROUND subroutine that is used in the case of non-isothermal wall channel, is the same as the GROUND subroutine used in isothermal wall channel, as given in Appendix C, with the following changes in group 13.

```
C------------------------------------- value = GRND6
      RETURN
 1318 CONTINUE
C------------------------------------- value = GRND7
      IF(ISTEP.EQ.1.AND.IZ.EQ.1) CALL GETZ(ZGNZ,GZ1,50)
      CALL ONLYIF(H1,H1,'WALL')
      CALL FN1(VAL,GZ1(IZ)*RG(6)+RG(7))
      RETURN
 1319 CONTINUE
C------------------------------------- value = GRND8
      IF(ISTEP.EQ.1.AND.IZ.EQ.1) CALL GETZ(ZGNZ,GZ1,50)
      CALL ONLYIF(H1,H1,'GLASS')
      CALL FN1(VAL,GZ1(IZ)*RG(8)+RG(9))
      RETURN
 1320 CONTINUE
C------------------------------------- value = GRND9
      RETURN
 1321 CONTINUE
C------------------------------------- value = GRND10
      RETURN
C*************************************************************
```

Appendix G

Heater Element

SIGRAFLEX is a pure graphite material.

Flexible foils (SIGRAFLEX-F) or
rigid laminated sheets (SIGRAFLEX-LH)

are produced by thermal exfoliation of graphite intercalation compounds. The resulting expanded graphite is then pressed or calendered to yield the finished material.

SIGRAFLEX heating elements in all manner of shapes

can be simply punched or cut out of the foils or laminated sheets by means of a knife and template.

Characteristic properties

- Suitable for use in air up to 500°C and in a reducing or inert atmosphere up to more than 3000°C
- Low specific gravity permitting very rapid heating and cooling; also low heat storage capacity
- Excellent thermal shock resistance
- Resistant to ageing
- Impermeable to gas and liquids
- Insensitive to deposits of carbon in carburizing processes under partial vacuum
- Laminates posses adequate mechanical strength and withstand rapid gas currents (an important consideration in vacuum furnaces using inert gas cooling)
- Not wetted by glass, ceramic or metal melts
- Excellent stability to chemicals
- Highly anisotropic electrical and thermal conductivity

Physical properties

Melting point	°C	approx. 3650 (sublimed)
Specific electrical resistivity		
(see Figures G.1 and G.2)		
(Bulk density 1.0 g/cm³, temperature 20°C)		
Laminate LH – parallel to the surface	Ω µm	8 – 9
Foil – parallel to the surface	Ω µm	10
– perpendicular to the surface	Ω µm	650
Anisotropy coefficient		65
Thermal conductivity		
(Bulk density 1.0 g/cm³, temperature 20°C)		
– parallel to the surface	W/mk	220
– perpendicular to the surface	W/mk	7
Thermal expansion		
(see Figure G.3)		
Mean coefficient of thermal expansion (20–1000°C)		
(Bulk density 1.7 – 1.9 g/cm³)	10^{-6}/°C	5 – 8
Shore hardness		
Bulk density 1.0 g/cm³		30
Bulk density 1.3 g/cm³		40
Elongation at failure	%	1.5 – 2
Flexural strength of Sigraflex LH (Bulk density 1.0 g/cm³)	N/mm²	1.3
Tensile strength (Thickness of foil 0.35 mm, bulk density 1.0 g/cm³)	N/mm²	5
Gas permeability (air)	cm²/s	$<10^{-5}$
Coefficient of emission (500°C) (see Figure G.4)		0.4
Bulk density (standard grades) (see Figure G.5)	g/cm³	0.3/0.7/1.0
Compressibility and recovery (see Figure G.6)		
Ash content	%	approx. 0.1

Ash content (average)	ppm				
Fe	30	Ti	4.4	V	1.3
Si	26	Ni	4.0	Mn	0.7
Na	10.5	Mg	2.0	Mo	0.3
Ca	9.7	Cr	2.3	Sn	0.2
Al	5.5	Cu	1.8	Pb	0.1

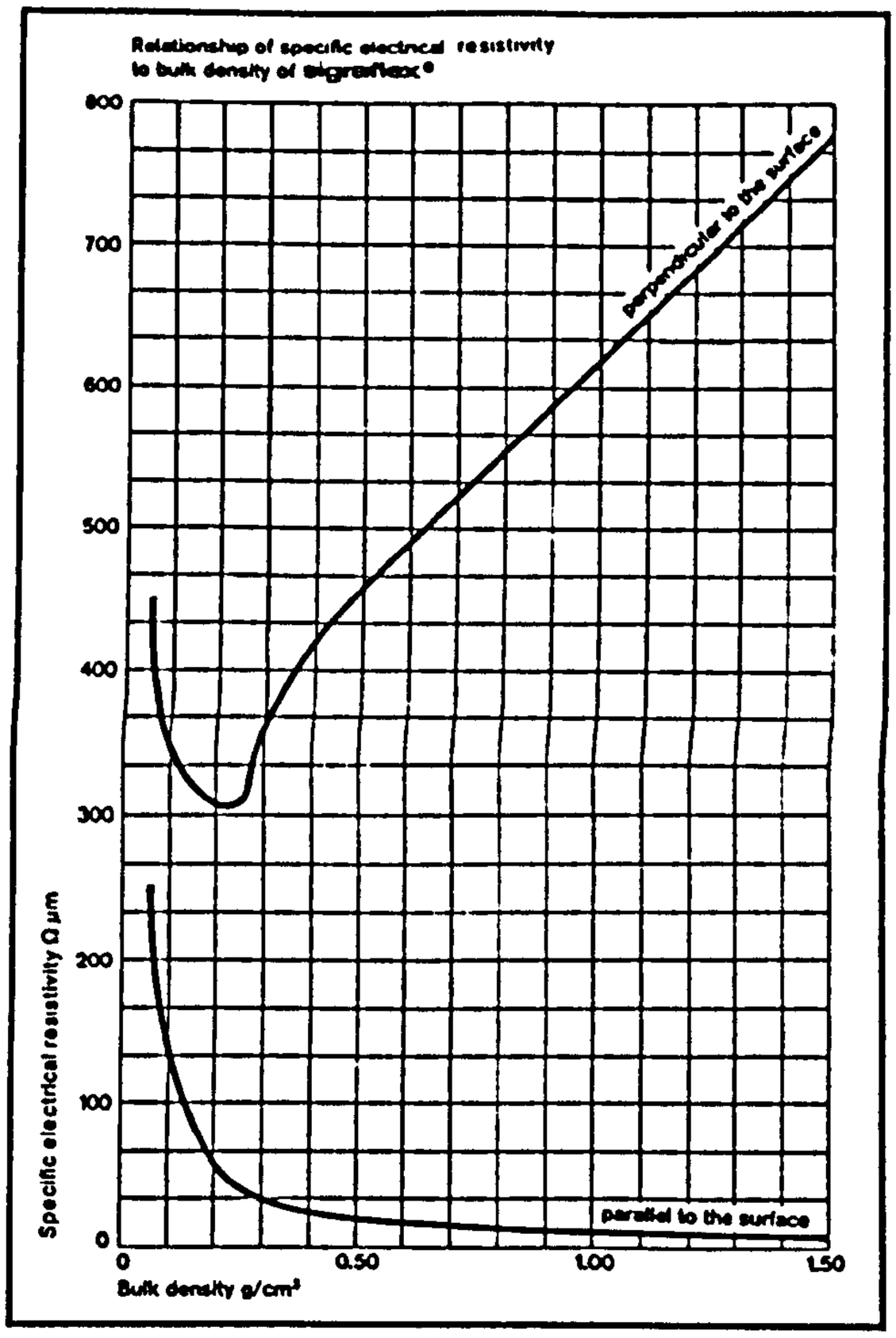

Figure G.1 Specific Electrical Resistivity

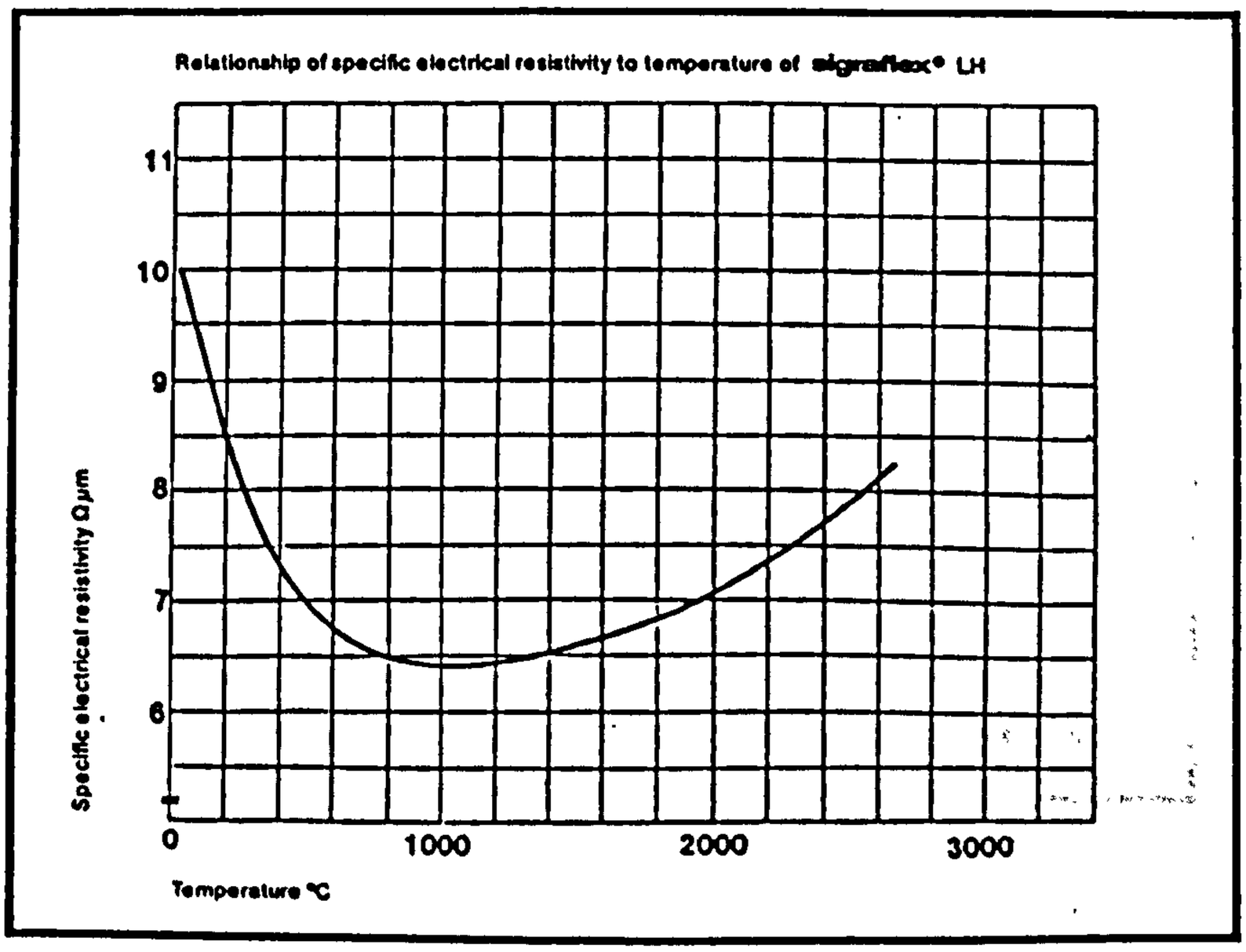

Figure G.2 Specific Electrical Resistivity

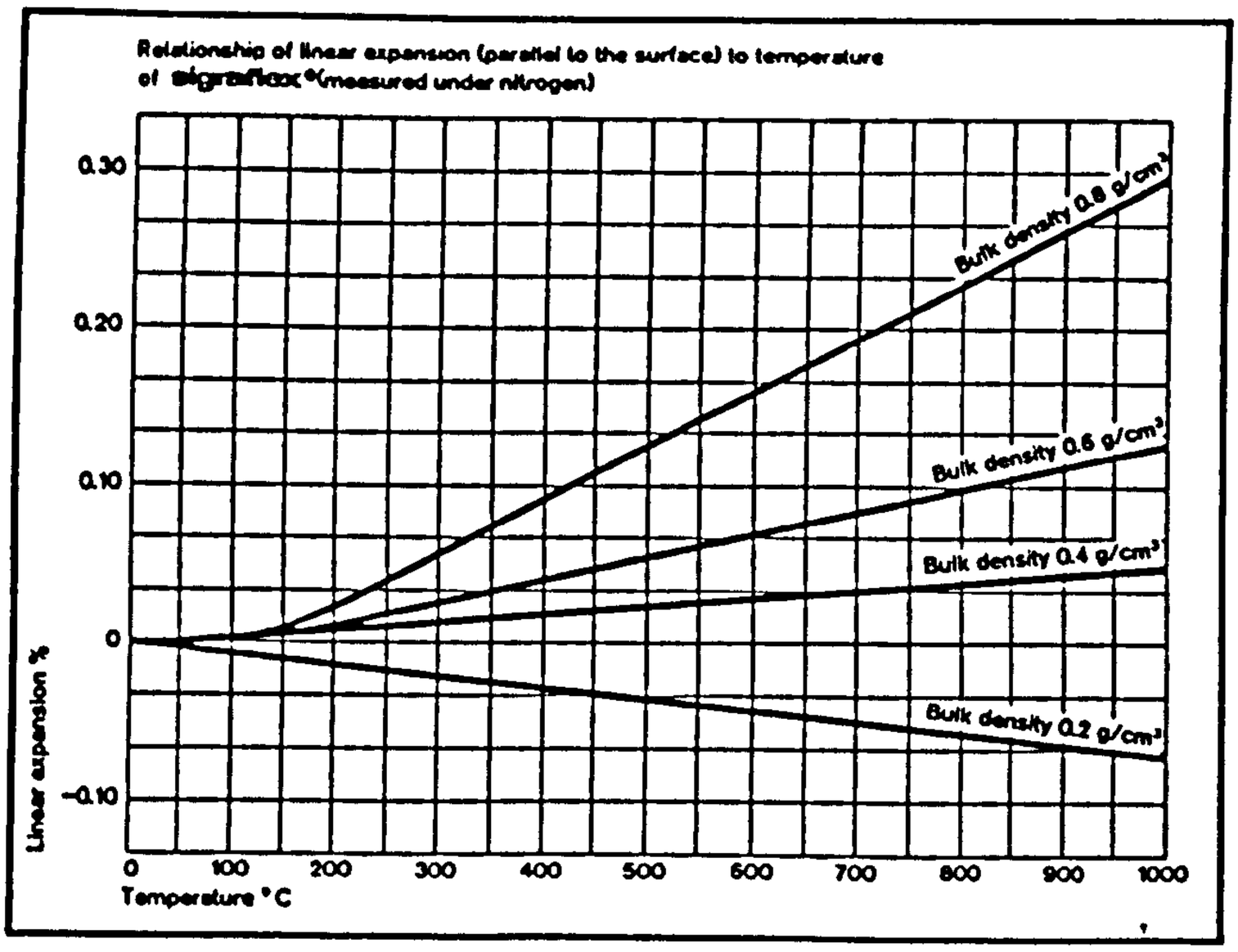

Figure G.3 Thermal Expansion

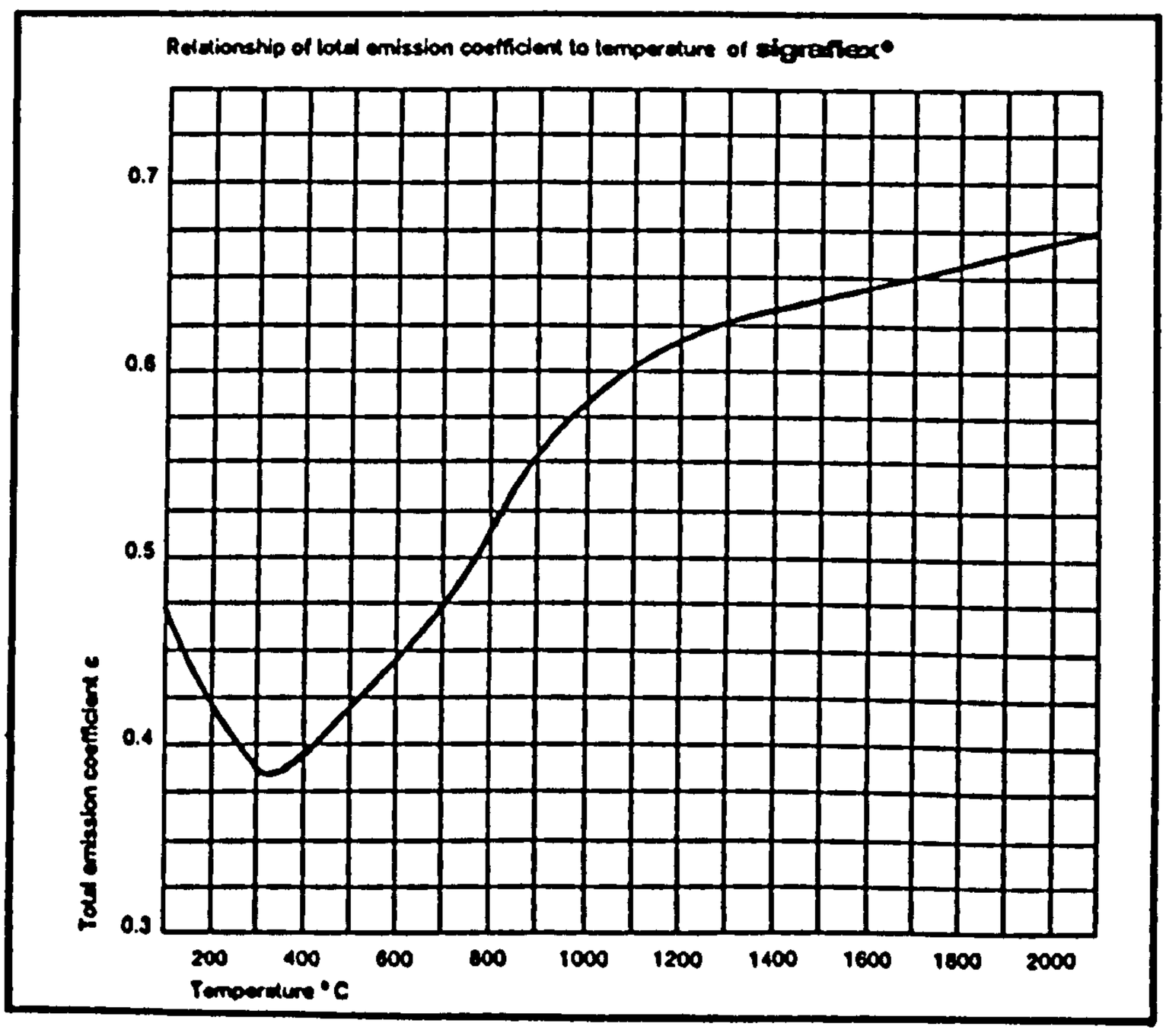

Figure G.4 Coefficient of Emission

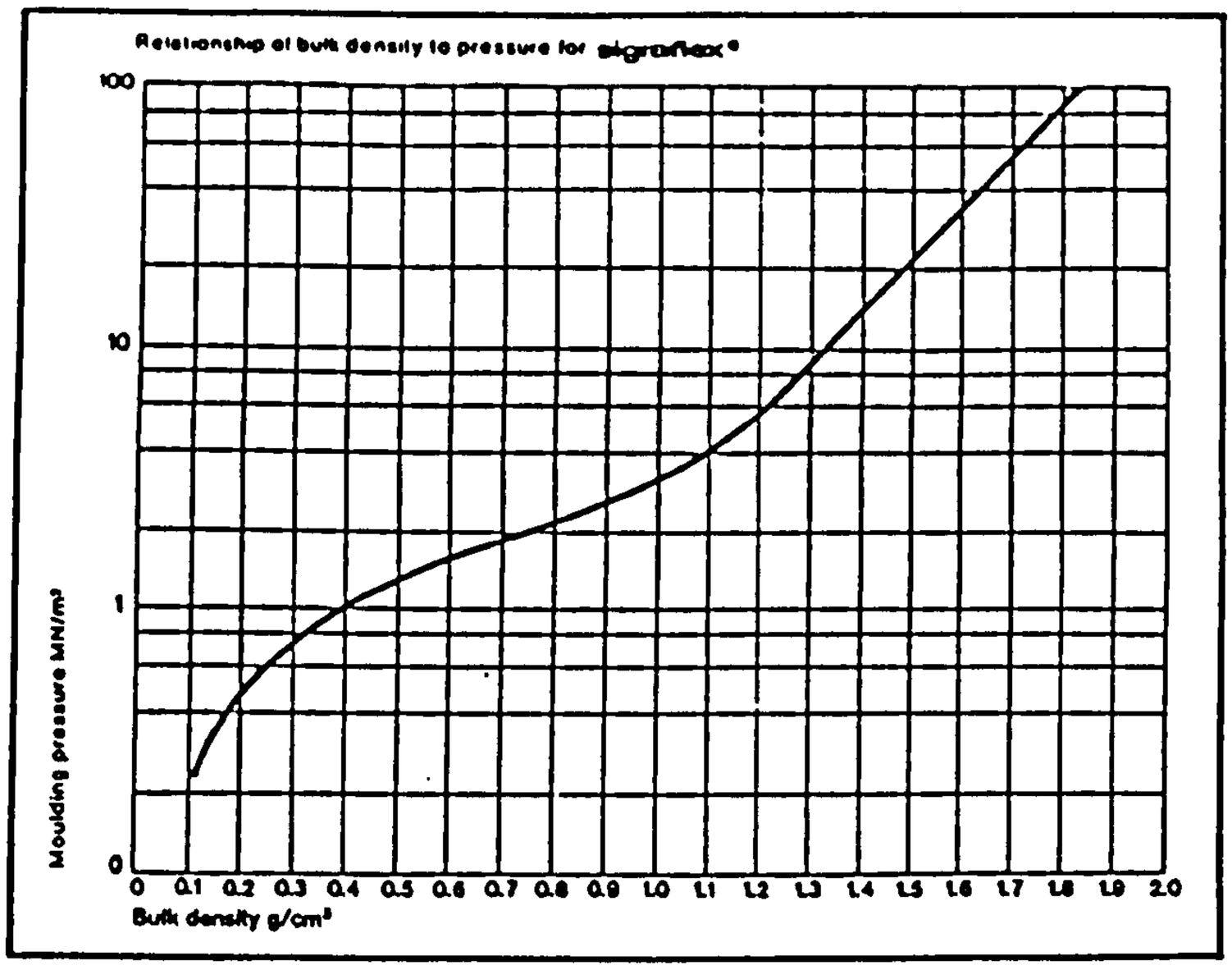

Figure G.5 Bulk Density

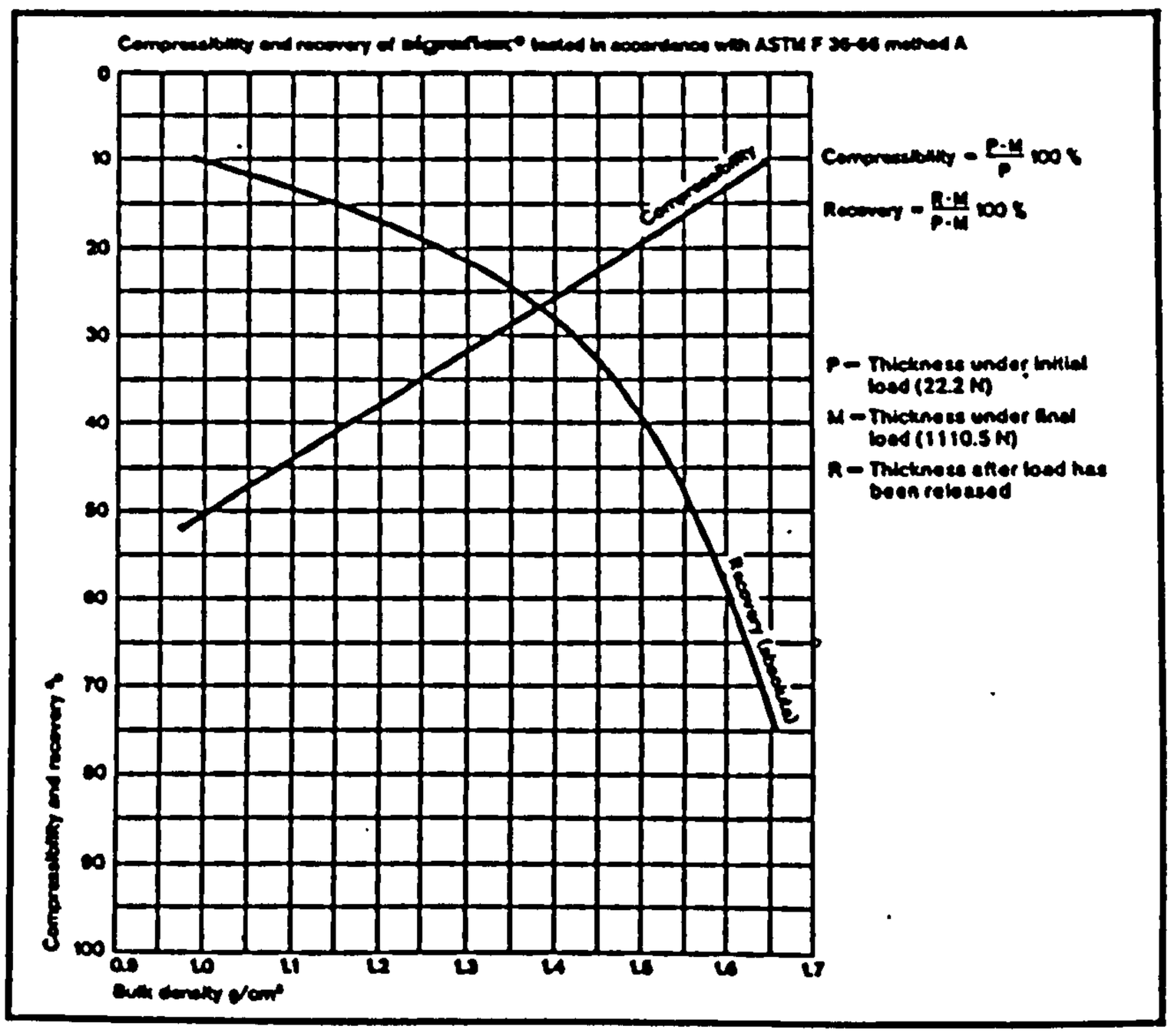

Figure G.6 Compressibility and Recovery

Appendix H

Insulation Material

TRITON **Kaowool** ceramic fibre

Board

(1260, 1400 & 1600)

Produced from refractory fibre compositions specially developed to give rigid, self-supporting forms.1400 & 1600 Board also contain a proportion of SAFFIL (R) Alumina Fibre.

Board is not wetted by most molten non-ferrous metals and has good resistance to spalling, thermal shock, and abrasion. The material can be easily cut and shaped.

Board contains a small percentage of organic binder to improve the handling strength, and this burns out on the first firing in use at approximately 200–300°C.

Sheet Size (mm)	:	1000 x 500
Thickness (mm)	:	5, 10, 25 (1260) * 5, 10, 15, 20, & 25 (1400/1600)

* Other thicknesses and sheet sizes also hardened Board can be supplied to special order by Converted Products Division.

General Properties	1260	1400	1600
Colour	White	White	White
Density (nominal) (kg/m^3)	250	200	160
Maximum service temperature (°C)	1260	1400	1600
Melting point (°C)	1680	–	–
Approximate weight loss on first firing in use (%)	4–6	5–10	5–10
Modulus of rupture (kPa) (Test based on B.S. 1902, after drying for 24 hours at 110°C)			
Unfired	1050	990	880
15 min. firing at 650°C	320	290	235

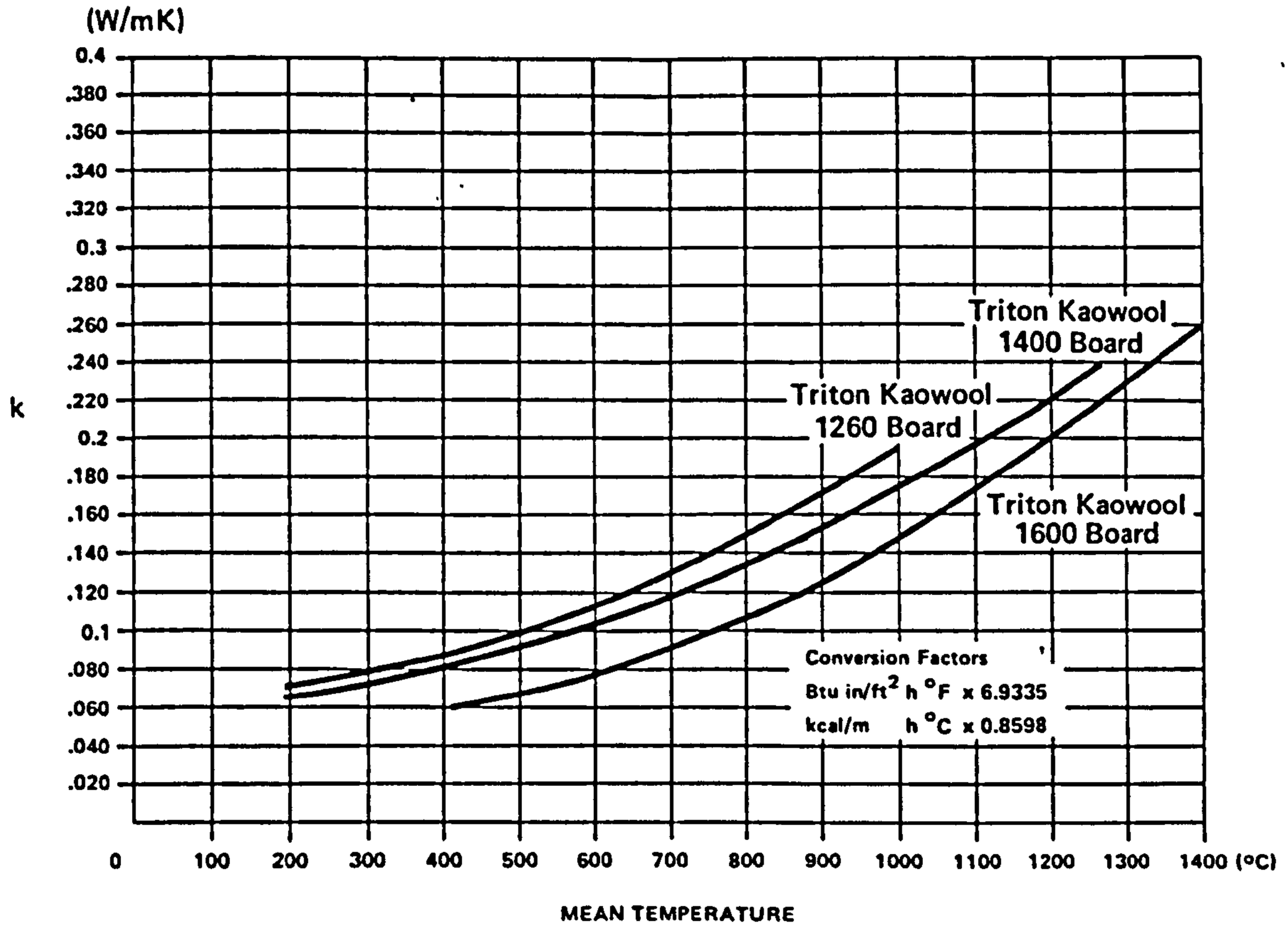

Typical applications

Iron & Steel	:	expansion joints, back-up insulation, heat shields, and mould base insulation
Non-Ferrous	:	tundish and launder covers in the casting of copper and copper-based alloys
Ceramics	:	hot-face lining for kilns and in construction of LTM kiln cars
Glass	:	back-up insulation in melting furnaces and protection of burners
Furnace Building	:	hot-face lining material (alternative to Blanket); back-up to solid refractories expansion joints.
Light Industry	:	lining combustion chambers in industrial and domestic boilers

® Saffil is the registered trademark of Imperial Chemical Industries Limited for alumina fibre.

TRITON **Kaowool** ceramic fibre

High Strength Paper

TRITON KAOWOOL High Strength Paper is manufactured from High Duty (1400 grade) fibre on conventional paper making machinery.

It has been specially developed for those industries where high strength, tough handling properties, excellent insulation and high service temperatures are of paramount importance.

Its high alumina content gives it a maximum use temperature of up to 1400°C.

The organic binder used to give the paper its excellent handling properties burns out on first firing without the production of the acidic fumes so common to other high strength, high flexibility ceramic fibre papers using neoprene based binder systems. The binder chosen has optimised the paper's tensile strength without impairing its flexibility.

Chemical Analysis

Typical major inorganic constituent analysis:

AL_2O_3	=	55%
SIO_2	=	45%

Approximately 7% acrylic polymer binder is used to give the paper its exceptional cold handling strength whilst retaining flexibility. This binder will burn out from 300°C.

Physical Properties

Colour =	White
Continuous use temperature	Up to 1400°C
Melting point	>1800°C
Approximate density (at rated thickness*)	230 kg/m³
Specific heat (980°C)	1.07k J/kg°K
Leachable Chlorides	<50 ppm

* (See thickness and roll sizes below)

TRITON KAOWOOL High Strength Paper possesses excellent resistance to chemical attack with the exception of hydrofluoric acid, phosphoric acid and strong alkalis, and it is unaffected by oil, steam or water.

Thermal Conductivity

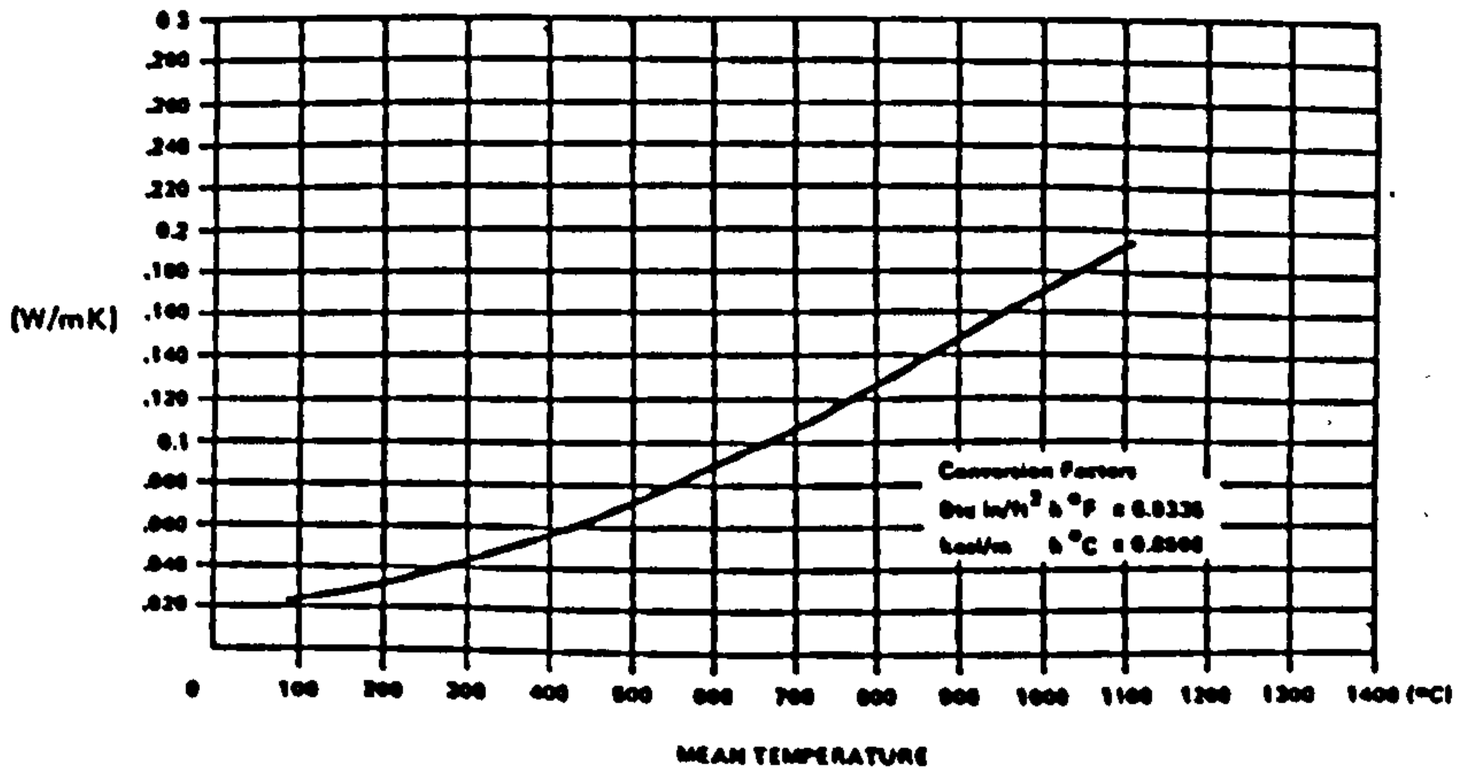

Electrical Properties

High Strength Paper is ideally suited for applications where both thermal and electrical insulation are required.

The electrical properties of the paper are as detailed below:

Resistivity
Normal atmospheric conditions, (23°C, 60% relative humidity) 10^{14} ohm–cm

Dielectric constant
Permittivity measurements were made at room temperature and humidity using a frequency 1583 Hz and gave an average figure of 1.2.

Dielectric strength – 4.0V/μm

Available Thicknesses and Roll Sizes

High Strength Paper is available in 0.5, 1.0 and 2.0 mm rated thicknesses. The "Rated Thickness" is the thickness measured under 50 kN/m² compression (as per the proposed B.S. method). (The uncompressed thickness will be approximately 20% greater than the rated thickness).

The paper is available ex stock in the following 500 mm wide roll lengths:

Rated Thickness	Roll Length and Weight	
0.5 mm	40 m (2.8 kg)	80 m (5.6 kg)
1.0 mm	20 m (2.3 kg)	40 m (4.6 kg)
2.0 mm	10 m (2.2 kg)	20 m (4.4 kg)

NB: 1000 mm and 250 mm widths in various lengths are available to order.

Typical applications

Launder applications
Hot tops
Casting heads
Parting media
Domestic gas and electric appliances
Gaskets
Lab equipment
Thermal and electrical insulation
Protection whilst brazing
Seals
Ladle applications
Mould liners
Fire protection applications
Expansion joints

Thermal Performances

The table below will be found useful in predicting the temperature drop across *High Strength Paper* for various hot-face working conditions.

Variation of cold face temperature °C with hot face temperature and Paper thickness

Hot Face Temp °C	Paper thickness in mm				
	0.5	1.0	2.0	4.0	6.0
200	161	135	109	85	72
400	–	275	218	156	131
600	–	–	333	250	205
800	–	–	–	343	290
1000	–	–	–	–	369
1200	–	–	–	–	442

Appendix I

HP-9845B Computer Program to Collect The Experimental Data

```
10    ! 69423A UTILITY PROGRAM ,9845B OR 9835A CONTROLLER HP-IB2
20    ! TYPE T THERMOCOUPLE
30    ! 69423A IN SLOT 1 OF MULTIPROGRAMMER
40    DIM C(12)
50    READ C(10),C(11),C(12)
60    READ C(7),C(8),C(9)
70    READ C(2),C(3),C(4),C(5)
80    BEEP
90    INPUT "NEW FILE NAME ?",Y$
100   CREATE Y$,14
110   ASSIGN #1 TO Y$
120   PRINTER IS 16
130   BEEP
140   PRINT "EXP. NO.:"&Y$
150   PRINT #1;Y$
160   PRINT
170   BEEP
180   INPUT "DATE OF THE EXP.( / / ) ?",Da$
190   PRINT "DATE OF THE EXP.:",Da$
200   PRINT #1;Da$
210   BEEP
220   INPUT "PLATE LENGTH ?",Me
230   PRINT "PLATE LENGTH =";Me
240   PRINT #1;Me
250   BEEP
260   INPUT "WIDTH ?",Wi
270   PRINT "WIDTH=";Wi
280   PRINT #1;Wi
290   PRINT
300   FOR K=1 TO 2
310   FOR J=1 TO 13
320   BEEP
330   INPUT "VERTICAL LOC.?",Ve
340   PRINT "VERTICAL LOC.:";Ve
350   BEEP
360   INPUT "CH. NO.:?",Ch
370   PRINT "CH. NO.:";Ch
380   BEEP
390   INPUT "HORIZONTAL LOC.?",Ho
400   PRINT "HORIZONTAL LOC.:";Ho
410   BEEP
420   INPUT "AIR VELOCITY=?",Ai
430   PRINT "AIR VELOCITY (M/SEC.)=";Ai
440   INPUT "Are These Values Satisfactory (Type Y Or N)?",Yn$
450   IF Yn$="Y" THEN 490
460   PRINT "Please Type In Your Value Again"
470   BEEP
480   IF Yn$="N" THEN 330
490   PRINT #1;Ve
500   PRINT #1;Ch
510   PRINT #1;Ho
520   PRINT #1;Ai
530   FOR I=1 TO 2
540   IF I=1 THEN Z$="A"
550   IF I=2 THEN Z$="B"
560   OUTPUT 723 USING "13A";"O160T"&Z$&"7T0260T"
570   OUTPUT 723 USING "2A";Z$&"X"
```

```
580   ENTER 723;R
590   R=FNOtd(R)
600   R=(R-4096)*10/4352
610   R=C(10)/(C(11)+LOG(-R))-C(12)
620   R=R*(C(7)+R*(C(8)+R*C(9)))*1E-6
630   FOR N=1 TO 6
640         !
650         OUTPUT 723 USING "6A,4D,6A";"0160T"&Z$,N,"T0260T"
660         OUTPUT 723 USING "2A";Z$&"X"
670         ENTER 723;T
680         T=FNOtd(T)
690         T=(T-(T>2047)*4096)*1E-5
700         T=(R+T)*1E6
710         F=C(1)+T*(C(2)+T*(C(3)+T*(C(4)+T*C(5))))
720         FIXED 2
730         PRINT "F=";F
740         PRINT #1;F
750   NEXT N
760   NEXT I
770   PRINT
780   NEXT J
790   PRINT "**********************"
800   NEXT K
810   ASSIGN * TO #1
820   ASSIGN #1 TO Y$
830   PRINTER IS 16
840   READ #1;Y$
850   PRINT "EXP. NO. :";Y$
860   READ #1;Da$
870   PRINT "DATE OF THE EXP.:";Da$
880   READ #1;Me
890   PRINT "PLATE LENGTH =";Me
900   READ #1;Wi
910   PRINT "WIDTH =";Wi
920   FOR L=1 TO 26
930   READ #1;Ve
940   PRINT "VERTICAL LOC.:";Ve
950   READ #1;Ch
960   PRINT "CH. NO.:";Ch
970   READ #1;Ho
980   PRINT "HORIZONTAL LOC.:";Ho
990   READ #1;Ai
1000  PRINT "AIR VELOCITY (M/SEC.)=";Ai
1010  FOR M=1 TO 12
1020  READ #1;F
1030  PRINT "F=";F
1040  NEXT M
1050  PRINT
1060  NEXT L
1070  ASSIGN * TO #1
1080  END
1090  DATA 3923.7225,13.158,273.2
1100  DATA 38.709457,3.7085566E-2,5.649552E-5
1110  DATA 2.5661297E-2,-6.1954869E-7,2.2181644E-11,-3.55009E-16
1120  !
1130  !
1140  ! THIS IS THE OTD FUNCTION
1150  !
1160  DEF FNOtd(A)
1170        RETURN A-2*INT(A/10)-16*INT(A/100)-128*INT(A/1000)-1024*INT(A/10000)-8
192*INT(A/100000)-(A>77777)*65536
1180  FNEND
```

```
580   ENTER 723;R
590   R=FNOtd(R)
600   R=(R-4096)*10/4352
610   R=C(10)/(C(11)+LOG(-R))-C(12)
620   R=R*(C(7)+R*(C(8)+R*C(9)))*1E-6
630   FOR N=1 TO 6
640         !
650         OUTPUT 723 USING "6A,4D,6A";"0160T"&Z$,N,"T0260T"
660         OUTPUT 723 USING "2A";Z$&"X"
670         ENTER 723;T
680         T=FNOtd(T)
690         T=(T-(T)2047)*4096)*1E-5
700         T=(R+T)*1E6
710         F=C(1)+T*(C(2)+T*(C(3)+T*(C(4)+T*C(5))))
720         FIXED 2
730         PRINT "F=";F
740         PRINT #1;F
750   NEXT N
760   NEXT I
770   PRINT
780   NEXT J
790   PRINT "**********************"
800   NEXT K
810   ASSIGN * TO #1
820   ASSIGN #1 TO Y$
830   PRINTER IS 16
840   READ #1;Y$
850   PRINT "EXP. NO. :";Y$
860   READ #1;Da$
870   PRINT "DATE OF THE EXP.:";Da$
880   READ #1;Me
890   PRINT "PLATE LENGTH =";Me
900   READ #1;Wi
910   PRINT "WIDTH =";Wi
920   FOR L=1 TO 26
930   READ #1;Ve
940   PRINT "VERTICAL LOC.:";Ve
950   READ #1;Ch
960   PRINT "CH. NO.:";Ch
970   READ #1;Ho
980   PRINT "HORIZONTAL LOC.:";Ho
990   READ #1;Ai
1000  PRINT "AIR VELOCITY (M/SEC.)=";Ai
1010  FOR M=1 TO 12
1020  READ #1;F
1030  PRINT "F=";F
1040  NEXT M
1050  PRINT
1060  NEXT L
1070  ASSIGN * TO #1
1080  END
1090  DATA 3923.7225,13.158,273.2
1100  DATA 38.709457,3.7085566E-2,5.649552E-5
1110  DATA 2.5661297E-2,-6.1954869E-7,2.2181644E-11,-3.55009E-16
1120  !
1130  !
1140  ! THIS IS THE OTD FUNCTION
1150  !
1160  DEF FNOtd(A)
1170        RETURN A-2*INT(A/10)-16*INT(A/100)-128*INT(A/1000)-1024*INT(A/10000)-8
192*INT(A/100000)-(A)77777)*65536
1180  FNEND
```

Appendix J

HP-9845B Computer Program to Analyze the Experimental Data

```
10    OPTION BASE 1
20    DIM F(20),H(15),U(15),O(15),T(15),Y(15),Tin(5),To(5),Ai(15)
30    DIM R(15),Cp(15),V(15),K(15),Ro(13),Z(15),Tw(15),Ti(15),Td(15)
40    DIM Tgi(15),Tave(15)
50    ASSIGN #1 TO "GAP102"
60    READ #1;Y$
70    READ #1;Da$
80    READ #1;Me
90    READ #1;Wi
100   FOR N=1 TO 2
110   FOR J=1 TO 13
120   READ #1;Ve
130   READ #1;Ch
140   READ #1;Ho
150   READ #1;Ai
160   FOR M=1 TO 12
170   FIXED 2
180   READ #1;F
190   F(M)=F
200   NEXT M
210   IF J=2 THEN 230
220   GOTO 270
230   Tin(N)=(F(10)+F(8)+F(9))/3+273
240   PRINT "Ti(N)=";Tin(N)
250   To(N)=(F(5)+F(11)+F(12))/3+273
260   PRINT "To(N)=";To(N)
270   NEXT J
280   NEXT N
290   ASSIGN * TO #1
300   ASSIGN #1 TO "GAP102"
310   PRINTER IS 0
320   READ #1;Y$
330   PRINT "EXP. NO. :";Y$
340   READ #1;Da$
350   PRINT "DATE OF THE EXP.:";Da$
360   ! PROPERTIES OF AIR "HEAT TRANSFER By J.P.HOLMAN"
370   FOR I=1 TO 5
380   READ R(I),Cp(I),V(I),K(I)
390   NEXT I
400   DATA 1.7684,1.0061,7.490,0.01809
410   DATA 1.4128,1.0053,9.490,0.02227
420   DATA 1.1774,1.0057,15.68,0.02624
430   DATA 0.9980,1.0090,20.76,0.03003
440   DATA 0.8826,1.0140,25.90,0.03365
450   READ #1;Me
460   PRINT "PLATE LENGTH=";Me
470   READ #1;Wi
480   PRINT "WIDTH =";Wi
490   ! ASPECT RATIO A=PLATE LENG./WIDTH
500   A=Me*100/Wi
510   FIXED 2
520   PRINT "ASPECT RATIO A =";A
530   FOR N=1 TO 2
540   FOR J=1 TO 13
550   READ #1;Ve
560   PRINT "VERTICAL LOC.:";Ve
570   READ #1;Ch
580   PRINT "CH. NO.:";Ch
590   READ #1;Ho
600   PRINT "HORIZONTAL LOC.:";Ho
```

```
610   READ #1;Ai
620   Ai(J)=Ai
630   PRINT "AIR VELOCITY (M/SEC.)=";Ai(J)
640   FOR M=1 TO 12
650   FIXED 2
660   READ #1;F
670   F(M)=F
680   PRINT "F=";F
690   NEXT M
700   IF Ch=2 THEN 1200
710   Tw(J)=(F(1)+F(2)+F(3))/3+273
720   Twp=Tw(J)
730   PRINT "AVERAGE WALL TEMP in deg (K)=";Tw(J)
740   Tgi(J)=(F(4)+F(5)+F(6))/3+273
750   Tgip=Tgi(J)
760   PRINT "AVERAGE GLASS INNER TEMP in deg (K) =";Tgi(J)
770   Tgo=(F(8)+F(9))/2+273
780   Tgop=Tgo
790   PRINT "AVERAGE GLASS OUTER TEMP in deg (K) =";Tgo
800   Taf=F(10)+273
810   PRINT "AMB. FRONT TEMP in deg (K) =";Taf
820   Tab=F(11)+273
830   PRINT "AMB. BACK TEMP  in  deg (K)=";Tab
840   Thb=F(12)+273
850   PRINT "HEATER BACK TEMP in deg (K)=";Thb
860   Z(J)=0
870   PRINT "Z=";Z(J)
880   Y(J)=0
890   PRINTER IS 0
900   PRINT TAB(2),"y/b";TAB(9),"Tw";TAB(19),"T";TAB(28),"Tgi";TAB(38),"Ti";TAB(
48),"To";TAB(56),"Ai"
910   T(J)=Tgi(J)
920   Ti(J)=Tin(N)
930   Td(J)=T(J)-Ti(J)
940   Ai(J)=0
950   PRINT Y(J);TAB(7),Tw(J);TAB(16),T(J);TAB(26);Tgi(J);TAB(36),Tin(N);TAB(45)
,To(N);TAB(54),Ai(J)
960   U(J)=0
970   O(J)=(T(J)-Ti(J))/(Tw(J)-Ti(J))
980   H(J)=U(J)*O(J)
990   PRINT TAB(3),"Y";TAB(12),"U";TAB(25),"O";TAB(38),"UO";TAB(50),"(LOCAL TEMP
 K)"
1000  PRINT USING 1500;Y(J),U(J),O(J),H(J),T(J)
1010  GOTO 1540
1020  FIXED 4
1030  Z(J)=Ho*1E-3
1040  PRINT "Z=";Z(J)
1050  FIXED 2
1060  Y(J)=Ho/(Wi*10)
1070  Tw(J)=F(1)+273
1080  Tw(J)=Twp
1090  !  AVERAGE AIR TEMP T(J) AT Y LOC.
1100  Tr=(F(2)+F(3)+F(4))/3
1110  T(J)=Tr+273
1120  In=INT(T(J)/50)-3
1130  IF In<1 THEN PRINT "T(J) IS LESS THAN 200 K";T(J)
1140  IF In>=5 THEN PRINT "T(J) IS GREATER THAN 400 k";T(J)
1150  Fr=(T(J)-(In*50+150))/50
1160  Ro(J)=R(In)+(R(In+1)-R(In))*Fr
1170  Tgi(J)=Tgip
1180  Ti(J)=(F(10)+F(8)+F(9))/3+273
1190  To=(F(5)+F(11)+F(12))/3+273
1200  Td(J)=T(J)-Ti(J)
```

```
1210  PRINT "Td(J)=";Td(J)
1220  PRINT TAB(2),"y/b";TAB(9),"Tw";TAB(19),"T";TAB(28),"Tgi";TAB(38),"Ti";TAB(
48),"To";TAB(56),"Ai"
1230  PRINT Y(J);TAB(7),Tw(J);TAB(16),T(J);TAB(26),Tgi(J);TAB(36),Ti(J);TAB(45),
To;TAB(54),Ai(J)
1240  ! AVERAGE AIR FILM TEMP in deg (K) 'Tf
1250  Tf=((Tw(J)+Tgi(J))/2+Ti(J))/2
1260  PRINT "AVERAGE AIR FILM TEMP in deg (K)=";Tf
1270  IF Tf<200 THEN PRINT "Tf IS LESS THAN 200 K";Tf
1280  IF Tf>=400 THEN PRINT "Tf IS GREATER THAN 400 K";Tf
1290  In=INT(Tf/50)-3
1300  IF In<1 THEN PRINT "Tf IS LESS THAN 200 K";Tf
1310  IF In>=5 THEN PRINT "Tf IS GREATER THAN 400 K";Tf
1320  Fr=(Tf-(In*50+150))/50
1330  R=R(In)+(R(In+1)-R(In))*Fr
1340  Cp=Cp(In)+(Cp(In+1)-Cp(In))*Fr
1350  V=V(In)+(V(In+1)-V(In))*Fr
1360  K=K(In)+(K(In+1)-K(In))*Fr
1370  ! PRINT "KINEMATIC VISCOSITY =";V;"1E-6 sq m/s"
1380  ! COEFFICIENT OF VOLUMETRIC THERMAL EXPANSION in deg (1/K) B
1390  B=1/Tf
1400  FLOAT 3
1410  ! PRINT "COEFFICINT OF VOLUMETRIC THERMAL EXPANSION in deg (1/K)=";B
1420  Tave(J)=(Tw(J)+Tgi(J))/2
1430  Gr=9.806*B*(Tave(J)-Ti(J))*(Wi/100)^3/(V*1E-6)^2
1440  PRINT "Gr =";Gr
1450  A=Me*100/Wi
1460  U(J)=Ai(J)*(Wi/100)/(V*1E-6*Gr)
1470  O(J)=(T(J)-Ti(J))/(Tw(J)-Ti(J))
1480  H(J)=U(J)*O(J)
1490  IF J>2 THEN 1500
1500  STANDARD
1510  PRINT TAB(3),"Y";TAB(12),"U";TAB(25),"O";TAB(38),"UO";TAB(50),"(LOCAL TEMP
 K)"
1520  IMAGE D.DD,4X,D.DDE,4X,MD.DDE,4X,MD.DDE,11X,DDD.DD
1530  PRINT USING 1500;Y(J),U(J),O(J),H(J),T(J)
1540  NEXT J
1550  J=14
1560  FIXED 4
1570  Z(J)=Wi/100
1580  FIXED 2
1590  Y(J)=1
1600  U(J)=0
1610  T(J)=Tw(13)
1620  Tw(J)=Tw(13)
1630  Tgi(J)=Tgi(13)
1640  Ti(J)=Ti(13)
1650  O(J)=(T(J)-Ti(J))/(Tw(J)-Ti(J))
1660  Ai(J)=0
1670  Td(J)=T(J)-Ti(J)
1680  H(J)=U(J)*O(J)
1690  FIXED 2
1700  PRINT TAB(2),"y/b";TAB(9),"Tw";TAB(19),"T";TAB(28),"Tgi";TAB(38),"Ti";TAB(
48),"To";TAB(56),"Ai"
1710  PRINT Y(J);TAB(7),Tw(J);TAB(16),T(J);TAB(26),Tgi(J);TAB(36),Ti(J);TAB(45),
To;TAB(54),Ai(J)
1720  PRINT TAB(3),"Y";TAB(12),"U";TAB(25),"O";TAB(38),"UO";TAB(50),"(LOCAL TEMP
 K)"
1730  PRINT USING 1500;Y(J),U(J),O(J),H(J),T(J)
1740  STANDARD
1750  FLOAT 3
1760  PRINT "THERMAL CONDUCTIVITY K W/m.c =";K
```

```
2260  PRINT "Rablog=";Rablog
2270  Rasb=Rab*Wi/Ve
2280  PRINT "Rasb=";Rasb
2290  Rasblog=LGT(Rasb)
2300  PRINT "Rasblog=";Rasblog
2310  Lbar=A/Grb
2320  PRINT "Lbar=";Lbar
2330  Xbar=Ve/(Wi*Grb)
2340  PRINT "Xbar=";Xbar
2350  PRINTER IS 0
2360  PRINT "V    =";V
2370  PRINT
2380  PRINT "Ve     =";Ve;TAB(22),"X      =";Xbar;TAB(44),"Lave   =";Lbar
2390  PRINT "Nug    =";Nug;TAB(22),"Hg     =";Hg
2400  PRINT "Nuw    =";Nuw;TAB(22),"Hw     =";Hw
2410  PRINT "Qf     =";Qf;TAB(22),"Vave   =";Vave
2420  Qd=Qdim*V*1E-6*Grb
2430  PRINT "Qd     =";Qd;TAB(22),"Qdim   =";Qdim
2440  PRINT "Mass   =";Mass
2450  PRINT "Qx     =";Qx;TAB(22),"Tx     =";Tx
2460  PRINT "Nuxave=";Nux;TAB(22),"Hxave =";Hx;TAB(44),"logNux=";Nuxlog
2470  PRINT "Twbar =";Twbar;TAB(22),"Tibar =";Tibar;TAB(44),"Tgibar=";Tgibar
2480  PRINT "Grave =";Grb;TAB(22),"logGr =";Grblog;TAB(44),"Tabar =";Tabar
2490  PRINT "Raave =";Rab;TAB(22),"logRa =";Rablog
2500  PRINT "Rasave=";Rasb;TAB(22),"logRas=";Rasblog
2510  PRINT "Nuglas=";Nuglass;TAB(22),"Hglass=";Hglass
2520  PRINT "Nuwall=";Nuwall;TAB(22),"Hwall =";Hwall
2530  PRINT "**********************************"
2540  STANDARD
2550  PRINTER IS 16
2560  REM ***** This is for drawimg *******
2570  FOR W=1 TO 4
2580 Set_up:        !
2590  PLOTTER IS 13,"GRAPHICS"
2600  GRAPHICS
2610  LIMIT 0,184,0,145
2620  LOCATE 30,120,20,98
2630  IF W=4 THEN 2660
2640  SCALE 0,100,0,100
2650  GOTO 2670
2660  SCALE 0,100,0,140
2670 Start_plot:      !
2680  FRAME
2690  AXES 10,10,0,0
2700  LINE TYPE 3
2710  FOR J=1 TO 14
2720  IF W=1 THEN 2760
2730  IF W=2 THEN 2780
2740  IF W=3 THEN 2800
2750  IF W=4 THEN 2820
2760  PLOT Y(J)*100,T(J)-273
2770  GOTO 2830
2780  PLOT Y(J)*100,O(J)*100
2790  GOTO 2830
2800  PLOT Y(J)*100,Ai(J)*100
2810  GOTO 2830
2820  PLOT Y(J)*100,U(J)*100000
2830  NEXT J
2840 Enhancements:      !
2850  UNCLIP
2860  LINE TYPE 1
2870 Label_axies:     !
2880  FOR A=0 TO 100 STEP 10
```

```
2890  MOVE A-4,-6
2900  LABEL A/100
2910  NEXT A
2920  LORG 2
2930  IF W>4 THEN 2960
2940  FOR B=0 TO 100 STEP 10
2950  GOTO 2960
2960  FOR B=0 TO 140 STEP 10
2970  MOVE -10,B
2980  IF W=1 THEN 3020
2990  IF W=2 THEN 3040
3000  IF W=3 THEN 3040
3010  IF W=4 THEN 3060
3020  LABEL B
3030  GOTO 3070
3040  LABEL B/100
3050  GOTO 3070
3060  LABEL B/100
3070  NEXT B
3080 Label_text:     !
3090  DEG
3100  SETGU
3110  IF W=1 THEN 3150
3120  IF W=2 THEN 3170
3130  IF W=3 THEN 3190
3140  IF W=4 THEN 3210
3150  MOVE 14,45
3160  GOTO 3220
3170  MOVE 14,55
3180  GOTO 3220
3190  MOVE 14,35
3200  GOTO 3220
3210  MOVE 14,45
3220  CSIZE 4,.5
3230  LDIR 90
3240  IF W=1 THEN 3280
3250  IF W=2 THEN 3300
3260  IF W=3 THEN 3320
3270  IF W=4 THEN 3340
3280  LABEL "t  (C)"
3290  GOTO 3350
3300  LABEL "0"
3310  GOTO 3350
3320  LABEL "Ai Air Velocity (M/SEC.)"
3330  GOTO 3350
3340  LABEL "U*(1E+03)"
3350  MOVE 75,9
3360  LDIR 0
3370  CSIZE 4,.5
3380  LORG 3
3390  LABEL "Y"
3400  CSIZE 4,.5
3410 Copies:     !
3420  EXIT GRAPHICS
3430  NEXT W
3440  STANDARD
3450  NEXT N
3460  STOP
3470  ASSIGN * TO #1
3480  END
```